

# Modeling of Ship Emissions and a Comparison of their Impact on Air Quality between Northern Europe and Eastern China

Dissertation

zur Erlangung des Doktorgrades der Naturwissenschaften  
an der Fakultät für Mathematik, Informatik und Naturwissenschaften  
Fachbereich Geowissenschaften  
der Universität Hamburg

vorgelegt von

**Daniel Alexander Schwarzkopf**  
geboren in Frankfurt am Main

Hamburg,  
Juni 2022



Universität Hamburg  
DER FORSCHUNG | DER LEHRE | DER BILDUNG



Helmholtz-Zentrum  
**hereon**



Fachbereich Erdsystemwissenschaften

---

Gutachter/innen der Dissertation: Prof. Dr. Kay-Christian Emeis  
Dr. Volker Matthias

Vorsitzender des Fach-Promotionsausschusses  
Erdsystemwissenschaften: Prof. Dr. Hermann Held

Dekan der Fakultät MIN: Prof. Dr. Heinrich Graener

Tag des Vollzugs der Promotion: 27.09.2022

## Eidesstattliche Versicherung | Declaration on Oath

Hiermit erkläre ich an Eides statt, dass ich die vorliegende Dissertationsschrift selbst verfasst und keine anderen als die angegebenen Quellen und Hilfsmittel benutzt habe.

I hereby declare upon oath that I have written the present dissertation independently and have not used further resources and aids than those stated.

23.11.2022

Hamburg, den | Hamburg, date

A handwritten signature in black ink, appearing to read 'Daniel Schmitt', with a long horizontal stroke extending to the right.

Unterschrift | Signature

# Abstract

Man-made influences have significantly changed the composition of the atmosphere during the last century. Enormous amounts of anthropogenic greenhouse gas emissions threaten to drive global warming to a point where its consequences could become catastrophic. Moreover, air pollution represents currently one of the greatest risks to human health worldwide. International shipping contributes to both of these problems on a global scale. Calculations hold it accountable for 2.2 % of CO<sub>2</sub>, 15 % of NO<sub>x</sub>, and 13 % of SO<sub>2</sub> of the respective total anthropogenic emissions in 2012. Regions that are particularly affected by air pollution from ships are, e.g., northern Europe or eastern China due to their high ship traffic. Analogous to global trade, merchant shipping is expected to continue to increase in the coming decades, and if not properly regulated, harmful ship emissions might increase as well.

Political actors, such as the International Maritime Organization (IMO), try to formulate effective management strategies that target the mitigation of adverse air quality impacts from ship emissions as well as a reduction of emitted greenhouse gases. However, this requires knowledge on the spatial and temporal distribution of ship emissions, as well as on their atmospheric dispersion and physicochemical transformations. Furthermore, potential legislative measures and technological pathways should be evaluated prior to their implementation to assess their performance against alternatives and identify possible drawbacks. Therefore, this doctoral thesis aims to investigate the effects of a potential future transition to cleaner and carbon-free fuels on ship emissions, as well as regional differences and/or similarities in the air quality impacts of ship emissions between northern Europe and eastern China.

To achieve these aims, the Modular Ship Emission Modeling System (MoSES) was developed. MoSES is independent of the region it is applied to and able to calculate spatio-temporally highly resolved ship emission data sets that are valuable for studying ship emissions. The emission calculation is based on a bottom-up approach, using data recorded from the automatic identification system (AIS) for ships and a ship characteristics database. In addition, several ship-type specific estimators were developed to account for ship characteristics data that is unavailable but required for the emission calculation.

For the research on ship emissions, two regions were of particular interest for this doctoral project. These are northern Europe, including the North and Baltic Sea (NBS), and eastern China, including the East China Sea, Yellow Sea, and Bohai Sea. Both are regions with high shipping densities, where ship emissions impact the air quality of populated coastal areas and large port cities. Using the MoSES model, ship emission inventories (EIs) for 2015 were calculated for both regions. In addition, uncertainties in the emission calculation were investigated, resulting from the choice of emission factors or unavailable ship characteristics data. A higher uncertainty was found for the ship EI generated for China, which was primarily due to less available information on ship engines of the regional fleet. For China, the main engine power had to be estimated for 67 % of the total main engine power of the regional fleet compared to 31 % for Europe.

In response to the IMO's current efforts to decarbonize the global shipping sector, a novel methodology was developed that is particularly useful to create decarbonization scenarios for the shipping industry. This methodology allows to modify and temporally evolve virtual representations of shipping fleets, e.g., to potential future shipping fleets. On the basis of these modified fleets, including their ship movements, scenario ship EIs can be calculated by the MoSES model.

Using this approach, three ship emission scenarios were generated for the NBS for the years 2025, 2040, and 2050. They concern a transition to ammonia as the main marine fuel in 2050, via liquefied natural gas as the main fuel in 2040. In addition, two different ammonia engine technologies were investigated, i.e., a combustion ignition engine (CI) option using marine diesel engine as pilot fuel and a spark ignition engine (SI) option using hydrogen as pilot fuel. Generally, the stronger emission reductions (shown below in brackets) were achieved with the SI technology, which is considered more advanced.

For 2050, a 40 % (47 %) reduction of CO<sub>2</sub> emissions from shipping was projected, but only a 22 % (44 %)

reduction of CO<sub>2</sub> equivalents compared to 2015. The reason for this difference is mainly attributable to an increase in N<sub>2</sub>O emissions. To contextualize these results to the IMO's decarbonization targets for 2050: These project a 50 % reduction of CO<sub>2</sub> emissions compared to 2008. Thus, differences need to be compensated in other ways, such as carbon capture and storage. In addition, air pollutant emissions were affected by the fuel transition: NO<sub>x</sub> emissions were reduced by 39 % (61 %), the different emitted PM components and SO<sub>2</sub> by 73–84 % in 2050 compared to 2015. The total annual ammonia slip from ammonia-fueled ships that were calculated for the NBS area was 930 Gg (35 Gg) in 2050.

Furthermore, difference in the regional impact of ship emissions on air quality between northern Europe and eastern China were investigated. An important factor in the comparison were the different levels of background air pollution between these regions, which can be classified as medium in Europe and high in China. Additional important factors were the regional shipping fleet and meteorological aspects.

For this study, two harmonized performed chemical transport model runs were carried out with the CMAQ model, using ship emission data calculated with MoSES. Annual mean pollutant concentrations in affected northern European coastal regions were 3 μg · m<sup>-3</sup> for NO<sub>2</sub>, below 0.3 μg · m<sup>-3</sup> for SO<sub>2</sub>, 2.5 μg · m<sup>-3</sup> for O<sub>3</sub>, and 1 μg · m<sup>-3</sup> for PM<sub>2.5</sub>. In eastern Chinese coastal regions these were 3 μg · m<sup>-3</sup> for NO<sub>2</sub>, 2 μg · m<sup>-3</sup> for SO<sub>2</sub>, 2–8 μg · m<sup>-3</sup> for O<sub>3</sub>, and 1.5 μg · m<sup>-3</sup> for PM<sub>2.5</sub>.

In heavily affected regions, such as large ports, the modeled contributions of ships on total ambient concentrations were in Europe 15 % for NO<sub>2</sub>, 0.3 % for SO<sub>2</sub>, 12.5 % for O<sub>3</sub>, and 1.25 % for PM<sub>2.5</sub> and in China 15 % for NO<sub>2</sub>, 6 % for SO<sub>2</sub>, 7.5 % for O<sub>3</sub> and, 2 % for PM<sub>2.5</sub>.

Thus, absolute pollutant concentrations from ships were in China slightly higher than in Europe, however, the relative impact was in China smaller due to higher emissions from other sectors. Compared to Europe, the higher level of atmospheric pollution, the characteristics of two different climate zones, and the summer monsoon were found to seasonally alter the chemical transformation processes of ship emissions in China. Especially in northern China, high PM concentrations during winter were found to inhibit the transformation of secondary aerosol precursors from ship emissions and reduce the impact of ship-related aerosols compared to Europe.

# Zusammenfassung

Durch den Einfluss des Menschen hat sich die Zusammensetzung der Atmosphäre im letzten Jahrhundert deutlich verändert. Gigantische Mengen anthropogener Treibhausgasemissionen sind der Auslöser für eine globale Erderwärmung, die droht katastrophale Folgen zu haben. Darüber hinaus stellt Luftverschmutzung derzeit die weltweit größte Gefahr für die menschliche Gesundheit dar. Der internationale Schiffsverkehr trägt seinen Teil zu diesen Problemen bei. Berechnungen zufolge hatte er einen Anteil von 2,2 % an CO<sub>2</sub>, 15 % an NO<sub>x</sub> und 13 % an SO<sub>2</sub> der jeweiligen anthropogenen Gesamtemissionsmengen im Jahr 2012. Regionen wie Nordeuropa oder Ostchina sind aufgrund ihres starken Schiffsverkehrs besonders von der Luftverschmutzung durch Schiffe betroffen. Analog zum Welthandel wird voraussichtlich auch die Handelschifffahrt in den kommenden Jahrzehnten weiter zunehmen. Erfolgt keine angemessene Regulierung, wird auch die Menge an schädlichen Schiffsemissionen weiter steigen.

Politische Akteure, wie die Internationale Seeschiffahrtsorganisation (IMO, International Maritime Organization), versuchen wirksame Strategien zu entwickeln, um die negativen Auswirkungen von Schiffsemissionen auf die Luftqualität zu mindern und den Ausstoß von Treibhausgasen zu reduzieren. Dies erfordert jedoch Kenntnisse über die räumliche und zeitliche Verteilung von Schiffsemissionen sowie über deren Dispersion und physikalisch-chemische Umwandlung in der Atmosphäre. Darüber hinaus sollten die Wirksamkeit legislativer Maßnahmen und technologische Neuentwicklungen vor ihrer Umsetzung auf ihre Wirksamkeit hin beurteilt sowie mögliche Nachteile ermittelt werden. Daher zielt die vorliegende Doktorarbeit darauf ab, die Auswirkungen eines möglichen künftigen Wechsels zu saubereren und kohlenstofffreien Kraftstoffen auf Schiffsemissionen zu untersuchen. Außerdem erfolgt eine Analyse regionaler Unterschiede und/oder Gemeinsamkeiten hinsichtlich der Auswirkungen von Schiffsemissionen auf die Luftqualität zwischen Nordeuropa und Ostchina.

Um diese Ziele zu erreichen, wurde das modulare Schiffsemissionsmodell (MoSES, Modular Ship Emission Modeling System) entwickelt. MoSES ist unabhängig von der zu modellierenden Region und in der Lage, räumlich und zeitlich hoch aufgelöste Schiffsemissionsdatensätze zu erzeugen, die für die Forschung an Schiffsemissionen von großem Nutzen sind. Die Emissionsberechnung basiert auf einem Bottom-up-Ansatz, bei dem Signaldaten aus dem automatischen Schiffsidentifikationssystem (AIS, Automatic Identification System) und eine Datenbank für Schiffseigenschaften verwendet werden. Darüber hinaus wurden mehrere schiffstypen-spezifische Funktionen entwickelt, um Schiffseigenschaften, die nicht bekannt, aber für die Emissionsberechnung erforderlich sind, abzuschätzen.

Für die Forschung an Schiffsemissionen waren für dieses Dissertationsprojekt zwei Regionen von besonderem Interesse. Diese sind Nordeuropa, einschließlich der Nord- und Ostsee (NBS, North and Baltic Sea), und Ostchina, inklusive dem Ostchinesischen Meer, dem Gelben Meer und dem Golf von Bohai. Beides sind Regionen mit hohem Schiffsverkehr, in denen Schiffsemissionen Einfluss auf die Luftqualität bewohnter Küstengebiete und großer Hafenstädte haben. Mithilfe des MoSES Modells wurden für beide Regionen räumlich und zeitlich hochaufgelöste Schiffs-Emissionsinventare (EIs) für das Jahr 2015 berechnet. Außerdem wurden Unsicherheiten in der Emissionsberechnung untersucht, die sich aus der Wahl der Emissionsfaktoren oder nicht verfügbarer Informationen zu Schiffseigenschaften ergeben. Eine größere Unsicherheit wurde für die Emissionsberechnung des Inventars für China festgestellt, was sich primär auf weniger verfügbare Informationen über die Leistung vieler Schiffsmotoren der regionalen Flotte zurückführen ließ. Für China musste die Leistung der Hauptmotoren für 67 % der gesamten Hauptmotorenleistung der regionalen Flotte geschätzt werden im Vergleich zu 31 % für Europa.

Als Reaktion auf aktuelle Ambitionen der IMO, den globalen Schifffahrtssektor zu dekarbonisieren, wurde eine neuartige Ansatz erarbeitet, der sich insbesondere zur Erstellung von Dekarbonisierungsszenarien für die Schifffahrt eignet. Dieser Ansatz ermöglicht es, virtuelle Darstellungen von Schiffsflotten zu modifizieren und zeitlich weiterzuentwickeln, z. B. zu möglichen zukünftigen Schiffsflotten. Auf der Grundlage solch einer modifizierten Flotte, inklusive ihrer Schiffsbewegungen, lassen sich mit dem MoSES-

Modell Emissionsinventare für Schiffsemissions-Szenarien berechnen.

Mittels dieses Ansatzes wurden für die NBS Region drei Schiffsemissionsszenarien für die Jahre 2025, 2040 und 2050 erstellt. In diesen wurde von einem Übergang zu Ammoniak als primärem Schiffskraftstoff im Jahr 2050 ausgegangen. Als Übergangslösung wurde verflüssigtes Erdgas (LNG, Liquefied Natural Gas) als primärer Kraftstoff im Jahr 2040 verwendet. Darüber hinaus, wurden zwei verschiedene Ammoniak-Motorentchnologien untersucht: eine Verbrennungsmotor-Option (CI, Combustion Ignition) mit Schiffsdiesel als Pilotkraftstoff und eine Fremdzündungsmotor-Option (SI, Spark Ignition) mit Wasserstoff als Pilotkraftstoff. Im Allgemeinen wurden stärkere Emissionsminderungen mit der SI-Technologie erzielt (in den folgenden Ergebnissen in Klammern), die als fortschrittlicher gilt.

Für 2050 wurde im Vergleich zu 2015 eine Verringerung der CO<sub>2</sub> Emissionen aus der Schifffahrt um 40 % (47 %) berechnet. Die Emissionen von CO<sub>2</sub>-Äquivalenten verringerten sich dagegen nur um 22 % (44 %). Der Grund dieser Differenz lag primär in einem Anstieg der N<sub>2</sub>O Emissionen. Um diese Ergebnisse in Kontext zu den Dekarbonisierungszielen der IMO für 2050 zu setzen: Diese legen eine 50-prozentige Reduktion der CO<sub>2</sub> Emissionen im Vergleich zu 2008 fest. Differenzen der in den Szenarien erhaltenen Ergebnisse müssten somit anderweitig, z. B. durch Carbon Capture and Storage kompensiert werden. Die Menge emittierter Luftschadstoffen wurde durch die Treibstoffumstellung ebenfalls beeinflusst: Für 2050 waren NO<sub>x</sub> Emissionen um 39 % geringer im Vergleich zu 2015 und die Emissionen verschiedener PM-Komponenten und SO<sub>2</sub> waren um 73–84 % reduziert. Die gesamten jährlichen NH<sub>3</sub>-Emission von ammoniak-betriebene Schiffe, die für die NBS Region berechnet wurden, lagen im Szenario für 2050 bei 930 Gg (35 Gg).

Außerdem wurden Unterschiede in den regionalen Auswirkungen von Schiffsemissionen auf die Luftqualität zwischen Nordeuropa und Ostchina untersucht. Ein wichtiger Faktor war der unterschiedliche Grad der Luftverschmutzung zwischen beiden Regionen, welcher in Europa als mittel und in China als hoch eingestuft werden kann. Weitere wichtige Faktoren waren die regionalen Schiffsflotten und meteorologische Aspekte.

Für diese Studie wurden zwei harmonisiert durchgeführte Chemietransportmodell-Läufe mit dem CMAQ-Modell vorgenommen, wobei mit MoSES berechnete Schiffsemissionsdaten verwendet wurden. Die mittleren jährlichen Schadstoff-Konzentrationen waren in betroffenen nordeuropäischen Küstenregionen  $3 \mu\text{g} \cdot \text{m}^{-3}$  für NO<sub>2</sub>, unter  $0.3 \mu\text{g} \cdot \text{m}^{-3}$  für SO<sub>2</sub>,  $2.5 \mu\text{g} \cdot \text{m}^{-3}$  für O<sub>3</sub> und  $1 \mu\text{g} \cdot \text{m}^{-3}$  für PM<sub>2.5</sub>. Für ostchinesische Küstenregionen lagen diese bei  $3 \mu\text{g} \cdot \text{m}^{-3}$  für NO<sub>2</sub>,  $2 \mu\text{g} \cdot \text{m}^{-3}$  für SO<sub>2</sub>,  $2\text{--}8 \mu\text{g} \cdot \text{m}^{-3}$  für O<sub>3</sub> und  $1.5 \mu\text{g} \cdot \text{m}^{-3}$  für PM<sub>2.5</sub>. In stark betroffenen Regionen, wie z. B. großen Häfen, betragen die Beiträge von Schiffen an den Luftschadstoff-Konzentrationen in Europa 15 % für NO<sub>2</sub>, 0.3 % für SO<sub>2</sub>, 12.5 % für O<sub>3</sub>, und 1.25 % für PM<sub>2.5</sub> und in China 15 % für NO<sub>2</sub>, 6 % für SO<sub>2</sub>, 7.5 % für O<sub>3</sub>, 2 % für PM<sub>2.5</sub>. Demnach waren die absoluten Schadstoff-Konzentrationen von Schiffen in China leicht höher als in Europa. Deren relative Auswirkungen waren jedoch in China aufgrund höherer Emissionen anderer Sektoren geringer. Im Vergleich zu Europa wurde festgestellt, dass in China der höhere Grad der Luftverschmutzung, die Charakteristiken zweier unterschiedlicher Klimazonen und der Sommermonsun die chemischen Umwandlungsprozesse von Schiffsemissionen in China saisonal verändern. Insbesondere für den Norden Chinas wurde festgestellt, dass hohe PM Konzentrationen im Winter die Umwandlung sekundärer Aerosolvorläufer aus Schiffsemissionen hemmen und die Auswirkungen schiffsbedingter Aerosole im Vergleich zu Europa verringern.



# Publications

The doctoral thesis was written within the framework of the following three core publications:

---

## Publication I:

A Ship Emission Modeling System with Scenario Capabilities,

**Daniel A. Schwarzkopf**, Ronny Petrik, Volker Matthias, Markus Quante, Elisa Majamäki, Jukka-Pekka Jalkanen,

Manuscript status: Accepted and published in

*Atmospheric Environment: X*, Volume 12, 2021, p. 100132,

ISSN 2590-1621,

<https://doi.org/10.1016/j.aeaoa.2021.100132>,

(<https://www.sciencedirect.com/science/article/pii/S2590162121000320>).

**Contributions:** Conceptualization: DAS, VM, MQ; Methodology: DAS; Software: DAS, RP; Validation: DAS, RP, EM, JPJ; Investigation: DAS; Data curation: DAS; Writing—original draft: DAS; Writing—review and editing: RP, VM, MQ; Supervision: VM, MQ; Project administration: VM, MQ; Funding acquisition: VM, MQ.

---

## Publication II:

Future Ship Emission Scenarios with a Focus on Ammonia Fuel,

**Daniel A. Schwarzkopf**, Ronny Petrik, Josefine Hahn, Volker Matthias, Markus Quante,

Manuscript status: Planned to be submitted to:

*Atmospheric Environment X*,

**Contributions:** Conceptualization: DAS, VM, RP; Methodology: DAS; Software: DAS; Validation: DAS, JH; Investigation: DAS; Data curation: VM, RP, DAS, JH; Writing—original draft: DAS; Writing—review and editing: JH, MQ; Supervision: VM, MQ; Project administration: VM, MQ; Funding acquisition: VM, MQ.

---

## Publication III:

Comparison of the Impact of Ship Emissions in Northern Europe and Eastern China,

**Daniel A. Schwarzkopf**, Ronny Petrik, Volker Matthias, Markus Quante, Guangyuan Yu, Yan Zhang

Manuscript status: Accepted and published in the special issue “*Atmospheric Shipping Emissions and Their Environmental Impacts*” in

*Atmosphere*, Volume 13(6), **2022**, p. 894,

<https://doi.org/10.3390/atmos13060894>,

(<https://www.mdpi.com/2073-4433/13/6/894>).

**Contributions:** Conceptualization: DAS, VM, MQ; Methodology: DAS, RP, VM, MQ; Software: DAS, RP; Validation: DAS; Formal Analysis: DAS; Investigation: DAS, RP, GY; Resources: VM, YZ; Data curation: DAS, RP; Writing—original draft preparation: DAS, RP, GY; Writing—review and editing: RP, VM, MQ, GY, YZ; Visualization: DAS; Supervision: VM, MQ, YZ; Project administration: VM, MQ, YZ; Funding acquisition: VM, MQ.

---



# Contents

<b>1. Introduction</b>	<b>1</b>
1.1. Air Pollution	1
1.1.1. Common Air Pollutants and their Health Effects	1
1.1.2. Sources and Sinks of Air Pollutants	2
1.1.3. Regulatory Measures for Air Pollution	3
1.1.4. Tropospheric Chemistry	4
1.1.4.1. Hydroxyl Chemistry	4
1.1.4.2. NO <sub>x</sub> Chemistry	5
1.1.4.3. O <sub>3</sub> Chemistry	5
1.1.4.4. SO <sub>2</sub> Chemistry	6
1.2. Greenhouse Gases	6
1.2.1. Common Greenhouse Gases and their Sources and Sinks	7
1.2.2. Regulatory Measures for Greenhouse Gases	8
1.3. Fundamentals of Air Quality Modeling	8
1.3.1. Emission Modeling	8
1.3.2. Meteorological Modeling	9
1.3.3. Chemistry Transport Modeling	9
1.3.3.1. Community Multi-scale Air Quality Model (CMAQ)	10
1.4. Air Pollutants and Greenhouse Gases from Ships and their Modeling	11
1.4.1. Modeling of Ship Emissions	12
1.4.2. Sulfur Emissions from Shipping and Corresponding Regulations	12
1.4.3. NO <sub>x</sub> Emissions from Shipping and Corresponding Regulations	13
1.4.4. Greenhouse Gas Emissions from Shipping and Corresponding Regulations	14
1.4.5. Recent and Current Focuses in Ship Emission Research	15
1.4.5.1. Ship Emissions in China	15
1.4.5.2. Potential Measures for the Reduction of Greenhouse Gas Emissions	16
<b>2. Scientific Question, Approach, and Structure of the Thesis</b>	<b>17</b>
2.1. Scientific Question	17
2.2. Approach	18
2.3. Structure of the Thesis	19
<b>3. Publication I: A Ship Emission Modeling System with Scenario Capabilities</b>	<b>21</b>
3.1. Model Description	22
3.1.1. AIS Data Tidying	22
3.1.2. Ship Movement	23
3.1.3. Ship Database Integration	23
3.1.4. Ship Definition	23
3.1.5. Emission Calculation	25
3.1.6. Emission Rastering	28
3.1.7. Ship Movement Compilation Data, Scenario Generation and Post-Processing	28
3.2. Model Application and Uncertainty Assessment	29
3.2.1. Preprocessing of AIS Data	29
3.2.2. Model Domain	29
3.2.3. Results	30
3.2.3.1. Spatial- and Temporal Distribution of Modeled Emissions	30

3.2.4.	Comparison with STEAM Ship Emission Data . . . . .	32
3.2.4.1.	Power Consumption . . . . .	33
3.2.4.2.	CO <sub>2</sub> . . . . .	33
3.2.4.3.	SO <sub>2</sub> and SO <sub>4</sub> . . . . .	34
3.2.4.4.	NO <sub>x</sub> . . . . .	35
3.2.5.	Uncertainty and Sensitivity Studies . . . . .	35
3.3.	Scenario Capability . . . . .	37
3.3.1.	Route Specific Sub-emission Inventories . . . . .	37
3.3.2.	Trade Volume Reduction Scenario . . . . .	38
3.4.	Conclusion . . . . .	39
<b>4.</b>	<b>Publication II: Future Ship Emission Scenarios with a Focus on Ammonia Fuel</b>	<b>41</b>
4.1.	Methodology . . . . .	41
4.1.1.	Reference Emission Inventory . . . . .	41
4.1.2.	Scenario Generation . . . . .	42
4.2.	Discussion of Scenario Emission Inventories . . . . .	44
4.2.1.	CO <sub>2</sub> Emissions . . . . .	45
4.2.2.	Methane Emissions . . . . .	46
4.2.3.	N <sub>2</sub> O Emissions . . . . .	47
4.2.4.	CO <sub>2</sub> Equivalent Emissions . . . . .	47
4.2.5.	NO <sub>x</sub> Emissions . . . . .	48
4.2.6.	Particulate Matter and SO <sub>2</sub> Emissions . . . . .	48
4.2.7.	CO and NMVOC Emissions . . . . .	49
4.2.8.	Ammonia Emissions . . . . .	49
4.3.	Concluding Summary and Outlook . . . . .	49
<b>5.</b>	<b>Publication III: Comparison of the Impact of Ship Emissions in Northern Europe and Eastern China</b>	<b>51</b>
5.1.	Materials and Methods . . . . .	52
5.1.1.	Model Simulations . . . . .	52
5.1.1.1.	Regions of Interest . . . . .	52
5.1.1.2.	Chemical Transport Model CMAQ - Setup and Forcing . . . . .	52
5.1.1.3.	Meteorological Forcing . . . . .	53
5.1.2.	Emissions Data . . . . .	53
5.1.2.1.	Anthropogenic Land-based Emissions for Europe . . . . .	53
5.1.2.2.	Anthropogenic Land-based Emissions for China . . . . .	53
5.1.2.3.	Biogenic Emissions . . . . .	54
5.1.2.4.	Ship Emissions in Northern Europe . . . . .	54
5.1.2.5.	Ship Emissions in China . . . . .	55
5.2.	Assessment of the Model Performance . . . . .	57
5.3.	Results and Discussion . . . . .	61
5.3.1.	NO <sub>2</sub> . . . . .	61
5.3.2.	SO <sub>2</sub> . . . . .	63
5.3.3.	Ozone . . . . .	64
5.3.4.	Fine Particulate Matter (PM <sub>2.5</sub> ) . . . . .	66
5.3.4.1.	Ammonium (NH <sub>4</sub> ) . . . . .	68
5.3.4.2.	Sulfate (SO <sub>4</sub> ) . . . . .	69
5.3.4.3.	Nitrate (NO <sub>3</sub> ) . . . . .	70
5.4.	Conclusions . . . . .	71
<b>6.</b>	<b>Summarising Discussion</b>	<b>73</b>
6.1.	Research Results . . . . .	73
6.2.	The Modular Ship Emission Modeling System (MoSES) . . . . .	75

6.3. Outlook . . . . .	76
<b>Bibliography</b>	<b>95</b>
<b>Abbreviations and Acronyms</b>	<b>97</b>
<b>List of Figures</b>	<b>104</b>
<b>List of Tables</b>	<b>106</b>
<b>A. Appendix</b>	<b>107</b>
A.1. Appendix for Publication I . . . . .	107
A.1.1. Fit Functions . . . . .	107
A.1.1.1. Gross Tonnage . . . . .	107
A.1.1.2. Total Main Engine Power . . . . .	107
A.1.1.3. Total Auxiliary Engine Power . . . . .	108
A.1.1.4. Service Speed and Main Engine RPM . . . . .	108
A.1.2. Gross Tonnage Class Averages . . . . .	109
A.1.3. Emission Factors . . . . .	109
A.1.3.1. Specific Fuel Oil Consumption (SFOC) . . . . .	109
A.1.3.2. Sulfur Dioxide (SO <sub>2</sub> ) . . . . .	110
A.1.3.3. Sulfate (SO <sub>4</sub> ) . . . . .	110
A.1.3.4. Nitrogen Oxides (NO <sub>X</sub> ) . . . . .	110
A.1.3.5. Black Carbon (BC) . . . . .	111
A.1.3.6. Primary Organic Aerosols (POAs) . . . . .	111
A.1.3.7. Mineral Ash (MA) . . . . .	111
A.1.3.8. Carbon Dioxide (CO <sub>2</sub> ) . . . . .	111
A.1.3.9. Carbon Monoxide (CO) . . . . .	112
A.1.3.10. Methane (CH <sub>4</sub> ) . . . . .	112
A.1.3.11. Non-Methane Organic Volatile Compounds (NMVOCs) . . . . .	112
A.1.3.12. Dinitrogen Oxide (N <sub>2</sub> O) . . . . .	113
A.1.3.13. Total Particulate Matter (PM <sub>tot</sub> ) . . . . .	113
A.1.3.14. Correction Factor for the Fuel Sulfur Dependency of PM . . . . .	113
A.1.4. Ship Energy Consumption at Berth . . . . .	113
A.1.5. AIS Navigational Status Values . . . . .	114
A.1.6. Engine Applications . . . . .	115
A.1.7. Total Monthly Ship Emissions in the North and Baltic Sea Domain . . . . .	115
A.1.8. List of Implemented Harbors . . . . .	115
A.1.8.1. North Sea . . . . .	115
A.1.8.2. Baltic Sea . . . . .	116
A.2. Appendix for Publication III . . . . .	117
A.2.1. Mapping for MEIC to SNAP Sectors and EDGAR Activity Codes . . . . .	117
A.2.2. Model Performance Data . . . . .	117
A.2.3. Pollutant Concentration Patterns . . . . .	120
A.2.3.1. NO <sub>2</sub> . . . . .	121
A.2.3.2. SO <sub>2</sub> . . . . .	122
A.2.3.3. Ozone . . . . .	124
A.2.3.4. PM <sub>2.5</sub> . . . . .	125
A.2.3.5. NH <sub>4</sub> . . . . .	127
A.2.3.6. NH <sub>3</sub> emissions . . . . .	128
A.2.3.7. NO <sub>3</sub> . . . . .	129
A.2.3.8. SO <sub>4</sub> . . . . .	130



# Preface

This doctoral thesis was developed at Helmholtz-Zentrum Hereon in cooperation with the Department of Earth System Sciences of the Faculty of Mathematics, Informatics and Natural Sciences (MIN) at the University of Hamburg. It is based on three scientific papers, of which two were published in an international peer-reviewed journal. The third paper is completed and will be submitted soon. All three papers are dealing with the overarching topic of ship emission modeling. Previously to this preface, an extended summary of the present work is given. Subsequent to this preface, the topics of anthropogenic air pollution, greenhouse gases, as well as air quality modeling, and the sub-topic of ship emission modeling are introduced in Chap. 1. The scientific questions that were the motivation for this thesis and an explanation of the approach used to answer them are described in Chap. 2. The publications produced during this doctorate are shown in Chap. 3, 4 and 5. The conclusions of this work as well as the answers to the scientific questions and an outlook are contained in Chap. 6.

Substantial parts of the research accomplished in this thesis contributed to the ShipCHEM project. The ShipCHEM project is a joint Sino-German research cooperation between Helmholtz-Zentrum Hereon and the Fudan University of Shanghai, co-funded by the National Science Foundation of China (NSFC) and the German Research Foundation (DFG, Deutsche Forschungsgemeinschaft, project number 645514). The research focus in the ShipCHEM project was to combine on-board emission measurements of ships with atmospheric chemistry transport modeling in order to estimate the contribution of shipping emissions to ambient air quality. The contributions made in this work concerned the construction of highly resolved shipping emission inventories, regional scale air quality simulations, and an analysis of differences and common features of ship emissions and their impacts on air quality between China and Europe (Chaps. 3 and 5).





# 1. Introduction

In the Anthropocene, our current geological epoch, humans became a driving force for the pollution of the Earth's atmosphere. Trillion tons of air and climate pollutants have been released, degrading the air we are breathing today, and more will follow this century. These pollutants endanger human health and that of other living species. They drive global warming towards a climatic change that poses an existential threat to life on our planet in its present form (Ramanathan, 2020).

In this doctoral thesis, computerized approaches were developed and applied that targeted the generation and evaluation of emissions data and their impacts on air quality. A focus was on the shipping sector and the generation of ship emission data that can describe the current situation as well as future developments. For this purpose, a model was developed that provides a particular flexibility for scenario creation and is thus able to generate the required data. The application of this model allowed to study a potential decarbonization pathway for the shipping sector that projected a transition towards ammonia as the primary used fuel. Furthermore, data sets for the regions of northern Europe and eastern China were generated and used as input for a chemistry transport model (CTM) to investigate differences in the impact of ship emissions between these two regions. This improved the understanding of the atmospheric effects of ship emissions and their impact on air quality in dependence of influencing parameters, such as the regional shipping fleet, the level of background atmospheric pollution and meteorological aspects.

## 1.1. Air Pollution

The problem of air pollution and the associated impact on human health go way back in human history. While in the past the main cause for air degradation and pulmonary diseases were wood fires, a shift towards fossil fuels and the Industrial Revolution intensified problems gradually (Jacobson, 2012). Today, the World Health Organization (WHO) states that air pollution is the world's greatest environmental health risk with annually seven million premature deaths resulting from exposure to air pollution (WHO, 2014). WHO data suggests an ubiquity of the problem: Almost 99% of the world's population lives in places where air pollution levels exceed the limits of WHO guidelines. These guidelines aim to reduce the detrimental health effects of air pollution (WHO, 2022). With clean air being a fundamental resource for every single person, measures must be taken to preserve this valuable good and minimize the risks of air pollution.

### 1.1.1. Common Air Pollutants and their Health Effects

The WHO defines air pollution as a contamination of the indoor or outdoor environment by any chemical, physical or biological agent that modifies the natural characteristics of the atmosphere. The most important pollutants referred to with this terminology are particulate matter (PM), nitrogen oxides (NO<sub>x</sub>), sulfur dioxide (SO<sub>2</sub>) and ozone (O<sub>3</sub>). All of them being harmful for public health and/or the environment.

Particulate matter is a collective term, describing small solid particles and liquid droplets that are found in the atmosphere. A sub-categorization of PM is often done according to particle size. Particles with an aerodynamic diameter of 2.5 μm and smaller are referenced to as PM<sub>2.5</sub> and particles with a diameter of 10 μm and smaller are described as PM<sub>10</sub> (European Environmental Agency, 2018). PM is especially harmful to the lower respiratory tract, being involved in the development of chronic obstructive pulmonary disease, lung cancer and cardiovascular diseases. The detrimental effects of PM are differing with particle sizes. While PM<sub>10</sub> is deposited in the bronchioles or alveoli of the lung, the smaller PM<sub>2.5</sub> is able to penetrate into the pulmonary alveoli and is thus more harmful. Long-term exposure to PM increases the risk of developing respiratory disorders (U. S. EPA, 2021a).

## 1. Introduction

Important components of PM are, e.g., black carbon (BC), primary organic aerosols (POAs) and mineral ash (MA). Black carbon, consisting mainly of pure carbon, originates from incomplete combustion and operates as a carrier of toxic and carcinogenic substances due to its porous structure (WHO, 2012). In the atmosphere, BC effectively absorbs solar radiation and decreases the Earth's albedo. When deposited on snow and ice, it enhances melting, which is an effect that is particularly important if BC is emitted in proximity to the polar caps (Bond et al., 2013). Primary organic aerosols are organic molecules, consisting of carbon and hydrogen, oxygen and/or nitrogen and sulfur that are directly emitted in a particulate form or phase (Bhattu, 2018). Mineral ashes represent the incombustible components of the fuel oil. These are, e.g., extraneous solids, residues of organometallic compounds and salts (Sarkar, 2015).

The term  $\text{NO}_x$  is a collective term for the gases nitrogen dioxide ( $\text{NO}_2$ ) and nitrogen monoxide (NO). Both are toxic gases that can form particles by atmospheric oxidation, acidify the environment as nitric acid ( $\text{HNO}_3$ , see Sect. 1.1.4.2 for details) and cause eutrophication (Paerl, 1995). Eutrophication is an enrichment of nutrients in water bodies, which can lead to excessive plant and algae blooms harmful for the ecosystem (Chislock et al., 2013). High concentrations are especially found in urban areas, where  $\text{NO}_2$  is linked to a reduced lung function of children. Long-term exposure increases the risk of bronchitis, myocardial infarction and lung cancer (WHO, 2022; Rasche et al., 2018; Hamra et al., 2015).

Similar to  $\text{NO}_x$ , sulfur dioxide is a toxic gas, which harms the respiratory tract. Atmospherically oxidized, it can contribute to particle formation or transform into sulfuric acid ( $\text{H}_2\text{SO}_4$ , which acidifies the environment (U. S. EPA, 2021b) (see Sect. 1.1.4.4). Health effects connected with a long-term exposure include asthma and chronic bronchitis, as well as preterm births (Farrow et al., 2020).

Ozone is a reactive oxygen species that fulfills a role as absorbent of mutagenic ultraviolet radiation in the earth's stratosphere. In the troposphere, however, it becomes an air pollutant that is harmful to human health and vegetation. Elevated concentrations can irritate the respiratory tract and deteriorate the lung function. Chronic exposure increases the risk of circulatory and respiratory mortality of all-causes (Turner et al., 2016). Moreover,  $\text{O}_3$  can damage vegetation, reduce the productivity of plants, and diminish agricultural crop yields (Chuwah et al., 2015).

Further air pollutants that are worth mentioning include: ammonia ( $\text{NH}_3$ ), which is an corrosive gas and plays an important role in particle formation, and carbon monoxide (CO) and (nonmethane) volatile organic compounds ((NM)VOCs), both are species important to consider in the formation of ground-level ozone.

### 1.1.2. Sources and Sinks of Air Pollutants

The sources of air pollutants are manifold. Usually, a differentiation is made between pollutants originating from human activities (anthropogenic sources) and pollutants originating from nature (biogenic sources). However, the dominant sources of air pollution are of anthropogenic nature, i.e. in particular the combustion of fossil fuels and biomass for energy generation and agriculture including livestock. Other important anthropogenic emission sectors include industrial activities, road and off-road traffic, aviation, and shipping (more information on emission from shipping can be found in Sect. 1.4). Biogenic air pollutant sources are, e.g., volcanoes ( $\text{SO}_2$ ,  $\text{NO}_x$ , PM), sand or dust (PM), lightning ( $\text{NO}_x$ ), natural wildfires (CO,  $\text{SO}_2$ , BC, PM), plants, animals, and micro-organisms (VOCs).

With respect to their source, air pollutants are also referenced to as primary and secondary pollutants. While primary pollutants are emitted directly from their source, secondary pollutants are formed by chemical or physical atmospheric processes from primary precursor pollutants. Examples for primary pollutants are  $\text{NO}_2$  and  $\text{SO}_2$ , which can be transformed into secondary PM by salification, e.g., with ammonia after an atmospheric oxidation. It is referred to Sect. 1.1.4 for further information on atmospheric reactions that form secondary air pollutants.

Air pollutant sinks are processes that permanently or semi-permanently remove a species from the atmosphere. This can be an absorption into the ground or ocean, a washing-out by rain, but also a transformation into another substance. The general life-cycle of an air pollutant, including sources and sinks, is illustrated in Fig. 1.1.

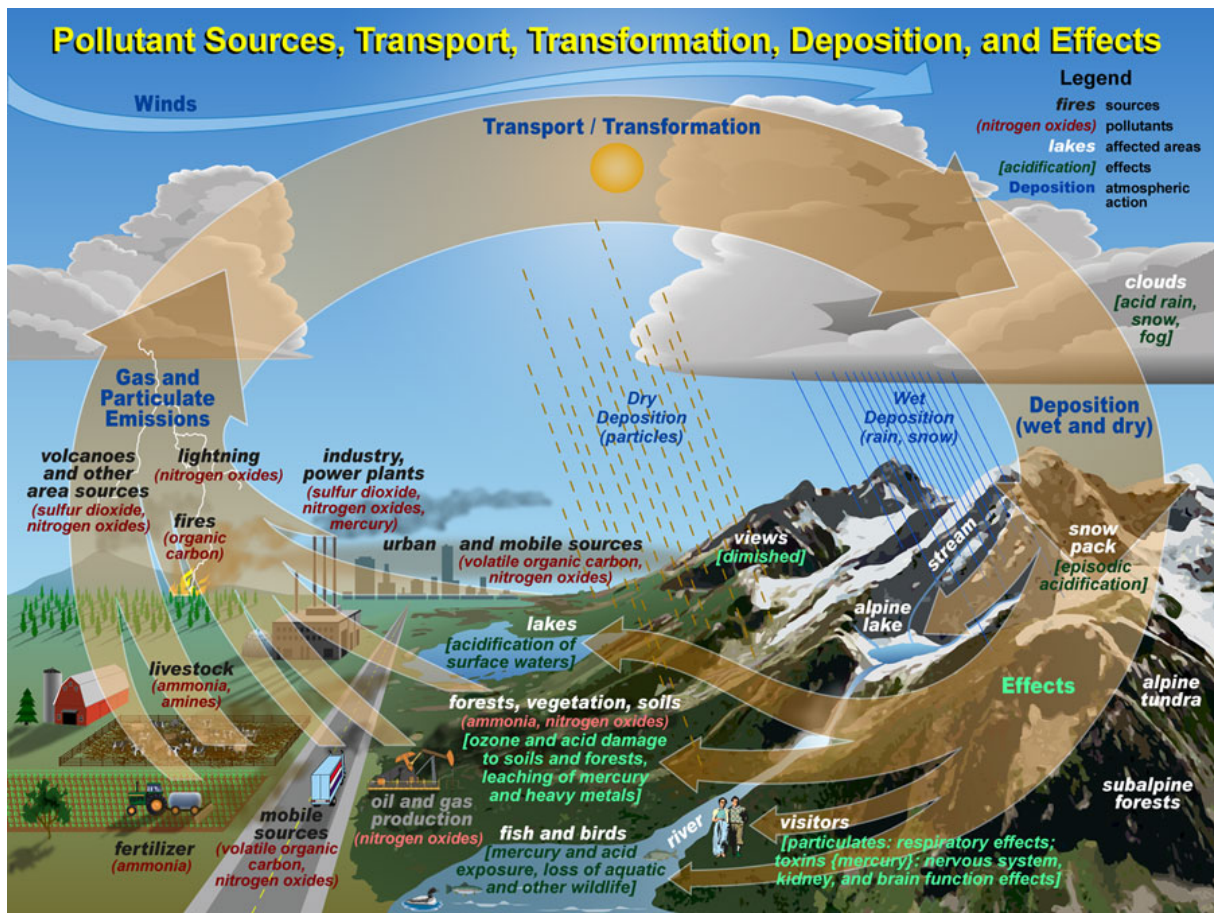


Figure 1.1.: Illustration of the atmospheric life-cycle of air pollutants from source to sink. Reprinted with permission from U.S. Fish & Wildlife Service (U. S. Fish and Wildlife Service, 2015).

### 1.1.3. Regulatory Measures for Air Pollution

To address and draw attention to the problem of air pollution, the WHO started in 1987 to periodically issue health-based air quality guidelines (AQGs) for the major health-damaging air pollutants (PM, O<sub>3</sub>, NO<sub>2</sub> and SO<sub>2</sub>, Table 1.1). Although not legally binding, they offer guidance to governments and the civil society in assessing the problem and developing policies that aim at a mitigation of health impacts from air pollution, based on a scientific basis. The earlier versions of the WHO's AQGs provided a foundation for legislation on air quality, in particular for the European countries, which brought the Ambient Air Quality Directive into force in 2008 (European Parliament and Council, 2008; WHO, 2021). The goals of this directive include the control of emissions from mobile sources, improvements of fuel quality, and the promotion and integration of environmental protection requirements into the transport and energy sector. It also contains an own set of European air quality guidelines that is shown in Table 1.1. Similar regulations were also implemented in other countries, e.g., in China. Its rapid economic growth of the recent decades and its role as the “factory of the world” made it with a global share of 18–35% the worldwide biggest emitter of air pollutants (Hoesly et al., 2018). The Chinese government, being aware of the problem, consistently updated and tightened its imposed exposure limits for air pollutants, which were first introduced in 1982 (Table 1.1). With the “Plan on the Prevention and Control of Air Pollution”, which was adopted in 2013, annual average PM<sub>2.5</sub> concentrations were effectively reduced by 28–40% in 2017 (China, State Council, 2013, 2018). Regional air pollution, however, persists on a high level until today (WHO, 2021).

Table 1.1.: World Health Organization (WHO) air quality guidelines (AQGs) for 2005 and 2021 (WHO, 2005, 2021), current European (European Commission, 2008) and Chinese air quality standards (class 2, GB 3095-2012 and HJ 633-2012).

Pollutant [ $\mu\text{g} \cdot \text{m}^{-3}$ ]	Averaging Time	WHO 2005 AQGs	WHO 2021 AQGs	EU Standards	Chinese Class 2 Standards
PM <sub>2.5</sub>	Annual	10	5	20	35
	24-hour	25	15	—	75
PM <sub>10</sub>	Annual	20	15	40	70
	24-hour	50	45	50	150
O <sub>3</sub>	Peak season	—	60	—	—
	8-hour	100	100	120	160
NO <sub>2</sub>	Annual	40	10	40	40
	24-hour	—	25	—	80
SO <sub>2</sub>	Annual	20	40	—	60
	24-hour	—	—	125	150

#### 1.1.4. Tropospheric Chemistry

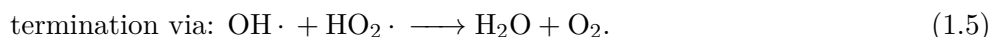
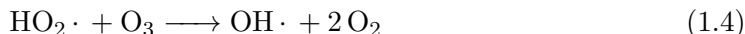
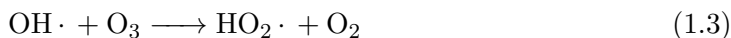
The main components of the Earth’s atmosphere are nitrogen, oxygen, inert gases, carbon dioxide and water vapor. Additionally, the atmosphere contains many different trace gases and pollutants, these are particularly found in the troposphere. With respect to air pollution, the most important species were introduced in Sect. 1.1.1. Photochemical processes, promoted by solar radiation, are of major importance for the dynamics of chemical transformations in the troposphere and their understanding. On the one hand, these reactions function as a source for secondary air pollutants, but on the other hand, they are also an important sink for the atmospheric trace gases. Hereby, hydroxyl radicals act as the main “cleaning agents” due to their oxidative capacity. The following section contains an overview of the main drivers of tropospheric chemistry and of the common reactions trace gases and pollutant species undergo. For this purpose, the knowledge presented in this section is mainly based on the current textbooks by Seinfeld and Pandis (2006) and Jacob (1999).

##### 1.1.4.1. Hydroxyl Chemistry

The main driver of tropospheric chemistry is the hydroxyl radical ( $\text{OH}\cdot$ ). In comparison to molecular oxygen and ozone,  $\text{OH}\cdot$  is highly reactive and functions as the major oxidant of the atmosphere. In the atmosphere, ozone can photolyze to singlet oxygen ( $\text{O}({}^1\text{D})$ ) according to Eq. (1.1). Hydroxyl radicals can then form by the reaction of an excited singlet oxygen species with a water molecule according to Eq. (1.2).



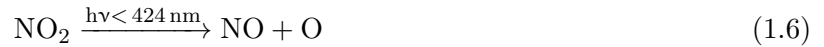
Hydroxyl radicals react with most atmospheric trace gases in the form of catalytic cycles in which  $\text{OH}\cdot$  is eventually regenerated. By Eq. (1.3) and the potential follow-up reaction of a hydroperoxyl radical with  $\text{O}_3$ , shown in Eq. (1.4), hydroxyl formation can also function as a significant sink for ozone,



Hydroxyl and hydroperoxyl radicals are often grouped together as  $\text{HO}_X$ .

### 1.1.4.2. NO<sub>x</sub> Chemistry

NO<sub>x</sub> is a group of chemical species that consists of the components NO and NO<sub>2</sub>. Both can interconvert rapidly during daytime in the presence of ozone, according to the Leighton relationship, shown in Eqs. (1.6)–(1.8).



It is noteworthy that according to Eqs. (1.6) and (1.7), high NO<sub>2</sub> concentrations can promote ozone formation. However, in connection to this, high NO concentrations favor O<sub>3</sub> degradation. This equilibrium, as well as influencing factors, is further discussed in Sect. 1.1.4.3.

During the day, NO<sub>2</sub> can be oxidized to nitric acid by hydrogen oxide radicals, according to Eq. (1.9),



M denotes in this equation a third molecule, required for stabilizing the addition intermediate. Due to absence of the photochemically produced OH during the night hours, a different pathway becomes dominant for the atmospheric removal of NO<sub>x</sub>. Following Eqs. (1.10)–(1.12) NO<sub>x</sub> is oxidized by ozone to nitric acid (HNO<sub>3</sub>) via the intermediate dinitrogen pentoxide (N<sub>2</sub>O<sub>5</sub>).



During the day, this pathway is hindered by a rapid photolysis of NO<sub>3</sub> back to NO<sub>x</sub>, following Eqs. (1.13) and (1.14).

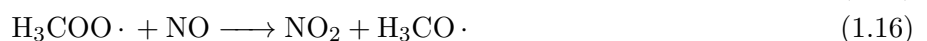
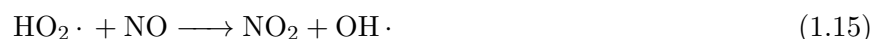


The high water-solubility of nitric acid favors a washing-out of the atmosphere before it can be photolyzed. In the presence of ammonia, HNO<sub>3</sub> can also convert via gas-phase-particle partitioning to particulate nitrate (Paerl, 1995).

### 1.1.4.3. O<sub>3</sub> Chemistry

Tropospheric ozone is a secondary air pollutant that is harmful to humans and plants (Sect. 1.1.1). However, as a precursor for hydroxyl radicals it also fulfills an important role in maintaining the oxidizing capacities of the atmosphere (see Eqs. (1.1) and (1.2)).

Its primary source in the troposphere is the photolysis of NO<sub>2</sub> in the NO<sub>x</sub> cycle, described in Eqs. (1.6) and (1.7). In this, hydro- or organic peroxy radicals (RO<sub>2</sub>·) are able to increase the NO<sub>2</sub>/NO-ratio by oxidation of NO, e.g., by the following two reactions, Eqs. (1.15) and (1.16),



The result is a net production of O<sub>3</sub>. Due to this reactivity, atmospheric reactions of VOCs and CO must be considered for an understanding of the concentrations of tropospheric ozone as they constitute substantial sources for hydroperoxy radicals. For simplicity, VOC chemistry is illustrated here by means of CO as surrogate, since the key aspects are similar.

## 1. Introduction

Carbon monoxide is oxidized in the atmosphere by hydroxyl radicals to produce CO<sub>2</sub> and hydroperoxyl radicals, as shown in Eq. (1.17),



As seen in Eq. (1.15)), HO<sub>2</sub> can oxidize NO and effectively increase ozone concentrations or self-react to hydrogen peroxide (H<sub>2</sub>O<sub>2</sub>, (1.18)). Hydrogen peroxide acts as a reservoir for HO<sub>X</sub> species. It can decompose photolytically to OH· (Eq. (1.19)) or disproportionate to HO<sub>2</sub> and water (Eq. (1.20)), the latter reaction effectively removes one OH· species.



In this regard, tropospheric ozone concentrations depend strongly on the amount of NO<sub>X</sub> during CO/VOC oxidation. While low NO<sub>X</sub> concentrations favor the chain-terminating reaction in Eq. (1.20) (referred to as NO<sub>X</sub>-limited conditions), high NO<sub>X</sub> concentrations favor Eq. (1.9) (VOC-limited conditions). Therefore, in dependence of environmental parameters, such as temperature, NO<sub>2</sub>/NO ratio and concentrations, and HO<sub>X</sub> concentrations, a NO<sub>X</sub> to VOC-ratio exists that corresponds to a peak production of tropospheric O<sub>3</sub> (Thornton et al., 2002). An approach for estimating environmental ozone concentrations is the empirical kinetic modeling approach (EKMA) by Dodge (1977), which is based on the generation of ozone concentration isopleths in dependence of NO<sub>X</sub> and VOC concentrations.

### 1.1.4.4. SO<sub>2</sub> Chemistry

In the troposphere, SO<sub>2</sub> can be physically removed by wet and dry deposition processes. Furthermore, it is oxidized by OH radicals to sulfur trioxide (SO<sub>3</sub>) after Eq. (1.21) and (1.22). With water vapor, SO<sub>3</sub> continues to react to sulfuric acid (H<sub>2</sub>SO<sub>4</sub>) by the reaction shown in Eq. (1.23).



Sulfuric acid is easily removed from the atmosphere by wet deposition. But similar to nitric acid, it can condense to form particles, e.g., in the presence of ammonia.

## 1.2. Greenhouse Gases

Greenhouse gases (GHGs) are gases that can absorb and emit light with a wavelength in the range of the thermal infrared spectrum (3–15 μm). Elevated GHG concentrations are the main drivers for an intensification of the greenhouse effect that is responsible for a gradual increase of the Earth's temperature. The reason for this is that energy, radiated by the Sun, gets trapped within the Earth's atmosphere. The planet's surface warms by absorbing solar energy, then re-emitting a part of the absorbed energy, and cooling again in the process. In the absence of GHGs, the re-radiated heat would traverse the atmosphere and escape back to space. The GHGs in our atmosphere, however, can absorb and capture this energy and radiate it isotropically. This way, approximately 50 % of the energy is redirected to the planet's surface and the process repeats itself. This results in an overall higher energy and heat uptake of the Earth system. A well-balanced amount of GHGs in our atmosphere is essential for life-friendly temperatures and makes the Earth a habitable place. Anthropogenic GHG emissions, however, have increased dramatically over the last century. At this rate they will cause our climate to spiral out of control if they are not rapidly reduced (IPCC, 2007).

The main anthropogenic sources of GHGs and air pollutants are the same, i.e. fossil fuel combustion, biomass burning, and agriculture. Their impact, however, is a different. Air pollutants, as described in

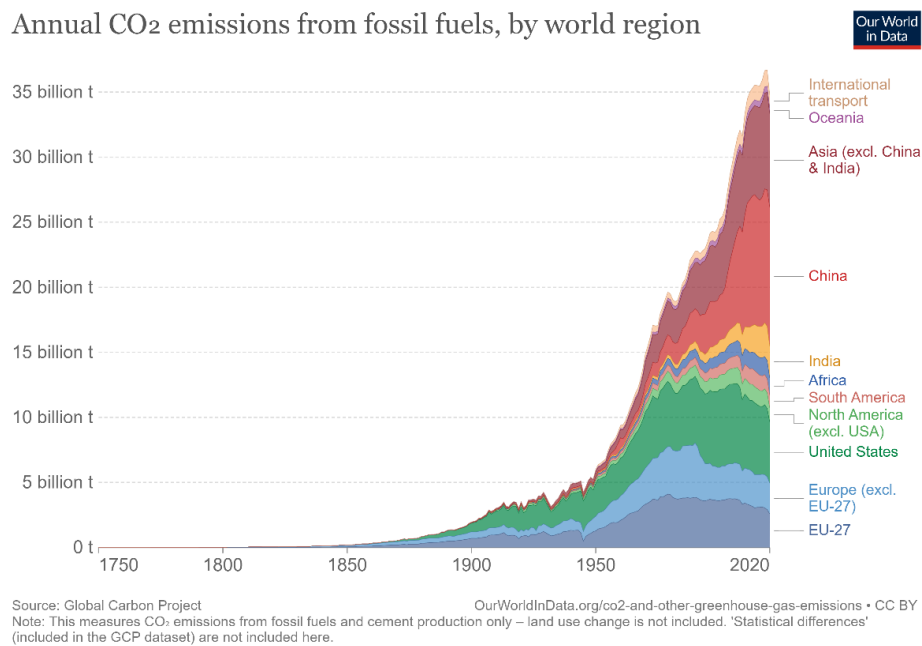


Figure 1.2.: Growth of annual production-based emissions of carbon dioxide (CO<sub>2</sub>) in tonnes by world region (Ritchie et al., 2020).

Sect. 1.1, directly affect human health when exposed to or cause environmental damage at ground level due to their harmful chemical or physical characteristics. The threat posed by GHGs, on the other hand, is of a secondary nature. Their potential to increase global temperatures can throw the entire climate system out of balance with catastrophic effects such as deadly heat waves, floods, droughts, fires etc. (Ramanathan, 2020).

### 1.2.1. Common Greenhouse Gases and their Sources and Sinks

The most important GHGs, emitted by human activity, are carbon dioxide (CO<sub>2</sub>), methane (CH<sub>4</sub>) and nitrous oxide (N<sub>2</sub>O). According to Olivier and Peters (2020), CO<sub>2</sub> accounted for a global share of 72 % on total anthropogenic GHG emissions in 2018, followed by CH<sub>4</sub> with 19 % and N<sub>2</sub>O with 6 %.

CO<sub>2</sub> is a gas that naturally occurs in the Earth's carbon cycle. However, this cycle is altered by human influence and the amounts of CO<sub>2</sub> released into the atmosphere dramatically increased through the combustion of fossil fuels for transportation and energy production. Simultaneously, natural CO<sub>2</sub> sinks as forests and soils are destroyed.

About 50 to 65 % of global methane emissions originate from anthropogenic sources. They mainly result from leakage in natural gas systems of industry and energy production, decomposition in landfills and from agricultural livestock. CH<sub>4</sub> stays in the atmosphere for 12 years on average and has a global warming potential of 25 CO<sub>2</sub> equivalents (IPCC, 2007).

Nitric oxide is a gas that occurs naturally as part of the Earth's nitrogen cycle. About 40 % of total N<sub>2</sub>O emissions originate from anthropogenic sources (IPCC, 2013). These are predominantly agricultural soil management activities as the application of fertilizers. It is also generated in the treatment of organic wastewater and forms as byproduct of combustion processes. Nitrous oxide has an atmospheric lifetime of 112 years and a global warming potential of 298 CO<sub>2</sub> equivalents.

Another very important GHG is water vapor (H<sub>2</sub>O). Water vapor is currently the dominant GHG in the atmosphere. Its concentrations, however, fluctuate regionally. Unlike the previously presented greenhouse gases, its concentrations are not directly related to human activity but rather indirectly via the so-called water vapor feedback. This term refers to an increase in atmospheric water vapor due to increased evaporation rates by the raising temperatures resulting from an enhanced greenhouse effect (Held and Soden, 2000; Schneider et al., 2010).

## 1. Introduction

In addition to its properties as an air pollutant, tropospheric ozone is also a potent greenhouse gas and the third most important along with CO<sub>2</sub> and CH<sub>4</sub>. As described in Sect. 1.1, O<sub>3</sub> is a photochemical product and not directly emitted from anthropogenic sources. Its tropospheric abundance is primarily controlled by the presence of NO<sub>x</sub> and VOCs in combination with the appropriate meteorological conditions (IPCC, 2001) (see Sect. 1.1.4.3).

### 1.2.2. Regulatory Measures for Greenhouse Gases

The topic of climate change, with GHG emissions as its main driver, has received overwhelming attention from scientific researchers and policy makers in recent years because of its importance. The Intergovernmental Panel on Climate Change (IPCC) fulfills an important role in assessing and communicating scientific evidence related to climate change to the international community. From 1988 up-to-now, five assessment reports have been published (the sixth report is currently being published), summarizing current knowledge about climate change, the socio-economic impacts and potential responses, and adaptation strategies (IPCC, 2022). An international legal framework, aiming at the reduction and stabilization of atmospheric greenhouse gas concentrations, was initiated 1992 by the United Nations with the Framework Convention on Climate Change (UNFCCC) and a corresponding international treaty (U. N., 1992). An extension of this treaty was the Kyoto Protocol, adopted in 1997, that committed the parties to a reduction of greenhouse gas emissions (UNFCCC, 1997). In the Paris Agreement of 2015, long-term goals were set to keep the increase of the global temperature below 2°C, compared to the pre-industrial level. The preferred target, however, was to limit the temperature increase to 1.5°C, as this would substantially reduce the risks and impacts of the resulting climate change (UNFCCC, 2016). In addition to these two international treaties, annual conferences on climate change were held in the framework of the UNFCCC, which served as formal meetings of the parties involved (Conference of the Parties, COP), to assess the progress made in dealing with climate change.

## 1.3. Fundamentals of Air Quality Modeling

Complementary to measurements, air quality modeling enables an improved assessment of the relationships between emissions of air pollution sources and their effects on ambient air quality. Common application tasks are:

- Determining the relative contributions of a specific emission source.
- Monitoring the compliance of air quality regulations.
- Predictions about the impacts of potential emission sources.
- Simulation of ambient air pollution concentrations under different policy or technological scenarios.

Comprehensive data sets are required for the operation of state-of-the-art air quality models, consisting primarily of emission and meteorological data. These data are often generated using upstream models, which are briefly introduced in the following Sects. 1.3.1 and 1.3.2. Sect. 1.3.3 describes chemistry transport models that are used for air quality modeling.

### 1.3.1. Emission Modeling

Emission models are representations of real, emission producing systems. They provide numerical estimations to the amounts of primary air pollutant and GHG emissions with spatial and temporal reference. The resulting products are referred to as emission inventories (EIs), which provide a basis for trends analyses, regional and local scale air quality modeling, an assessment of regulatory impacts, and exposure modeling (U. S. EPA, 2022).

So called top-down and bottom-up approaches are the two major methods applied in emission models. Top-down approaches usually start from a known “bulk” amount of emissions that e.g., specify a total emission value for a national or regional level. The share of a specific activity on this “bulk” emission must be spatially and temporally allocated over the working domain by the model to generate an EI.



This is achieved by using spatial surrogates and temporal profiles that are representative of the activity. An example for top-down modeling is a bulk emission value for residential heating in Germany that is distributed according to a population density grid as spatial surrogate.

Bottom-up approaches, on the other hand, directly calculate an emission amount generated by an activity for which spatially and temporally fine-resolved data is available. To do this, activity specific emission factors (EFs) are needed that approximate emission quantities to the respective activity (Eq. (1.24)).

$$Emission_{total} = Activity \cdot EF \quad (1.24)$$

An example for a bottom-up approach are ship emissions that are calculated for every individual ship in a working domain, according to time-referenced position data. Usually, both methods are combined for the creation of comprehensive and accurate EIs. This is necessary because the detailed input data required for bottom-up modeling is often not for all emission sources available. Furthermore, bottom-up models can be computationally demanding. However, an exclusive use of top-down approaches may lead to an insufficient accuracy of the EIs for applications that require high spatial or temporal resolution.

To cope with the widely varying emission activities and data sources, emission models need to provide a special flexibility to meet the requirements of current research. The bottom-up Modular Ship Emission modeling System (MoSES) for high-resolution modeling of ship emissions was created in the frame of the present work. It is described in detail in Chap. 3. In addition, several self-conceptualized scripts were created that allow to temporally resolve and compile emission data sets in analogy to top-down approaches. Other emission models that were used in the frame of this doctoral project are the top-down Highly Modular Emission Model (HiMEMO) for nonshipping anthropogenic emission sectors. HiMEMO is a modular toolbox for emission calculation that is currently under development at the Helmholtz-Zentrum Hereon. Biogenic emission data were generated with the bottom-up Model of Emissions of Gases and Aerosols from Nature (MEGAN) in version 3 (Guenther et al., 2012, 2020).

### 1.3.2. Meteorological Modeling

As a driver for the modeling of pollutant concentrations from emissions data, meteorological fields are needed as input for a CTM. The meteorological field data for northern Europe and eastern China that were required for the model runs with the CTM CMAQ (see Sect. 1.3.3.1 and Chap. 5) were generated with the regional weather forecasting COSMO model in climate mode (COSMO-CCLM) (Rockel et al., 2008). COSMO-CCLM is embedded into the COSMO model, which is used for numerical weather prediction (Doms and Schättler, 2002; Doms et al., 2011; Baldauf et al., 2011). It solves the nonhydrostatic compressible equations for the atmosphere. The prognostic quantities are: momentum, temperature and pressure as well as the budget equations for water constituents, i.e. water vapour, cloud water, rain water, cloud ice, snow and sleet/hail. In order to use the meteorological fields with the CMAQ, a preprocessor (LM-MCIP) was necessary that interpolated and reformatted the data.

### 1.3.3. Chemistry Transport Modeling

The atmosphere is a complex system, in which a multitude of interdependent physical and chemical processes occur at any given time. Chemistry transport models (CTMs) are numerical models that try to simulate these processes that can be categorized into atmospheric fluxes, chemical reactions (production and loss), and deposition (by gravity or washing out) of one or more chemical species. The results of a CTM include spatiotemporally-referenced variables, such as air pollutant concentrations and deposition rates. For numeric models, the knowledge of the operation principles allows an integrated understanding of the described system. Thus, combined with the information from ambient measurements, CTMs allow us to study the reactivity of atmospheric processes and to progress in a comprehensive understanding of the atmosphere.

According to Seinfeld and Pandis (2006), a distinction between two principle approaches is made in the formulation of a CTM:

1. In Lagrangian approaches a fluid particle is described by its trajectory, e.g., an air parcel transported by local winds. For this, the location of the air parcel must be known as well as meteorological

## 1. Introduction

parameters, such as the temperature and the wind speed. With the exception of emissions, no mass exchange is allowed for the air parcel with its surroundings.

2. Eulerian approaches calculate the velocity of a fluid particle in dependence of its position and time. In practice, this means that in an Eulerian model the concentrations of atmospheric species are simulated in a fixed array of geo-referenced computational cells. The cells are placed adjacent to each other; the complete area spanned by the set of cells is called a domain. Matter and energy transport is allowed between adjacent cells for each time step. Today, most state-of-the-art CTMs are based on the Eulerian approach.

For calculating concentration fields, a Eulerian CTM approximates the time dependent concentration  $c$  of every considered species  $i$  in a well-mixed box of length  $l$  and height  $h$  after the following form, shown in Eq. (1.25),

$$\frac{\delta c_i}{\delta t} = \sum E_i + \sum P_i - \sum L_i + v_{adv} \frac{c_i^0 - c_i}{l} + v_v \frac{c_i^{ab} - c_i}{h} - v_{dep} \frac{c_i}{h}. \quad (1.25)$$

In this equation,  $E$  is a term describing the emission sources.  $P$  and  $L$  are physicochemical production and loss rates, respectively, which are calculated on the basis of a set of chemical equations implemented in the CTM. The term  $v_{adv}(c^0 - c)/l$  describes the advection where  $v_{adv}$  is the advection wind velocity and  $c^0$  the upwind concentration. Entrainment and detrainment are described by the term  $v_v(c^{ab} - c)/h$ , where  $v_v$  is the ventilation velocity for exchange with the air above the box and  $c^{ab}$  the concentration above the box. The calculation of this transport depends on previously calculated meteorological fields which are fed to the CTM (Sect. 1.3.2). Finally, the term  $v_{dep}c/h$  describes species loss due to deposition with the rate  $v_{dep}$ .

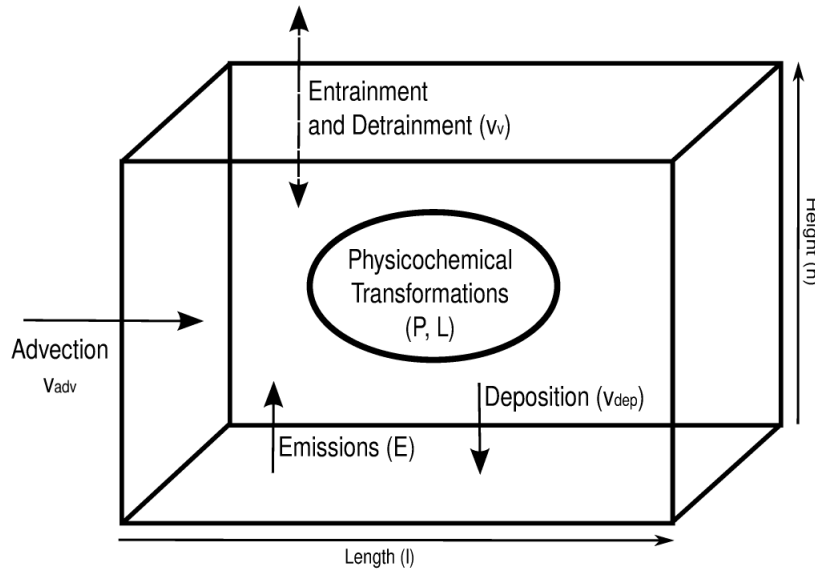


Figure 1.3.: Schematic representation of an Eulerian box model.

The CTM applied in this work is the Community Multi-scale Air Quality (CMAQ) model, which is based on an Eulerian approach. It is described in the following Sect. 1.3.3.1.

### 1.3.3.1. Community Multi-scale Air Quality Model (CMAQ)

The Community Multi-scale Air Quality (CMAQ) model is a multi-scale, time-integrating atmospheric Eulerian CTM developed by the U.S. Environmental Protection Agency (Byun and Ching, 1999; Byun and Schere, 2006). CMAQ has a regional scope, which means that, in contrast to a global model, only a specified area is modeled, which is referred to as domain (see also Sect. 1.3.3). To produce useful results, regional models require information on the emission fluxes at the boundaries of their domain. This information is called “boundary conditions” and can be acquired from global models. The calculation of the atmospheric

transport is based on an averaged form of the primitive equations and on input data about meteorological fields (see Sect. 1.3.2).

CMAQ was built in a modular approach and includes several modules for physical and chemical process that are important in a chemistry transport model (U. S. EPA, 1999):

Horizontal and vertical advection processes are treated separately by CMAQ. This is possible because the principal transport motion in the atmosphere is horizontal. Vertical motion often relates to an interaction of dynamics and thermodynamics. In general, the mass conservation of the continuity equation applies to advection processes.

Vertical diffusion is represented in CMAQ by the Asymmetric Convective Method (Pleim and Chang, 1992). Under convective conditions (warming surface), this method mixes heated air vertically until the temperature of the rising air equals the ambient temperature. Vertical diffusion under non-convective conditions (cooling surface), as well as horizontal diffusion are represented by eddy diffusion.

The chemistry module in CMAQ is responsible for the chemical production and the loss of atmospheric species. Different chemistry modules are supported that usually separate chemical reactions into gas-phase, aqueous-phase and, aerosol chemistry. For this work the Carbon Bond Mechanism in its 2005 version was used with an updated toluene chemistry, molecular hydrolysis, and rate constants (CB05-TUCL) was used (Yarwood et al., 2005; Whitten et al., 2010; Sarwar et al., 2011). It covers a total of 238 reactions and uses an approach, where chemical species are lumped into 24 groups of aerosols and 83 groups of gas species.

Particles are represented in CMAQ by three log-normally distributed particle modes that cover different groups of particle sizes, i.e. the Aitkin mode, the accumulation mode and the coarse mode with a mean diameter of  $0.03\ \mu\text{m}$  ( $\sigma = 1.7$ ),  $0.3\ \mu\text{m}$  ( $\sigma = 2$ ), and  $6\ \mu\text{m}$  ( $\sigma = 2.2$ ), respectively. Typically, the bulk of the particle mass in the atmosphere corresponds to the accumulation mode (Binkowski, 1999). Particles from the Aitkin and accumulation mode can roughly be referred to as  $\text{PM}_{2.5}$  with the majority of them having a aerodynamic diameter smaller than  $2.5\ \mu\text{m}$ .

In addition, important cloud-based processes are considered in CMAQ. These are aqueous chemical reactions, the vertical mixing of pollutants, and the removal of pollutants by wet deposition.

## 1.4. Air Pollutants and Greenhouse Gases from Ships and their Modeling

An important part of today's transportation sector is the shipping industry. With more than 80 % of the world's merchandise trade volume transported by ships, ocean-going vessels are the backbone of international trade. In the last 20 years, international maritime trade experienced an average growth of approximately 3 % per year. To meet the increased demand, the number and freight capacity of freight vessels grew accordingly (UNCTAD, 2020). With respect to their emissions per cargo volume, ships can be considered as a relatively environmentally friendly mode of transportation (IMO, 2009). However, at the current time an overwhelming majority of vessels are powered by reciprocating marine diesel engines, which in total consume more than 300 Mtonnes of fossil fuels annually (Fridell, 2018). The combustion of such large quantities of fuel oils are responsible for significant amounts of air pollutants and GHGs. Estimations made in the Third IMO Greenhouse Gas Study held international shipping accountable for 2.2 % of  $\text{CO}_2$ , 15 % of  $\text{NO}_x$ , and 13 % of  $\text{SO}_2$  emissions in 2012 (IMO, 2014). Additionally, emissions from ships can contain carbon monoxide CO and NMVOCs as well as methane, nitrous oxide and PM. The PM emitted by ships is usually comprised of sulfate  $\text{SO}_4^{2-}$ , water associated with sulfate  $\text{SO}_4^{2-} \times \text{H}_2\text{O}$ , black carbon (BC), mineral ash (MA), and primary organic aerosols (POAs).

In Sect. 1.1 it was explained that these pollutants are responsible for a variety of cardiopulmonary diseases and environmental problems; Sect. 1.2 showed the significance of GHG emissions for global warming. Ship emissions are a significant contributor to these problems. Especially, because 70 % of pollutants from shipping are emitted within 400 km of coastal regions and ports, rather than in the open ocean or unpopulated regions Corbett et al. (2007); Eyring et al. (2010).

The first globally concerted provisions to reduce GHG emissions from international shipping were made in the Kyoto Protocol in 1997. As a specialized agency of the United Nations, the International Maritime Organization (IMO) is the global standard-setting authority to enforce environmental regulations for international shipping. In accordance with the targets set in Kyoto Protocol, the IMO added the new

Annex VI to the International Convention for the Prevention of Pollution from Ships (MARPOL) in 1997 (IMO MEPC, 1997). The Annex VI entered into force on 19 May 2005 and targeted the prevention of air pollution from ships and their contribution to local and global air pollution. A revised Annex VI with significantly tightened emission limits was adopted in October 2008 and entered into force on 1 July 2010. Several amendments to MARPOL Annex VI targeting air quality were enacted in the following years. Their regulating aspects and corresponding research studies are discussed in the following sections. For regulations targeting sulfur oxides, it is referred to Sect. 1.4.2 and for nitrogen oxides to Sect. 1.4.3. Measures adopted for monitoring and reducing GHG emissions from ships are described in Sect. 1.4.4.

### 1.4.1. Modeling of Ship Emissions

Around the same time as the adoption of the Kyoto Protocol, the first global ship emission inventories were compiled (Olivier et al., 1996; Corbett and Fischbeck, 1997) and research on ship emissions and their impact was intensified (Endresen et al., 2003; Corbett and Koehler, 2003; Eyring et al., 2005; Dalsøren et al., 2009). Ships were confirmed as a significant source of global air pollution by the scientific community (Corbett and Fischbeck, 1997; Endresen et al., 2003; Dalsøren et al., 2009). Temporal and spatial resolution of ship emission inventories were initially achieved by evaluating ship arrival and departure tables, data from the Automated Mutual-Assistance Vessel Rescue System (AMVER) or the International Comprehensive Ocean-Atmosphere Data Set (ICOADS) (Corbett and Fischbeck, 1997; Endresen et al., 2003; Eyring et al., 2005; Dalsøren et al., 2009). The amount of emitted pollutants was based on averaged parameters in top-down approaches using proxy data on vessel fuel consumption and/or cargo turnover (Corbett and Fischbeck, 1997; Corbett and Koehler, 2003; Trozzi and Vaccaro, 1999; Eyring et al., 2005; Dalsøren et al., 2009). The introduction of the Automatic Identification System (AIS) in 2005 facilitated the acquisition of ship traffic data immensely and provided an enormous potential for improved accuracy in ship emission modeling. The usage of AIS is regulated in the SOLAS convention, maintained by the IMO, which requires every ship larger than 300 gross tons (GT) to carry a transceiver and regularly report and send position signals. For ship emission modeling, several activity-based methods were developed that rely on AIS data and allow an estimation of ship emissions for confined regions or for specific sectors (e.g., port areas or cruise shipping (Chen et al., 2016; Leong et al., 2015; Simonsen et al., 2018)). Many of these are able to generate temporally and spatially resolved emission inventories that can be analyzed and further used for air quality modeling studies. Beneath their area of application, these models differ in their complexity, e.g., the calculation of a ship's power demands, the determination of ship activities, and the applied EFs. While more sophisticated concepts can consider resistances from external influences (Johansson et al., 2017a; Winther et al., 2014), more simplistic approaches rely on engine load factors and ship characteristics to calculate power consumption (Goldsworthy and Goldsworthy, 2015; Coello et al., 2015; Aulinger et al., 2016; Fan et al., 2016; Simonsen et al., 2018; Kwon et al., 2019). An example for a model that can implement a high level of detail is the Ship Traffic Emission Assessment Model (STEAM) developed by the Finnish Meteorological Institute (FMI) (Jalkanen et al., 2009, 2012; Johansson et al., 2017a). Winther et al. (2014) derived ship power functions using their generic ship design model (SHIP-DESMO) to set up AIS-based ship emission inventories for the Arctic (Kristensen, 2012, 2013; Kristensen and Lützen, 2013). An approach for ships traveling the North Sea was developed by Aulinger et al. (2016). It considers a ship's power consumption and EFs based on engine load factors.

### 1.4.2. Sulfur Emissions from Shipping and Corresponding Regulations

The sulfur species in ship emissions, i.e.  $\text{SO}_2$  and  $\text{SO}_4^{2-}$  are combustion products of residue sulfur compounds in the ship fuel (Eqs. (1.26) and (1.21–1.23)) (Müller, 2000; Seinfeld and Pandis, 2006).



Thus, the amount of  $\text{SO}_x$  emissions depends directly on the sulfur content of the fuel (FSC). Due to this simple relationship, the FSC was subject to the first regulations made by the IMO in MARPOL Annex VI. In 2012, global limits for the FSC in ship fuels were introduced by the IMO, allowing a maximum of 3.5 % m/m (mass/mass) (IMO MEPC, 2008b). From the beginning of 2020, this global sulfur cap was

further tightened to 0.5 % (IMO MEPC, 2016). In addition to global sulfur limits, sulfur emission control areas (SECAs) were introduced, one at the North American coastline and another in the North and Baltic Sea. The latter is sometimes referred to as the European gateway to international trade and subject to high shipping densities with ship routes that border the densely populated coastal regions of northern European. Furthermore, several large port cities are located in this area, e.g., Rotterdam, Antwerp, or Hamburg. In this SECA, the FSC for ships is more strictly limited with a max. of 1.5 % m/m allowed since 2007, of 1 % since July 2010 and of 0.1 % since the beginning of 2015 (IMO MEPC, 2008b). Several studies investigated the effects of sulfur control measures on air quality. Lauer et al. (2009) concluded that a globally reduced FSC within 200 NMs of coastal regions reduces near surface sulfate significantly. Contemporaneously unabated NO<sub>x</sub> emissions, however, promote a strong increase of NO<sub>3</sub> aerosols that counteract lower sulfate concentrations. Furthermore, a reduced albedo was modeled due to less cloud coverage along ship routes where SO<sub>4</sub> aerosols can act as cloud condensation nuclei. With respect to the introduced SECA regulations, similar conclusion were drawn by Matthias et al. (2010) and Jonson et al. (2015) from modeling studies for the North Sea and for the NBS region. The Interreg project EnviSuM identified a reduction of sulfur-related ship emissions in the Baltic Sea between 2014 and 2016 by 87 % of SO<sub>2</sub> and 36 % of PM<sub>2.5</sub>. It was estimated that 500–1,000 premature deaths and a large number of nonlethal cases of heart attacks and strokes are prevented every year by the SECA; even in countries further away from the Baltic Sea (Repka et al., 2019). Global and regional model calculations by Jonson et al. (2020) found that, in addition to the European SECA, the IMO’s global sulfur cap since 2020 was able to reduce ship-related PM<sub>2.5</sub> concentrations and sulfur deposition in European coastal regions further.

With China being one of the world’s most exporting countries, its economic performance comes at the price of high freight ship traffic off its coast. China is home to seven of the ten largest container ports worldwide; in 2019 they handled nearly 30 % of the world’s container port throughput (TEU) (Lloyds’ List, 2020; UNCTAD STAT). China’s coastal regions are suffering from a similar, ship-related air quality degradation as northern Europe and the improvements of the designated SECAs encouraged the Chinese government to establish a nationally legislated Domestic Emission Control Area (DECA) in 2019. The scope of this area ranges 12 nautical miles from the Chinese coastline as well as from the coast of Hainan Island, including also the Chinese megaports. Ships sailing these areas are required to use fuel with a maximum FSC of 0.5 %. For berthing ships, this regulation was tightened to a FSC of 0.1 %, effective as of 2020. (China, Ministry of Transport, 2018). The effect of the DECA on air quality has been investigated in several studies. Liu et al. (2018) determined that this policy reduced PM<sub>2.5</sub> and SO<sub>2</sub> concentrations in the Pearl River Delta (PRD) by 2.7 and 9.5 %, respectively. Possible benefits from a larger DECA were investigated by Feng et al. (2019). Here, ships up to 96 NM from shore were found to contribute substantially to PM<sub>2.5</sub>. Accordingly, Zhao et al. (2020) could show that the DECA decreased the contribution of ship emissions to PM<sub>2.5</sub> by 71 % but that a stricter fuel-sulfur limit and an expansion of the DECA to 100 NM from coast might even achieve a reduction of 86 %.

The effect of cleaner marine fuels that resulted from the IMO’s global sulfur cap since 2020 has been investigated by Sofiev et al. (2018). They concluded that the usage of low-sulfur fuels reduced ship-related premature mortality and morbidity by 34 and 54 %, respectively, in 2020. However, marine fuels still account for approximately 250,000 deaths annually but stricter standards could bring additional health benefits. Furthermore, the usage of low-sulfur fuels was estimated to increase anthropogenic climate forcing by 3 % due to a reduction of ship-related aerosols by approximately 80 %.

### 1.4.3. NO<sub>x</sub> Emissions from Shipping and Corresponding Regulations

The formation of NO and NO<sub>2</sub> in combustion engines is mainly based on the oxidation of dissociated nitrogen from injected air under high temperatures (> 1800 K after the Zeldovich mechanism, Eqs. (1.27)–(1.29)) (Zeldovich, 1946; Heywood, 2018),



## 1. Introduction

After emission,  $\text{NO}_x$  can transform according to the chemical reactions introduced in Sect. 1.1.4.  $\text{NO}_x$  originating from ships was found to increase surface ozone levels over the eastern Atlantic and western Europe by 4–6 ppbv (Huszar et al., 2010). Furthermore, it significantly affects ozone levels near coastal zones (Tagaris et al., 2017). Geels et al. (2012) estimated the conversion rate of  $\text{NO}_2$  from ship exhausts to  $\text{HNO}_3$  at 5 h and the total atmospheric lifetime of  $\text{NO}_x$  at 24 h. Since  $\text{NO}_x$  emissions cannot be easily controlled by the fuel composition as  $\text{SO}_x$ , three “Tiers” were defined by the IMO, each stricter in regulating allowed exhaust  $\text{NO}_x$  limits. The exact limits depend on a ship’s construction date and its engine’s revolutions per minute (RPM). Currently, they can be complied with current engine technologies or engine control such as exhaust gas recirculation (EGR) or exhaust gas after-treatment such as Selective Catalytic Reduction (SCR). Nitrogen emission control areas (NECAs) were defined by the IMO, which correspond in their extent to the designated SECAs (see Sect. 1.4.2). Outside of a NECA, Tier I regulations apply to vessels built on or after 2000; Tier II regulations apply to vessels built as of 2011; Tier III regulations are valid for ships built in or after 2016 and which are sailing in the North American NECA or from ships built as of 2021 and which are sailing in the Baltic and North Sea NECA (IMO MEPC, 2008a, 2014). Since these regulations only apply to new built ships, it should be noted that the full  $\text{NO}_x$ -reducing effect of the NECA is not immediate but increases over subsequent years. An assessment report by Hammingh et al. (2012) concluded that the total years of life lost due to air pollution in the North Sea littoral states would be reduced by nearly one percent until 2030 as a result of the NECA. Health benefits from a NECA would exceed the costs for international shipping in 2030 even in the least favorable of the regarded situations. Winnes et al. (2016a) project that a NECA reduces  $\text{NO}_x$  emissions by 66 % in 2040, compared to 2010. Karl et al. (2019a) estimate a  $\text{NO}_x$  reduction from shipping by 80 % in the Baltic Sea, with respect to 2012. The reduction in secondary particulate nitrate is estimated to be 24 % as a result of the NECA. Furthermore, it was recognized that lower  $\text{NO}_x$  levels are critical for a sustained attenuation of ozone concentrations in the Baltic Sea region. An estimation for the reduction of  $\text{NO}_x$  emissions in the NBS region by the implemented NECA is also given by the scenarios shown in Chap. 4. These are: 13 % for 2025, 57 % for 2040, and 39 % for 2050. However, it should be noted that these projections include a major fuel type change to LNG in 2040 and to ammonia in 2050.

### 1.4.4. Greenhouse Gas Emissions from Shipping and Corresponding Regulations

With the amendment of Annex VI to the MARPOL Convention of 1997, the Marine Environment Protection Committee (MEPC) was not only tasked with the mitigation of ship-related air pollution, but was also invited to develop viable strategies to reduce  $\text{CO}_2$  emissions from ships (IMO MEPC, 1997). In this context, the First IMO GHG Study was published in 2000 and estimated the contribution of global shipping on total anthropogenic  $\text{CO}_2$  emissions at 1.8 % (IMO, 2000). A resolution at the 23rd IMO assembly in December 2003 that concerned the reduction of GHG emissions from ships strengthened the commitment of the MEPC in their task (23rd IMO Assembly, 2004). The Second IMO GHG Study was published in 2009 and estimated that in 2007 globally 880 Mts of  $\text{CO}_2$  were emitted from international shipping. This corresponded to a share of 2.7 % on total anthropogenic  $\text{CO}_2$  emissions (IMO, 2009).

In July 2011, the first regulation, the Ship Energy Efficiency Management Plan (SEEMP), was adopted that targets a reduction of GHG emissions by mandatory minimum energy efficiency levels for the work every ship undertakes (e.g.,  $\text{CO}_2$  emissions per tonne-mile) (IMO MEPC, 2011). The second reduction measure is the Energy Efficiency Design Index (EEDI) and entered into force from the beginning of 2013. It requires newly built ships with a gross tonnage over 400 to meet efficiency targets that increase with each year. Initially, EEDI reduction factors required ships built until 2025 to be at least 30 % more efficient compared to ships built in 2014 (IMO MEPC, 2016). However, for several ship types these measures were subsequently tightened, now requiring an efficiency gain by 50 % until 2022 (IMO MEPC, 2018a). The IMO expects the EEDI measure to have a great long-term impact and that it is able to reduce emissions from international shipping by approximately 85 %. The SEEMP measures, instead, were aiming at a short to medium-term effect. By 2050, these two packages combined are expected to reduce  $\text{CO}_2$  from shipping by up to 1.3 Gt per year (IMO, 2014).

A Third and Fourth IMO GHG Study, published in 2014 and 2020, respectively, estimated international shipping to be responsible for 977 Mt of  $\text{CO}_2$  equivalents (2.76 %) in 2012 and 1.076 Gt (2.89 %) in 2018

(IMO, 2014, 2020). To put these numbers into perspective, the shipping sector would be the 6th largest CO<sub>2</sub> emitter if considered as a country (Balcombe et al., 2019).

In 2018, the IMO's MEPC established the "Initial IMO Strategy on reduction of GHG emissions from ships", a framework for further actions targeting the GHG mitigation from ships (IMO MEPC, 2018b). The stated goal of this strategy is the reduction of total annual GHG emissions from shipping by at least 50 % until 2050, compared to 2008. Possible candidate short- mid- and long-term measures to achieve this goal are currently under discussion. These include for the short term, e.g., a further tightening of the existing EEDI and SEEMP packages or operational measures, such as ship-speed optimizations. For the mid- and long-term perspective, alternative low- or zero-carbon fuels and innovative market-based concepts are being discussed. A short overview of possible concepts, technologies and ideas for the reduction of GHG emissions from ships can be found in Sect. 1.4.5, which discusses recent and current research focuses on the topic of ship emissions.

### 1.4.5. Recent and Current Focuses in Ship Emission Research

The previous sections presented current legislation targeting ship emissions and studies investigating their effects. However, there are many recent and current studies that elucidate aspects of the topic of ship emissions that were previously neglected, have become technically feasibly or more important in recent years. This section intends to give an overview of these studies and of recent and current trends in the research on ship emission.

A major overview of scientific studies analyzing the NBS region has already been given in Sects. 1.4.2 and 1.4.3 on sulfur and NO<sub>x</sub> emissions and corresponding regulations. interdisciplinary projects, such as Clean North Sea Shipping (CNSS) and Sustainable Shipping and the Environment of the Baltic Sea Region (SHEBA) are noteworthy and complete the overview (CNSS project, 2014; SHEBA project, 2018). Both were initiated by the EU and investigate impact from shipping in a comprehensive approach, as they consider environmental stressors and technological aspects in addition to the emissions of ships.

On a global scale, a high resolution bottom-up ship emission inventory was calculated and analyzed by Johansson et al. (2017a) with the STEAM model. CO<sub>2</sub> emissions from 376,219 ships were estimated at 831 Mt, NO<sub>x</sub> at 20.9 Mt, SO<sub>x</sub> at 9.69 Mt and PM<sub>2.5</sub> at 1.49 Mt in 2015. In this inventory, tankers, cargo, and container ships were found to be responsible for more than 75 % of CO<sub>2</sub> emissions.

#### 1.4.5.1. Ship Emissions in China

According to the global inventory by Johansson et al. (2017a), East Asia, with its main actor China, is one of the regions most impacted by ship emissions. Promoted by a rapid economic growth, China has become the worldwide biggest emitter of anthropogenic air pollutants with a share of 18–35 % (Hoesly et al., 2018). In recent years, the topic has received increasing attention in the scientific community and research efforts have intensified. Initial studies on ship emissions in China have been reviewed by Zhang et al. (2017). A recent study by Chen et al. (2017) developed the first national-scale ship emission inventory for China with a high spatial resolution. Liu et al. (2016) showed that shipping emissions in East Asia accounted for 16 % of global CO<sub>2</sub> emissions from ships in 2013. Accompanying air pollutants were held accountable for 14,500–37,500 premature deaths per year and even more cases of adverse health effects. Lv et al. (2018) found that shipping increased PM<sub>2.5</sub> concentrations in eastern China on average by 5.2 μg · m<sup>-3</sup> in 2015. Vessels within 12 NM of the coastline could be held mainly responsible for this.

Several studies exist that took a closer look at the situation in the three major shipping centres in China, i.e. the Pearl River Delta (PRD) port cluster, the Yangtze River Delta (YRD) port cluster, and the Bohai Rim. Wan et al. (2020) produced EIs for 2018 for all three regions. He found that the YRD was responsible for almost 50 % of total ship emissions in China. Ship EIs for the PRD were also developed by Li et al. (2016) and Chen et al. (2019). Chen et al. (2019) found that ships in the PRD increased PM<sub>2.5</sub> concentrations regionally by 1.4 μg · m<sup>-3</sup> and ozone by 1.9 ppb which corresponded to 466 and 346 premature deaths, respectively. The spatial and seasonal dynamics in the YRD were investigated by Fan et al. (2016) and Feng et al. (2019) who concluded that more than 60 % of ship emissions are emitted within 100 km of the coastline and are highest during spring. However, due to atmospheric transport by onshore winds, ship-

## 1. Introduction

related PM<sub>2.5</sub> concentrations in Shanghai were highest during the summer monsoon (up to 4.62  $\mu\text{g} \cdot \text{m}^{-3}$ ). Chen et al. (2018) found that also for the Bohai Rim region ship traffic is a nonnegligible source of air pollutants. On annual average, ships were found to be responsible for 5.9 % of PM<sub>2.5</sub> concentrations with highest contributions during summer (12.5 %) and lowest during winter (0.9 %).

### 1.4.5.2. Potential Measures for the Reduction of Greenhouse Gas Emissions

In Sect. 1.4.4 it was introduced that a decarbonization of the shipping sector is important for the global reduction of GHG emissions. As the international legislative body, the IMO formulated ambitious targets for the upcoming years. The measures to achieve these targets remain yet unclear, leaving room for ideas from different disciplines. That a transition away from traditional carbon-rich fossil fuels is need, is almost certain. However, no policies or incentives for ship owners and stakeholders exist at current that specifically regulate the use of alternative fuels. Different alternatives are under discussion of which biodiesels, methanol (MeOH), liquefied natural gas (LNG), hydrogen (H<sub>2</sub>), and ammonia NH<sub>3</sub> are currently the most promising candidates for ocean-going vessels. Recently, numerous studies have examined the feasibility of these fuels in terms of technological, economical, and environmental aspects (Aakko-Saksa and Lehtoranta, 2019; Balcombe et al., 2019; DNV-GL, 2020; Wang and Wright, 2021). Although fuels, such as biodiesels, MeOH, and LNG can benefit from existing infrastructure and produce significantly fewer air pollutants when combusted, their potential to reduce GHG emissions is insufficient for achieving the targets set by the IMO (see Sect. 1.4.4). The rapid growth of bunkering infrastructure makes LNG currently one of the most promising short-term alternatives to conventional fuel oils. Hydrogen and ammonia stand out since they are carbon-free and have high energy densities. Hydrogen, however, is currently the most expensive alternative. Its wider adoption in the short-term is hindered by economical factors and the lack of an adequate infrastructure. The usage of ammonia might overcome these hurdles: It is inexpensive and currently produced in large scales for agricultural fertilization and for a variety of chemical applications. Several technical key issues remain in the design of ammonia propulsion systems, which include poor combustion properties and the toxicity and corrosiveness of NH<sub>3</sub>. The different strengths and weaknesses of these potential candidates as future ship fuels emphasize that there currently is no single path to a successful GHG reduction strategy. However, a scenario presented in Chap. 4 investigates the promising pathway of a major fuel type transition towards ammonia until 2050, with LNG as an interim solution, from an emission modeling perspective.

Considerable fuel savings and thus a reduction of GHG emission can also be attained by technologies and operational measures that improve vessel efficiency, such as wind or solar assistance, slow-steaming, paints and hull-coatings to reduce fouling, or waste heat recovery. Policy options could target market-based mechanics, such as emission control via subsidies, pricing, or regulated emission quantities (ITF/OECD, 2018; Balcombe et al., 2019). The potential of a trade-driven ship emission reduction is shown in a study by Wang et al. (2021). They estimated that the optimization of trading-partnerships could significantly reduce travelling distances of merchant ships and thus in an ideal case reduce CO<sub>2</sub> emissions by 38 %. In this regard, an expiration of fossil fuels is expected to be accompanied by a decline in maritime trade as fossil fuels constitute a substantial portion of the maritime freight capacity, i.e. 41 % in 2016 (ITF/OECD, 2018; Ankathi et al., 2022).



## 2. Scientific Question, Approach, and Structure of the Thesis

### 2.1. Scientific Question

Air pollution currently represents one of the greatest threats to human health worldwide. Furthermore, it is the cause for severe environmental damage. Global warming is fueled by enormous amounts of anthropogenic GHG emissions and threatens to unbalance the climate system, which may lead to catastrophic events and poses a great risk for humankind. The shipping sector is a contributor to these problems since it is responsible for almost 3% of global GHG emissions and for an even greater share on the most important air pollutants (IMO, 2014, 2020). Current projections assume a further growth of the shipping industry, which can exacerbate global warming and air pollution in the future if no proper regulations are implemented (UNCTAD, 2019, 2020). Scientific research on atmospheric emissions made it possible to recognize and raise awareness for these problems in the first place. However, knowledge on the subtopic of ship emissions, their formation, atmospheric physicochemical transformations, and impacts on air quality allows us to deal with the associated implications. Political and economic actors can use this knowledge to formulate effective management strategies for ship emissions that aim at the mitigation of GHG emissions and adverse air quality impacts. This includes the identification of ship emission hotspots, the monitoring of ship-related air pollution, and an evaluation of the effectiveness of active regulations as well as of potential future legislation and technologies.

A modeling approach for studying ship emissions and their impacts on air quality requires accurate ship emission data with high spatial and temporal resolution. For the development of a model that is capable of producing this data, methodological questions, such as the following, are important to ask: What fundamental data are available that can be used for ship emission modeling? How can a shipping fleet be modeled, including important ship characteristics and ship movements? What are important emission-producing activities and maneuvers of ships? How can these activities be spatiotemporally resolved and efficiently implemented in a model? How detailed does the implementation of these activities need to be or what approximations are acceptable to still obtain useful results? Furthermore, when developing a ship emission model, it is important to consider the intended areas of application. With the IMO's stated goal of a globally decarbonized shipping sector and the pending transformations to achieve this goal, a flexible methodology for investigating this development is of great importance. As explained in Sect. 1.4.5, a clear pathway to decarbonize the shipping sector remains unclear at present. However, carbon-free fuels are most likely an essential part of a strategy. For this reason, it is important to assess the feasibility, prospects of success and potential consequences of the ideas and measures that are currently being considered to reduce carbon emissions in shipping. The use of scenarios is a viable approach in scientific modeling to investigate such measures and evaluate possible future outcomes. Guidance to produce realistic decarbonization scenarios and requirements that a ship emission model must meet in order to create useful scenarios can be determined by answering questions, such as: What are currently the most promising decarbonization ideas, measures, and strategies? What transport economical and technological developments can be expected in the shipping sector in the future? How can a future shipping fleet and their corresponding emissions be modeled? Particularly, in context of the two previous questions. What flexibilities must a model provide to implement such scenarios?

However, for the research on ship emissions, it is not only the temporal dimension that is of importance, and which can be studied through scenarios, as described earlier. The spatial dimension also proves important, as shipping is a globally operated industry and significantly affects air quality by emitting  $\text{NO}_x$ ,  $\text{SO}_2$ , and  $\text{PM}_{2.5}$  in many regions worldwide. Coastal regions near major shipping routes and port cities where many people are potentially exposed to air pollutants are particularly affected by ship emissions.

Densely shipped regions, such as the North and Baltic Seas in northern Europe or the Bohai, East, and South China Seas in eastern China, ship emissions and their impacts have been investigated in several studies, as discussed in Sect. 1.4. Large port cities are located in northern Europe, e.g., Rotterdam, Antwerp, or Hamburg. The region is subject to significant but not serious air pollution. Eastern China is home to several of the world's largest ports, e.g., Shanghai, Ningbo-Zhoushan, or Shenzhen. China's tremendous economic growth of the recent decades and its role as "factory of the world" are reasons that led to a very high level of anthropogenic air pollution. Although both areas have been studied in their own right, a comparison between regional ship emissions and their impacts has not been done up to now. The complex nature of the atmosphere makes questions regarding regional differences or similarities in the physicochemical transformations and impacts of the emitted pollutants on air quality nontrivial to study. In addition, there are obvious differences between the two regions whose influence on the impact of ship emissions on air quality is important to investigate. In this context, questions such as the following are crucial to ask for investigating this topic: What role have meteorological aspects or regional weather phenomena in the impacts of ship emissions? Are there differences in the regional shipping fleet that can account for potential differences in ship emission impacts? And in particular: How do the different levels of air pollution influence atmospheric chemistry and the impact of ship emissions on air quality? Chemistry transport models combined with ship emission data allow to study such questions by simulating atmospheric processes and the transformation and dispersion of emitted substances that lead to their ambient concentrations.

In conclusion of the preceding remarks, this thesis aims to provide an answer to scientific issues and previously raised questions, summarized by the following overarching scientific questions.

*What are the regional differences and/or similarities in air quality impacts of ship emissions between northern Europe and eastern China?*

*How does a future transition to cleaner and carbon-free fuels affect ship emissions?*

In order to answer these central scientific questions, this thesis addresses two additional questions concerning methodological challenges:

*What general approach is required to calculate useful and spatiotemporally highly resolved ship emission data?*

*How can future ship emission scenarios be created, particularly scenarios related to a decarbonization of the shipping sector?*

## 2.2. Approach

Growing atmospheric pollution can be monitored and quantified by means of analytical methods. This can be done by maintaining a wide network of measurement stations, e.g., at more than hundred stations of the European Monitoring and Evaluation Programme (EMEP), which is complemented by national networks. Similarly, countries as China maintain a large network of more than a thousand stations established in the frame of its "Plan on the Prevention and Control of Air Pollution" in 2013 (China, State Council, 2013). These measurements can be used to determine long-term trends, but also to monitor compliance with applicable air pollution regulations. However, although the number of stations in national and transnational networks is constantly growing, a station can represent only a single point measurement. To complement measured data, numerical air quality modeling became increasingly feasible and popular with the strong increase in computing power during the last decades. Air quality models are capable of calculating uniform, comprehensive, and spatiotemporally referenced air pollutant concentrations. They even allow for estimations in regions with no measured data available. In addition, all processes in a model are clearly defined and thus comprehensible. Air quality models allow the recreation of historic situations and more importantly, the prediction of air quality in future scenarios, investigating potential policy or technological options. Assessing future developments is particularly important in times of emerging climate change and provides a scientific guidance for political decision makers.

In order to address the scientific questions, described in Sect. 2.1, which were the motivation for this work, a multi-model approach was chosen that is illustrated in Fig. 2.1. The key components of this approach are introduced and briefly explained in the following sections.

The development of the Modular Ship Emission Modeling System (MoSES) solved the first methodological challenge and enabled the calculation of temporally and spatially highly resolved ship emissions data. A detailed description of this model and its functionalities can be found in publication I presented in Chap. 3. In conjunction with a novel approach for generating ship emission scenarios, MoSES was also used to calculate future ship emission inventories for the North and Baltic Sea for the years 2025, 2040, and 2050. These include expected fleet developments and describe a potential pathway to a decarbonized shipping sector by a transition to cleaner and carbon-free fuels. The according Publication II is constituted in Chap. 4.

Finally, ship emission inventories for northern Europe and eastern China, calculated with MoSES, were used in an applicative study with a chemistry transport model for the year 2015. The performance of this method was estimated by a comparison of the model results with measured air quality data. An evaluation of the obtained results focused on differences and similarities of ship emission impacts on air quality between China and Europe.

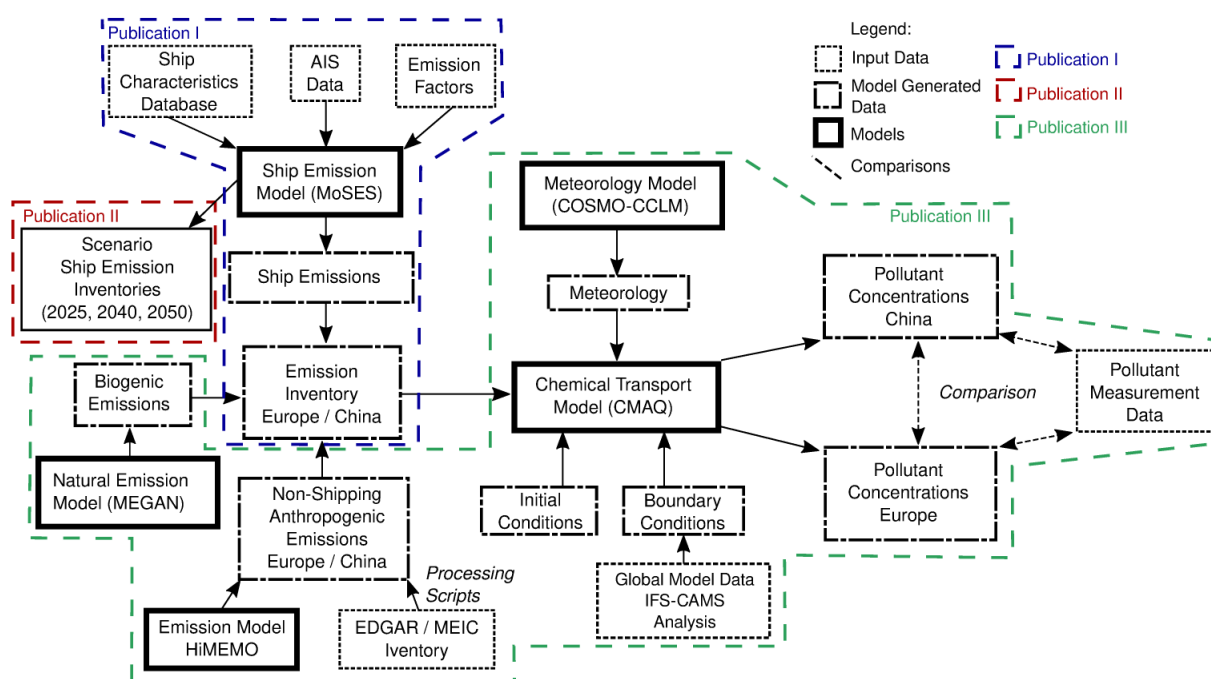


Figure 2.1.: Outline of the multi-model approach that was applied in this work to answer the scientific questions. External input data are marked by a dotted frame, model generated data by a dash-dotted frame and models are marked by a bold frame. An approximate reference of the work packages to the individual publications is given by the colorized, dashed frames.

## 2.3. Structure of the Thesis

Chap.1 of this thesis gives a general introduction to current problems arising from anthropogenic air pollution and greenhouse gas emissions. For this, the most relevant pollutant species are described in brief, including their effects on human health and on the environment as well as their sources and sinks. Furthermore, chemical reactions are introduced that are important for the atmospheric formation and removal of these species.

The next sections describe the fundamentals of air quality modeling, particularly with respect to the methods of emission, meteorological and air quality modeling.

A comprehensive overview is given of the role that shipping, and that particularly ship emissions, have

## *2. Scientific Question, Approach, and Structure of the Thesis*

in the topics of air pollution and greenhouse gas emissions. The current regulating policies are explained that target the mitigation of air pollutants and GHG emissions from ships. Relevant scientific studies are presented that refer to these policies and examine their effects. In addition, a scientific overview for ship emission modeling is provided and its state-of-the-art. Furthermore, recent and current focuses in ship emission research are described. These include the stricter regulations and the increased research interest for ship emissions in China and potential pathways for a decarbonization of the shipping sector

Chap. 2 presents the scientific questions that are answered by this thesis. Furthermore, it describes the approach taken to do this.

Chap. 3 contains the first publication, which concerns the Modular Ship Emission modeling System (MoSES), which was developed during this dissertation project. MoSES is a bottom-up ship emission model that allows the regionally independent creation of temporally and spatially highly resolved ship emission inventories. Its design allows for an extended flexibility in the modeling procedure, which makes it particular useful for creation of scenario. Its application is exemplified by the generation of an emission inventory of the North and Baltic Sea for the year 2015 that was also used for a model validation against the established Ship Traffic Emission Assessment Model (STEAM).

Chap. 4 contains the second publication that introduces a novel approach for scenario generation. In conjunction with the MoSES model, this approach was used to create three future scenario ship emission inventories for the years 2025, 2040, and 2050 that express current decarbonization efforts by a major fuel type change in the shipping industry from fossil fuels towards ammonia via liquefied natural gas as transitional solution.

Chap. 5 contains the third publication in which MoSES generated ship emission inventories are used in a chemistry transport model to estimate ship-related pollutant concentrations for northern Europe and eastern China in 2015. A comparison regarding the impact of ship emissions on air quality is made between these regions, which are particularly distinct in terms of their background air pollution levels.

Chap. 6 summarizes the scientific findings of this thesis that were dealt with in detail in the three publications in the Chaps. 3, 4, and 5. Furthermore, it draws an overarching conclusion and answers to the scientific questions formulated in Sect. 2.1. An outlook to further relevant research on the topic of ship emissions and air quality modeling in extension to the present work is given in Chap. 6.3.

### 3. Publication I: A Ship Emission Modeling System with Scenario Capabilities

The following chapter corresponds, apart from minor changes, to the publication of the same name authored by:

*Daniel A. Schwarzkopf, Ronny Petrik, Volker Matthias, Markus Quante, Elisa Majamäki, Jukka-Pekka Jalkanen*

and published in the Elsevier journal:

*Atmospheric Environment: X*, Volume 12, **2021**, p. 100132, ISSN 2590-1621.  
<https://doi.org/10.1016/j.aeaoa.2021.100132>.

#### Abstract

A bottom-up modular ship emission modeling system (MoSES) is presented that calculates highly spatiotemporally resolved ship exhaust emissions, based on ship position data recorded from the automatic identification system. MoSES is built in a modularized architecture, which guarantees good expandability. Several ship-type specific methods have been developed for estimating missing ship characteristics that are important for ship emission modeling, such as the gross tonnage, main or auxiliary engine power, engine rating or the service speed, since these characteristics are often not available in present data. Additionally, most recent emission factors for sulfate and black carbon were derived from literature that cover formerly neglected low-sulfur fuels. MoSES is demonstrated by the creation of an emissions inventory for the North and Baltic Sea region, but it may readily be applied to other regions as well. The results were evaluated and compared to ship emission data calculated with the established Ship Traffic Assessment Model (STEAM 3). A good agreement with the daily shipping activity and CO<sub>2</sub> emissions was found, although fewer emissions were calculated with MoSES for SO<sub>2</sub>, SO<sub>4</sub> and NO<sub>x</sub> due to differences in the method for calculating the power consumption, the assumed fuel sulfur content, and applied emission factors. Furthermore, the impact of different emissions factors and uncertainties due to missing ship characteristics has been investigated. Additionally, extensive functionalities for scenario generation were implemented that allow the modification of a ship fleet in a model run. A filtering algorithm was developed to support scenario generation by the creation of sub-emission inventories. These contain only emissions of ships moving between two specific harbors or points of interest. This feature is demonstrated for the ship traffic between the five busiest harbors in the North Sea among each other, and between the English Channel. The scenario capability of the model is exemplified on a case based on sub-emission inventories, that investigates a decreased trade volume between representative ports of mainland Europe and the United Kingdom.

#### Acknowledgement

This work was funded by the German Science Foundation (DFG) in the framework of the DFG-NSFC funded project “ShipChem” (DFG project nr. 645514) and supported by the BSH funded project “SeAir” (BSH contract code: 10042629, Hereon contract code: 430/2018).

### 3.1. Model Description

For bottom-up modeling of ship emissions, five key steps were formulated, namely, the loading and processing of AIS data (Sect. 3.1.1), the construction of a ship route (Sect. 3.1.2), fetching of ship characteristics from a database (Sect. 3.1.3) and allocation to the respective ship (including the estimation of missing quantities, Sect. 3.1.4), the calculation of emissions (Sect. 3.1.5) and the rastering of emissions (Sect. 3.1.6). These steps were implemented as modules containing the data and processing methods for each distinct modeling step. Since these modules can be self-reliant and arranged differently, this concept contributes to the model's flexibility. A potential for prospective extension and augmentation of the model functionality is provided by this modular structure, e.g., the implementation of additional emission factors, methods for power or ship characteristics estimation or interpolation routines. A scheme of the modeling process used for this work is shown in Fig. 3.1.

It should be emphasized that versatile functionality for scenario generation is provided by an expandable toolbox that is able to modify a shipping fleet created from an AIS data set. Thereby, representations of modeled ships and their movement and routes may be altered individually, either for specific groups or for the whole fleet. This approach refers to realistic circumstances and is designed to improve emission inventories for scenarios regarding future trends, regulations or technologies in the shipping sector. Further explanation of this approach can be found in Sect. 3.1.7.

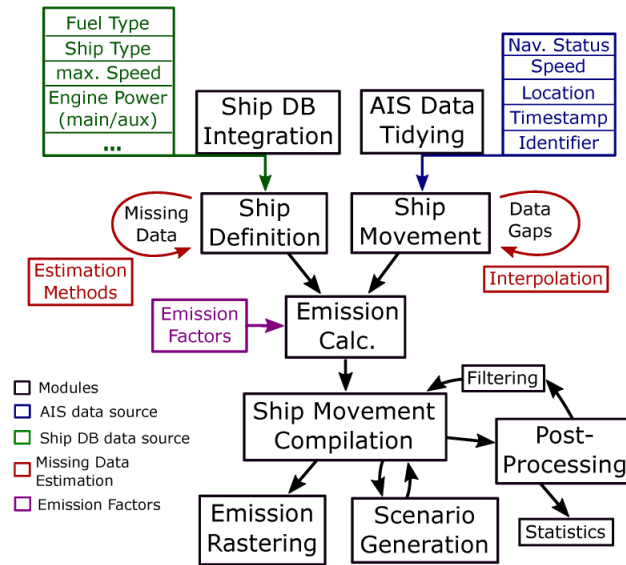


Figure 3.1.: Schematic representation of the modeling process in MoSES. Black boxes represent modules and functions of the model. Blue boxes contain input data from AIS. Green boxes represent data from a ship database. Red boxes represent internal methods to fill in data gaps. Violet boxes represent data regarding emission factors.

#### 3.1.1. AIS Data Tidying

The foundation of the bottom-up modeling approach used in this work is the data transmitted via AIS. This information can be categorized into three classes:

1. Static ship data, e.g., IMO or MMSI number, ship name, ship type, length or draught;
2. Dynamic ship data, e.g., timestamp, position, speed over ground or navigational status; and
3. Voyage data, e.g., draught, destination.

Since there is no obligation to send the complete set of information via AIS, data that are important for emission modeling are often missing, especially for smaller non-commercial ships. At the beginning of each model run, the AIS data is checked for errors. More specifically, this means that signals containing wrong coordinates are removed. Furthermore, signals are excluded when their transmitted speed over ground

exceeds a selectable threshold. For the model runs presented in this work, this threshold was set to 50 kn, as higher speeds are unreasonable for the majority of ships. Nonetheless, velocities higher than the chosen threshold may originate from AIS transceivers installed on airplanes or hovercrafts employed in the marine environment. Ship speeds below zero, which may arise due to the effect of wind and waves on berthing ships, were set to zero. Furthermore, signals with missing timestamps are removed prior to running the model. Finally, every distinct ship in the data set is identified by its IMO and/or MMSI number.

### 3.1.2. Ship Movement

For each identified ship, a route will be created from the available AIS data. In this regard, a route consists of route segments, each of which is created from the data of two temporally consecutive AIS signals. Every route segment is initially characterized by a timestamp, a time interval, coordinates, the average ship speed between its two AIS signals and a navigational status. In a later stage of the modeling process additional attributes are calculated for each route segment, e.g., energetic quantities, emission factors and emission values (see Sect. 3.1.5).

Since unrealistic coordinate changes may be present in AIS data, due to malfunctioning GPS systems or multiple use of the same IMO or MMSI number, a consistency check of the created routes is necessary. To do so, the average speed of each route segment is calculated by its length and duration. If the speed threshold of 50 kn is exceeded, the faulty signal will be excluded and a new route segment will be determined.

To ensure that each ship route segment only spans a distance that is significantly smaller than the spatial resolution chosen for the model run and thus, to prevent accumulation of emissions, two interpolation algorithms are implemented. The first algorithm is universally applicable and splits a route segment recursively, until its distance falls below a specified threshold. Considering that interpolation affects a route segment, which is represented as a straight line between two coordinates of AIS signals, ship movement over land may occur with this procedure. To address this problem, the route interpolation method developed by Aulinger et al. (2016) can be alternatively applied. This routine sets newly interpolated route segments of ship movement along previously defined common shipping routes in the area.

### 3.1.3. Ship Database Integration

For the accurate estimation of ship emissions, information is required that is not transmitted via AIS. Therefore, MoSES contains an interface to integrate one or multiple ship databases (e.g., by IHS Markit). The database is queried by a ship identifier, i.e., usually the IMO or MMSI number. The attributes of interest that can be currently processed by the model are as follows: draught, fuel type, gross tonnage, length, fuel type code and propulsion type, engine revolutions per minute (RPM, for main and auxiliary engine), ship type, service speed, total engine power (main and auxiliary engine), width, SFOC and year of build of the ship. Since the static section of the AIS data can contain complementary or more recent ship information (see Sect. 3.1.1), a preprocessor is available that allows its inclusion through the ship database interface.

### 3.1.4. Ship Definition

During a model run a definition is created for every identified ship, that allocates and compiles all ship characteristics important for emission calculation. Since multiple data sources may be available (e.g. ship databases, AIS data) these are differently prioritized. For the model runs presented herein, the highest priority was attributed to the used IHS Markit 2020 ship database. Attributes missing in the ship database are subsequently assigned from the less prioritized auxiliary ship database that was created from static AIS data as explained in Sect. 3.1.3. The least prioritized method queries the AIS data for the desired attribute, e.g. the service speed of a ship. If multiple values are extracted from AIS data the most frequently occurring is used.

If a ship or important ship attribute is not present in the databases or external data sources the missing information is estimated based on the available data. Since many estimation methods distinguish between

ship types, this information needs to be determined at an early stage. The model differentiates between the following 10 ship types plus an undefined class:

- Bulk
- Cargo and Container
- Cruise
- Fishing
- Military
- Passenger and Ro-Ro
- Pleasurecraft
- Tanker
- Tug
- Other
- Undefined

These types were derived from ship-type code classifications taken from the Marine Cadastre Project 2018 by the U.S. National Oceanic and Atmospheric Administration. Ship-type codes are usually transmitted as data in AIS. The type “Other” is assigned to ships for which type information is available but does not fit to one of the implemented types. These are e.g. dredging or drilling ships, patrol or research vessels. If no ship-type information is present, the type “Undefined” is assigned. A further subdivision of the ship types for modeling purposes or scenario generation is possible.

To derive missing ship attributes, fit functions that relate known to unknown quantities were created from more than 140000 ships in the IHS Markit 2020 database (with a gross tonnage  $> 100$ ) for every implemented ship type. Estimation of the gross tonnage ( $GT$ ) can be done by two sets of functions: one as a function of the ship’s length ( $L$ ), and one as of the draught ( $D$ ). As proposed by Hulskotte and Denier van der Gon (2010) a near cubic relationship of  $GT$  to  $L$  or  $D$ , shown in Eq. (3.1) was used.

$$GT(x) = a \cdot x^b \quad \text{with } x \equiv L \text{ or } D \quad (3.1)$$

While using  $L$  as an independent variable, the factor  $a$  has a range of 0.01–0.055, and the exponent  $b$  has a range of 2.6–3.3 for the different ship types (see Appendix A.1.1.1 for details). When no information about  $L$  is present,  $GT$  will be derived from  $D$ . For  $x \equiv D$ , the exponent has a range of 1.5–6.2 (Appendix A.1.1.1). If neither  $L$  nor  $D$  is known, the model relies on  $GT$  class averages created from the IHS Markit 2020 database (Appendix A.1.2). A special case is represented by the ship type “Undefined”. Since large vessels are mostly commercially used, and the data available about commercial vessels are usually better available, the assumption was made that ships, for which type and size information is missing, are small. Thus, these ships were assigned an arbitrarily gross tonnage of 500, which corresponds to the size of many small fishing vessels or pleasurecrafts. This value is confirmed for the North/Baltic Sea (see Sect. 3.2.5 for details).

As proposed by Denier van der Gon and Hulskotte (2009) and Flodström (1997), a relationship proportional to the square root of a ship’s gross tonnage ( $GT$ ), shown in Eq. (3.2), was used to derive the total main engine power ( $P_{main}$ ).

$$P_{main}(x) = a \cdot \sqrt{GT}. \quad (3.2)$$

The factor  $a$  is in the range of 51–178 for the different ship types (Appendix A.1.1.2).

The main engine RPM ( $RPM_{main}$ ) and the service ship speed ( $S_{ser}$ ) were implemented as asymptotic functions of the form shown in Eq. (3.3). The total main engine power ( $P_{main}$ ) was used as the independent variable  $x$ . The numerical parameter  $a$  represents the horizontal asymptote on the right side with a range from 15 to 26, and  $b$  represents the response of the function when  $x$  is zero. It is in the scope of 5–12. The factor  $c$  is an independent variable in the range from  $-10$  to  $-7$  (Appendix A.1.1.4).

$$RPM_{main}(x) \text{ or } S_{ser}(x) = a + (b - a) \cdot e^{-cP_{main}}. \quad (3.3)$$



The exponential model was chosen to reflect the assumption that large marine diesel engines usually drive propellers with a large diameter and low pitch. Since the engine RPM cannot fall below zero, an asymptotic behavior was implemented. Although ultra-low-speed marine diesel engines can run at approximately 60 RPM, lower ratings are very rare. Thus, the allowed RPM values were capped at this point and estimated values that are smaller are rectified to 60 RPM.

For estimating  $S_{ser}$ , an asymptotic exponential relationship to  $P_{main}$  was used because most ships are not designed for high velocities but rather for efficient performance. Thus, a cap for the speed slightly above common cruise velocities is reasonable.

A dependency of the total auxiliary engine power  $P_{aux}$  from  $P_{main}$  was implemented by the linear function in Eq. (3.4) through the origin,

$$P_{aux}(x) = a \cdot P_{main}. \quad (3.4)$$

Although a proportionality of  $P_{aux}$  to a ship's size ( $GT$ ) is reasonable, a linear dependency of  $P_{main}$  was chosen because it yielded better results. The complete set of fit functions can be found in Appendix A.1.1.3.

Some of the queried data regarding ship characteristics need further processing to be used in the model, e.g., the fuel type code and propulsion type code. Currently, the model distinguishes among nine fuel types. It is important to mention that the two oil-based fuels, namely, distilled fuel (DF) and residual fuel (RF), account for more than 99 % of used fuel types in the 2015 North/Baltic Sea model run presented in this work. Other considered types are gas boil-off (GBO), liquefied natural gas (LNG), nuclear energy, coal, methanol, liquefied petroleum gas and liquefied volatile organic compounds (burnt in steam turbines or boilers). If present, the fuel type can be determined from a ship's fuel type code. When information about the fuel type is missing, it can be estimated depending on the engines RPM and a survey by Zeretzke (2013) that claims that 95 % of engines running between 60 and 300 RPM and 70 % of engines running in a range of 300–1500 RPM use residual fuel. The remaining vessels use distillate fuel.

Since the implemented EFs by Zeretzke (2013) use the engine applications classified by IMO MEPC (2008a), they are determined on the basis of a ship's propulsion type (see Appendix A.1.6).

From a ship's year of build, information about its engine efficiency and applicable legal regulations can be deduced. If this information is unavailable, it will be assigned by a decision table set up by Aulinger et al. (2016).

### 3.1.5. Emission Calculation

Due to the modularized architecture of the model, emission factors, as well as other methods that are important for ship emission modeling, can be changed. Furthermore, this structure allows for the easy updating of existing methods or even to add new features or emission factors. The quantities and methods currently implemented are explained in the following.

Previous to emission calculation, the navigational status for all route segments is evaluated. Depending on the result, emissions are calculated for the main and auxiliary engine for moving ships or for the auxiliary engines only for berthing ships. The navigational status can adopt 16 different values and is usually transferred in characters or as a numerical code in the dynamic section of the AIS data (see Appendix A.1.5 for possible values).

The main engine load for every route segment is calculated to obtain an estimation of a ship's power consumption. It is described by Eq. (3.5) (Goldsworthy and Goldsworthy, 2015; Aulinger et al., 2016).  $EL$  and  $S$  are the instantaneous engine load factor and speed, respectively.  $S_{ser}$  is the service speed of the vessel.

$$EL = \left( \frac{S}{S_{ser}} \right)^3 \quad (3.5)$$

Due to a lack of information about a vessel's auxiliary engine load, it is set as static value between 0 and 1 for each individual ship type, to suit the different auxiliary power demands. An approach by Whall et al. (2002) recommends 0.3, which was used as the default.

The energy consumption  $E$  of a ship in the time interval of  $\Delta T$  is calculated with the engine load  $EL$  and the total power of the main or auxiliary engines  $P$ , which is found using Eq. (3.6),

$$E = \Delta T \cdot (EL_{main} \cdot P_{main} + EL_{aux} \cdot P_{aux}). \quad (3.6)$$

The energy consumption of berthing ships can either be calculated using a static auxiliary engine load factor, as for moving ships, or by a method based on studies about the fuel consumption of vessel's in harbors (Hulskotte and Denier van der Gon, 2010; Simonsen et al., 2018; CNSS project, 2014). A detailed description of this concept can be found in the Appendix A.1.4.

The specific fuel oil consumption (SFOC) of the main and auxiliary engines is determined via parameterizations created by Zeretzke (2013) from test bed measurements at Germanischer Lloyd Hamburg. These are available for different engine size classes and engine applications with the  $EL$  as independent variable. Additionally, a method for determining the SFOC introduced by Jalkanen et al. (2012), and adopted in the 3rd IMO GHGS, was implemented. This method considers a higher fuel consumption for faster-rated engines and a better efficiency for newer engines. In addition to SFOCs for oil-based fuels, this approach contains SFOCs for LNG-driven ships, gas boil-off, and steam turbines. Compared to these two estimation methods, SFOC values can be queried from a database. A decreased efficiency for engines that are operated outside their standard rating is taken into account by a load-dependent correction factor IMO (2014) or by applying the parabolic relationship derived by Jalkanen et al. (2012).

The sulfur content of the fuel (FSC) used by a ship is important for quantifying the emitted amount of some pollutants and especially for  $SO_x$ . Thus, it must be determined previous to the emission calculation. Since the actual sulfur content of ship fuels varies with each batch and is typically not known for modeling purposes, average values and SECA limits are used. The annually averaged global FSCs for residual and distillate fuel oils, determined in the IMO's sulfur monitoring program, are implemented for the years 2010–2018 and can be updated with values of future releases (IMO MEPC, 2018a). If a ship sails in the waters of a designated SECA, it must comply with the established sulfur limits. Consequently, maximum permitted sulfur limits are used if the values from the IMO's sulfur monitoring program are exceeded. Since the average FSC depends on the date and area, the model can determine it automatically for each route segment. Alternatively, desired values may be entered for the model run. Next to the unknown true sulfur content of the fuel batch, an additional uncertainty regarding  $SO_x$  emissions is introduced by ships not complying to the sulfur regulations. Although, in the North/Baltic Sea SECA the number of registered non-compliant ships in 2015 was small, with 2.8 % (OECD, 2016), the effect on  $SO_x$  concentrations can be significant, keeping in mind that SECA limits differed from the global limits by a factor of 35 in 2015. Another uncertainty with opposing effect is introduced by SECA-compliant fuels, which most likely will have a FSC below the allowed limits. Considering these two uncertainties the true average FSC will be in between and thus, using the SECA FSC limits seems to be a reasonable approximation.

The emission factors used in the model are power based with the unit  $g * kWh^{-1}$ . The currently implemented factors for gases and aerosols and their sources and dependencies are listed in Table 3.1.

$SO_2$  emissions are directly dependent on a ship's SFOC and FSC. This relationship is used for  $EF_{SO_2}$ , which is determined for every route segment. According to IMO (2014), approximately 98 % of the sulfur in fuel will be oxidized to  $SO_2$  during combustion, which is considered in the calculation.

The amount of formed sulfate ( $SO_4$ ) is also dependent on the SFOC and the FSC, with reduced sulfate emissions occurring during the use of low-sulfur fuels.  $EF_{SO_4a}$  was derived for dry sulfate from a literature research and has the form shown in Eq. (3.7),

$$EF_{SO_4}(SFOC, FSC, EL) = SFOC \cdot FSC \cdot CR_{SO_4}(EL) \cdot \frac{M(SO_4)}{M(S)} \quad (3.7)$$

$M(S)$  and  $M(SO_4)$  are hereby the molar mass of sulfur and sulfate, respectively,  $CR_{SO_4}(EL)$  is the conversion rate of sulfur to sulfate depending on the engine load  $EL$ , that is  $0.01 + EL \cdot 0.035$  for RF and  $0.01 + EL \cdot 0.004$  for DF (Kasper et al., 2007; Lack et al., 2011; Petzold et al., 2010, 2011; Yu et al., 2020; Shen and Li, 2020; Yu et al., 2020). Two other methods for calculating sulfate emissions are also implemented.  $EF_{SO_4b}$  utilizes a fixed conversion rate of 2 %, representing the remaining fraction of the fuel sulfur that is not converted to  $SO_2$ .  $EF_{SO_4c}$  depends only on the FSC and was derived by Jalkanen et al. (2012), based on measurement data from the IMO (2009). In comparison to the latter two methods, the newly derived EF yields much lower sulfate emissions for ships using low-sulfur fuels, e.g., ships in the SECA in the North/Baltic Sea.

Water associated with sulfate in particles is important for determining the total weight of particulate emissions and was implemented as  $EF_{SO_4w}$  and depends on the FSC.

Table 3.1.: In MoSES considered gases and aerosols with the different implemented emission factors, their sources and dependencies.

Pollutant	Identifier	EF source	EF dependencies	Comments
Sulfur dioxide (SO <sub>2</sub> )	EF <sub>SO2</sub>	—	SFOC, FSC	S to SO <sub>2</sub> conversion rate of 2 %
Sulfate (dry, SO <sub>4</sub> <sup>2-</sup> )	EF <sub>SO4a</sub>	This publ.	SFOC, FSC, EL	S to SO <sub>4</sub> conversion rate depends on FSC
	EF <sub>SO4b</sub>	3rd IMO GHGS	SFOC, FSC	S to SO <sub>4</sub> conversion rate of 2 %
	EF <sub>SO4c</sub>	Jalkanen (2012)	FSC	S to SO <sub>4</sub> conversion rate of 5 %
Water assoc. with SO <sub>4</sub> (SO <sub>4</sub> × H <sub>2</sub> O)	EF <sub>SO4w</sub>	Jalkanen (2012)	FSC	—
Nitrogen oxides (NO <sub>x</sub> )	EF <sub>NOXa</sub>	Zeretzke (2013)	EL, engine type/size	Tier 1 and 2
	EF <sub>NOXb</sub>	3rd IMO GHGS	Fuel type, engine speed	Tier 0–2
Black carbon (BC)	EF <sub>BCa</sub>	Aulinger (2016)	EL, fuel type	—
	EF <sub>BCb</sub>	Jalkanen (2012)	EL	—
Primary organic aerosols (POAs)	EF <sub>POAa</sub>	Aulinger (2016)	—	—
	EF <sub>POAb</sub>	Jalkanen (2012)	EL	—
Mineral ash excl. metal sulfates (MA)	EF <sub>MAa</sub>	This publ.	SFOC, FSC	—
	EF <sub>MAb</sub>	Aulinger (2016)	Fuel type	—
	EF <sub>MAc</sub>	Jalkanen (2012)	EL	—
Carbon dioxide (CO <sub>2</sub> )	EF <sub>CO2</sub>	3rd IMO GHGS	Fuel type, SFOC	—
Carbon monoxide (CO)	EF <sub>CO</sub>	3rd IMO GHGS	Engine type/speed, EL	—
Methane (CH <sub>4</sub> )	EF <sub>CH4</sub>	3rd IMO GHGS	Fuel type, engine speed	—
Non-methane volatile Organic compounds (NMVOCs)	EF <sub>NMVOCa</sub>	3rd IMO GHGS	Engine type/speed	—
	EF <sub>NMVOCb</sub>	EMEP/EEA (2019)	EL, engine speed	—
Dinitrogen oxide (N <sub>2</sub> O)	EF <sub>N2O</sub>	3rd IMO GHGS	Engine type/speed	—
Particulate matter (PM <sub>tot</sub> )	EF <sub>PMa</sub>	3rd IMO GHGS	Fuel type, engine Speed	incl. wet SO <sub>4</sub> <sup>2-</sup> and POAs as defined
	EF <sub>PMb</sub>	EMEP/EEA (2019)	EL, fuel type	by the IMO.

PM is defined by the IMO as substance including sulfate, water associated with sulfate ash and organic carbons. EF<sub>PMa</sub> described in the 3rd IMO GHGS determines the total particulate matter including all these components (PM<sub>tot</sub>). EF<sub>PMb</sub> has a similar form and was implemented from EMEP/EEA (2019). Even though it does not depend on the FSC, it considers increased PM emissions for low engine loads and a different emission pattern for berthing ships. Another method for determining the amount of PM in ship emissions has been proposed by Jalkanen et al. (2012) as the sum of SO<sub>4</sub>, SO<sub>4</sub> × H<sub>2</sub>O, BC, POA and MA emissions. In this respect it is noteworthy that the summed PM of the latter method yields approximately 10 % higher PM emissions in the presented model runs compared to PM<sub>tot</sub>. The EFs for PM<sub>tot</sub> include a correction factor for low main engine loads as described in Starcrest (2013) and account for the dependency of the FSC with a function that was fit to the data in the 3rd IMO GHGS (Appendix A.1.3.14).

EFs for the individual components of particulate matter, BC, POA and MA were implemented from Aulinger et al. (2016). Both of the latter, EF<sub>POAa</sub> and EF<sub>MAb</sub>, depend on the engine and fuel type in use. For EF<sub>BCa</sub> an engine load-dependent correction factor is applied, as BC emissions are known to increase significantly at low loads (Lack and Corbett, 2012). A second set of EFs for these three particulates were implemented from Jalkanen et al. (2012). In contrast to EF<sub>BCa</sub>, EF<sub>BCb</sub> has no correction factor for low loads but considers a decreased engine efficiency at non-standard rating with the parabolic function derived by Jalkanen et al. (2012). EF<sub>POAb</sub> includes a correction function that increases POA emissions at low loads. The EF<sub>MAa</sub> was derived for MoSES from a literature research and yielded a dependency of the FSC that is not implemented in any of the other EFs for this particulate. A fit to the measured values gives the linear relationship in gkWh<sup>-1</sup> shown in Eq. (3.8),

$$EF_{MA}(FSC, SFOC) = 0.02 \cdot FSC \cdot SFOC \quad (3.8)$$

$FSC$  is the fuel sulfur content and  $SFOC$  the specific fuel oil consumption in  $\text{g} \cdot \text{kWh}^{-1}$  (Moldanová et al., 2009; Agrawal et al., 2010; Lack et al., 2011; Petzold et al., 2011; Khan et al., 2013; Winnes et al., 2016b; Shen and Li, 2020).

Emission factors for  $\text{NO}_X$  for diesel engines need to consider the three  $\text{NO}_X$  emissions Tiers defined in IMO MEPC (2008a, 2014). Depending on a ship's year of construction, different  $\text{NO}_X$  emission limits must be complied with. The time frame preceding the  $\text{NO}_X$  regulations is referenced herein as Tier 0. For Tier 1 and 2, engine load-dependent functions for the main engine applications E2 and E3 were implemented with  $EF_{\text{NO}_Xa}$ . They were further subdivided in engine size classes. According to Zeretzke (2013), no engine load dependency could be found for the auxiliary engines; rather, there is a correlation of  $\text{NO}_X$  emissions to the total auxiliary engine power. In contrast to  $EF_{\text{NO}_Xa}$ ,  $EF_{\text{NO}_Xb}$ , from the 3rd IMO GHGS, considers slightly lower  $\text{NO}_X$  emissions for residual than for distillate fuels. The latter is available for Tiers 0–2 and differentiates between low- and medium-speed main engines, gas- and steam turbines. The same differentiation for engine speeds is made in  $EF_{\text{N}_2\text{O}a}$ , which was also implemented from the 3rd IMO GHGS.

Even though the carbon content in each individual fuel type might differ slightly,  $\text{CO}_2$  emissions are not altered for different engine types or duty cycles. Therefore, the implemented  $EF_{\text{CO}_2}$  from the 3rd IMO GHGS is a linear function for each fuel type, which are dependent on the  $SFOC$ .

A set of EFs for carbon monoxide ( $EF_{\text{CO}}$ ), methane ( $EF_{\text{CH}_4}$ ), and NMVOCs ( $EF_{\text{NMVOC}a}$ ), described in the 3rd IMO GHGS, are implemented. They do not differ regarding RF- or DF-usage but slightly decrease with increasing engine speed. Specific EFs are implemented for steam boilers, gas turbines and LNG-fueled engines. CO and NMVOCs result from incomplete fuel combustion. Thus, CO emissions are corrected for small engine loads ( $0.2 > EL > 0.02$ ) by a load-dependent function. For diesel-fueled engines, steam boilers and gas turbines the magnitude of methane emissions is approximately 2 % of NMVOC emissions (Cooper and Gustafsson, 2004). The second, more elaborate  $EF_{\text{NMVOC}b}$  was implemented from EMEP/EEA (2019) and considers increased emissions for low engine loads or berthing ships.

After all emission factors and the  $SFOC$  were determined, emissions were calculated with Eq. (3.9),

$$M_p = EF \cdot E. \quad (3.9)$$

Hereby  $M_p$  is the mass of the pollutant in g,  $EF$  is the emission factor in  $\text{g} \cdot \text{kWh}^{-1}$ , and  $E$  is the energy in kWh.

### 3.1.6. Emission Rastering

For storing and further processing of the calculated emissions (e.g., as emission input in a chemical transport model) every identified ships' emissions are rastered onto a grid with the temporal and spatial resolution and the spatial extent specified for the model run. Emissions of the main and auxiliary engines may be rastered onto separate grids. Additionally, a grid containing the power consumption or a ship density may be created. The ship density is deduced from the time a ship spends in a grid cell. The time each ship gets to distribute across grid cells corresponds to the chosen temporal resolution for the model run, e.g., if the chosen temporal resolution is hourly, each ship gets to distribute one hour in each time step across the grid cells it traversed. The amount of "ship time" each traversed grid cell gets assigned is proportional to the fraction of time the ship spent in this grid cell.

### 3.1.7. Ship Movement Compilation Data, Scenario Generation and Post-Processing

In addition to storing the model run's emission data on grids (Sect. 3.1.6), they are compiled with the corresponding ship's movement (Sect. 3.1.2) and technical data (Sect. 3.1.4). This compiled shipping fleet data constitutes the basis for several important features:

- It is the starting point for model runs on the basis of previously executed runs. Different options may be chosen for this re-run, e.g., emission factors or grid size.
- It allows a statistical evaluation of the model run's shipping fleet. This includes ship characteristics and the information pertaining to if a ship characteristic had to be estimated or was available through a database. This allows an assessment of uncertainties in the model run.

- Individual ships, ship groups or ship types and their emissions may be filtered from the whole fleet and be used for separate model runs. The results can be compared to the total emissions or investigated in terms of spatial or temporal patterns.
- For investigating ship movements or routes between specific harbors or other regions of interest (e. g. Hamburg and Rotterdam or the English Channel) and quantifying their emissions, a method was developed that allows the creation of sub-emission inventories that contain only emissions from ship sailing between these regions.
- Tools for modifying the modeled shipping fleet can be applied to single ships or ship groups and are available for dynamic values, e.g., ship speed, and/or static ship characteristics, e.g., engine power, gross tonnage, ship type, fuel type.
- Ships can be added to or removed from the fleet; existing ships can be duplicated and their movement set can be temporally shifted. The adding or removal of ships from the fleet can be repeated until a percentage increase or decrease in ships or freight volume is met. These procedures are possible not only for the complete movement of a ship but also for a ship route between harbors or regions of interest. In this regard a route is one travel of a ship, e.g., sailing from Hamburg to Rotterdam, or vice versa. These routes can be identified, and any of them may be removed or duplicated. This procedure is then repeated for other ships traveling on the same route until a specific criteria is met, e.g., a decreased trade volume. Other travels these ships made in the modeled time frame remain unchanged. This allows a realistic increase or decrease of shipping activity when creating scenarios.
- All of these changes are applied previous to emission rastering and are thus not confined to a previously chosen spatial and temporal resolution.

## 3.2. Model Application and Uncertainty Assessment

For testing purposes, MoSES has been set up for a domain that includes the North and Baltic Sea regions. The quality of the used AIS data set was assessed and the obtained emission inventory was evaluated in terms of the emission's spatial and temporal distribution. The results were compared to data from the Ship Traffic Assessment Model (STEAM3) (Jalkanen et al., 2009, 2012; Johansson et al., 2013, 2017a). An estimation of the uncertainties encountered during the modeling process was carried out, and the scenario capability of the model is shown in two examples.

### 3.2.1. Preprocessing of AIS Data

The AIS data used for the underlying study was collected by the European Maritime Safety Agency (EMSA) and was acquired from the Federal Maritime and Hydrographic Agency of Germany (BSH). Previous to the actual model run, the AIS signal data with erroneous ship name character coding was removed. This concerned only 0.002 % of the data, and the error due to removal of these signals was considered to be negligibly small. Other methods for data pertaining to “tidying” were applied automatically at the beginning of a model run and were explained in Sect. 3.1.1. On average, 0.95 % of the data had to be removed due to transgressing the maximum allowed speed, which was set herein to 50 kn. Where possible, missing IMO numbers in AIS signal data were derived from other signals in the data set on the basis of MMSI numbers. It has to be noted that the currently available data set lacks satisfactory coverage in locations far from shoreline. The data is mainly compiled from records of land-based AIS stations and less from satellites, the latter being a more reliable option for recording data in the open sea. These data gaps were filled by the interpolation routine described in Sect. 3.1.2.

### 3.2.2. Model Domain

The AIS data covers the area between the longitude and latitude ranges from  $-5.00^\circ$  to  $31.41^\circ$  and  $48.32^\circ$  to  $68.37^\circ$ , respectively. The spatial extent of the modeled North/Baltic Sea domain was chosen in accordance

with this data range. The resolution of the grid is  $0.069^\circ$  in  $x$  (East – West) and  $0.036^\circ$  in  $y$  (North – South) direction, which corresponds to approximately 4 km.

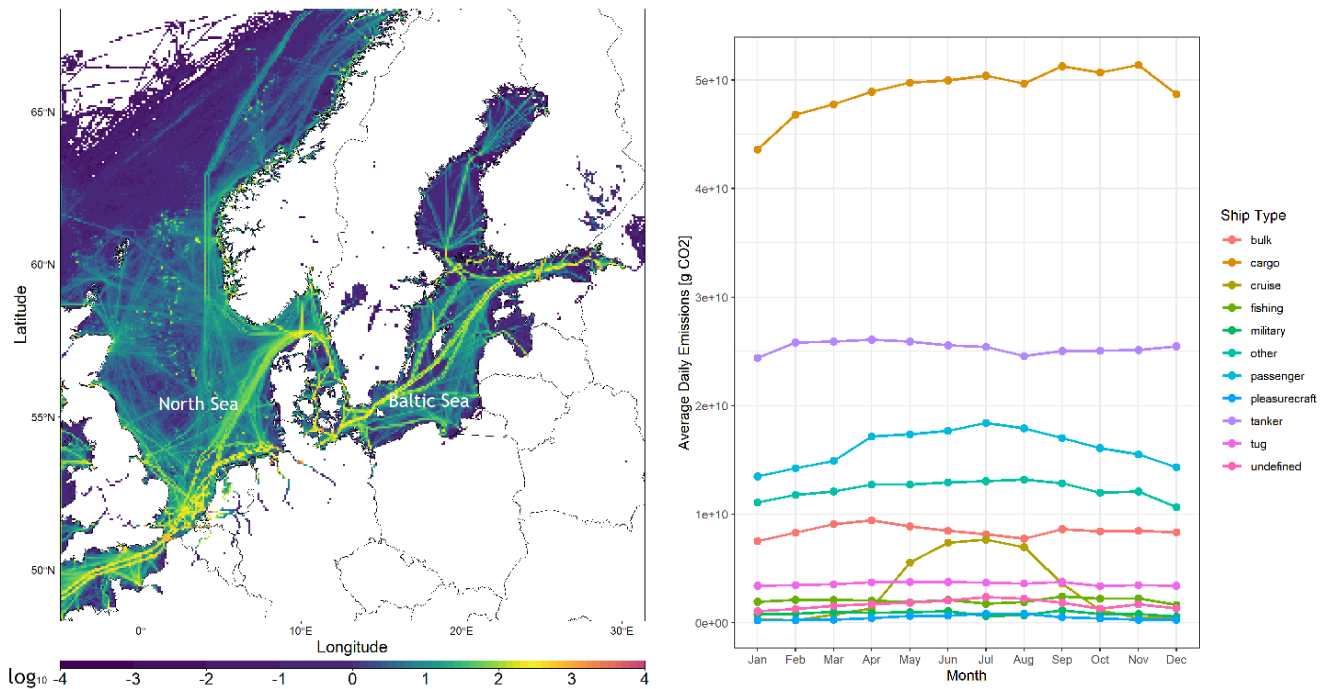


Figure 3.2.: Calculated CO<sub>2</sub> emissions in  $\text{g} \cdot (\text{m}^2 \cdot \text{year})^{-1}$  on a logarithmic scale for the year 2015 in the chosen model domain including the North and Baltic Sea. The spatial resolution is approximately  $4 \times 4 \text{ km}^2$  (left). Monthly change of CO<sub>2</sub> emissions in 2015 for each ship type averaged to one day (right).

### 3.2.3. Results

The model runs were carried out for the year 2015 in an hourly resolution. In total, the data of almost 900 unitmillion AIS signals was processed. Overall, for 20 hours distributed throughout the year, no AIS data was recorded by the AIS transceiver stations. This translates to a temporal signal coverage of 99.8%. The total number of identified ships per month varied over the year. In early and late 2015, approximately 22,000 different vessels were present, while during the summer months, this number rose to more than 30,000 ships sailing in the domain. Of their number, 58% were using DF, approximately 41% RF and less than 1% other fuel types, such as LNG, methanol or coal. While the number and activity of identified cargo ships and tugs remained constant throughout the year, an increased activity of fishing vessels could be observed in March/April and October/November, which corresponds to the herring fishing season (German Federal Agency for Nature Conservation, 2020). In the summer months, a spike in ship counts could be observed for pleasurecrafts and passenger-related ships. The number of undefined ships increased in the summertime as well, most of which were probably small private vessels. This observation explains the higher total ship counts observed during that time.

#### 3.2.3.1. Spatial- and Temporal Distribution of Modeled Emissions

The model domain includes the North and Baltic Sea, which are two regions with a high shipping density. The main shipping routes in these regions are clearly visible based on the emission inventory shown in Fig.3.2. The largest route passes through the English Channel, leads around Denmark, and splits in the Baltic Sea, with one track heading into the Gulf of Finland and the other into the Gulf of Bothnia. Many small routes separate from the main route to aim for the eastern side of the United Kingdom, the Norwegian coast and the biggest European container ports such as Le Havre, Felixstowe, Antwerp, Rotterdam, Bremerhaven and Hamburg.

The calculated annual emissions for the North/Baltic Sea domain in total for the year 2015 and for each individual ship type can be found in Table 3.2 (see Appendix A.1.7 for monthly total emissions). The EFs used for this model run were chosen to reflect actual conditions and the complexity of combustion in ship engines in the best possible way. They are in the references of Table 3.1:  $EF_{SO_2}$ ,  $EF_{SO_{4a}}$ ,  $EF_{SO_{4w}}$ ,  $EF_{NOX_a}$  for Tier 1, 2 and  $EF_{NOX_b}$  for Tier 0,  $EF_{CO_2}$ ,  $EF_{CO}$ ,  $EF_{CH_4}$ ,  $EF_{N_2O}$ ,  $EF_{NMVOC_b}$ ,  $EF_{PM_b}$ ,  $EF_{MA_a}$ ,  $EF_{BC_a}$ ,  $EF_{POA_b}$ . When available for a ship, the SFOC from a database was used in combination with the parabolic function described by Jalkanen et al. (2012). Otherwise, the SFOC was calculated using the method presented in Zeretzke (2013).

In general, more emissions could be observed during summer than in the winter months, which is in accordance with the observed monthly ship counts. On average, approximately 40 % of  $CO_2$ ,  $NO_X$ ,  $CO$ ,  $N_2O$  and POA emissions and 35 % of  $SO_2$ ,  $SO_4$ , NMVOC, BC, MA and PM emissions originated from cargo ships. A slight increase of this ship type's emissions could be observed for the beginning of the year. Since methane is mostly emitted by ships using LNG as fuel, it has special emission patterns. This fuel type is rarely used by cargo ships and thus, they have only an average share of 8 % on  $CH_4$  emissions. To tankers, an average share of 20 % in the emissions of  $CO_2$ ,  $NO_X$ , POA, BC,  $CO$ , NMVOC,  $N_2O$  and PM, 15 % in  $SO_2$ ,  $SO_4$  and MA and a share of 32 % in  $CH_4$  could be ascribed. No seasonality was found for tanker traffic. The different proportions of the pollutants in comparison to cargo ships can be explained by their fuel type dependency. DF was used by 66 % of the number of tank ships, RF by 33 % and LNG by almost 1 % of the ships. Passenger ships in the modeled domain have a share in 15 % of  $CO_2$ ,  $NO_X$ ,  $SO_2$ ,  $SO_4$ , POA, MA and  $N_2O$  emissions, 10 % of PM, NMVOC and BC and 42 % of  $CH_4$  emissions. Most passenger ships are commuting on predefined routes between the European mainland and the UK, or connecting Germany, Denmark and many of the Eastern European countries with the Scandinavian countries over the Baltic Sea. A weak seasonal effect was found for this ship type with slightly higher emissions during summertime than in the winter. Passenger ships are with 90 % of their numbers predominantly fueled by DF. Additionally, this ship type has with 1.7 % the highest percentage of LNG- or methanol-driven ships. Emissions of cruise ships show a strong seasonality. Due to a very small activity in winter, which is confined to the English Channel, their amount of emissions is very small during that time. In spring, they start traveling along the Norwegian coast, and in summer their routes cover the whole North and Baltic Sea region, except the Gulf of Bothnia. Emission shares for this type rise to approximately 6 % in the summer. The seasonality of cruise and passenger ships is in agreement with the expectation that there is a higher demand in summer due to the higher temperatures and holidays. Most of the cruise ships in the domain use DF (93 %), the remaining ships use RF. Ships of other types, such as fishing vessels, tugs and undefined ships, usually have a small share of 1–3 % in the total emissions. The share in PM and  $SO_2$  can rise to 6 and 13 %, respectively, for fishing ships in the fishing season in spring and autumn, since they predominantly use RF. It is noteworthy that despite their large count, especially in the summertime, "Undefined" ships contribute only a very small percentage to the total emissions. For most of these ships, other important characteristics besides the information about their type is not available, and they are thus assumed to be small. Further discussion about ships of type "Undefined" can be found in Sect. 3.2.5. In general, the emissions of military ships and pleasurecrafts have a negligibly small share in the total emissions, with less than 1 %. For military ships, this is in accordance with their very small count, which is observed throughout the whole year. However, it is noteworthy that they are excluded from obligation to transmit AIS data, which represents an uncertainty in the model results. Pleasurecrafts are responsible for only very few emissions despite their large count during summer (12 % of total ship counts). They mainly use DF, and their size is small. However, because most of these kind of vessels may not be using AIS and are generally sailing close to the coast, the impact of their emissions on human health should not be neglected (Johansson et al., 2020). Ships compiled under the type "Other" account for 10 % of total emissions for most pollutants. Showing no seasonality, they have an increased share in BC, with 16 % and NMVOC and PM with 20 % due to an equal use of RF and DF by the number of ships and a frequent operation at low loads. A major part of methane emissions is produced by ships using LNG as a fuel source; the spatial and temporal distribution of this pollutant is strongly dependent on the deployment of such ships. The model results for 2015 show that these fuels are especially used by commuting passenger ships on routes between Denmark and the other Scandinavian countries. For

LNG-carriers, which are predominantly found on the major shipping routes and at the Norwegian coast, this is also a common fuel source.

Table 3.2.: Modeled emissions in Gg/year for the North/Baltic Sea Domain 2015 in total and for each individual ship type.

Ship Type	SO <sub>2</sub>	SO <sub>4</sub>	SO <sub>4</sub> xH <sub>2</sub> O	NO <sub>x</sub>	BC	POA	MA	CO <sub>2</sub>	CO	CH <sub>4</sub>	NM VOC	N <sub>2</sub> O	PM <sub>tot</sub>
All	31.20	0.76	0.59	897.97	13.89	17.96	0.32	44886.43	38.31	7.77	11.12	2.36	29.83
Bulk	1.52	0.03	0.02	55.42	0.72	1.13	0.02	3085.58	2.58	0.05	0.52	0.16	1.71
Cargo	10.99	0.25	0.19	352.60	4.88	6.94	0.11	17917.36	14.58	0.65	3.69	0.91	11.01
Cruise	0.65	0.01	0.01	24.98	0.27	0.49	0.01	1097.34	1.06	0.02	0.16	0.07	0.70
Fishing	1.45	0.05	0.04	14.23	0.27	0.32	0.01	742.38	0.60	0.01	0.2	0.04	0.61
Military	0.28	0.01	0.01	6.96	0.15	0.15	0.00	312.51	0.27	0.00	0.14	0.02	0.29
Passenger	4.41	0.12	0.10	132.84	1.67	2.42	0.05	5906.64	5.38	2.97	1.21	0.32	3.88
Pleasurecr.	0.14	0.00	0.00	3.45	0.09	0.08	0.00	171.29	0.14	0.00	0.08	0.01	0.15
Tanker	4.78	0.10	0.08	176.34	2.69	3.49	0.05	9254.73	7.99	2.49	2.14	0.48	5.71
Tug	1.26	0.03	0.03	24.68	0.61	0.61	0.01	1305.36	1.14	0.04	0.56	0.07	1.15
Other	3.38	0.09	0.07	93.85	2.27	2.05	0.03	4475.96	4.09	1.52	2.14	0.26	4.01
Undefined	2.34	0.07	0.06	12.65	0.27	0.28	0.02	617.28	0.48	0.01	0.23	0.03	0.62

### 3.2.4. Comparison with STEAM Ship Emission Data

For quality assessment, a comparison was carried out between ship emissions calculated with MoSES and ship emissions calculated with the established Ship Traffic Assessment Model (STEAM 3) described in detail by Jalkanen et al. (2009, 2012) and Johansson et al. (2013, 2017a). STEAM combines AIS data and ship-specific technical information obtained from IHS Markit to model the fuel use and emissions of each vessel. The STEAM emission calculation is performed using two different AIS data sources. The first one is global vessel activity data obtained from Orbcomm that is recorded by both, terrestrial- and satellite-based AIS receivers. The corresponding ship emission inventory covers the whole Baltic and North Sea region and is referred here as STEAM-Worldpool. The second data set is collected by the Baltic Marine Environment Protection Commission - Helsinki Commission (HELCOM) and covers only the Baltic Sea region. It is referred to here as STEAM-HELCOM. Since the coverage of the HELCOM data is higher in the Baltic Sea region, it is a more reliable data source than the Worldpool data for creating emission inventories. It should be mentioned that the major part of the HELCOM data covering the Baltic Sea, except data recorded by the Russian authorities, is also contained in the EMSA data set, which was used with MoSES. The spatial resolution of both STEAM emission data sets is 4 km<sup>2</sup>, which is similar to the inventory calculated with MoSES. The spatial grids and the temporal frequency of STEAM and MoSES emission inventories are harmonized prior comparison of ship emission totals and fluxes.

For capturing seasonal shipping trends, a comparison was conducted in January and July of the year 2015. The focus was placed on the hydrographic regions North Sea, Baltic Sea and the combined region of Kattegat and Skagerak (Table 3.3). It is noteworthy that the North Sea region includes the English Channel only up to 4°W, until the end of the SECA. Moreover, the Baltic Sea region does not include the three basins of the Gulf of Riga, the Gulf of Finland and the Gulf of Bothnia. On the one hand, the spatial coverage of the ship emission data sets does not allow a thorough investigation of the aforementioned basins. Furthermore, the smaller basins were found to be very sensitive to the source of AIS data. A comparison of the monthly total emissions is shown in Table 3.3, where the values are given as the percentage of the emission ratio obtained from dividing MoSES results by emissions calculated with STEAM.



Table 3.3.: Hydrographic regions used for the comparison of MoSES with STEAM, along with the ratio between MoSES emission values and STEAM emission values, given as percentage. For the Baltic Sea region two data sets for comparison, STEAM-Worldpool (Baltic Sea Worldpool) and STEAM-HELCOM (Baltic Sea HELCOM), were available. Kattegat and Skagerrak were considered as an additional third region.

Region	Size [km <sup>2</sup> ]	Month	Power Cons.	CO <sub>2</sub>	SO <sub>2</sub>	SO <sub>4</sub>	NO <sub>x</sub>
North Sea	606635	Jan.	87	96	72	15	78
		Jul.	71	77	58	13	66
Skagerak & Kattegat	68787	Jan.	84	98	71	13	76
		Jul.	84	95	71	13	80
Baltic Sea Worldpool	217829	Jan.	89	104	78	12	84
		Jul.	82	92	70	11	79
Baltic Sea HELCOM	217829	Jan.	88	102	77	12	84
		Jul.	90	102	77	12	89

### 3.2.4.1. Power Consumption

The gridded ship power consumption calculated by both models shows a difference of approximately 10–18 %, with the exception of July for the North Sea, which has a deviation of approximately 30 %. Hereby, a smaller power consumption was calculated by MoSES (Table 3.3). This deviation is probably due to differences in the method for calculating the power consumption, e.g., by the inclusion of ship specific resistances in the STEAM model and the assumed load of auxiliary engine usage. Another factor could be the differing estimation methods regarding installed main and auxiliary engine power for ships, for which these quantities are not known. However, reasons for the larger gap between total power consumption in the North Sea of 29 %, for the month July, are not clear at the present time. An incompleteness of the Worldpool data set, e.g., due to bad satellite coverage, may be the case, which could lead to higher emission estimates due to uncertainties in ship movement interpolation or additional estimates of missing ship characteristics. This assumption is based on a comparison of the STEAM-HELCOM to the STEAM-Worldpool emission inventory for the Baltic Sea, which yields 8 % less power consumption for the latter in July, while for January the values are equal. Additionally, a different handling of unidentified ships in the two models creates larger deviations in July compared to January and in the North Sea compared to the Baltic Sea, since the number and activity of unidentified ships is higher in this time frame and region. This difference for July systematically translates to the comparison of the following emissions of gas- and particle species.

### 3.2.4.2. CO<sub>2</sub>

In terms of emissions, CO<sub>2</sub> is the species best suited to reflect differences in the shipping activity, since it directly depends on the consumed fuel. Table 3.3 shows that the estimated emission totals of CO<sub>2</sub> are almost equal for all three compared regions, aside from the North Sea in July. Relating this finding to the comparison of the power consumption suggests that a higher SFOC in MoSES balances a lower calculated power consumption, since these are the two main impact factors when determining CO<sub>2</sub> emissions. An analysis of the daily variation of CO<sub>2</sub> emissions was also done for both inventories (Fig. 3.3). There is a good linear correlation between MoSES and STEAM-HELCOM and -Worldpool for the Baltic Sea in January, with  $R = 0.98$ . For July,  $R$  is 0.98 and 0.77 for STEAM-HELCOM and STEAM-Worldpool, respectively. For the North Sea in January, the correlation is lower, i.e., 0.88 in January and 0.44 for July. The low correlation in July might be explained by the higher count of unidentified ships in addition to

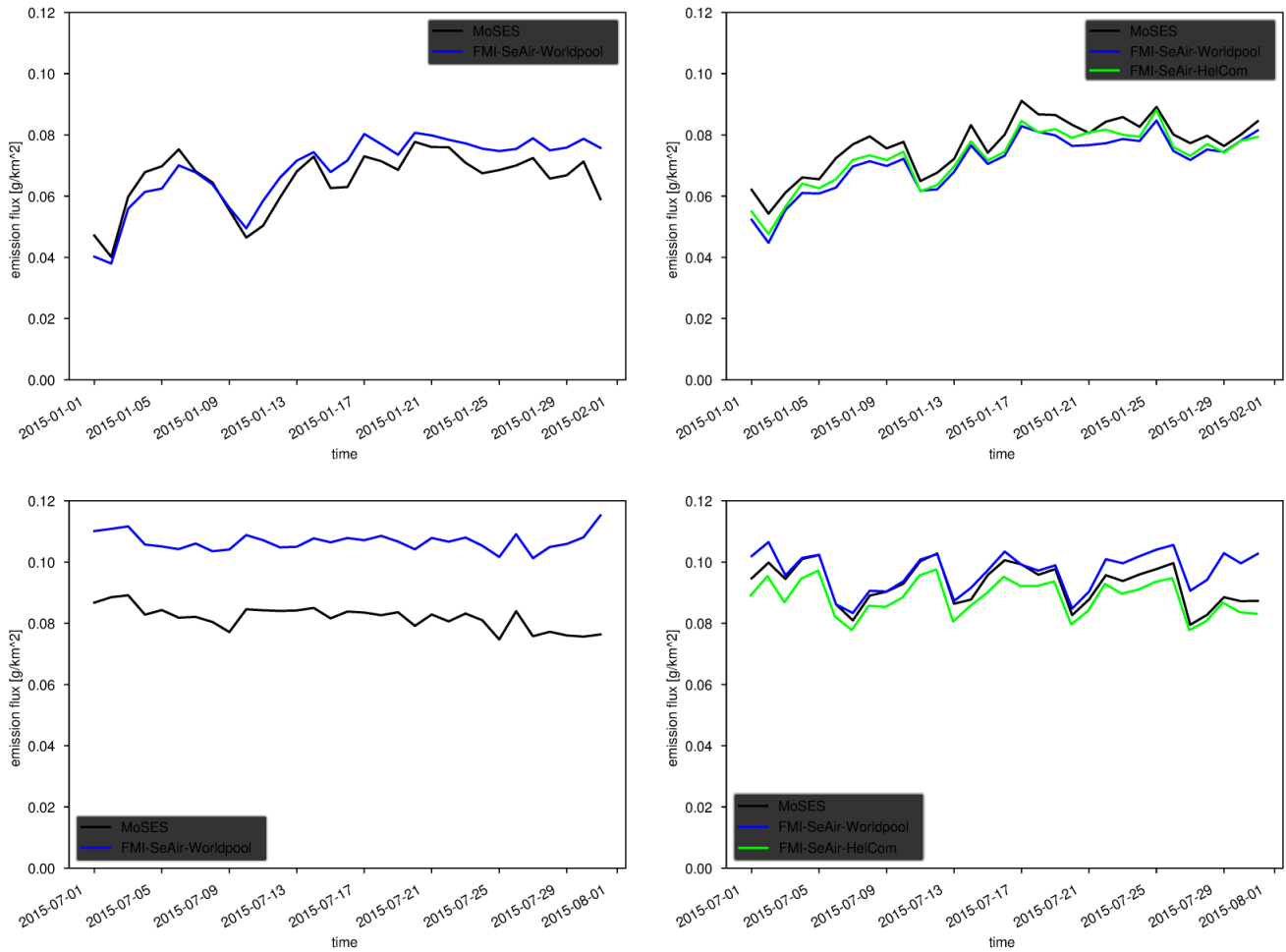


Figure 3.3.: Comparison of the daily CO<sub>2</sub> emissions [g/km<sup>2</sup>] calculated with MoSES and STEAM for the North Sea (left) and the Baltic Sea (right). The results are shown for January 2015 (top panel) and July 2015 (bottom panel).

the deviations found for the calculated power consumption. Considering this, not only the total emission values but also the daily modeled shipping activity is mainly in good agreement with each other.

### 3.2.4.3. SO<sub>2</sub> and SO<sub>4</sub>

For CO<sub>2</sub>, the emissions calculation of SO<sub>2</sub> strongly relies on the SFOC, although it additionally depends on the FSC. The comparison shows 30 % lower emissions in the North Sea and 20 % lower emissions in the Baltic Sea for MoSES. This discrepancy is explained by a lower fuel sulfur content that is applied to distillate fuels in MoSES, which is used by approximately 60 % of the number of ships, sailing in the area. The calculated average for the FSC was determined at 0.08% in the MoSES inventory. Since the STEAM model assumes a FSC of 0.1 % for all oil-based fuel types (SECA limit), the observed difference in SO<sub>2</sub> emissions corresponds to the 20 % difference in FSC. In this respect, an uncertainty in the actual FSC, introduced by ships non-compliant to the sulfur regulations, is noteworthy. Since ships burning non-compliant fuel in a declared SECA can easily have 35 times higher sulfur emissions and the number of non-compliant ships is unclear, the correct FSC to be applied remains uncertain. However, most of these breaches of law might occur close to SECA borders in the North Sea and the English Channel.

The calculation of sulfate with MoSES using  $EF_{SO_4a}$  results in emission totals being 6–7 times lower than the sulfate emissions reported by STEAM. On the one hand, this is due to the lower average FSC, as mentioned for SO<sub>2</sub>. On the other hand,  $EF_{SO_4a}$  yields a sulfur to sulfate conversion rate for low-sulfur fuels, which is lower than the often applied 2–5 % for high-sulfur fuels (see Eq. 3.7 for details, Petzold

et al. (2010)). Thus, SO<sub>4</sub> emission totals of MoSES are significantly smaller than those of STEAM, which uses a conversion rate of 5.2 %.

#### 3.2.4.4. NO<sub>x</sub>

For comparison, all NO<sub>x</sub> emissions were considered as NO equivalents. Relatively small differences are found between the emission inventories of the two models, i.e., 20 % fewer emissions for the North Sea and 10–15 % fewer emissions with MoSES for the Baltic Sea. The slightly smaller amount in MoSES is explained by the lower power consumption and different applied NO<sub>x</sub> emission factors. While the EF for NO<sub>x</sub> in STEAM is based on the limit value requirements of IMO's Annex VI, which regulates the total weighted cycle emission limit, EF<sub>NO<sub>x</sub>a</sub> applied in MoSES is based on test-bed measurements implemented on ships by Germanischer Lloyd. For ships built prior to the year 2000, no NO<sub>x</sub> regulations apply and emission factors are even more unclear; this is even more true when considering an effect of engine aging, which is in MoSES not considered for NO<sub>x</sub> emissions.

In conclusion, it could be shown that ship emission inventories and shipping activity modeled with MoSES agrees well with ship emissions gleaned from the established STEAM model, considering the uncertainties discussed in previous sections. Differences occur due to the use of different EFs, differences in the calculation of ship power consumption, and other parameters under discussion as the fuel sulfur content.

#### 3.2.5. Uncertainty and Sensitivity Studies

As already seen in Sect. 3.2.4, in ship emission modeling, a large uncertainty is afflicted with the choice of EFs, since they directly affect calculated emissions. This is particularly true for the pollutants that compose PM, as their amounts vary significantly between studies due to differences in methodology, sampling and analysis techniques (IMO, 2014). One of the strengths of MoSES is its flexibility in applied EFs. To have an impression of the associated uncertainty, emissions were calculated using different EFs than the ones used in Sect. 3.2.3.1. The modeling was conducted for January and July to cover the seasonal effects. As previously described, two methods for the estimation of a ship's SFOC are currently implemented, one from Zeretzke (2013) and one from the 3rd IMO GHGS. The difference between both methods can be demonstrated by means of SO<sub>2</sub> and CO<sub>2</sub>, with 8 % higher emissions obtained with the SFOCs from the 3rd IMO GHGS.

The biggest differences due to a change of EFs were found for the components of particulate matter. EF<sub>SO<sub>4</sub>a</sub> results in 80 % fewer sulfate emissions compared to EF<sub>SO<sub>4</sub>b</sub>, and the former assumes a sulfur to sulfate conversion rate of 2 %. Since the majority of the model domain is located in the European SECA, ships are obliged to run on low-sulfur fuels. The FSC dependency of EF<sub>SO<sub>4</sub>a</sub> results in a sulfur-to-sulfate conversion rate much lower than 2 %. For black carbon, the difference between the implemented EF<sub>BCa</sub> and EF<sub>BCb</sub> is small, with 5 % higher emissions using the former. In contrast, a comparison of EF<sub>POAa</sub> and EF<sub>POAb</sub> results in 100 % higher emissions with the latter. The comparison of EF<sub>MAa</sub> shows 80 % lower emissions compared to EF<sub>MAb</sub> and 94 % compared to EF<sub>MAc</sub>. The reason for this is the consideration of the FSC in EF<sub>MAa</sub>.

The results reflect the previously mentioned high level of uncertainties for particle emissions, which are introduced by the applied EFs. However, it should be noted that some methods in use may neglect dependencies that are important for accurate predictions or are outdated because they are based on high sulfur fuels.

Although the quality of available input data for ship emission modeling improved significantly after the introduction of the AIS, many uncertainties originating from these data remain, as already discussed by Jalkanen et al. (2014). While smaller temporal gaps without recorded AIS data can be interpolated by algorithms, large data gaps can seriously distort the model results. Erroneous coordinates can usually be filtered out, while an uncertainty remains when wrong coordinates are introduced due to wrongly transmitted IMO or MMSI number. AIS signals belonging to airplanes or hovercrafts in the maritime environment, which are equipped with an AIS transmitter, can introduce unreasonably high velocities to the AIS data. These must be excluded from the calculation to avoid unreasonably high emissions. At

the domain boundaries, emissions can accumulate due to emission calculation between the pre-exit and post-entering signal of the ship. In particular, small domains with a long modeling time frame are prone to this error. The magnitude of this error can be reduced by specifying a temporal threshold that inhibits emission calculation if the interval between two consecutive AIS signals is too long. For the model run presented herein, this interval was set to 48 hours. It is noteworthy that this method also interferes with large temporal data gaps occurring inside the domain. Wind and waves exerting force on a sailing ship can increase or decrease its fuel consumption. Based on studies by Jalkanen et al. (2009) and Huang et al. (2018) the introduced error during ship emission modeling is in the range of  $\pm 2$  %, when creating emission inventories for large regions, as the North and Baltic Sea. Because the improvements in emission calculations are most likely small and the amount of additional data needed is large, MoSES does not consider effects of wind and waves.

An uncertainty due to a lack of ship characteristics data is almost inevitable in ship emission modeling. As shown in Table 3.4, the percentage of ships with missing quantities that are crucial for emission calculation is more than 60 %. The majority of these ships are considered to be small. In contrast, for only 6 % of ships with an assigned IMO number the engine power had to be estimated. In Sect. 3.1.4, several methods were introduced to derive missing ship characteristics based on available data. To get an estimate of the error that is associated with this procedure, uncertainty studies were performed for the ship attributes describing main and auxiliary engine power, main engine RPM, service speed and gross tonnage. Emission inventories were calculated for January and July 2015, with the values of estimated ship attributes set to the lower or upper limit of a 95 %, 50 % and 25 % prediction band. The calculation of these limits was based on a linear approximation described in Bates and Watts (2007). Error propagation was considered for ship attributes that depend on estimated input data. Since it is unreasonable for any ship characteristics to be  $\leq 0$ , the lower uncertainty limit for the estimation was restricted at 1. In general, a higher fraction of ship characteristics had to be estimated for July due to the increased number of small pleasurecrafts in summer, mentioned in Sect. 3.2.3.1. These small crafts are less often recorded in a database and thus, less information about them is available.

The error shown in Table 3.4 is cumulative since the gross tonnage is the basis for engine power estimation, and this is used in turn for most other attributes. Since data about auxiliary engines is scarce, a large uncertainty is inherent to their emissions. The uncertainty due to estimating the main engine RPM and the service speed is in comparison small, as these do not directly influence the estimated power consumption, and the estimation of the service speed is improved by including the vessel speed information contained in the AIS data. It is also noteworthy that an increase of the service speed decreases the engine load according to Eq. (3.5) and thus results in a lower approximated power consumption and emissions.

Since ship characteristics will not consistently be over- or underestimated, a second approach based on the calculated prediction bands was applied. The value of each estimated ship characteristic was distributed randomly in the range of the prediction band limits according to the probability of a modified normal distribution (R. Norm.). The normal distribution was modified in the respect that it had to be cut-off for the lower limits to avoid negative values for ship characteristics. Consequently, the outcome was not symmetrical. A general increase of up to 20 % of the calculated CO<sub>2</sub> emissions was the result. The sensitivity of CO<sub>2</sub> emission calculation for the different estimated characteristics is shown in Table 3.4.

Table 3.4.: The percentage of ships for which an attribute was estimated with the lower and upper percentual uncertainty this ship attribute has on the calculation of CO<sub>2</sub> emissions. The values are given as an average of the months January and July.

Attribute	Dependencies	Prc. Est.	Upper Limit			Lower Limit			R. Norm.
			95 %	50 %	25 %	95 %	50 %	25 %	95 %
<i>GT</i>	—	60.78	+31 %	+17 %	+11 %	-12 %	-9 %	-6 %	+8 %
<i>P<sub>main</sub></i>	<i>GT</i>	61.72	+62 %	+28 %	+16 %	-14 %	-12 %	-8 %	+9 %
<i>P<sub>aux</sub></i>	<i>P<sub>main</sub></i>	96.08	+104 %	+75 %	+39 %	-30 %	-26 %	-19 %	+20 %
<i>RPM<sub>main</sub></i>	<i>P<sub>main</sub></i>	66.00	+62 %	+30 %	+18 %	-14 %	-9 %	-6 %	+9 %
<i>S<sub>max</sub></i>	<i>P<sub>main</sub></i>	86.74	+61 %	+23 %	+15 %	-13 %	-1 %	-3 %	+9 %

Another uncertainty in the modeling process are ships of the “Undefined” type, i.e., ships for which no type information is available. Usually, this lack of information is accompanied by missing ship characteristics, and the missing type makes the estimation less accurate. As a first indicator for choosing an appropriate estimation method, the assumption was made for these vessels to be rather small. The spatial distribution of “Undefined” ships in the emission inventory supports this assumption, as most activity has been found to be close to coastal regions, especially in the waters of Norway, Denmark, Germany, Netherlands and Belgium. Small ships usually do not sail far into the open sea, and smaller vessels sailing on rivers are usually not obliged to send an AIS signal, which may explain the small amount of data transmitted. To fill this knowledge gap, the estimation methods used for ship type “Fishing” were also applied to “Undefined” ships. From the IHS Markit 2020 data, it is evident that most fishing vessels are small, and it is assumed that this is a good approximation. A more quantitative indication for the size of “Undefined” ships could be obtained by evaluating the ship length data occasionally transmitted via AIS. Thus, an average from over 9000 ships yielded a length of 44 m, which corresponds to a gross tonnage of 562 when applying the appropriate fit function. This is in good agreement with the value of 500 GT used in the model for vessels that do transmit neither length nor gross tonnage.

### 3.3. Scenario Capability

The methods for scenario generation implemented in MoSES allow various adaptations of a previously generated shipping fleet. In particular, subsets of the modeled fleet can be created, which contain only the ship traffic on specific routes between harbors or other points of interest. Furthermore, a modeled shipping fleet can be examined and modified in terms of its composition, ship number, ship characteristics and movement parameters, e.g., gross tonnage, engine power, fuel type, speed and timestamp. Emission calculation with different EFs or rastering of the data with a specific temporal and spatial resolution can be done after the ship fleet is modified. The following scenarios are application examples of these implemented methods. They quantify the emissions of ships traveling between the five busiest harbors in the North/Baltic Sea and the English Channel and estimate emission savings due to a trade volume reduction between representative harbors of the European Mainland and the United Kingdom.

#### 3.3.1. Route Specific Sub-emission Inventories

For demonstrating the scenario capabilities of MoSES, sub-emission inventories were created for the ship traffic between the five busiest European ports in the model domain in 2015, according to Eurostat (2018). In descending cargo turnover these are Rotterdam, Antwerp, Hamburg, Bremerhaven and Felixstowe. They account in total for 5.1 % of the CO<sub>2</sub> emissions calculated for the North/Baltic Sea domain described in Sect. 3.2.2. Since the main shipping route to North Europe leads through the English Channel, the emissions resulting from the traffic between the mentioned harbors and this region was also determined. The total share of CO<sub>2</sub> emissions between the five busiest ports and the Channel could be quantified to 4.8 %. The breakdown of the CO<sub>2</sub> emission to routes between individual harbors or the English Channel can be found in Table 3.5. The amount of emissions determined between the five considered ports and the English Channel is in accordance with their rank as busiest container port; thus, Rotterdam has the highest share of emissions, followed by Antwerp, Hamburg, Bremerhaven and Felixstowe. The applied method is limited to direct routes between these harbors and is currently not able to consider ship routes with intermediate stops in other harbors. Additionally, a ship needs to spend more than 30 minutes in the harbor region before a route is counted. This avoids the wrong assignment of routes when ships sail closely past harbors, e.g., in rivers.

The ships traveling between the five harbors are predominantly freight ships, e.g., cargo/container ships and tankers with a size of approximately 5000 gross tons and above. In the traffic with the English Channel the ship size shifts to higher gross tonnages (Fig. 3.4).

Table 3.5.: Share in CO<sub>2</sub> emissions from ships sailing between the five busiest ports, the English Channel and all other implemented ports in the North/Baltic Sea region. The values cover both directions and are given as fraction of the total emissions in the model domain. Values that are not available or redundant are marked as “n.a.”.

	Rott.	Antw.	Hamb.	Bremh.	Felixs.	Engl. Chan.
Rott.	n.a.	1.93	0.66	0.28	0.38	2.03
Antw.	n.a.	n.a.	0.55	0.42	0.13	1.47
Hamb.	n.a.	n.a.	n.a.	0.14	0.13	0.47
Bremh.	n.a.	n.a.	n.a.	n.a.	0.03	0.31
Felixs.	n.a.	n.a.	n.a.	n.a.	n.a.	0.51
Other	12.13	10.3	4.56	3.03	1.42	17.74

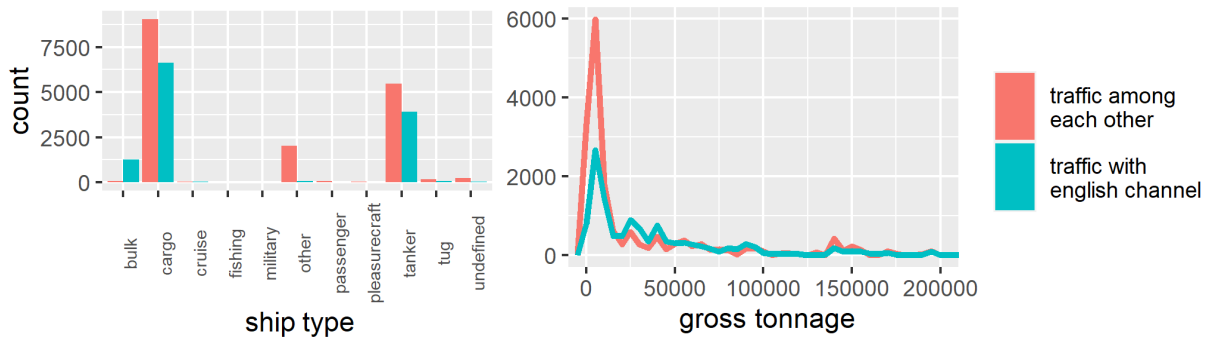


Figure 3.4.: Ship type and gross tonnage distribution of ships traveling between the five busiest ports in the North and Baltic Sea Region and the English Channel.

As shown in Table 3.5, the generation of sub-emission inventories can not only be done for the traffic between individual harbors or areas but also for a multitude. To demonstrate this, ship traffic emissions between the five busiest ports with each of the other 150 implemented ports in the domain were calculated (see Appendix A.1.8 for a list of implemented harbors). This was also done for the traffic to and from the English Channel, which could be held accountable for almost 18 % of the CO<sub>2</sub> emitted by ships in 2015, with a surplus of 4 % from ships entering the region.

### 3.3.2. Trade Volume Reduction Scenario

On the basis of the route-specific emission inventories created in the previous Sect. 3.3.1, an example scenario was created concerning a decreased cargo turnover between representative ports of the European Mainland and the United Kingdom. For this purpose, the traffic in 2015 between the relevant harbors, Rotterdam, Antwerp, Hamburg and Bremerhaven with Felixstowe, was considered. Almost 1300 different ships were found sailing on these routes, 91 % of which were cargo ships, 7 % were tankers, and the remaining 2 % were other ship types. To approximate the total trade volume, each trip between one of the four mentioned harbors with Felixstowe was counted and multiplied by the gross tonnage of the respective ship. Subsequently, ship routes from cargo ships and tankers were removed at random from the whole set of routes until a trade volume reduction of 10 %, 20 % and 30 % was obtained. The calculated CO<sub>2</sub> emissions of the reduced transport can be found in Table 3.6. It should be mentioned that the reported reductions consider only the ship-related emissions; emission reductions due to changed harbor activities are not captured by the applied method. The nonlinearity between the reduced trade volume and the corresponding emission decrease reflects the fuel-efficiency gain that is associated with larger cargo ships.

Table 3.6.: Reduction of trade volume and corresponding CO<sub>2</sub> emission reduction in an example scenario.

<b>Reduction of trade vol.</b>	<b>none</b>	<b>10 %</b>	<b>20 %</b>	<b>30 %</b>
CO <sub>2</sub> emissions [Gg]	355	308	268	221
Emission reduction	0 %	13 %	24 %	38 %

### 3.4. Conclusion

With this study, we introduced the flexible and modular ship emission model MoSES for emission inventories generation. The model contains various emission factors for 13 species, including the most recent emission factors for sulfate and black carbon. As a first application, a temporally and spatially high-resolved ship emission inventory for the North and Baltic Sea was modeled and evaluated in terms of total emissions, as well as for the contribution of individual ship types. Information about ship characteristics, e.g., fuel type, gross tonnage or engine power, is gathered or estimated during the modeling process and may be used for a statistical evaluation of the modeled shipping fleet. The model is independent of the region of interest, as long as the relevant AIS data is supplied. An interface to connect and query several databases for ship characteristics is provided. For the presented model, the IHS Markit 2020 database and an auxiliary database, which is created from the AIS data, were utilized. To cope with the occasional lack of ship characteristics that are important for emission calculation, parameterizations based on easier accessible quantities were derived.

To assess the quality of the modeled emission inventory, a comparison with ship emission data for the same region calculated with the STEAM model was carried out. A good agreement of both calculated shipping activities was found, although in general, fewer emissions were obtained due to differences in the power- and fuel consumption and emission factors.

Since implemented emission factors and methods for determining the specific fuel oil consumption (SFOC) of ships are changeable for each model run, this provides an opportunity for comparison. A difference of 8 % of CO<sub>2</sub> and SO<sub>2</sub> emissions was found when using different methods for determining the SFOC. The biggest differences by varying emission factors were found for sulfate and mineral ash emissions with up to 80 % and 100 %, respectively.

The frequent lack of knowledge about crucial ship characteristics encouraged an assessment of the associated uncertainty present in emission calculations. The sensitivity of the model to the ship characteristic estimation methods was determined within 95 %, 50 % and 25 % prediction bands for the parameterizations. For an 95 % prediction band, the error of the calculated CO<sub>2</sub> emissions due to ship characteristic estimation was determined to be +8 % for gross tonnage, +9 % for main engine power and +20 % for auxiliary engine power estimation.

Furthermore, the present model provides versatile functionality for scenario generation via a toolbox that can modify a modeled shipping fleet, created from AIS data. Thus, modifications are done in a way that remains close to realistic conditions, e.g., an increase in shipping will be expressed by new ships joining the fleet or existing ships sailing more often. The possibility of creating route-specific ship emission inventories is shown by an assessment of ship traffic and the resulting emissions between the five busiest harbors in the regions. Approximately 5.1 % of the CO<sub>2</sub> emissions in the North and Baltic Sea could be attributed to ship traffic between the five busiest harbors of the region, and 4.8 % could be attributed to the traffic between these five harbors and the English Channel. An example scenario, which combines the different implemented methods for scenario creation in MoSES, assesses the emission decrease due to a decreasing trade volume between the representative ports of the European mainland and the United Kingdom. This toolbox for scenario creation is currently used for studies about the effect of policies and new technologies on air quality, with a focus on emission abatement. The ship emission model will be embedded within a comprehensive emission model that is currently under development that will allow the combination of emissions from shipping with emissions from other sectors. MoSES was created to generate temporally and spatially highly resolved emission inventories. These emission inventories are typically used for air quality

### *3. Publication I: A Ship Emission Modeling System with Scenario Capabilities*

studies, considering atmospheric transport and chemical transformation, but may also be used, e.g. for the assessment of health or socioeconomic impacts. Continuing air quality studies, utilizing the generated emission inventory and considering future scenarios, are currently carried out.



## 4. Publication II: Future Ship Emission Scenarios with a Focus on Ammonia Fuel

The following chapter corresponds to a planned publication authored by:

*Daniel A. Schwarzkopf, Ronny Petrik, Josefine Hahn, Volker Matthias, Markus Quante.*

It is planned to be submitted to:

*Atmospheric Environment X.*

### Abstract

Current efforts by the International Maritime Organization (IMO) to decarbonize the shipping sector have gained momentum, although the exact path to achieve this goal is currently unclear. However, it can be safely assumed that alternative cleaner and zero-carbon fuels will be key components in a strategy. In this work, three ship emission scenarios for 2025, 2040 and 2050 were developed that cover the area of the North and Baltic Seas. They aim at a fundamental transition in the usage of marine fuels towards ammonia as the mainly used fuel in 2050, via an intermediate step in 2040 with liquefied natural gas as the main fuel. Additionally, expected trends and developments for the shipping sector were implemented, i.e., a fleet growth by vessel size and number. Efficiency improvements were included that are in accordance with the Energy Efficiency Design Index of the IMO. The scenarios were created using a novel method based on modifications to a virtual shipping fleet. The vessels in this fleet were subject to decommission and renewal cycles that adapt them to the scenario's target year. Emissions for this renewed shipping fleet were calculated with the Modular Ship Emission Modeling System (MoSES). With respect to ammonia engine technology, two cases were considered. The first case deals with compression-ignition engines and marine gas oil as pilot fuel, the second case treats spark-ignition engines and hydrogen as the pilot fuel. The first case is considered better feasible until 2050. Reductions with the first case in 2050 compared to 2015 were 40 % for CO<sub>2</sub> emissions. However, CO<sub>2</sub> equivalents were only reduced by 22 % with the difference mainly resulting from increased N<sub>2</sub>O emissions. NO<sub>x</sub> emissions were reduced by 39 %, different PM components and SO<sub>2</sub> between 73 % to 84 % for the same target year. The estimated NH<sub>3</sub> slip from ammonia-fueled ships in the North and Baltic Seas was calculated to be 930 Gg in 2050. For the second ammonia engine technology that is considered more advanced, emission reductions were generally stronger and ammonia emissions smaller.

### Acknowledgements

This research was supported by the BSH funded project “SeAir” (BSH contract code: 10042629, Hereon contract code: 430/2018).

### 4.1. Methodology

#### 4.1.1. Reference Emission Inventory

The reference ship emission inventory that was the basis for the scenario emission inventories (EIs) was generated using the bottom-up approach of the MoSES model. Details about the model and emission factors (EFs) applied can be found in Schwarzkopf et al. (2021). The reference EI, is based on North and Baltic Sea AIS data for the year 2015, compiled by the European Maritime Safety Agency (EMSA). The

vessel characteristics required for the emissions calculation were either used from the IHS Markit 2020 database or extracted from the AIS data. Missing data were estimated with the ship type-specific methods implemented in the MoSES model. The computational domain of the EI was located in northern Europe and ranged from 48.32°N to 68.37°N and 5°W to 31.41°E. The resolution of the gridded EI was 0.069° in east–west and 0.036° in north–south direction. This corresponded to approximately 4 km. In addition to the EI, a virtual shipping fleet was generated from the AIS data. This virtual fleet compiles vessel movements, the respective ship characteristics, the emissions and the energy consumed.

#### 4.1.2. Scenario Generation

In analogy to the reference EI, the scenario EIs were generated using a bottom-up approach. However, the data basis is not the AIS data, but rather a modified version of the virtual shipping fleet that was produced alongside the reference EI for 2015. The scenario EIs for the years 2025, 2040 and 2050 cover the same domain and have the same resolution as the reference EI.

The modified virtual shipping fleets for the scenarios were created using a scenario creation toolbox implemented in the MoSES model and a novel, general approach that is based on physical fleet developments. The underlying data and steps of this approach can be adjusted and individually executed to provide a flexibility for the scenario generation by a modified shipping fleet. In this work, a virtual fleet was renewed by implementing changes to vessels that reflect currently foreseeable legislation, trends in fleet development and technological advances. The projections distinguish between six of the 11 ship types considered in MoSES, namely “Bulk”, “Cargo”, “Cruise”, “Passenger”, “Tanker” and “Other”. The ship type “Tugs” was included in the category “Other”, because no specific data were available. Due to lack of data, no changes were made for ships of type “Fishing”, “Military”, “Pleasurecraft”, and for ships whose type could not be determined (“Undefined”). The exclusion of fleet developments for the latter three ship types was justified by their small contribution to total emissions, which for CO<sub>2</sub> was determined to be 1.8 % for fishing vessels, 0.2 % for pleasurecrafts and 1 % for undefined vessels.

In the first step of scenario creation, all ships that had exceeded the average lifetime for their respective ship type in the target year of the scenario were identified. Estimates for the average lifetime from Winnes et al. (2016a) were used and are shown in Table 4.1. All ships identified in this regard were “renewed”, which means they were modified in several ways, these are as follows. First, the year of build of a ship was incremented by the life-cycle expectations of its type. This ensured that the EFs complied with the respective regulations when the emissions were recalculated. In particular for NO<sub>x</sub> emissions this was important, because in the North and Baltic Seas ships must comply with the NO<sub>x</sub> Tiers set by the IMO (IMO MEPC, 2008a, 2014).

To account for trends in shipbuilding, the capacity of the renewed vessel was increased by up-scaling their gross tonnage. Likewise, the ship engine size was increased. The capacity increase followed the data from Fridell et al. (2016), which are shown in Table 4.1. Since the values in Table 4.1 refer to an average capacity increase of the entire fleet, an effective capacity increase factor ( $c_{eff}$ ) was determined for each scenario and ship type based on the ships available for renewal and their summed capacity in gross tons ( $c_{avail}$ ). The factor  $c_{eff}$  was calculated using equation 4.1 to cover the average capacity growth of the entire fleet with the vessels available for renewal,

$$c_{eff} = (c_{tot} \cdot c_{rel}) / c_{avail} + 1. \quad (4.1)$$

The relative capacity as a fraction  $c_{rel}$  is shown in Table 4.1 as percentage and  $c_{tot}$  is the total capacity in gross tons of the entire shipping fleet.

The up-scaling of engine power for “renewed” ships was performed using the ship-type specific estimation models described in Schwarzkopf et al. (2021). These were used to scale main engine power using the gross tonnage and the auxiliary engine power using main engine power. In addition, a weighting factor was calculated when actual engine performance data was available from a database for the respective vessels. The weighting factor was determined as the ratio between the actual engine power and the estimated engine power from the respective estimation model. It was applied during the up-scaling procedure to preserve information from the database and reduces the error from the estimation model. In addition, an

Table 4.1.: Increase in number of ships and capacity increase in percent for all three scenarios, based on Fridell et al. (2016). Annual efficiency increases based on IMO Energy Efficiency Design Index and average ship lifetimes from Winnes et al. (2016a) for the ship types considered.

Ship type / Year	Ship number incr. [%]			Capacity incr. [%]			Eff. incr. [%] annual	Lifetime [y]
	2025	2040	2050	2025	2040	2050		
Bulk	2	5.1	7.2	5.1	12.5	19.1	0.99	19
Cargo <sup>a</sup>	8.3	22.2	11.0	10.9	26.9	37.9	0.82	26
Cruise	10.5	28.2	41.6	4.6	9.9	12.2	0.74	27
Passenger	12.1	30.8	43.1	13.8	35.4	48.1	0.69	27
Tanker	12.7	34.7	51.8	22.5	64.9	101.0	0.73	26
Other	4.6	9.9	12.2	4.6	9.9	12.2	0.69	25

<sup>a</sup> For the ship type Cargo, the sum for container and general cargo ships was used, weighted by the ship type distribution, according to the UNCTAD Report 2020.

efficiency coefficient  $e$  was introduced for each ship with  $0 < e \leq 1$  that is in accordance to the IMO Energy Efficiency Design Index (EEDI) and directly affected the calculated energy consumption,

$$E = EL \cdot P_{tot} \cdot \Delta t \cdot e \quad (4.2)$$

In Equation (4.2),  $E$  is the energy consumption of the ship,  $EL$  is the engine load,  $P_{tot}$  the ship's engine power, either for main or auxiliary engines, and  $\Delta t$  a time interval. The efficiency factor for a ship was calculated individually for each ship, depending on the annual efficiency increase and the number of years valid for an efficiency increase (i.e. EEDI measures are valid from 2013 and no efficiency increase is considered after 2040). The annual efficiency increase data can be found in Table 4.1.

If needed, a scenario shipping fleet could be created in multiple renewal cycles. For the scenarios presented, one cycle was run for the 2025 shipping fleet, two cycles were run for 2040 and three for 2050. The number of required cycles should be oriented to the average ship lifetime divided by the difference in years between the year of the target scenario and the year of the reference shipping fleet. However, for the present scenarios, intervals smaller (10–15 years) than the average vessel lifetimes (19–27 years) were chosen to implement a trend towards a generally newer fleet. This was considered plausible, as future technological advances will encourage the construction of new ships.

The next steps in the scenario building process involved a projected distribution of fuel types according to their share of total ship energy consumption. The respective shares of fuel types were chosen according to the Engine Use and Transitions Scenario 11 of DNV-GL (2020), which considers a reduction of CO<sub>2</sub> emissions from global shipping by 50% in 2050 compared to 2008. The corresponding data for this are shown in Table 4.2. This scenario projects a transition to ammonia as the primary fuel in 2050 over LNG as the most common fuel in 2040. Biodiesels are included here among the distillate fuels.

Table 4.2.: Percentage of energy consumption by fuel type for the reference emissions inventory (2015) and the three scenarios created (2025, 2040, 2050), according to DNV-GL (2020).

Fuel type / Year	2015	2025	2040	2050
Residual fuel	14.97	12.75	10	1
Distillate fuel	83.93	73.75	22	23
LNG	1.19	13.5	57	33
MeOH	0.05	0	1	2
NH <sub>3</sub>	0	0	10	40

In order to distribute the fuel types accordingly, it was first necessary to use MoSES to calculate the total energy consumption for each individual ship and for the entire fleet of ships. Subsequently, the fuel

used by each ship in the virtual fleet was changed until the desired energy share was achieved. Where possible, the original fuel types were retained and newer technologies such as LNG and, in particular, methanol and ammonia were preferred for ships of a more recent build. The MoSES model is then used to calculate the emissions of each vessel in the renewed virtual fleet based on up-scaled engine power, efficiency improvements, applicable regulations, and redistributed fuel types. To produce the EIs, the calculated emissions were rastered to predefined hourly grids. Details of the associated procedure and the applied EFs for the traditional fossil fuel oil are described in Schwarzkopf et al. (2021). The emission values for LNG and methanol engines were analogous to those in the Fourth IMO GHG Study. EFs for ammonia engines are based on estimates and preliminary results by Ntziachristos et al. from the Laboratory of Applied Thermodynamics of the University of Thessaloniki and are shown in Table 4.3 (Westlye et al., 2013; Laval et al., 2020).

Two cases for ammonia technology were distinguished. The first case is referred to as “uncontrolled” and assumes a compression-ignition engine with marine gas oil (MGO) as pilot fuel. This technology leaves fossil fuel emissions per kWh that are equivalent to about 20% of the emissions from traditional marine diesel engines fueled solely by MGO. The second case is referred to as “controlled” and involves a spark-ignition engine using hydrogen as the pilot fuel.

Table 4.3.: Emission factors (EFs) for ammonia-fueled engines for an “uncontrolled” case describing a compression-ignition engine using marine gas oil as pilot fuel and a “controlled” case describing a spark ignition engine using hydrogen as pilot fuel. The EFs are based on preliminary results from Ntziachristos et al. from the Laboratory of Applied Thermodynamics of the University of Thessaloniki.

<b>Emission Species</b>	<b>EF [g/kWh] uncontrolled</b>	<b>EF [g/kWh] controlled</b>
CO <sub>2</sub>	110	0
CO	0.09	0
SO <sub>2</sub>	0.065	0
SO <sub>4</sub> <sup>b</sup>	0.0013	0
PM	0.036	0
NO <sub>x</sub>	10	3 <sup>c</sup>
N <sub>2</sub> O	0.778	0.015
NH <sub>3</sub>	31.2	1.17

<sup>b</sup> For this EF, 2% of SO<sub>2</sub> emissions are assumed. <sup>c</sup> This EF considers the application of selective catalytic reduction (SCR) or exhaust gas recirculation (EGR)

A final step in scenario building concerned a trend towards an increasing number of ships. Since it was difficult to predict on which shipping routes and in which areas in the North Sea and Baltic Sea more ships will be needed and used in the future, a uniform approach was chosen to reflect this development. For this purpose, the energy consumption and emissions were increased according to the projections for an increasing ship number by Kalli et al. (2013), as shown in Table 4.1

## 4.2. Discussion of Scenario Emission Inventories

In the following section, the observed emission trends in the created scenarios are explained, starting from the reference year 2015 to the three scenario years 2025, 2040 and 2050. Furthermore, a distinction is made between the “uncontrolled” and “controlled” cases, which refer to the ammonia engine technology used. However, in view of current developments, an application of the technology considered in the uncontrolled case seems more plausible for the year 2050. The technology considered in the controlled case can presumably be expected to emerge temporally after the uncontrolled case (de Vries, 2019). For the uncontrolled case, the evolution of total emission levels for the scenario years considered are shown in Fig. 4.1. For the emission species that differ compared to the controlled case, the developments are shown in Fig. 4.2.

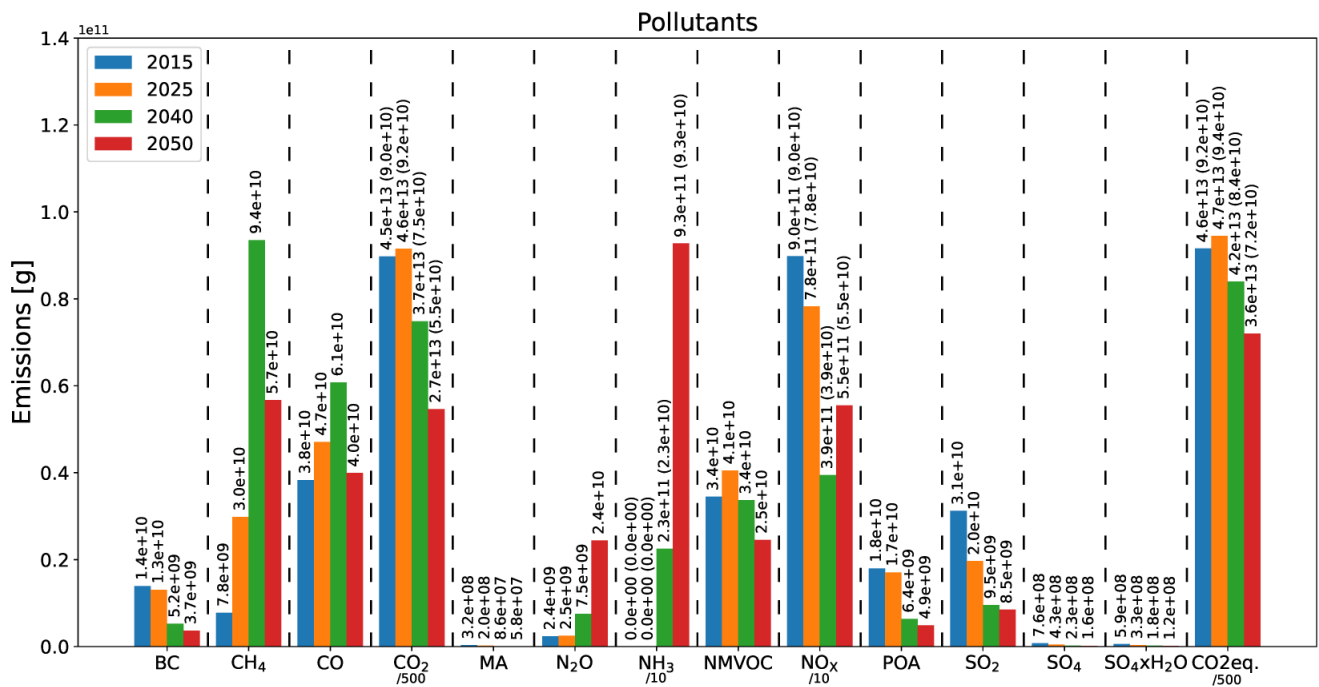


Figure 4.1.: Development of total annual emissions from 2015 to 2050 in the North and Baltic Sea domain. For NH<sub>3</sub>-powered engines a compression-ignition engine with marine diesel oil as pilot fuel is considered, which is referred to as the “uncontrolled” case. Values for CO<sub>2</sub> were divided by 500, for NH<sub>3</sub> by 5, for NO<sub>x</sub> by 10, and for CO<sub>2</sub> equivalents by 500 to fit the scale.

The modeled scenarios assume a broad fuel transition to ammonia by 2050 to meet the decarbonization targets set by the IMO. This transition is planned to proceed via LNG as the main ship fuel used in 2040. Emissions were generally reduced by the IMO’s EEDI measures that required an increasing efficiency of new ship generations built from the beginning of 2013. An offsetting effect to the increased efficiency came from the growing number and size of ships (the latter going in hand with higher engine power) to meet the demands of global trade.

#### 4.2.1. CO<sub>2</sub> Emissions

Compared to 2015, CO<sub>2</sub> emissions in the uncontrolled case were modeled to increase by 2% in 2025, decrease by 18% in 2040 and by 40% in 2050 (Fig. 4.1). In the controlled case a CO<sub>2</sub> reduction of 47% could be achieved from 2015 to 2050 (Fig. 4.2). The increase of CO<sub>2</sub> emissions by 2025 was based on fleet growth trends by vessel size and number. These trends outweighed the lower CO<sub>2</sub> emissions from LNG-fueled ships (approximately 13% lower CO<sub>2</sub> emissions per gram of fuel, versus residual and distillate fuels), which were increasing in number until 2025 (IMO, 2020). In the 2040 scenario, a higher percentage of ships used LNG as a bridging technology (57%). In addition, it was assumed that 10% of ships will use ammonia as fuel. In the uncontrolled case, CO<sub>2</sub> emissions from ships using NH<sub>3</sub> as fuel were not zero but reduced by approximately 83%, compared to traditional marine engines powered by fuel oil. In the controlled case, CO<sub>2</sub> emissions are truly carbon-free due to the use of hydrogen as pilot fuel. Both effects together led to a trend reversal and an overall decrease in CO<sub>2</sub> emissions. For the 2050 scenario, 40% of the energy demands in shipping were projected to be met by ammonia, resulting in further reductions in CO<sub>2</sub> emissions.

The designated target of the IMO is a reduction of CO<sub>2</sub> emissions from global shipping by at least 50% in 2050 compared to 2008 (IMO MEPC, 2018b). The CO<sub>2</sub> reductions in the uncontrolled case of this study were short of 10 percentage points (40% CO<sub>2</sub> decrease) to achieve the IMO target. In the controlled case, CO<sub>2</sub> reductions were only short of 3 percentage points (47% CO<sub>2</sub> decrease). For achieving a reduction of 50%, differences in CO<sub>2</sub> emissions need to be compensated, e.g., by processes such as Carbon Capture

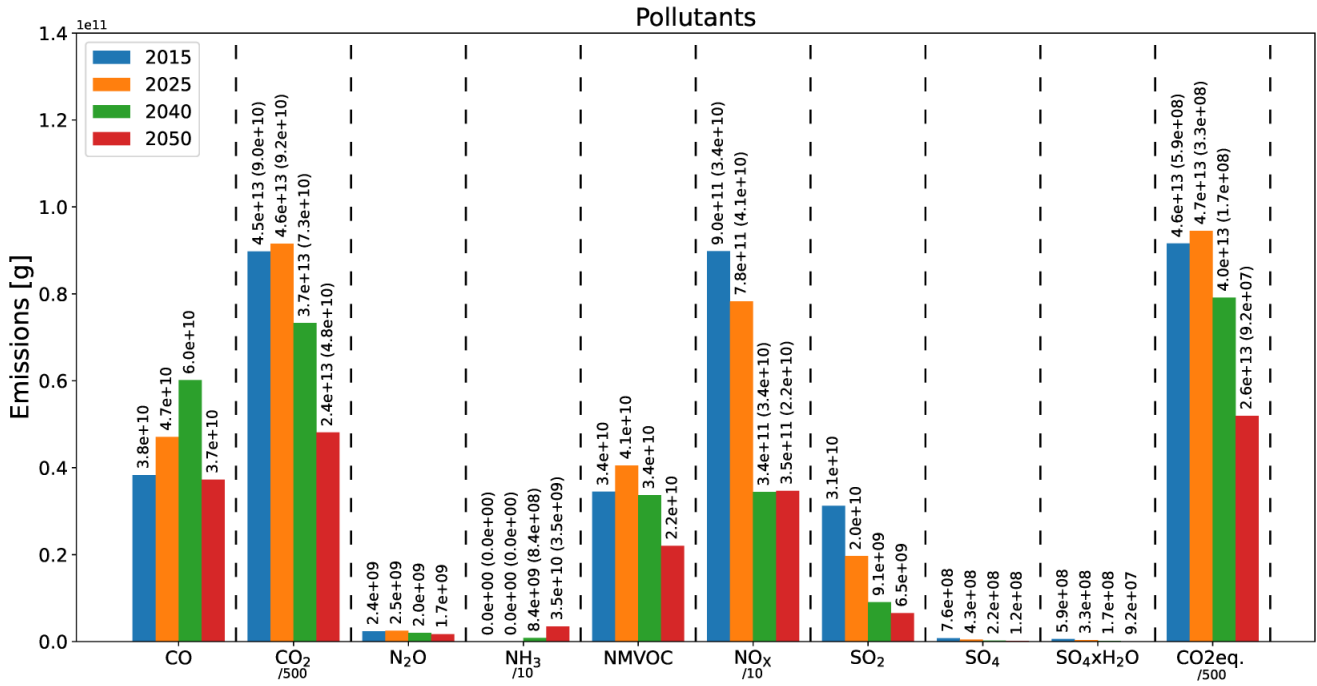


Figure 4.2.: Development of total annual emissions from 2015 to 2050 in the North and Baltic Sea domain. For NH<sub>3</sub>-powered engines a spark-ignition engine with hydrogen as pilot fuel is considered, which is referred to as the “controlled” case. The figure shows only emission species whose development is different in the controlled case than in the uncontrolled case. Values for CO<sub>2</sub> were divided by 500, for NH<sub>3</sub> by 10, for NO<sub>x</sub> by 10 and for CO<sub>2</sub> equivalents by 500 to fit the scale.

and Storage during fuel production, which were not considered here. Furthermore, this study compares the CO<sub>2</sub> reductions between the years 2050 and 2015. However, results from Kalli et al. (2013) suggest that the total CO<sub>2</sub> emissions in the North and Baltic Seas SECA region varied only little between the years 2009 and 2015. Thus, a comparison between the years 2050 and 2008 might be similar to the results presented here.

The spatially distributed CO<sub>2</sub> emission fluxes [ $\text{g} \cdot \text{m}^{-2} \cdot \text{year}^{-1}$ ] of the reference EI for 2015 on a logarithmic scale are shown in Figure 4.3 (a). Figures 4.3 (b)–(d) show the percent change in CO<sub>2</sub> emissions for the three future scenarios, compared to the reference EI. In particular, in Figure 4.3 (b), the characteristics of the scenario-building method are visible from the differences in percentage CO<sub>2</sub> reductions. In 2025, CO<sub>2</sub> reductions were still small compared to 2015. In some areas, especially in domestic and coastal regions and in the North Sea between Scotland and Norway, no change or even an increase of CO<sub>2</sub> emissions could be observed. These observations could be attributed to fishing vessels and pleasurecrafts as well as vessels whose type could not be determined. All these ships usually sail near the coast and due to a lack of data they were not changed in the scenario shipping fleets. A similar observation was made for regions and routes on which mainly newer ships were deployed, as these were not renewed for the 2025 scenario fleet. Nevertheless, in these areas and on these routes, the number of ships was increased and accordingly the emissions compared to 2015. However, overall emissions in these regions were generally low. In 2040 and 2050, a significant decrease in CO<sub>2</sub> is clearly visible along the main shipping routes in the English Channel, along the northern European coastline and in the Baltic Sea (Figures 4.3 (c) and (d)).

#### 4.2.2. Methane Emissions

Emissions of methane increase by 61 % from 2015 to 2025. They peaked in 2040 by an increase of 1105 % and were still increased by 631 % in 2050, compared to 2015. The reason for this was the increasing number of LNG-fueled ships. LNG-fueled marine engines can leak unburned methane, which is known as methane slip, which is responsible for the largest part of CH<sub>4</sub> emissions. To effectively reduce the GHG emissions

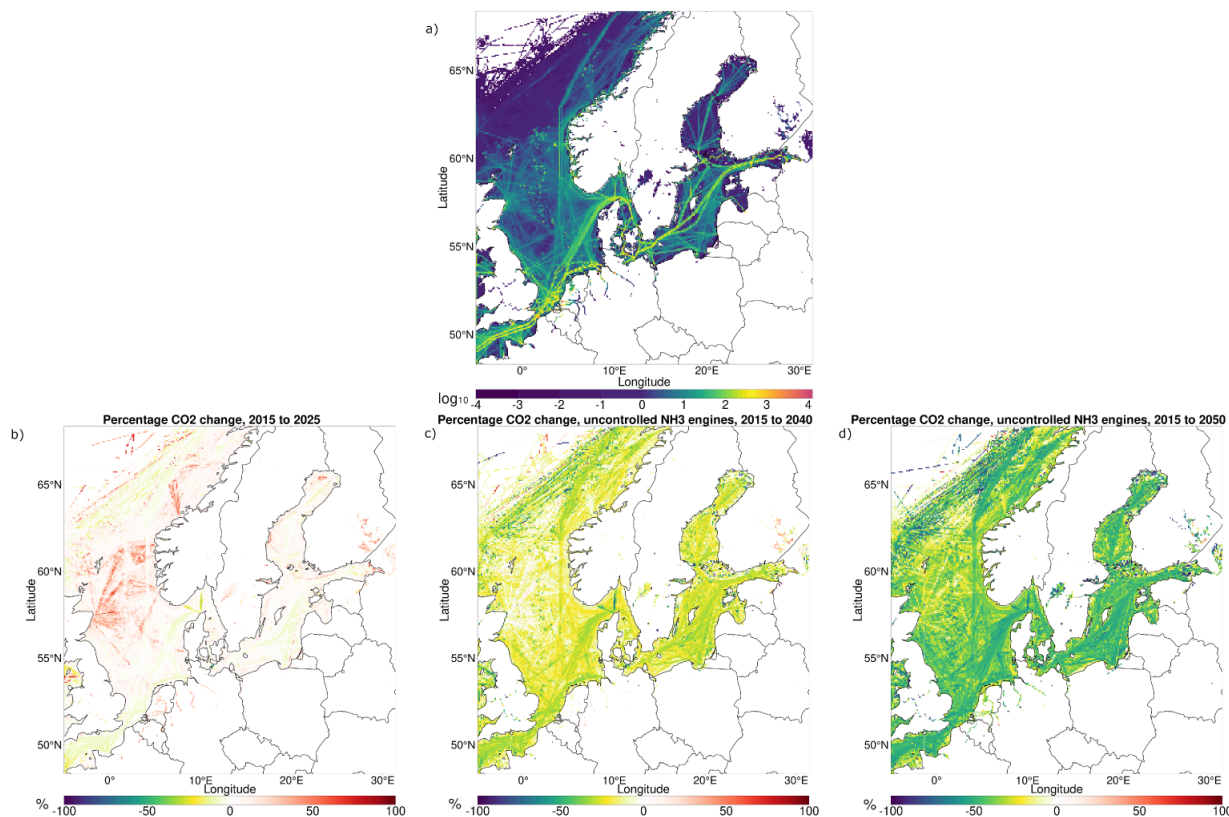


Figure 4.3.: CO<sub>2</sub> emission fluxes in  $[g \cdot m^{-2} \cdot year^{-1}]$  from the reference emission inventory (2015, **a**) and the percentage change from the scenario emission inventories for the years 2025 (**b**), 2040 (**c**), and 2050 (**d**), compared to the reference.

from the shipping sector, this must be carefully considered, as the global warming potential (GWP) of methane is 25 CO<sub>2</sub> equivalents (Forster et al., 2007) and can outweigh the savings in CO<sub>2</sub> emissions.

This could impede the ambitious GHG reduction targets and demonstrates the need for discerning control that targets methane slip from LNG-fueled ships. Therefore, this topic was included in the list of candidate short-term measures of the IMO's GHG reduction strategy (IMO MEPC, 2018b). In addition, at the COP26 climate summit, more than 100 countries pledged to reduce methane emissions (EU, 2021).

### 4.2.3. N<sub>2</sub>O Emissions

The third important GHG emitted by ships is nitrous oxide (N<sub>2</sub>O). Similar to NO<sub>x</sub>, nitrous oxide is a byproduct in internal combustion engines that forms from the air that is injected into the cylinders. The use of ammonia as a marine fuel can increase emissions of N<sub>2</sub>O due to additional nitrogen from ammonia combustion. Nitrous oxide is very potent as a greenhouse gas with a GWP of 298 CO<sub>2</sub> equivalents (Forster et al., 2007). Nitrous oxide was projected to increase by 4% in the 2025 scenario due to the implemented fleet growth. In the uncontrolled case for the 2040 scenario a 213% increase in N<sub>2</sub>O emissions was estimated compared to 2015 due to the deployment of the first ammonia-fueled ships (Fig. 4.1). In 2050, a 900% increase was estimated compared to 2015. A reduction of nitrous oxide emissions by a different engine technology or through better control of the combustion process might be possible. This is reflected by the calculations for the controlled case, which projects a reduction of nitrous oxide emissions by only 17% in the 2040 scenario and by 29% in 2050 with respect to 2015 (Fig. 4.2).

### 4.2.4. CO<sub>2</sub> Equivalent Emissions

The effect of the scenario projections on the development of total GHG emissions is illustrated by means of their CO<sub>2</sub> equivalents in Figures 4.1 and 4.2. From 2015 to 2025 CO<sub>2</sub> equivalents were modeled to increase

by 2%. Compared to 2015 CO<sub>2</sub> equivalents in 2040 were reduced by 9% in the uncontrolled case and 13% in the controlled case. In the 2050 scenario the reductions were 22% and 44%, respectively. Besides CO<sub>2</sub>, methane and nitrous oxide were considered for the calculation of CO<sub>2</sub> equivalents. An additional consideration of BC with a 100 year GWP of 900 in the calculation of CO<sub>2</sub> equivalents (IMO, 2020) significantly increased the reductions due to a decreased use of fuel oils. In the uncontrolled case, changes in CO<sub>2</sub> equivalent emissions, including BC, were +0.2% in 2025, -20% in 2040 and -31% in 2050. In the controlled case, these changes were also +0.2% in 2025, -24% in 2040 and -50% in 2050. These results show the significant differences in overall GHG reductions between the NH<sub>3</sub>-engine technologies used. In the controlled scenario for 2050, only 7% of the reduction potential could be attributed to CO<sub>2</sub> without considering the GWP of BC. The major part of 15% could be achieved by a better control of nitrous oxide. A greater reduction potential of 15% was associated with nitrous oxide, which is accessible by a better control of N<sub>2</sub>O emissions. These results suggest not only CO<sub>2</sub> is important in future legislation that aims at reducing GHG emissions in the shipping sector. Especially emissions of N<sub>2</sub>O need to be included in future regulation measures if a transition towards ammonia as a more climate-friendly fuel is to succeed. The results also highlight the significant contribution of BC to CO<sub>2</sub> equivalent emissions from ships, which can be easily reduced by transitioning to cleaner and carbon-free fuels.

#### 4.2.5. NO<sub>x</sub> Emissions

Nitrogen oxide emissions decreased by 13% in the 2025 scenario compared to 2015 (Figures 4.1 and 4.2), primarily due to MARPOL Annex VI NO<sub>x</sub> control requirements and the implementation of an NECA in the North and Baltic Seas (IMO MEPC, 1997, 2016). Accordingly, ships that were renewed during the scenario generation had a more recent year of build and thus needed to comply to stricter emission limits. In addition, the higher number of LNG-fueled ships reduced total NO<sub>x</sub> emissions, as they generally emit less NO<sub>x</sub> and often even have emissions below the limits of the IMO Tier III Regulation. In 2040 the number of new built ships, that had to comply with the NECA regulations, increased. In addition, the share of energy consumed by LNG-fueled vessels increased significantly by 57% compared to 2015. For ammonia-fueled ships the amount of NO<sub>x</sub> emissions also depends on the technology used and is different for the uncontrolled and controlled cases. The NO<sub>x</sub> EFs for the uncontrolled case were about equal to the Tier II limits, which resulted in a 39% NO<sub>x</sub> emissions decrease in the 2050 scenario, compared to 2015. Compared to the 2040 scenario this represented an increase by 41%. The NO<sub>x</sub> EFs for the controlled case were in the magnitude of the Tier III limits. This resulted in a NO<sub>x</sub> reduction of 62% in the 2040 scenario and of 61% in the 2050 scenario, compared to 2015. In this context, it should be noted that NO<sub>x</sub> emissions from ammonia-fueled engines could be further reduced through the application of selective catalytic reduction (SCR) or exhaust gas recirculation (EGR) technologies (Mounaïm-Rousselle and Brequigny, 2020).

#### 4.2.6. Particulate Matter and SO<sub>2</sub> Emissions

The reduced use of conventional oil-based fuels in marine engines also led to a reduction in particulate emissions. Particulate matter in ship emissions consists of black carbon (BC), mineral ash (MA), primary organic aerosols (POAs), sulfate (SO<sub>4</sub>) and water associated with sulfate (SO<sub>4</sub> × H<sub>2</sub>O), which were projected to be reduced between 73% and 84% in the 2050 uncontrolled scenario (Fig. 4.1). Slightly higher reductions were expected in the controlled case (Fig. 4.2). SO<sub>2</sub> emissions are reduced analogously. In the 2025 scenario, the reductions were mainly based on the shift from DF to LNG, since LNG generally produces fewer particles in burning and contains very little sulfur. In the 2025 scenario, the reductions were mainly due to the switch from DF to LNG, which produces fewer particulates when burned. This is also attributable to its lower sulfur content. In the 2040 and 2050 scenarios, particulate emissions were further reduced due to the continued increase in the share of LNG and NH<sub>3</sub>-fueled ships. In the controlled case, emissions from ammonia combustion could be considered nearly free of primary particulates.



#### 4.2.7. CO and NMVOC Emissions

Non-methane volatile organic compounds (NMVOC) and CO emissions increased by 21 % and 24 %, respectively, in the 2025 scenario compared to 2015 (Figures 4.1 and 4.2). The amount of NMVOC emissions from marine diesel engines and LNG-fueled ships is of a comparable magnitude. However, carbon monoxide emissions are higher for LNG-fueled vessels. For this reason, CO emissions increased further for the 2040 scenario, alongside the increasing number of LNG-powered ships. For this reason, CO emissions continued to rise in the 2040 scenario, analogously to the increasing number of LNG-fueled ships. For the uncontrolled and controlled case, NMVOC emissions were at similar levels in the 2040 scenario as in 2015, as additional emissions from fleet growth were offset by the deployment of ammonia-fueled vessels and the EEDI measures (Figures 4.1 and 4.2). Since experimentally determined EFs were not available for NMVOC emissions from ammonia engines, they were estimated to be 20 % of the NMVOC EFs for marine diesel engines in the uncontrolled case to match the amount of pilot fuel used. In the uncontrolled 2050 scenario, CO emissions increased by 5 % and NMVOC emissions decreased by 27 % compared to 2015, due to the high number of ships operating on carbon-free ammonia (Fig. 4.1). For the controlled case, a decrease of 3 % was modeled for CO and of 35 % for NMVOC emissions (Fig. 4.2). The slightly lower emission totals in the controlled case were based on the assumption that ship emissions from ammonia engines are almost free of CO and NMVOCs, which are both carbon compounds.

#### 4.2.8. Ammonia Emissions

With the introduction of ammonia-powered ships, ammonia slip emerged as a problem. According to Ntziachristos et al, ammonia slip is in the order of 8 % of the  $\text{NH}_3$  consumed for the technology used in the uncontrolled case. Ammonia emissions of 930 Gg were calculated for the uncontrolled 2050 scenario in the regarded domain (Fig. 4.1). With the technology of the controlled case ammonia slip was reduced to approximately 100 ppm, resulting in only 4 % of  $\text{NH}_3$  emissions, compared to the uncontrolled case. This reduced ammonia emissions to 35 Gg for the controlled 2050 scenario (Fig. 4.2). It should be noted that this ammonia slip, in conjunction with  $\text{NO}_x$  and  $\text{SO}_2$  emissions from shipping, is expected to increase concentrations of secondary ammonium aerosols near the shipping lanes, especially in the uncontrolled case. Furthermore, the toxicity of ammonia can be directly harmful to organisms and cause environmental acidification and nitrification (Asman et al., 1998).

### 4.3. Concluding Summary and Outlook

This publication presents a novel methodology for generating ship emission scenarios. The methodology allows to simulate physical fleet developments, such as the decommissioning and renewal of ships, fuel type changes and efficiency gains, implemented through changes to a virtual shipping fleet. Subsequently, the emissions of this fleet can be calculated with the MoSES ship emission model, so that the complex relationships between the energy consumption of several thousand ships and the corresponding emissions can be handled in a computational model. The methodology presented is generally applicable to enable a flexible scenario design, but it is particularly useful for the generation of future scenarios.

One use case for this approach is shown in this work by the creation of three ship emissions inventories for the future scenario years 2025, 2040, and 2050. They cover a domain located in northern Europe that includes the North and Baltic Seas. Motivated by the IMO's increased efforts to decarbonize the shipping sector and the growing urgency to reduce GHG emissions, the scenarios examine the impact of a broad fuel transition to ammonia in 2050 via LNG as an interim solution in 2040. With respect to the ammonia-engine technology, two cases were distinguished. One case assumes a compression-ignition engine with marine gas oil as pilot fuel and is referred to as "uncontrolled", the other involves a spark-ignition engine using hydrogen as the pilot fuel and is referred to as "controlled". Emission reductions were in general stronger for the controlled case, however, it is assumed that the technology of the uncontrolled case is more feasible by 2050. In addition, a growing fleet by ship size and number is considered as well as efficiency improvements in accordance with the IMO's EEDI measures.

#### 4. Publication II: Future Ship Emission Scenarios with a Focus on Ammonia Fuel

Compared to the reference ship emission inventory for 2015 CO<sub>2</sub> emissions decreased by 40 % for the uncontrolled 2050 scenario. However, for CO<sub>2</sub> equivalents the reduction was only 22 % (or 31 % by including BC in the calculation of CO<sub>2</sub> equivalents). This difference was primarily due to a tremendous increases of methane and nitrous oxide emissions by 613 % and 900 %, respectively.

NO<sub>x</sub> emissions were calculated to be reduced by 39 % in the uncontrolled 2050 scenario, which includes reductions associated with the implemented NECA in the North and Baltic Seas. CO emissions were calculated to increase slightly by 5 %, and NMVOC emissions decreased by 27 %. The phasing-out of marine fossil fuels reduced emissions of SO<sub>2</sub> and primary particulate matter from shipping by more than 73 %. However, NH<sub>3</sub>-slip from ammonia-fueled ships emerged as a new emission species from shipping. For the study region, it amounted to 930 Gg in the uncontrolled 2050 scenario and, in combination with NO<sub>x</sub> and SO<sub>2</sub>, has the potential to promote the formation of secondary particles near the shipping routes. It should be noted that this slip can be significantly reduced, e.g., by the different technological approach regarded in the controlled case, which reduced ammonia-slip to approximately 4 % compared to the uncontrolled case.

To investigate how the projections in these ship emission scenarios affect pollutant concentrations and air quality in the North and Baltic Seas, chemistry transport modeling studies are currently being conducted with the presented ship emission inventories. Future work in the context of ship emission scenarios could address further developments that might be expected in the future. However, the impact of some of these development is unclear or difficult to quantify at the present time. These include e.g., a non-compliance of ships to cleaner fuels, different engine technologies or possible new legislation, aimed at the mitigation of GHG emissions and/or air pollution. In addition, shore power could play a larger role for berthing ships in the future, which would reduce ship emissions in larger port areas. Moreover, no rerouting of important shipping lanes was considered, e.g., via a possible Arctic route, which may open under ongoing climate change.

## 5. Publication III: Comparison of the Impact of Ship Emissions in Northern Europe and Eastern China

The following chapter corresponds, apart from minor changes, to the publication of the same name authored by:

*Daniel A. Schwarzkopf, Ronny Petrik, Volker Matthias, Markus Quante, Guangyuan Yu, Yan Zhang,*

and published in the special issue of the MDPI Journal:

*“Atmospheric Shipping Emissions and Their Environmental Impacts”*

*Atmosphere*, Volume 13(6), **2022**, p. 894, <https://doi.org/10.3390/atmos13060894>.

### Abstract

It is well known that ship emissions contribute significantly to atmospheric pollution. However, the impact on air quality can regionally vary, as influenced by parameters such as the composition of the regional shipping fleet, state of background atmospheric pollution, and meteorological aspects. This study compared two regions with high shipping densities in 2015. These include the North and Baltic Seas in Europe and the Yellow and East China Seas in China. Here, a key focal point is an evaluation of differences and similarities of the impacts of ship emissions under different environmental conditions, particularly between regions with medium (Europe) and high air pollution (China). To assess this, two similarly performed chemical transport model runs were carried out with highly resolved bottom-up ship emission inventories for northern Europe and China, calculated with the recently developed MoSES model, publicly available emissions data for nonshipping sources (EDGAR, MEIC). The performance of the model was evaluated against measurement data recorded at coastal stations. Annual averages at affected coastal regions for NO<sub>2</sub>, SO<sub>2</sub>, O<sub>3</sub> and PM<sub>2.5</sub> were modeled in Europe to be 3, below 0.3, 2.5, 1 and in China 3, 2, 2–8, 1.5, respectively, all given in µg/m<sup>3</sup>. In highly affected regions, such as large harbors, the contributions of ship-related emissions modeled in Europe were 15 %, 0.3 %, –12.5 %, 1.25 % and in China were 15 %, 6 %, –7.5 %, 2 %, respectively. Absolute pollutant concentrations from ships were modeled slightly higher in China than in Europe, albeit the relative impact was smaller in China due to higher emissions from other sectors. The different climate zones of China and the higher level of atmospheric pollution were found to seasonally alter the chemical transformation processes of ship emissions. Especially in northern China, high PM concentrations during winter were found to regionally inhibit the transformation of ship exhausts to secondary PM, and reduce the impact of ship-related aerosols, compared to Europe.

### Acknowledgements

This research and APC were funded by the German Research Foundation (DFG) in the framework of the DFG-NSFC funded project “ShipChem” with the DFG project nr. 645514 and supported by the BSH funded project “SeAir” (BSH contract code: 10042629, Hereon contract code: 430/2018).

## 5.1. Materials and Methods

### 5.1.1. Model Simulations

#### 5.1.1.1. Regions of Interest

Model domains were prepared for the two regions of interest for which this study compared the air quality impact of ship emissions. The region of northern Europe was covered by a domain hereafter referred to as SC12NSBS. It includes the North and Baltic Seas and is shown in Fig. 5.1 (left). China was represented by a domain that is located in East Asia and is hereafter referred to as CNC12 (Fig. 5.1 right). It includes the coastline of China, including the Bohai Sea, the Yellow Sea, the East China Sea and parts of the South China Sea. Both domains have the same extent in kilometers and include not only the main local shipping routes but also densely populated coastal regions, whose air quality is affected by ship exhausts. Two  $12 \times 12 \text{ km}^2$  Lambert conformal grids were set up for the chemistry transport modeling (see Sect. 5.1.1.2 for details). Both grids consisted of  $196 \times 196$  cells.

Two chemical transport simulations were performed for each domain: One represented a “base” case that included emissions from all sectors, and the other represented a “no ships” case, omitting ship emissions (see Sect. 5.1.2). The pollutant concentrations originating from shipping were then determined by the zero-out method, in which the “no ships” case is subtracted from the “base” case.

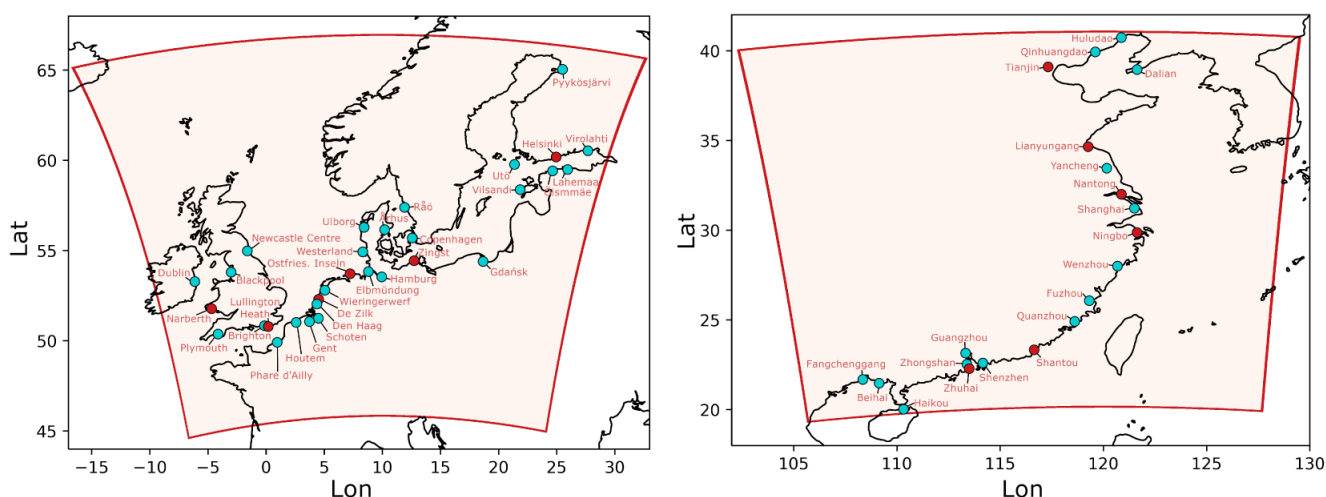


Figure 5.1.: Modeled domains for northern Europe (**left**, SC12NSBS) and eastern China (**right**, CNC12) that were created for the comparison. Also shown are the air quality monitoring stations that were considered in an evaluation of the model performance. The red dots represent selected stations whose comparison data are exemplarily shown in the original publication in Sect. 5.2. The full evaluation data of all stations can be found in the appendix.

#### 5.1.1.2. Chemical Transport Model CMAQ - Setup and Forcing

The Community Multiscale Air Quality model (CMAQ) by Byun and Ching (1999); Byun and Schere (2006) in version 5.2, a chemistry transport model, was used and set up with the carbon bond 5 photochemical mechanism (CB05-TUCL) (Yarwood et al., 2005; Whitten et al., 2010; Sarwar et al., 2011) and the AE6 aerosol mechanism. The CMAQ run was performed for 2015 after a previous spin-up time of 2 weeks to adapt to the initially homogeneous concentration fields and atmospheric conditions. The model considered 30 vertical layers from the ground surface up to a 100 hPa pressure level, which was located at approximately 8 km. Twenty of these layers were below an altitude of 2000 m. The lowest layer had a height of approximately 42 m and was located at approximately 21 m.

The simulations for China and Europe were nested into preceding, overarching CMAQ simulations that covered larger areas at a coarser resolution (36 km for Europe and 24 km for China) but used the same emission sources as the 12 km runs. The chemical conditions at the boundaries of these larger domains

were taken from the Integrated Forecast System - Copernicus Atmosphere Monitoring Service (IFS-CAMS) analysis (Inness et al., 2019). The data were available from the MARS archive at the European Centre for Medium-Range Weather Forecasts (ECMWF) and the CAMS Atmosphere Data Store (ECMWF-CAMS, 2021). Particle and gas concentration fields of the IFS-CAMS data are usually provided on a T511 spectral grid with 137 vertical levels, but due to retrieval issues, data on a  $0.5^\circ \times 0.5^\circ$  grid were used. The IFS-CAMS data were temporally and spatially remapped onto the boundary of the overarching domains. Chemical and particle species were converted to match the species used in CMAQ.

### 5.1.1.3. Meteorological Forcing

One important difference between the regions of interest was the characteristic of the atmospheric large-scale circulation. Therefore, reliable meteorological data are needed to calculate the transport and transformation of gas species and aerosol particles as realistically as possible. The meteorological forcing was realized by atmospheric simulations with the community model COSMO-CLM (version 5.0-clm15) (Rockel et al., 2008), which is embedded into the COSMO model used for numerical weather prediction (Doms and Schättler, 2002; Doms et al., 2011; Baldauf et al., 2011). To simulate radiative transfer, an extension of the COSMO model for MACv2 transient aerosol climatology was used (Kinne, 2019).

The atmospheric simulations were performed using forcing data from global models as initial and boundary conditions, i.e. the MERRA2 reanalysis (Gelaro et al., 2017) for the SC12NSBS domain and the JRA-55 reanalysis (Kobayashi et al., 2015; Harada et al., 2016) for the CNC12 domain. The simulations for Europe were performed on a grid with a resolution of  $0.06^\circ \times 0.06^\circ$ . To ensure that the atmospheric fields in the transient model integration were in accordance with the observations over the whole period, a nudging technique was used as described in Petrik et al. (2021). The reader is referred to this publication to find more information about the setup of the atmospheric model (setup “CCLM-oF-SN”). Regarding the simulations over eastern Asia, a domain with a resolution of  $0.11^\circ \times 0.11^\circ$  was used that consisted of  $315 \times 315$  grid points.

The initialization of the soil proved a challenging task since the forcing data from the global model did not provide sufficient information consistent with the soil parameterization of the regional model. In the southeastern Asia region, the characteristics of soil drying and soil wetting are very different for the various climates. Different spin-up experiments for the soil were performed. The results suggested that at least one complete monsoon season and one complete winter season were needed: only then could the water reservoir be reasonably filled up, and the solution converged to a balanced state. In particular, the soil levels below one meter required a considerable amount of time. Additionally, the region of northern China, where precipitation events occur only rarely.

## 5.1.2. Emissions Data

The emissions data fed to CMAQ were compiled from different sources for 2015 and preprocessed to an hourly resolution.

### 5.1.2.1. Anthropogenic Land-based Emissions for Europe

For the SC12NSBS domain in Europe, land-based emission data were based on the CAMS-REGAP-EU emission inventory for 2015 in version 3.1. The data set comprises annual anthropogenic emission totals for 13 GNFR sectors (Granier et al., 2019) (<https://permalink.aeris-data.fr/CAMS-REG-AP>, last accessed: 16 September 2021). The emissions were prepared utilizing the internally available Highly Modular Emission Model (HiMEMO). A temporal distribution up to a one-hour resolution was achieved using temporal profiles from the LOTOS-EUROS model, which were used to simulate a daily schedule of emissions from the GNFR sectors.

### 5.1.2.2. Anthropogenic Land-based Emissions for China

For the CNC12 domain, emissions data from the Multiresolution Emission Inventory for China (MEIC) were used for nonshipping, land-based emission sources (Li et al., 2017; Zheng et al., 2018; Li et al., 2014, 2019b;

Liu et al., 2015; Tong et al., 2018; Liu et al., 2020; Peng, L., Zhang, Q., Yao, Z., Mauzerall, D. L., Kang, S., Du, Z., Zheng, Y., Xue, T., and He, 2019). The monthly, gridded emissions of the MEIC inventory had an original spatial resolution of  $0.25^\circ \times 0.25^\circ$ . The emission inventory (EI) contained data for the five emission sectors: “Agriculture”, “Industry”, “Power”, “Residential” and “Transportation”. The following chemical species and compound groups were included: black carbon (BC), CO, NH<sub>3</sub>, NO<sub>x</sub>, organic compounds (OC), PM<sub>2.5</sub>, PM<sub>coarse</sub>, SO<sub>2</sub> and VOC species that were pre-categorized into the functional groups considered in the CB05 chemistry mechanism.

For the other countries that were completely or partially included in the CNC12 domain, monthly, gridded emissions from EDGAR v5.0 were used at a  $0.1^\circ \times 0.1^\circ$  spatial resolution. The EDGAR inventory covered 9 pollutants, i.e. BC, CO, NH<sub>3</sub>, NMVOC, NO<sub>x</sub>, OC, PM<sub>10</sub>, PM<sub>2.5</sub> and SO<sub>2</sub>, of 27 activities that are based on IPCC 1996 and 2006 sector codes (see appendix Sect. A.2.1). All nonshipping anthropogenic emissions were distributed from a monthly to an hourly resolution. The individual temporal patterns for countries and sectors were considered by applying the high-resolution temporal profiles developed by Crippa et al. (2020). For this, the five sectors of the MEIC inventory were mapped to fit EDGAR activities (see appendix Sect. A.2.1). A sector-wise vertical distribution up to 1106 m was carried out by applying the height profiles described in Bieser et al. (2011b).

To be compatible with the application in CMAQ, NO<sub>x</sub> emissions were split into NO and NO<sub>2</sub> at a ratio of 90 to 10 for road traffic and 95 to 5 for all other sectors. Furthermore, NMVOC emissions from EDGAR were split sector-wise according to a profile of the Netherlands Organisation for Applied Scientific Research (TNO) into the functional groups of the CB05 mechanism. PM<sub>2.5</sub> splits were applied from the SMOKE for Europe emission model by Bieser et al. (2011a).

### 5.1.2.3. Biogenic Emissions

Emissions from biogenic sources were calculated with the Model of Emissions of Gases and Aerosols from Nature (MEGAN) in version 3 for both model domains (Guenther et al., 2012, 2020). MEGAN was driven by the same meteorological data preprocessed for CMAQ (see Sect. 5.1.1.3.) Vegetation data tables were used unmodified from the official MEGAN resources (MEGAN LAI, 2021). SPOT/PROBA V LAI1 from GEOV1 products was chosen as an alternative input for leaf area index (LAI) data in MEGAN (Baret et al., 2013).

### 5.1.2.4. Ship Emissions in Northern Europe

The ship EI for northern Europe was created with the MoSES model using data from the automatic identification system (AIS) that were recorded by the European Maritime Safety Agency (EMSA), which was acquired from the Federal Maritime and Hydrographic Agency of Germany (BSH). The European inventory covered the area between the longitude and latitude ranges  $-5.00^\circ$ – $31.41^\circ$  and  $48.32^\circ$ – $68.37^\circ$ , respectively. The spatial resolution was  $0.069^\circ$  in the  $x$  (east–west) and  $0.036^\circ$  in the  $y$  (north–south) directions, which corresponded to approximately 4 km. The temporal resolution was hourly. A detailed description of this ship EI and details about the bottom-up methods used for the calculation can be found in Schwarzkopf et al. (2021). To cover the whole computational SC12NSBS domain (Fig. 5.1, left), the ship emission inventory was augmented at the northern and western boundary with data from the Ship Traffic Assessment Model (STEAM) described in detail in Jalkanen et al. (2009, 2012); Johansson et al. (2013, 2017b). The STEAM data were part of the CAMS-GLOB-SHIP dataset (v2.1) and can be downloaded at the Emissions of Atmospheric Compounds and Compilation of Ancillary Data website (ECCAD, 2021). The emission inventory of MoSES was scaled up to fit the grid of the STEAM data (regular lon.-lat. with a  $0.1^\circ$  resolution) and then merged.

Table 5.1 lists the gas and aerosol species included in the ship EIs, together with a reference to the source of the EFs used. NO<sub>x</sub> emissions were split into NO and NO<sub>2</sub> in the ratio of 92 to 8 for shipping. NMVOCs were split according to data from the Finnish Meteorological Institute (FMI), which was consistent with the results from CIMAC (2008) PM<sub>2.5</sub> emissions from ships were split with data from the SMOKE for Europe emission model (Bieser et al., 2011a). Finally, the merged data set was fed into the CMAQ model as emission input.

### 5.1.2.5. Ship Emissions in China

The ship EI for China covered the area between the longitude and latitude ranges 133.15°–102.09° and 44.47°–15.54°, respectively. The AIS data used for this inventory were obtained through a collaboration with the Shanghai Maritime Department. The ship EI for China generated from these data, had a spatial resolution of 0.039° in the  $x$  (east–west) and the  $y$  (north–south) directions, corresponding to approximately 4 km. The temporal resolution is hourly. For better comparability of the model results, the same parameters and EFs were used with MoSES for this EI as for the EI of northern Europe (Table 5.1, see also for details (Schwarzkopf et al., 2021)).

Table 5.1.: Gas and aerosol species included in the ship emission inventories (EIs), with sources of the emission factors (EFs) used.

Pollutant	EF source
Sulfur dioxide (SO <sub>2</sub> )	—
Sulfate (SO <sub>4</sub> <sup>2-</sup> )	Schwarzkopf et al. (2021)
Water associated with sulfate (SO <sub>4</sub> × H <sub>2</sub> O)	Jalkanen et al. (2012)
Nitrogen oxides (NO <sub>x</sub> )	Zeretzke (2013)
Black carbon (BC)	Aulinger et al. (2016)
Primary organic aerosols (POAs)	Jalkanen et al. (2012)
Mineral ash excl. metal sulphates (MA)	Schwarzkopf et al. (2021)
Carbon dioxide (CO <sub>2</sub> )	IMO (2014)
Carbon monoxide (CO)	IMO (2014)
Methane (CH <sub>4</sub> )	IMO (2014)
Nonmethane volatile organic compounds (NMVOCs)	EMEP/EEA (2019)
Dinitrogen oxide (N <sub>2</sub> O)	IMO (2014)
Particulate matter (PM <sub>tot</sub> )	EMEP/EEA (2019)

The spatial distribution of CO<sub>2</sub> emission fluxes for 2015 in the CNC12 domain and monthly, normalized emission totals for each considered species are illustrated in Fig. 5.2. The monthly variation in ship emissions showed two minima. The first minimum was registered in February during the long public holidays of the Chinese Spring Festival, and the second minimum was seen during the summer months, which corresponded to the summer fishing moratorium. In contrast, higher fishing activities and corresponding emissions were found in spring and autumn. Similar observations were also made by Chen et al. (2017) and Fan et al. (2016).

For the calculation of ship emissions, 10 ship types were differentiated plus an “Undefined” class, used for ships for which no type information was present. These were Bulk, Cargo and container, Cruise, Fishing, Military, Passenger and Ro-Ro, Pleasurecraft, Tanker, Tug and Other. The annual emissions for 2015 are shown in Table 5.2 as totals and for the individual ship types. The majority of emissions could be accounted for by freight ships. Hereby, cargo ships, including container and Ro-Ro cargo ships, had the largest share, with an annual average of 38 % of SO<sub>2</sub>, SO<sub>4</sub> and MA, 45 % of NO<sub>x</sub>, CO<sub>2</sub>, CO, NMVOC, N<sub>2</sub>O, BC and POA and 10 % of CH<sub>4</sub> and 43 % of PM<sub>tot</sub> emissions. A decreased activity for this ship type was modeled in February and March. Bulk freighters instead accounted for only 1 % of SO<sub>2</sub>, SO<sub>4</sub> and MA, 14 % of CO<sub>2</sub>, CO, NO<sub>x</sub> and N<sub>2</sub>O, 3 % of CH<sub>4</sub>, 9 % of NMVOC and BC, 11 % POA and 5 % PM<sub>tot</sub> emissions. The share of tankers, the last type of freight ships considered, was 7 % of the emissions of SO<sub>2</sub>, SO<sub>4</sub>, MA and PM<sub>tot</sub>. They also accounted for 11 % of the emissions of NO<sub>x</sub>, CO<sub>2</sub>, CO and N<sub>2</sub>O, 80 % of CH<sub>4</sub> and 9 % of NMVOC, BC and POA. In total, freight ships accounted for approximately 50–70 % of ship emissions and for almost all methane emissions. The emission share of fishing vessels in the model domain was 5 % of SO<sub>2</sub>, SO<sub>4</sub> and MA, 3 % of NO<sub>x</sub>, CO<sub>2</sub>, CO, NMVOC, N<sub>2</sub>O, BC, POA and PM<sub>tot</sub> and 1 % of CH<sub>4</sub> emissions. A seasonality for emissions from fishing vessels was observed, with increased emissions in April and May and October. An explanation for this was the summer fishing ban in the South China Sea enforced since 1999 (<https://www.fao.org/fishery/en/facp/chn>, last accessed: 14 December 2021). This resulted in a decrease in CO<sub>2</sub> emissions to 1 % in June, which increased to 5 % during peak periods.

Tugs and passenger ships accounted for only 2–3 % of the emissions of the species considered. Cruise ships, military ships and pleasurecrafts accounted for a negligible share of all emissions species considered, with less than 1 %. In this context, it should be noted that AIS is not a reliable source for tracking military vessels. Ships of other types, grouped under the type “Other” (e.g. dredging or drilling ships, patrol or research vessels) accounted for 17 % of SO<sub>2</sub>, SO<sub>4</sub>, MA and PM<sub>tot</sub>, 9 % of NO<sub>x</sub>, CO, N<sub>2</sub>O and POA, 8 % of CO<sub>2</sub>, 2 % of CH<sub>4</sub> and 13 % NMVOC and BC emissions. Ships for which no type could be determined due to missing data were assigned the type “Undefined”. Various assumptions had to be made for this type, which usually included estimations of the engine power and fuel type. When vessel size information was not available, “Undefined” ships were considered small, and an approximated gross tonnage of 500 was found to be plausible (Schwarzkopf et al., 2021). This result was supported by the two assumptions that large and commercial vessels are considered more reliable in transmitting information via AIS and that the available vessel characteristics databases are more reliable for larger vessels.

In the CNC12 domain, undefined ships are responsible for approximately 26 % of SO<sub>2</sub>, SO<sub>4</sub> and MA, 14 % of NO<sub>x</sub> and CO<sub>2</sub>, 13 % of CO, NMVOC and N<sub>2</sub>O, 3 % of CH<sub>4</sub> and 16 % of PM<sub>tot</sub>, POA and BC emissions. Numerically, nearly 57 % of the vessels had to be classified as “Undefined”; no information on installed main engine power was available for nearly 92 % of them. This corresponds to a share of 67 % of all vessels for which the installed main engine power had to be estimated. Similar findings were made by Zhang et al. (2019) for the PRD, where unidentified ships accounted for 49 % of CO<sub>2</sub> emissions. This introduces an uncertainty to the calculated emissions due to the estimations that had to be made. In comparison, 11 % of undefined ships by number were found in the European EI. Estimations about the main engine power had to be made for more than 56 % of ships and for 31 % of the total on ships installed main engine power.

In both regions, oil-based residual and distillate fuels are predominant, being used by more than 99 % of registered vessels. However, in China, 65 % of vessels were found using residual fuels, compared to 37 % in Europe. The vast majority of the remaining ships use distillate fuels. The more frequent application of residual fuels is, in addition to the differing legal regulations, responsible for higher SO<sub>x</sub> and particle emissions in China.

Of the more than 110,000 of different vessels registered in China in 2015 and of the nearly 22,000 registered in Europe, 4090 vessels were found in both regions. Most of them, 95 %, were freight ships, with a gross tonnage over 5,000. This was plausible, as larger ships are usually deployed for this long voyage. They were distributed among the ship types considered: 38 % bulk freighters, 35 % cargo and container ships, 23 % tankers, 2 % other ships. The remaining ship types make up less than 1 %.

Table 5.2.: Modeled ship emissions in Gg · year<sup>-1</sup> for China in 2015 in total and for each individual ship type.

Ship Type	SO <sub>2</sub>	SO <sub>4</sub>	SO <sub>4</sub> xH <sub>2</sub> O	NO <sub>x</sub>	CO <sub>2</sub>	CO	CH <sub>4</sub>	NM VOC	N <sub>2</sub> O	BC	MA	POA	PM <sub>tot</sub>
All	486.55	14.38	11.22	1,678.98	85,325.01	70.3	5.97	21.93	4.36	29.94	4.98	39.87	89.34
Bulk	6.43	0.13	0.10	219.43	12,144.84	9.95	0.20	1.95	0.60	2.81	0.07	4.53	6.80
Cargo	181.93	5.28	4.12	750.25	39,012.88	31.12	0.58	10.22	1.94	13.66	1.86	17.98	38.18
Cruise	0.63	0.02	0.02	8.33	363.08	0.34	0.01	0.06	0.02	0.10	0.01	0.18	0.29
Fishing	26.17	0.77	0.60	51.23	2,445.1	2.01	0.03	0.67	0.13	1.03	0.27	1.42	3.68
Military	0.37	0.01	0.01	0.94	43.38	0.04	0.00	0.02	0.00	0.02	0.00	0.02	0.05
Passenger	10.69	0.35	0.27	45.98	1,925.97	1.82	0.03	0.59	0.12	0.74	0.11	0.99	2.19
Pleasurec.	1.11	0.03	0.02	2.17	103.08	0.09	0.00	0.05	0.01	0.05	0.01	0.05	0.15
Tanker	31.89	0.99	0.77	177.59	8,978.86	8.43	4.83	1.88	0.48	2.54	0.33	3.60	7.33
Tug	15.91	0.49	0.38	27.90	1,600.8	1.36	0.03	0.59	0.09	0.74	0.16	0.85	2.33
Other	81.46	2.45	1.91	150.52	6,679.75	5.89	0.10	2.94	0.38	3.54	0.83	3.78	11.13
Undef.	129.96	3.85	3.00	244.63	12,027.27	9.26	0.16	2.96	0.60	4.70	1.33	6.46	17.22



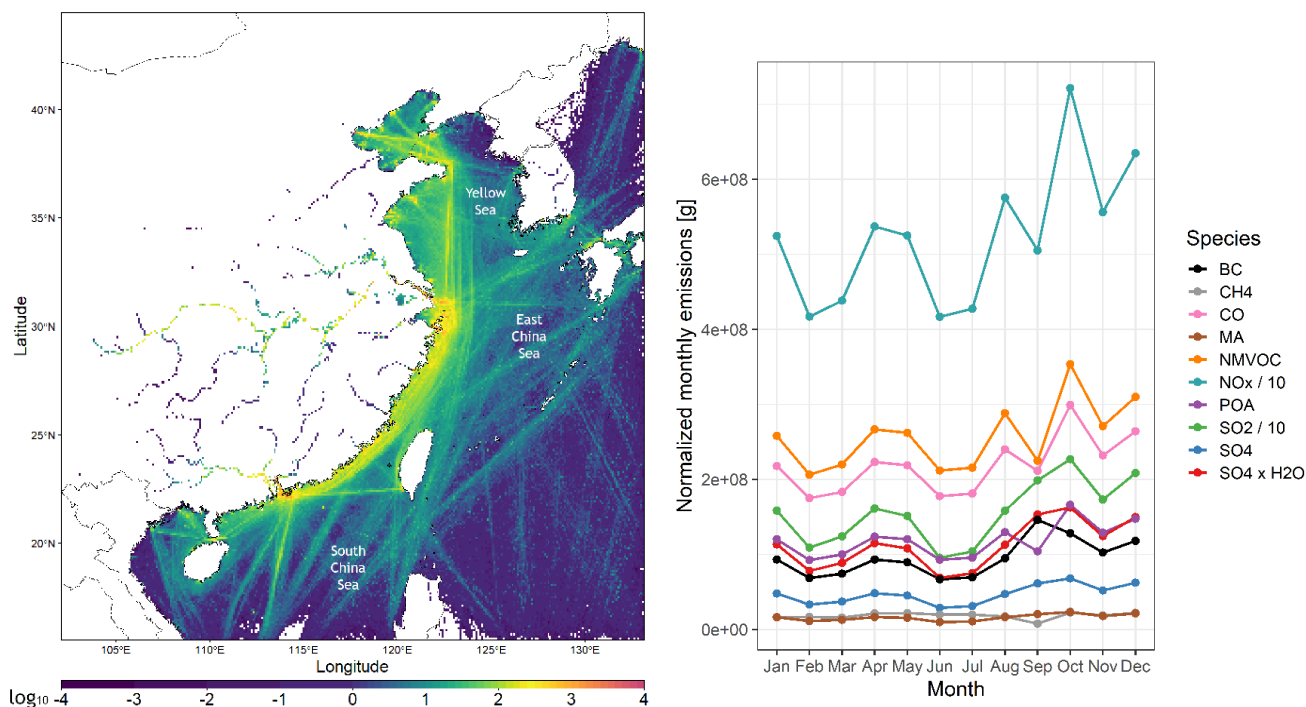


Figure 5.2.: Calculated CO<sub>2</sub> emission fluxes in  $\text{g} \cdot \text{m}^{-2} \cdot \text{year}^{-1}$  plotted on a logarithmic scale for the Chinese domain 2015. The spatial resolution is approximately  $4 \times 4 \text{ km}^2$  (left). Monthly emissions of black carbon (BC), CH<sub>4</sub>, CO, mineral ash (MA), nonmethane volatile organic compounds (NMVOCs), NO<sub>x</sub>, primary organic aerosols (POAs), SO<sub>2</sub>, SO<sub>4</sub> and SO<sub>4</sub> × H<sub>2</sub>O in 2015, normalized to one day (right). Values of NO<sub>x</sub> and SO<sub>2</sub> were divided by 10 to fit the scale.

## 5.2. Assessment of the Model Performance

To assess the reliability and performance of the model results for the European SC12NSBS and Chinese CNC12 domains, they were compared with publicly available air quality data from the European Environment Agency (EEA) and the Chinese authorities. The data for Europe were acquired from the Air Quality e-Reporting (AQER) repository, which contains data from 2013 onwards (EEA, 2021). The data for China were acquired from the China National Environment Monitoring Centre (<http://www.cnemc.cn>, last accessed: 27 April 2022).

Since the focus was on the influence of ship emissions, measurement data from monitoring stations in coastal regions near the major shipping routes were evaluated. Note that a point measurement at the station site and an average concentration in a  $12 \times 12 \text{ km}$  grid cell enclosing the station were compared. Therefore, the measured concentrations may not be fully representative of the grid cell, as the resolution of the regional model does not allow for the consideration of small-scale measurement conditions and effects near the station. Although the uncertainties of this method are hard to estimate, it can be seen as a performance indicator for the model.

A comparison of the concentration time series was performed (for NO<sub>2</sub> and SO<sub>2</sub>, emissions were included in the comparison), and statistical quantifiers were calculated from the hourly concentrations for each pollutant. These include the geometric mean for all stations, two arithmetic mean values calculated using only positive or negative normalized mean biases (NMB<sub>pos</sub>, NMB<sub>neg</sub>) and the arithmetic mean of the Spearman correlation coefficients. Only stations with data availability greater than 60% of hourly measurements for 2015 were considered for comparison. A total of 29 stations in the SC12NSBS domain and 20 stations in the CNC12 domain were considered (their locations are shown in Fig. 5.1). A comparison of the modeled “base” case concentrations with the measured data is shown in Tables 5.3 and 5.4 for each domain. These include statistical quantifiers calculated with data from all stations. For pollutant and station-specific NMBs and correlation coefficients for the modeled “base” and “no ships” case, refer to the appendix, Tables A.17 to A.24. A high correlation coefficient was an indicator of the representativeness of

the time profiles used for the concentration patterns at the monitoring station. A correlation was considered for a coefficient greater than or equal to 0.5. The correlation was considered “good” if the coefficient was equal to or greater than 0.7.

Table 5.3.: Comparison of modeled NO<sub>2</sub>, SO<sub>2</sub>, O<sub>3</sub> 8-hour mean and PM<sub>2.5</sub> concentrations of the modeled “base” case in  $\mu\text{g} \cdot \text{m}^{-3}$  with measurements in the SC12NSBS domain. Based on all 29 considered stations in Europe, the mean correlation coefficient (Mean Corr.) and two values, calculated as the mean of either positive or negative normalized mean biases are shown (NMB<sub>pos</sub>, NMB<sub>neg</sub>). For the latter two values, the number of stations used for the calculation is given in parentheses.

Station	NO <sub>2</sub>		SO <sub>2</sub>		O <sub>3</sub> 8-hour mean		PM <sub>2.5</sub>	
	Mean <sub>mod</sub>	Mean <sub>meas</sub>	Mean <sub>mod</sub>	Mean <sub>meas</sub>	Mean <sub>mod</sub>	Mean <sub>meas</sub>	Mean <sub>mod</sub>	Mean <sub>meas</sub>
Dublin	3.05	4.94	—	—	—	—	—	—
Blackpool	2.47	11.46	—	—	68.55	49.39	8.17	5.78
Narberth	1.60	1.63	0.37	0.68	75.12	61.09	—	—
Plymouth	2.27	13.53	—	—	76.77	45.59	8.52	9.33
Brighton	4.77	10.72	—	—	72.40	51.52	—	—
Lull. Heath	4.44	4.79	0.28	0.95	73.98	53.61	—	—
Newcastle	6.06	25.56	—	—	66.52	36.56	7.96	7.80
Phare d’Ailly	—	—	—	—	76.09	59.62	—	—
Houtem	7.19	7.12	1.19	1.07	64.51	47.15	9.65	8.12
Gent	13.51	23.40	0.94	1.23	50.48	32.78	10.57	11.15
Schoten	17.79	21.26	—	—	45.04	29.50	10.87	10.79
Den Haag	17.91	22.20	—	—	39.51	33.29	—	—
De Zilk	12.99	9.83	0.73	0.95	48.49	42.27	9.73	6.61
Wieringerwerf	5.30	8.55	—	—	68.96	44.15	8.93	6.04
Ostf. Inseln	3.43	6.39	0.14	0.40	72.08	55.72	—	—
Elbmündung	5.33	9.56	—	—	67.33	47.54	—	—
Hamburg	12.12	26.39	1.07	3.28	—	—	—	—
Westerland	1.34	2.17	0.09	0.26	77.55	61.91	—	—
Ulborg	1.54	2.77	—	—	73.55	61.99	—	—
Århus	3.23	9.61	—	—	72.37	50.36	—	—
Råö	—	—	—	—	74.34	62.74	—	—
Copenhagen	7.13	12.32	—	—	66.14	53.76	—	—
Zingst	2.95	3.73	0.21	0.39	72.69	57.10	—	—
Gdańsk	5.80	10.44	1.67	2.17	—	—	—	—
Vilsandi	0.98	1.37	0.11	0.27	75.61	65.64	—	—
Utö	1.16	2.25	0.10	0.30	74.56	66.32	4.00	3.45
Õismäe	3.65	5.13	0.39	0.47	67.60	51.05	—	—
Helsinki	5.90	14.01	1.00	0.61	58.39	44.94	4.84	4.22
Lahemaa	1.33	1.61	0.23	0.53	65.52	50.24	—	—
Virolahti	1.56	2.74	0.26	0.21	67.24	47.51	3.87	4.19
Pyykösjärvi	3.00	6.61	—	—	51.92	43.39	—	—
<b>Mean NMB<sub>pos</sub></b>	0.398(1)		0.365(10)		0.27(28)		0.164(9)	
<b>Mean NMB<sub>neg</sub></b>	−0.38(28)		−0.266(6)		<i>n.a.</i> (0)		−0.03(2)	
<b>Mean Corr.</b>	0.617		0.279		0.659		0.377	

All of the 29 stations in the SC12NSBS domain in Europe were background monitoring stations in less densely populated locations, e.g., suburban or rural stations were preferred in the selection. NO<sub>2</sub> concentrations were often underpredicted by the model, indicated by 28 of 29 stations having a negative NMB. For 6 of the 29 stations a correlation coefficient of 0.7 or greater was found. For 26 stations, the coefficient was greater than or equal to 0.5. In general, the NMB was higher for stations where lower concentrations were modeled. When comparing the “base” with the “no ships” case, lower concentrations were found at all stations, which highlights the importance of including ship emissions in the model. Consequently, a higher absolute NMB was calculated, indicating a poorer agreement between the “no ships” and the measurements. This was consistent with the assumption that shipping is an important source of air pollution for many of these stations because they were located near major shipping routes. Considering the correlation, differences were not so clear since the disparities between the “base” and “no ships” cases were small.

In the SC12NSBS domain, SO<sub>2</sub> concentrations were generally low at the stations considered, mostly below  $1 \mu\text{g} \cdot \text{m}^{-3}$ . In comparison to the measurements, the modeled SO<sub>2</sub> concentrations were often overestimated, as 10 of the 16 stations had an NMB greater than zero. A correlation coefficient greater than

0.5 was calculated for only one station. The low correlation could be explained by the overall low SO<sub>2</sub> concentrations, which are both difficult to measure and model. The correlation differences between the “base” and “no ships” cases were generally small.

The distinct diurnal concentration changes and seasonal trends of the O<sub>3</sub> 8-hour mean were well represented in the model results, as shown by correlations greater than 0.5 for all 28 stations. For 9 stations, the correlation was greater than 0.7. The average NMB of 0.27 indicated that concentrations at all 28 stations were systematically overestimated. This overestimation was most concise in spring and autumn. Furthermore, large daily fluctuations were often not captured well by the model. In general, the correlation was better for the “base” case than for the “no ships” case. The performance gain of the model by including ship emissions was small for most stations. However, for stations close to the port cluster of Rotterdam and Antwerp, i.e. Schoten, De Zilk and Den Haag, the performance gain was significant. The observed ozone reduction by ship exhausts in this region is also visible in concentration patterns, which are shown in Fig. 5.6 (a)–(c) and are discussed later.

Of the 29 stations in total, PM<sub>2.5</sub> was only measured at 11 sites in the Netherlands, Belgium, England and Finland. According to the NMB, the modeled concentrations were mostly overestimated. For two stations, a correlation equal to or greater than 0.5 was calculated; for none, a correlation equal to or greater than 0.7. The low correlation was explained in terms of the complex nature of ambient PM<sub>2.5</sub> concentrations. The chemical and physical transformations that generate particulate matter, and that particles themselves undergo mostly depend on location-specific parameters. Local events can generate high fluctuations in hourly measurements, which are difficult to reproduce with a regional model. However, the correlation coefficient increased at all regarded stations by the inclusion of ship emissions. The NMB decreased for some cases due to an overestimation of the concentrations.

The 20 stations in the CNC12 domain in China are located in or close to large coastal cities (Table 5.4).

Table 5.4.: Comparison of modeled NO<sub>2</sub>, SO<sub>2</sub>, O<sub>3</sub> 8-hour mean and PM<sub>2.5</sub> concentrations of the modeled “base” case in  $\mu\text{g} \cdot \text{m}^{-3}$  with measurements in the CNC12 domain. Based on all 20 considered stations in China, the mean correlation coefficient (Mean Corr.) and two values, calculated as the mean either from positive or negative normalized mean biases are shown (NMB<sub>pos</sub>, NMB<sub>neg</sub>). For the latter two values, the number of stations used for the calculation is given in parentheses.

Station	NO <sub>2</sub>		SO <sub>2</sub>		O <sub>3</sub> 8-hour mean		PM <sub>2.5</sub>	
	Mean <sub>model</sub>	Mean <sub>meas</sub>	Mean <sub>mod</sub>	Mean <sub>meas</sub>	Mean <sub>mod</sub>	Mean <sub>meas</sub>	Mean <sub>mod</sub>	Mean <sub>meas</sub>
Dalian	53.68	29.53	24.74	19.59	26.28	64.12	43.42	33.98
Huludao	16.78	29.73	7.85	33.10	52.85	48.38	31.79	40.38
Qinhuangdao	29.04	38.01	14.51	28.64	31.46	30.50	38.45	30.11
Tianjin	56.95	33.53	29.83	19.00	4.32	29.99	59.93	50.52
Lianyungang	15.05	24.31	4.75	22.07	57.19	60.35	42.26	39.82
Yancheng	18.57	19.60	3.75	15.53	59.14	72.76	41.12	35.52
Nantong	36.79	30.45	11.84	23.50	37.06	62.88	42.19	45.28
Shanghai	59.11	39.21	27.09	14.70	21.57	60.07	41.51	41.10
Ningbo	44.97	37.27	16.06	14.36	36.73	50.95	37.51	35.30
Wenzhou	30.72	38.75	9.05	11.96	51.90	33.98	36.03	37.29
Fuzhou	23.77	28.92	6.19	5.78	70.80	40.27	34.67	24.41
Quanzhou	24.96	21.22	9.87	8.60	63.49	46.82	44.64	23.66
Shantou	15.01	16.98	6.05	11.64	78.48	61.95	42.11	28.22
Shenzhen	47.27	30.07	15.55	7.93	27.79	48.69	48.70	25.08
Guangzhou	58.01	41.38	20.86	10.96	22.08	26.21	52.25	32.91
Zhongshan	20.33	23.39	7.03	9.99	64.65	33.83	48.02	26.30
Zhuhai	14.25	23.30	5.03	7.03	79.18	51.72	45.85	23.98
Haikou	6.92	11.34	2.98	4.84	85.70	44.20	37.56	17.73
Beihai	5.38	12.10	4.93	7.90	92.03	65.84	42.38	19.20
Fangchenggang	5.04	10.45	4.48	4.89	87.99	36.73	41.99	24.14
<b>Mean, NMB<sub>pos</sub></b>	0.402(12)		0.512(9)		0.544(18)		0.439(17)	
<b>Mean, NMB<sub>neg</sub></b>	−0.283(8)		−0.38(11)		−0.1(2)		−0.06(3)	
<b>Mean Corr.</b>	0.477		0.398		0.628		0.408	

NO<sub>2</sub> concentrations were overestimated at 12 of the 20 stations, but at 9 of these 12 stations, the NMB was only small ( $\leq 0.1$ ). An underprediction was found for 8 stations, of which 7 had an NMB lower than

–0.1. No general systematic was found for this observation. An analysis of the  $\text{NO}_2$  emissions that were used as input for the model run leads to manifold reasons. For stations bordering the Bohai Sea, emissions were either too high or too low. In Jiangsu Province, summer and winter trends were not well captured.  $\text{NO}_x$  emissions were also too high for the stations in Shanghai and Ningbo; in the case of Shanghai, this may be related to the location of the monitoring station, which is on the Huangpu River, while the corresponding model cell covers a large part of the urban center. A comparison of the model results with the measurements in the PRD showed that the diurnal trend was more pronounced in the model than in the measurements. At the three southernmost stations, emissions were found to be too low. A correlation coefficient greater than 0.5 was found for 8 stations; no station had a correlation greater or equal 0.7. The low correlation might be explained by the urban environments in which most stations are located, which has a large influence on the hourly concentration patterns. Nevertheless, the main concentration features could be reproduced for most stations with the applied time profiles, although some concentration peaks were slightly shifted in time.

In general, the measured and modeled  $\text{SO}_2$  concentrations at stations in China were much higher than those in Europe. The model underestimated the concentrations of  $\text{SO}_2$  at 11 and overestimated them at the other 9 stations. The correlation coefficient was greater than or equal to 0.5 for 7 stations and was not greater than or equal to 0.7 for any station. In contrast to Europe, better correlations were calculated, which is probably related to the higher  $\text{SO}_2$  concentrations. An examination of the emissions at the measurement sites suggested that  $\text{SO}_2$  emissions were mainly too high at station sites in the YRD or PRD. Too low emissions were frequently found at northern stations, e.g., Huludao, Qinhuangdao, Lianyungang and Yancheng.

Similar to Europe, the diurnal ozone fluctuations were well modeled, but concentrations were overestimated at 17 of 20 stations. However, the correlations were greater than or equal to 0.5 at 16 stations and greater than or equal to 0.7 at 7 stations. In general, the correlation coefficients in China were higher for the northern stations than for the southern stations. In the north, overestimations were observed mainly during summer, while this trend was reversed in the south, which is presumably related to the regionally different climate zones. While the strong daily  $\text{O}_3$  fluctuations in Europe were often underestimated, the results for China were in better agreement. The largest improvements from the inclusion of ship emissions were found in southern China, e.g., Quanzhou, Fuzhou and Wenzhou. In the large port clusters in the YRD or PRD, the impact of ships on ozone concentrations was small.

Compared to the measurement data, the modeled  $\text{PM}_{2.5}$  concentrations were overestimated. A correlation coefficient greater than or equal to 0.5 was calculated for 7 stations all located in the northern part of the domain, i.e., Wenzhou, and at stations further north with a steady increase in correlation up to 0.69 at Qinhuangdao. Additionally, a small NMB was calculated for these stations. In southern China, the model performance for  $\text{PM}_{2.5}$  was worse. While the mean of the 10 stations, including Fuzhou and those farther south, had an average NMB of 0.66, the average NMB for Wenzhou and the 10 stations further north was 0.11. Based on this observation, it is assumed that the model performs better in the calculation of  $\text{PM}_{2.5}$  concentrations for the temperate climate zone.

In summary, the model performance was found to be satisfactory in both domains; however, different conclusions were drawn for Europe and China. The predominantly underestimated  $\text{NO}_2$  concentrations in Europe, although with good correlations, suggest a systematic bias. The under- and overestimates in China and the moderate correlations indicate inconsistencies in the emission inventory and occasional difficulties of the model in describing  $\text{NO}_2$  concentrations under the local meteorological conditions and atmospheric background. The better performance and correlation for  $\text{SO}_2$  in China is related to the difficulties in modeling and measuring the low concentrations that occur in Europe. The pronounced diurnal trends in ozone concentrations were well captured in both domains, as reflected by high correlation coefficients, but a systematic overprediction of ozone concentrations was found for both regions. Concentrations of  $\text{PM}_{2.5}$  were mostly overpredicted in both domains. Furthermore, it is noteworthy that in China the accuracy for modeled  $\text{PM}_{2.5}$  concentrations increased at sites further north, which might be related to the temperate climate. However, caution must be exercised in interpreting these observations, as consideration of the immediate environment of the measurement site and small-scale effects is only limited to  $12 \times 12$  km resolved model runs. It should also be emphasized that the stations selected for Europe are mostly

nonurban background stations, while most of the monitoring stations in China are located in or near major cities. Moreover, differences in the methodologies and sources that were used to create the nonshipping anthropogenic EIs are hardly avoidable. For the CNC12 domain, a second model run was carried out, in which anthropogenic, nonshipping emissions for China were used from the EDGAR instead of the MEIC inventory. The EDGAR inventory has a higher resolution of  $0.1^\circ$ , compared to  $0.25^\circ$  in MEIC. However, the results obtained with EDGAR showed higher overestimations, compared to MEIC. This was especially the case for  $\text{NO}_2$  and  $\text{O}_3$ . Thus, it was decided that the MEIC inventory would be more reliable for China.

### 5.3. Results and Discussion

Pollutants from ship exhausts can be transported over land by onshore winds to degrade air quality in populated areas. During this transport, a portion is removed from the atmosphere by wet and dry deposition processes. Furthermore, chemical reactions are responsible for the formation of secondary pollutants and particulates. For the latter, ammonia emissions from agriculture play a significant role. Rates for the relevant chemical transformations generally increase with temperature. In contrast, nucleation and coagulation of the particulation processes are facilitated at lower temperatures. All of these processes are considered within CMAQ and result in concentration patterns that are discussed and compared for northern Europe and eastern China.

In general, primary pollutants from shipping had the largest impact close to densely shipped routes (e.g., the Yangtze River, the English Channel or the southern North Sea) and in the vicinity of large port clusters (e.g., in the YRD, PRD or Rotterdam/Antwerp/Amsterdam). In Europe, prevailing southwesterly winds transported pollutants towards populated areas. In China, prevailing south and southeasterly winds transported ship emissions onto coastal regions, especially over the flat terrain of the Lower Yangtze Plain (LYP) and North China Plain (NCP). Meteorological conditions proved to be more important for an understanding of the seasonal patterns of ship pollutant concentrations than fluctuations in ship traffic (Yu et al., 2021). In particular, the East Asian monsoon is a dominant factor for emissions from a marine environment. Secondary pollutants generally have a higher atmospheric lifetime and can thus be encountered farther away from marine shipping lanes. They were found to have a higher impact on extended coastal regions in both domains.

For an interpretation of the results and an assessment of the impact ship emissions have on air quality, total regional pollutant concentrations must be considered, as well as the contribution from ships only. This was done for the pollutant species  $\text{NO}_2$  (Sect. 5.3.1),  $\text{SO}_2$  (Sect. 5.3.2), ozone (Sect. 5.3.3),  $\text{PM}_{2.5}$  (Sect. 5.3.4) and the main components of  $\text{PM}_{2.5}$  from shipping, ammonium (Sect. 5.3.4.1), sulfate (Sect. 5.3.4.2) and nitrate (Sect. 5.3.4.3). The contribution of shipping was determined by the zero-out method, i.e. by subtracting the results of a model run with omitted ship emissions from a model run that considers all emission sources. All concentration fields shown in the following are annual averages, unless otherwise specified. Seasonally averaged concentration fields are found in the appendix to avoid disrupting the reading flow by their large numbers (Sect. A.2.3). All concentrations are given in  $\mu\text{g} \cdot \text{m}^{-3}$ . The contribution of shipping to the total pollutant concentrations is shown as a percentage.

#### 5.3.1. $\text{NO}_2$

Nitrogen dioxide emissions are mainly the result of nitrogen oxidation during combustion processes.  $\text{NO}_2$  plays an important role in the formation of ground-level ozone (see Sect. 5.3.3) and as a precursor of PM (Sect. 5.3.4 and 5.3.4.3).

In Europe, annual average concentrations of  $15\text{--}20 \mu\text{g} \cdot \text{m}^{-3}$  were modeled near major cities and industrialized areas, e.g., London, Paris, Prague, the Rhine-Ruhr or Rhine-Main metropolitan regions. The overall highest  $\text{NO}_2$  concentrations of  $30\text{--}35 \mu\text{g} \cdot \text{m}^{-3}$  were modeled in the area of the Rotterdam/Antwerp/Amsterdam port cluster (Fig. 5.3 (a)).

In the coastal regions of mainland Europe bordering the North Sea and the southeastern coast of the United Kingdom,  $1\text{--}4 \mu\text{g} \cdot \text{m}^{-3}$   $\text{NO}_2$  could be attributed to shipping, even up to  $100\text{--}150$  km from the coastline (Fig. 5.3 (b)). The contribution of shipping to total  $\text{NO}_2$  varied between 20 and 40% in these

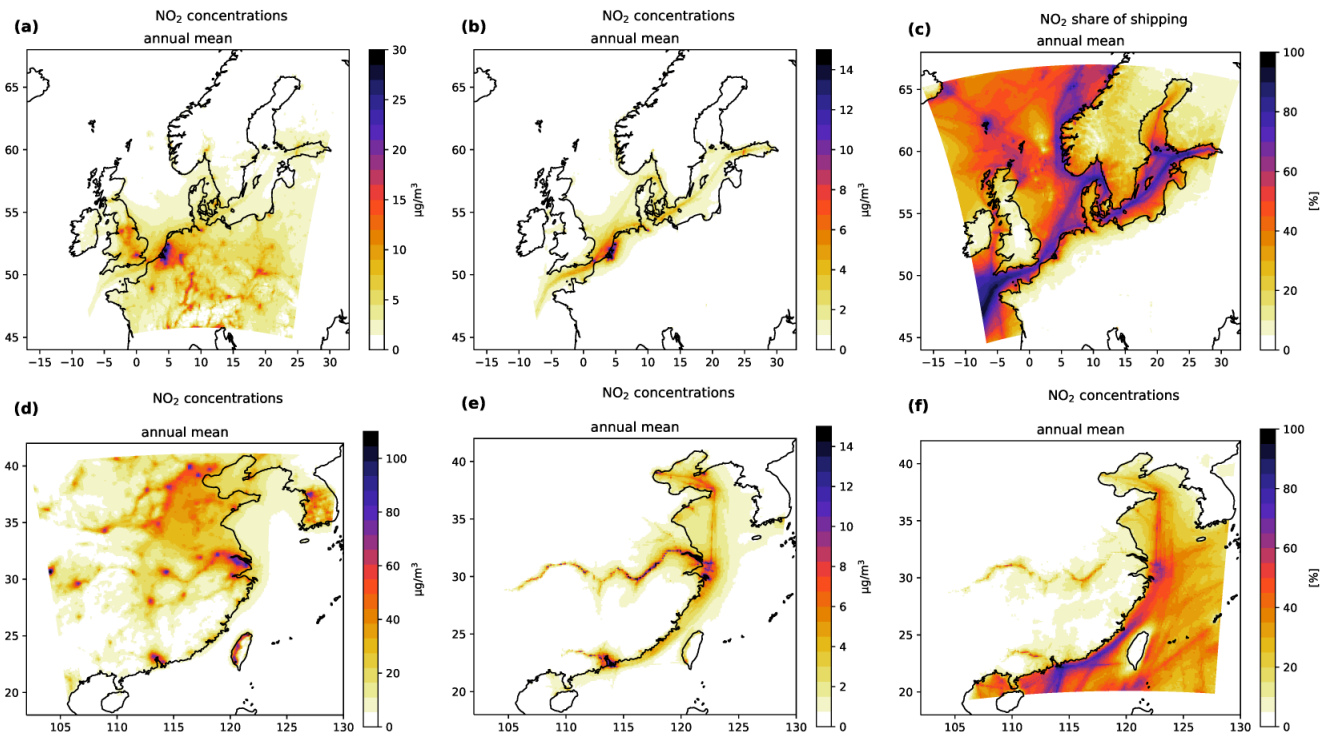


Figure 5.3.: Annual averages of NO<sub>2</sub> concentrations in the SC12NSBS domain in Europe (a–c) and the CNC12 domain in China (d–f). NO<sub>2</sub> concentrations [ $\mu\text{g} \cdot \text{m}^{-3}$ ] from all emission sources are shown in (a,d), from shipping only in (b,e) and the share of NO<sub>2</sub> concentrations from shipping on total NO<sub>2</sub> concentrations [%] is shown in (c,f).

regions. In ports, almost 50% of NO<sub>2</sub> could be attributed to ships (Fig. 5.3 (c)). Due to higher shipping activities in spring and summer, slightly higher concentrations were modeled for these seasons (Fig. A.2). In winter and autumn, the contribution of shipping to total NO<sub>2</sub> was lower as NO<sub>2</sub> emissions from residential heating increased and shipping activity decreased. (Fig. A.3).

In China, the concentrations of NO<sub>2</sub> were mostly in the range of 20 to 50  $\mu\text{g} \cdot \text{m}^{-3}$ . In densely populated regions, large cities and heavily industrialized areas, NO<sub>2</sub> concentrations reached 60 to 90  $\mu\text{g} \cdot \text{m}^{-3}$ , e.g., in Jiangsu, Tianjin, Hebei, the PRD, Shanghai, Beijing and the Sichuan Basin (Fig. 5.3 (d)).

The impact of shipping on regional NO<sub>2</sub> concentrations was most evident in the YRD, PRD, the associated rivers, the LYP and NCP. NO<sub>2</sub> concentrations were in the range of 2 to 8  $\mu\text{g} \cdot \text{m}^{-3}$  but could locally increase up to 13  $\mu\text{g} \cdot \text{m}^{-3}$  (Fig. 5.3 (e)). Vessel traffic was found to be responsible for 10–20% of the NO<sub>2</sub> concentrations in the major port clusters and the LYP and NCP. The highest contribution of up to 50% to the total NO<sub>2</sub> concentrations was modeled in parts of the Yangtze and Pearl Rivers (Fig. 5.3 (f)). In large parts of the Chinese coast, onshore pollutant transport and the impact of NO<sub>2</sub> by ships were small. In autumn and particularly in winter, higher ship-induced NO<sub>2</sub> concentrations and an extended dispersion were modeled, especially close to the Yangtze River (Fig. 5.4 (a) and Fig. A.6). This was consistent with the results of Shah et al. (2020) and could be explained by the longer lifetimes of NO<sub>x</sub>. High NO<sub>2</sub> and SO<sub>2</sub> concentrations from other sectors created oxidant-limited conditions during these seasons that reduced the conversion rate for NO<sub>2</sub>-depleting reactions, such as conversion to nitrate or nitric acid. Additionally, atmospheric oxidants such as ozone or hydroxyl radicals were less readily formed in winter due to lower solar irradiance. Furthermore, the frequent northerly and northwesterly winds during winter were able to transport more pollutants from shipping and other sectors from coastal regions to the open ocean. Combined with the reduced shipping activity, this explained the lower contribution of ships to NO<sub>2</sub> in coastal areas during this season. The relatively low concentrations over the Yellow Sea in autumn could be related to dilution by cold air currents from the northeast (Yu et al., 2021).

When the two regions were compared, approximately 2.5 times higher NO<sub>2</sub> concentrations were found in China. With only slightly higher ship-related NO<sub>2</sub> concentrations in China, the relative contribution of

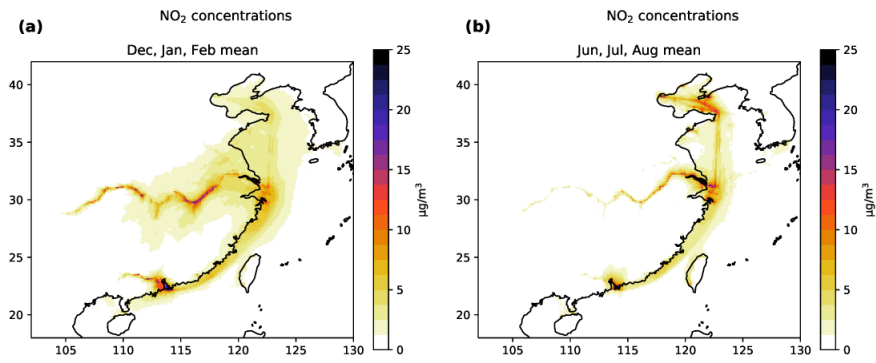


Figure 5.4.: Seasonal averages of  $\text{NO}_2$  concentrations [ $\mu\text{g} \cdot \text{m}^{-3}$ ] from shipping in the CNC12 domain in China for winter (a) and summer (b).

$\text{NO}_2$  from ships was 30–40 % and thus higher in European ports. Furthermore,  $\text{NO}_2$  concentrations from ships showed little seasonality in Europe, with slightly higher concentrations in spring and summer. In China, reduced  $\text{NO}_2$  concentrations were modeled in spring and summer, especially in the southern coastal regions (Fig. 5.4 (b) and Fig. A.5). Higher deposition rates during the summer monsoon were responsible for this observation. Furthermore, high overall  $\text{NO}_2$  concentrations in China during winter resulted in increased transport and a further dispersion of  $\text{NO}_2$  from shipping in inland areas (Fig. 5.4 (b)).

### 5.3.2. $\text{SO}_2$

Sulfur dioxide emissions are mainly generated by the combustion of fossil fuels. Similar to  $\text{NO}_2$ , it can form secondary aerosols by oxidation, e.g., sulfate (Sect. 5.3.4 and 5.3.4.2).

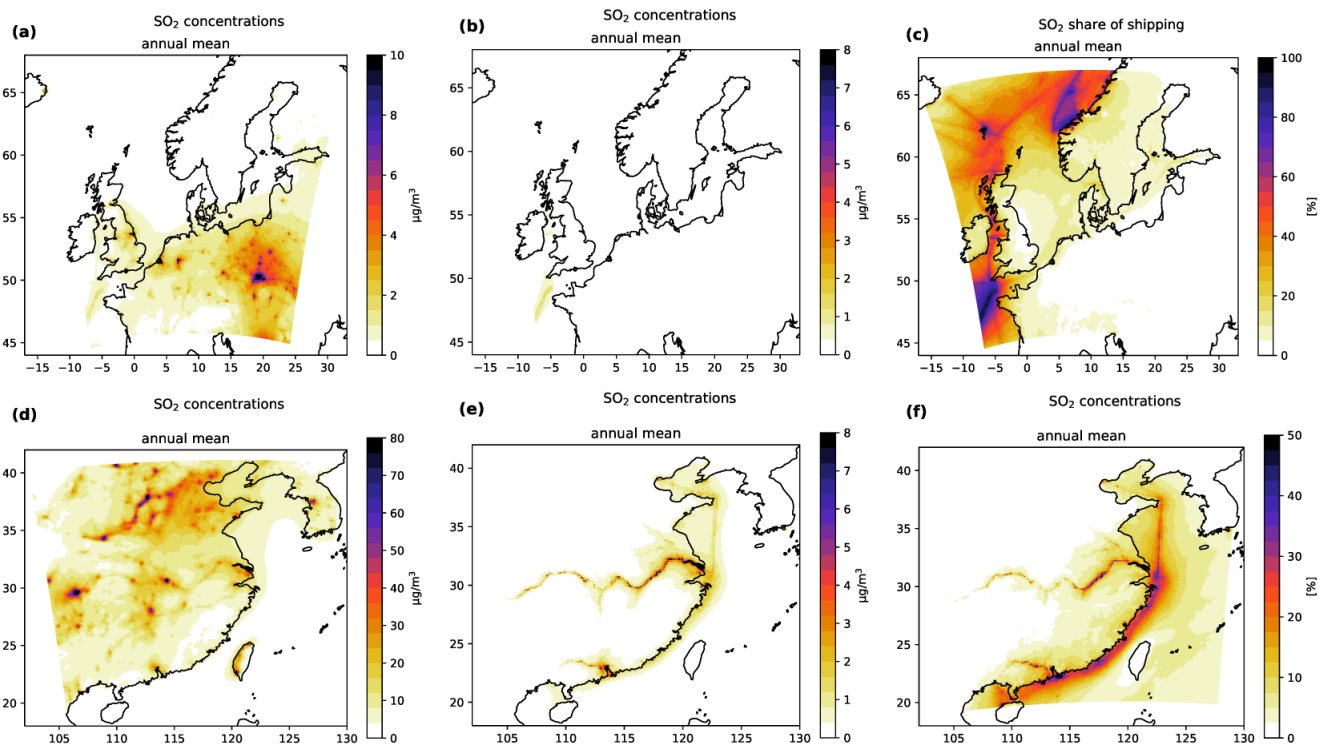


Figure 5.5.: Annual averages of  $\text{SO}_2$  concentrations in the SC12NSBS domain in Europe (a–c) and in the CNC12 domain in China (d–f).  $\text{SO}_2$  concentrations [ $\mu\text{g} \cdot \text{m}^{-3}$ ] from all emission sources are shown in (a,d), from shipping only in (b,e) and the share of  $\text{SO}_2$  concentrations from shipping on total  $\text{SO}_2$  concentrations [%] is shown in (c,f).

In Europe, SO<sub>2</sub> was emitted mainly from coal power plants, e.g., in the Rhine-Ruhr region in Germany or in the Polish provinces of Lodz, Opole and Silesian. Elevated concentrations of 12.5 µg · m<sup>-3</sup> were common near these coal power plants, and concentrations up to 4 µg · m<sup>-3</sup> were modeled in large parts of Poland (Fig. 5.5 (a)). In winter and autumn, SO<sub>2</sub> concentrations were higher due to residential heating (Fig. A.7).

Since an SECA was introduced in the North Sea and Baltic Sea in early 2015, SO<sub>2</sub> from shipping has become less important as an air pollutant. Nevertheless, small contributions of less than 0.3 µg · m<sup>-3</sup> (15 % of total SO<sub>2</sub>) were modeled in the vicinity of the ports of Rotterdam, Amsterdam, Antwerp and Hamburg. From outside of the SECA, SO<sub>2</sub> concentrations of similar magnitude were transported from the major shipping routes to the coastal regions of Brittany (40 %). Furthermore, concentrations of up to 0.8 µg · m<sup>-3</sup> (50–70 %) were modeled in port cities on the east coast of Ireland and the west coast of the United Kingdom (Fig. 5.5 (d)).

In 2015, 64 % of the Chinese domestic energy consumption was produced using coal power plants (26 % in Europe) (Qi et al., 2016; Redl et al., 2021)). This difference was reflected in higher atmospheric SO<sub>2</sub> concentrations (Fig. 5.5 (d)). In densely populated and industrialized regions, annual averages of 30 µg · m<sup>-3</sup> were modeled with local concentration peaks of up to 100 µg · m<sup>-3</sup>. Similar to NO<sub>2</sub>, ship traffic contributed the most to SO<sub>2</sub> in the major port clusters in the YRD, PRD and along the Yangtze River, with concentrations ranging from 4 to 8 µg · m<sup>-3</sup> (30–40 %). SO<sub>2</sub> concentrations of 1 to 3 µg · m<sup>-3</sup> (10–20 %) were modeled along large parts of the coastline (Fig. 5.5 (e), (f)). The seasonal patterns of SO<sub>2</sub> were similar to those of NO<sub>2</sub>. Concentrations were higher in winter and autumn, especially in the YRD and PRD port clusters and along navigated rivers (Fig. A.11). It is assumed that, similar to NO<sub>2</sub>, chemical conversion and deposition of SO<sub>2</sub> from shipping was inhibited due to high SO<sub>2</sub> emissions from other sectors.

When comparing the two regions, atmospheric SO<sub>2</sub> concentrations in China were found to be approximately 6 times those in Europe. For similar reasons as for NO<sub>2</sub>, reverse seasonal trends between the two regions were also modeled for SO<sub>2</sub>.

### 5.3.3. Ozone

Tropospheric ozone is known to be harmful to the respiratory tract and is also a potent greenhouse gas (IPCC, 1995, 2001). O<sub>3</sub> is a photochemical product for which formation solar radiation is the most important factor. However, concentrations of tropospheric ozone are also controlled by the availability of reaction partners, such as NO<sub>x</sub> and VOCs. For this reason, high VOC/NO<sub>x</sub> ratios can produce NO<sub>x</sub>-limited conditions that favor ozone formation and usually occur in rural areas. Vice versa, low VOC/NO<sub>x</sub> ratios and VOC-limited conditions are common in urban centers and promote O<sub>3</sub> titration. By this means, ship emissions that contain NO<sub>x</sub> and VOCs can have a significant influence on regional ozone concentrations. With respect to the comparison with measurements in Sect. 5.2, it must be noted that ozone concentrations were systematically overestimated in both domains.

In Europe, annual averages of 8-hour max. ozone concentrations over land were modeled in the range of 75 to 90 µg · m<sup>-3</sup> (Fig. 5.6 (a)). Due to high cloud coverage in Europe during the summer months of 2015, especially over the North Sea, the United Kingdom and the Scandinavian countries, the modeled O<sub>3</sub> concentrations were lower for summer than spring (Fig. A.13). However, this result needs to be interpreted with care, as the ozone overestimation was found to be higher in spring than in summer.

Due to high NO<sub>x</sub> emissions from shipping and VOC-limited conditions in the area of the harbors of Rotterdam, Antwerp and Hamburg, O<sub>3</sub> concentrations were reduced to approximately 70–80 µg · m<sup>-3</sup> by NO<sub>x</sub>-promoted ozone decomposition. This corresponded to an ozone reduction of 10 to 15 µg · m<sup>-3</sup> and a relative reduction of 10 to 15 % (Fig. 5.6 (b), (c), illustrated ozone concentrations here represent annual averages instead of averages of the O<sub>3</sub> 8-hour max.). In other areas of the SC12NSBS domain, ship emissions increased ozone by 1–3 µg · m<sup>-3</sup> (1–3 %). The reduction potential was stronger in winter when the solar irradiation was lower (Fig. 5.7 (a)). During summer, a ship-related increase in ozone concentrations by 4 to 8 µg · m<sup>-3</sup> (5–10 %) was modeled in Denmark, southern Sweden, Norway and northern Germany, as well as in coastal regions bordering the Baltic Sea and the English Channel (Fig. 5.7 (b) and Figures A.14 and A.15).

In China, average values of 8-hour max. ozone concentrations were modeled between 140 and 150 µg · m<sup>-3</sup>. Values were lower in the southern- and northernmost coastal regions, 100–120 µg · m<sup>-3</sup> (Fig. 5.6 (d)). Re-



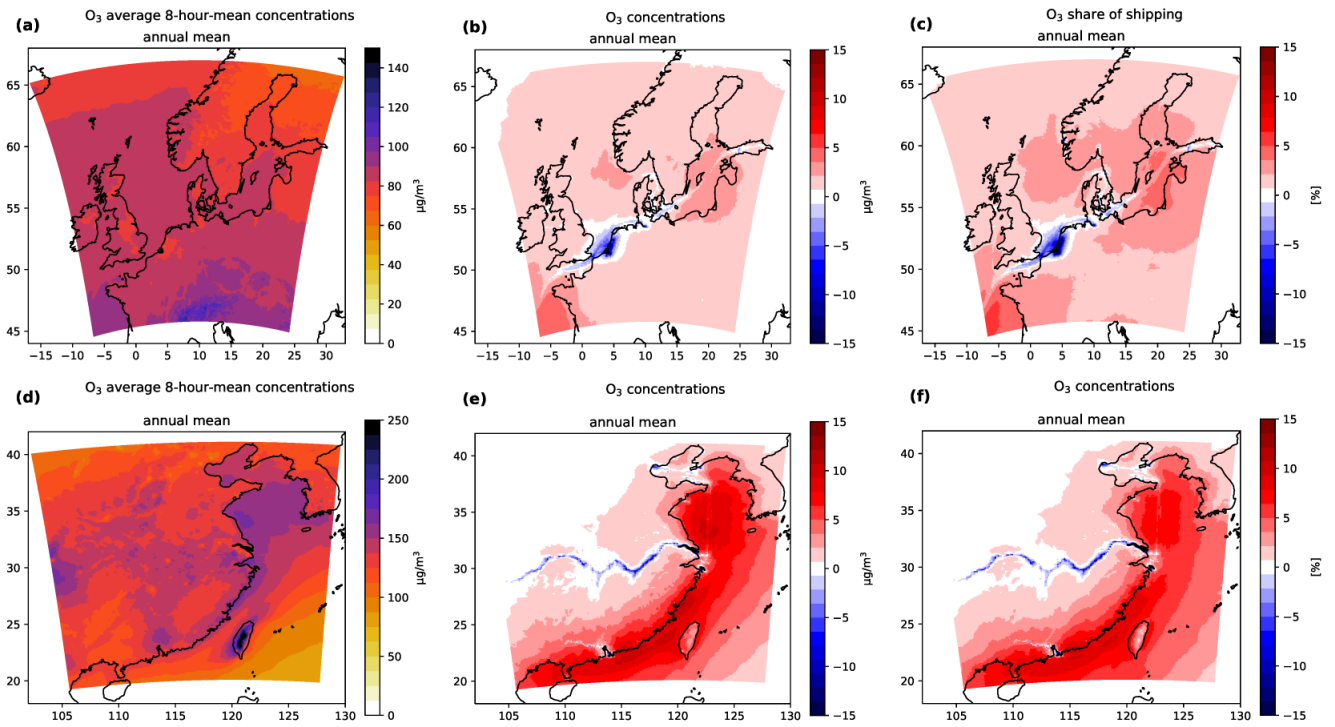


Figure 5.6.: Annual averages of  $O_3$  concentrations in the SC12NSBS domain in Europe (a–c) and in the CNC12 domain in China (d–f). Annual averages of 8-hour max.  $O_3$  concentrations [ $\mu\text{g} \cdot \text{m}^{-3}$ ] from all emission sources are shown in (a,d), annual averages from shipping only in (b,e) and the share of  $O_3$  concentrations from shipping on total  $O_3$  concentrations [%] is shown in (c,f).

Regarding the seasonality of  $O_3$ , different factors had to be considered for mainland China. While in the winter radiation was lower, especially in the northeast, high  $\text{NO}_x$  emissions from residential heating promoted ozone decomposition. Furthermore, an increased aerosol load was able to take up gaseous precursors relevant for ozone formation (Li et al., 2019a). Consequently,  $O_3$  concentrations were very low (e.g., in the LYP and NCP during winter, often less than  $50 \mu\text{g} \cdot \text{m}^{-3}$ ).

In China, an ozone reduction from ship emissions of  $5\text{--}15 \mu\text{g} \cdot \text{m}^{-3}$  could mainly be observed along the Yangtze River. As in Europe, the reason for this was a smaller  $\text{VOC}/\text{NO}_x$  ratio, which decreased through ship emissions. At the large port cluster in the YRD and PRD, VOC-limited conditions were plausible; however, the impact of  $\text{NO}_x$  from ships on ozone degradation was small. An explanation for this was the low relative contributions of ships to the total  $\text{NO}_2$  concentrations, which were lower than, for example, in Rotterdam/Antwerp. This was also consistent with the results in Sect. 5.2, which indicated that the inclusion of ship emissions has little effect on ozone concentrations in the YRD and PRD. Increased ozone concentrations due to ship emissions were found along the southern coastline by  $4\text{--}8 \mu\text{g} \cdot \text{m}^{-3}$  (5–8%) and by approximately  $2\text{--}3 \mu\text{g} \cdot \text{m}^{-3}$  along the northern coastline (Fig. 5.6 (e) and (f)). Here, it was plausible that ozone whose formation was promoted by ship emissions in marine environments might have been transported to coastal regions by onshore winds. During spring and especially in summer, higher  $O_3$  concentrations from ships were shifted towards the northeast, while in autumn and winter, high concentrations were shifted to the southeast (Figure 5.7 (c) and Figures A.17 and A.18). Due to less irradiation during winter, a seasonal reduction in  $O_3$  concentrations through ship emissions was modeled in the PRD, the YRD and along the Yangtze River. An ozone reduction during winter was also evident in the Bohai and Yellow Seas, where it was plausible that  $\text{NO}_x$  was transported from northern China and the Korean Peninsula to the marine environment to create VOC-limited conditions. Concentrations were reduced by approximately  $10\text{--}20 \mu\text{g} \cdot \text{m}^{-3}$  (10–20%) in the YRD, PRD and near the Yangtze and by  $2 \mu\text{g} \cdot \text{m}^{-3}$  (2%) at the northern coastline.

In contrast to Europe, ozone concentrations in China were less reduced by ship emissions, especially in the large port clusters. This could be attributed to the lower contribution of shipping to total  $\text{NO}_2$

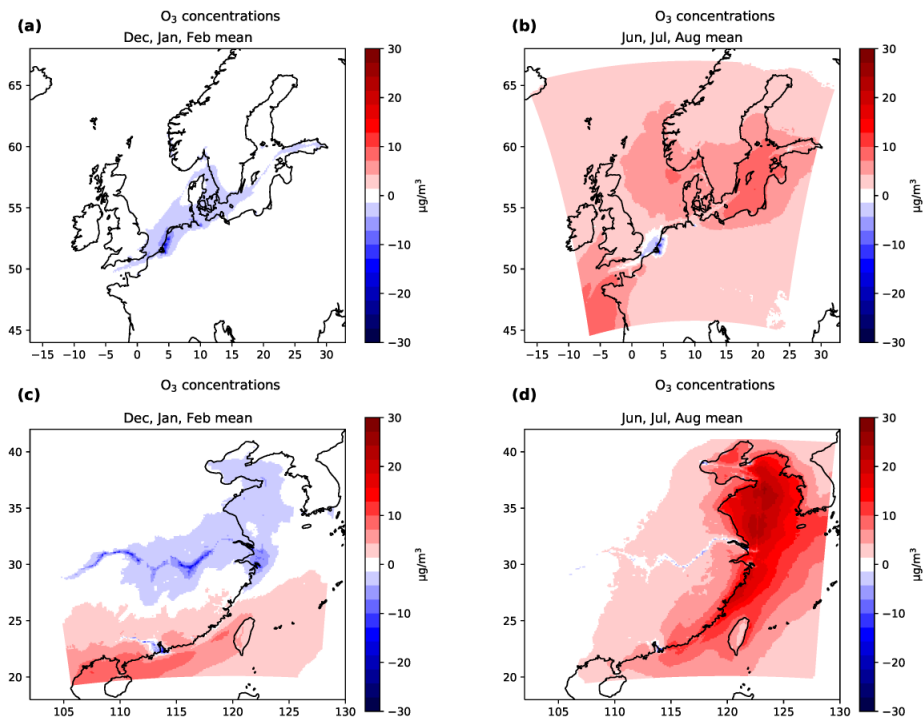


Figure 5.7.: Seasonal averages of O<sub>3</sub> concentrations [ $\mu\text{g} \cdot \text{m}^{-3}$ ] from shipping in the SC12NSBS domain in Europe for winter (a), summer (b) and in the CNC12 domain in China for winter (c) and summer (d).

concentrations in China. In addition, ship emissions increased ozone formation in many coastal regions that were close to the major shipping lanes. However, in China this observation was much more pronounced than in Europe, as significant amounts of ozone formed in marine areas were transported to land. A similar seasonality for O<sub>3</sub> was modeled for northern Europe and northern China, with lower O<sub>3</sub> concentrations in winter and autumn (Fig. 5.7 and Figures A.17 and A.14). A reversal of this seasonality was found for the subtropical climate zone of southern China.

### 5.3.4. Fine Particulate Matter (PM<sub>2.5</sub>)

With respect to its source, PM<sub>2.5</sub> is divided into primary and secondary particles. Primary PM<sub>2.5</sub> is emitted directly from the emission source. With respect to ship emissions, these are sulfate, water associated with sulfate, BC, MA and POAs. However, the major impact of PM<sub>2.5</sub> from shipping usually stems from secondary nitrate and sulfate particles, which are formed in atmospheric chemical reactions from the precursors NO<sub>x</sub> and SO<sub>2</sub>. Normally, these form as the ammonium salts (Sect. 5.3.4.1): ammonium sulfate (Sect. 5.3.4.2) and ammonium nitrate (Sect. 5.3.4.3). The oxidation rate for these compounds, as well as nucleation and particle growth, depends on environmental parameters (e.g., temperature, solar radiation and humidity). Furthermore, the availability of reaction partners such as ammonia (NH<sub>3</sub>), hydroxyl radicals (OH<sup>·</sup>) and ozone (O<sub>3</sub>) is of importance. The high atmospheric lifetime of aerosol species enables PM<sub>2.5</sub> from shipping to be transported hundreds of kilometers away from the main shipping routes to inland areas (U. S. EPA, 2009).

In Europe, the highest annual average PM<sub>2.5</sub> concentrations of 12–15  $\mu\text{g} \cdot \text{m}^{-3}$  were modeled in neighboring states of the North Sea, close to the major shipping lanes, i.e., northern France, England, northern Germany and especially Belgium and the Netherlands (Fig. 5.8 (a)). In these regions, the formation of secondary aerosols was promoted by high ammonia emissions from agriculture, which were highest during spring, the main season for fertilization (Fig. A.19); see also Sects. 5.3.4.1, 5.3.4.2 and 5.3.4.3).

Ship emissions were relevant precursors for the formation of secondary particulates and contributed approximately 10% to the modeled concentrations (1 to 1.25  $\mu\text{g} \cdot \text{m}^{-3}$ , Fig. 5.8 (b), (c)). The main spatial patterns were preserved during all seasons; however, the most impacted region shifted eastwards during

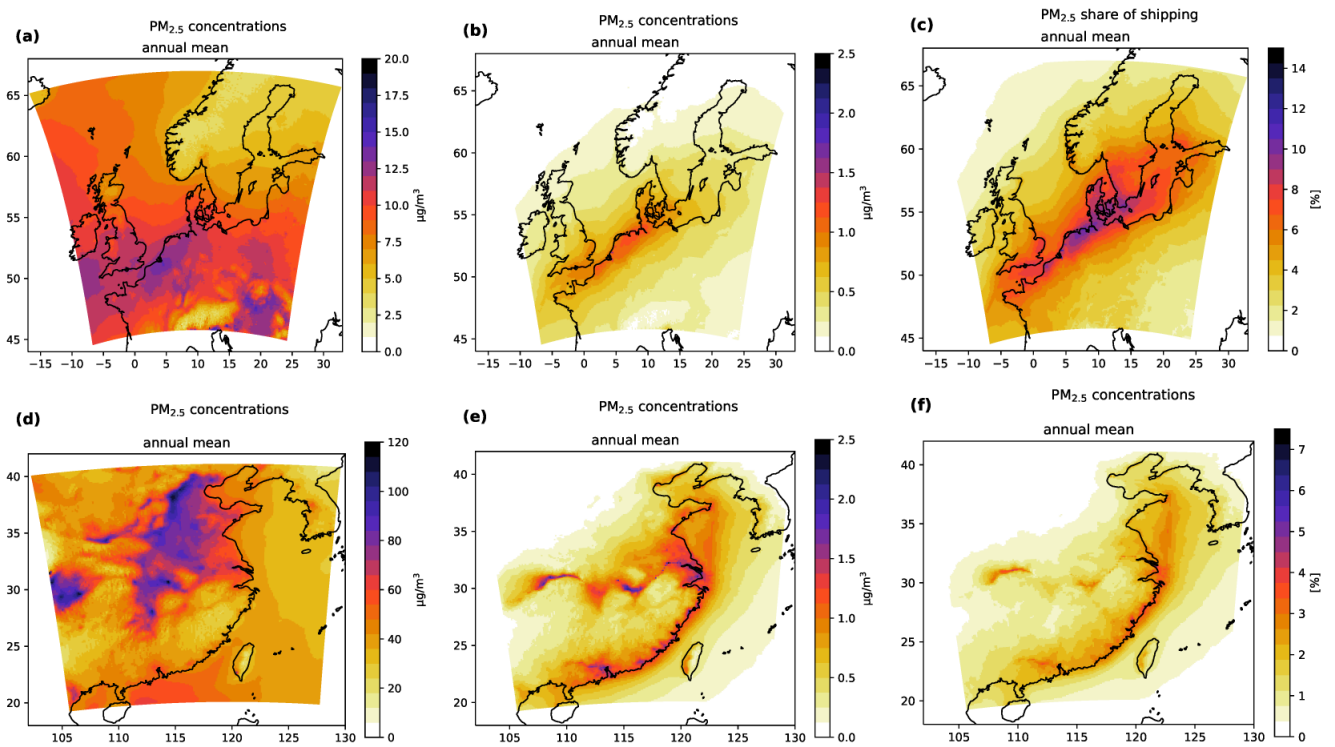


Figure 5.8.: Annual averages of  $\text{PM}_{2.5}$  concentrations in the SC12NSBS domain in Europe (a–c) and in the CNC12 domain in China (d–f).  $\text{PM}_{2.5}$  concentrations [ $\mu\text{g} \cdot \text{m}^{-3}$ ] from all emission sources are shown in (a,d);  $\text{PM}_{2.5}$  concentrations only from shipping are shown in (b,e); the share of  $\text{PM}_{2.5}$  concentrations from shipping in the  $\text{PM}_{2.5}$  concentrations from all sources [%] is shown in (c,f).

winter to northern Germany and Denmark. In summer, the field with the highest concentrations was stretched along the English Channel and the North Sea coastline of the European mainland. This observed shift corresponded to the frequent southwesterly wind direction in winter and the westerly wind directions in summer. During spring, it is evident that ship emissions, combined with the higher ammonia emissions, result in a strong increase in ship-related  $\text{PM}_{2.5}$  concentrations (Fig. 5.9 (c)).

In China, the highest annual average concentrations of  $100\text{--}125 \mu\text{g} \cdot \text{m}^{-3}$  were modeled in megacities and regions with high traffic and industry densities, e.g., Chongqing and Chengdu in the Sichuan Basin, Wuhan and the Beijing-Tianjin-Hebei city cluster (Fig. 5.8 (c)). During winter,  $\text{PM}_{2.5}$  concentrations were highest, with concentrations up to  $150\text{--}200 \mu\text{g} \cdot \text{m}^{-3}$  (Fig. A.22). Although China has a large agricultural sector, a concise increase in  $\text{PM}_{2.5}$ , promoted by high ammonia emissions from agricultural fertilization, which has its main season here during summer, could not be observed.

$\text{PM}_{2.5}$  concentrations of  $1\text{--}1.5 \mu\text{g} \cdot \text{m}^{-3}$  from shipping were modeled along large parts of the Chinese coastline and in the LYP and NCP; concentrations of  $2 \mu\text{g} \cdot \text{m}^{-3}$  were found in the vicinity of the port cluster in the YRD and PRD and in parts of the Yangtze River. The share of shipping on total  $\text{PM}_{2.5}$  concentrations in China was 2–3% small due to the high  $\text{PM}_{2.5}$  contributions from other sectors (Fig. 5.8 (e) and (f)). Remarkably, almost no ship-related impact on  $\text{PM}_{2.5}$  concentrations was modeled in northeastern China during winter (Fig. 5.9 (e)). It is assumed that in winter, the ratio of aerosol precursors from other sectors was too high to allow significant particle generation from ship emissions. Furthermore, lower concentrations were modeled for spring and summer along the southern coastline due to the higher temperatures and a higher deposition during the rainy season (Fig. 5.9 (f) and (g)).

In summary, it can be said that the modeled  $\text{PM}_{2.5}$  concentrations were approximately 6 times higher in China than in Europe. The  $\text{PM}_{2.5}$  concentrations due to ship traffic were on a similar level, resulting in a lower contribution from ships to total  $\text{PM}_{2.5}$  concentrations. Notable differences in seasonality were found between the two regions (Fig. 5.9).

To gain better insight into these aspects, the main components of  $\text{PM}_{2.5}$ , ammonium, sulfate and nitrate

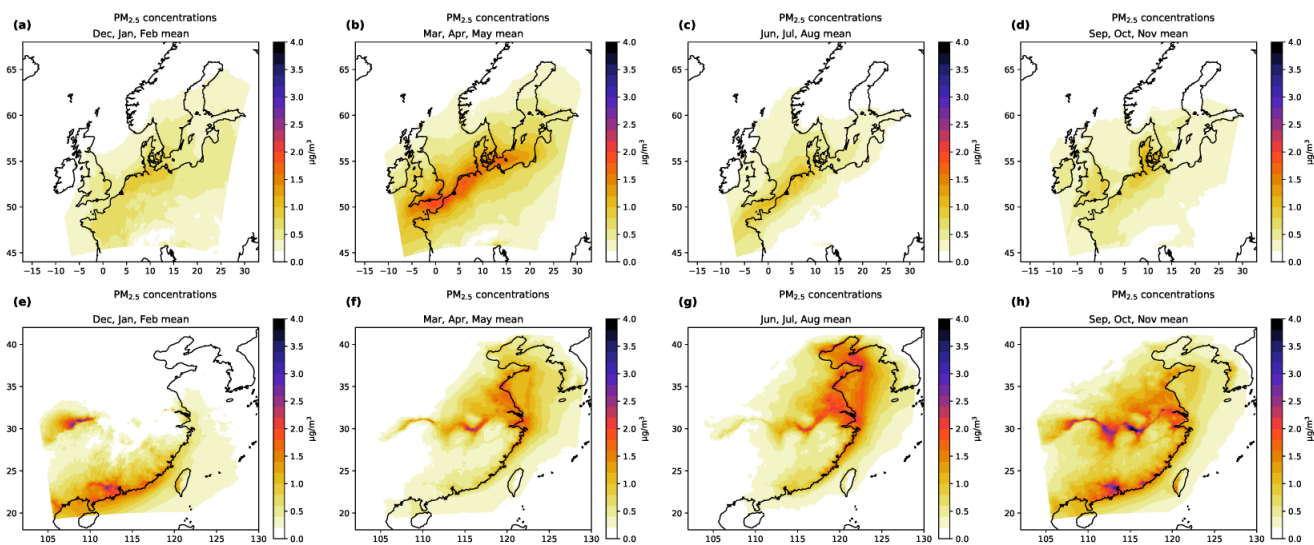


Figure 5.9.: Seasonal averages of  $\text{PM}_{2.5}$  concentrations [ $\mu\text{g} \cdot \text{m}^{-3}$ ] from shipping in the SC12NSS domain in Europe for winter (a), spring (b), summer (c), autumn (d) and in the CNC12 domain in China for winter (e), spring (f), summer (g) and winter (h).

concentrations were analyzed for both regions in the following sections. Hereby it was to consider that particle formation is strongly dependent on microclimatic conditions, such as temperature, humidity, concentrations of oxidants and precursors, and the presence of pre-existing aerosols (Baek et al., 2004; Pathak et al., 2009).

#### 5.3.4.1. Ammonium ( $\text{NH}_4$ )

Ammonium is a typical secondary aerosol component originating mainly from agricultural ammonia emissions. The modeled ammonium concentrations presented in this chapter refer to the  $\text{NH}_4^+$  mass component in secondary aerosols, i.e., approximately the sum of the mass of ammonium sulfate and ammonium nitrate particles minus the mass of sulfate and nitrate.

In both regions, a strong seasonality and temperature dependency could be seen for the formation of ammonium particles with higher concentrations during winter and lower concentrations during summer. Seasonality was less pronounced for ammonium from shipping.

In Europe, ammonium originating from ship emissions increased aerosol pollution by  $0.2 \mu\text{g} \cdot \text{m}^{-3}$  in most coastal regions bordering the main shipping routes (Fig. 5.10 (b)). Analogous to the total  $\text{PM}_{2.5}$ , elevated ammonium concentrations of  $0.4 \mu\text{g} \cdot \text{m}^{-3}$  were modeled in coastal regions of mainland northern Europe in spring. These are generated by ammonia from agricultural fertilization in combination with ship emissions (Fig. A.25 and A.31). The lowest impact of ammonium from shipping was observed in summer, when high temperatures impeded the nucleation of particles. An approximate contribution of 20% to total ammonium concentrations in Europe could be ascribed to ships (Fig. 5.10 (c)). This contribution could rise up to 40–50% during summer, when fewer precursor species from other emission sectors were present.

In China, ammonium from shipping was modeled in concentrations of  $0.2 \mu\text{g} \cdot \text{m}^{-3}$  along the coastline. Higher concentrations of  $0.3\text{--}0.4 \mu\text{g} \cdot \text{m}^{-3}$  were found in the YRD, along the Yangtze, and in the LYP and the NCP (Fig. 5.10 (e)). The contribution of shipping to ammonium was 12% on the southeast coast and 8% in the northeast coastal regions (Fig. 5.10 (f)). Distinct regional and seasonal differences were evident in the model results. Similar to  $\text{PM}_{2.5}$ , no contribution of shipping to ammonium was modeled in northeast China during winter. Due to the rainy season in spring and summer, almost no ammonium contributions from shipping were modeled at the southern coastline (Fig. A.29).

A comparison of the two regions showed that ammonium concentrations in China were approximately 5 times higher than those in northern Europe, which was in agreement with the results of the modeled  $\text{PM}_{2.5}$  totals (Fig. 5.10 (a) and (d)). The contribution from shipping, however, was in both domains on a similar scale. In China, the spatial pattern of  $\text{NH}_4$  concentrations corresponded better to ammonia emissions,

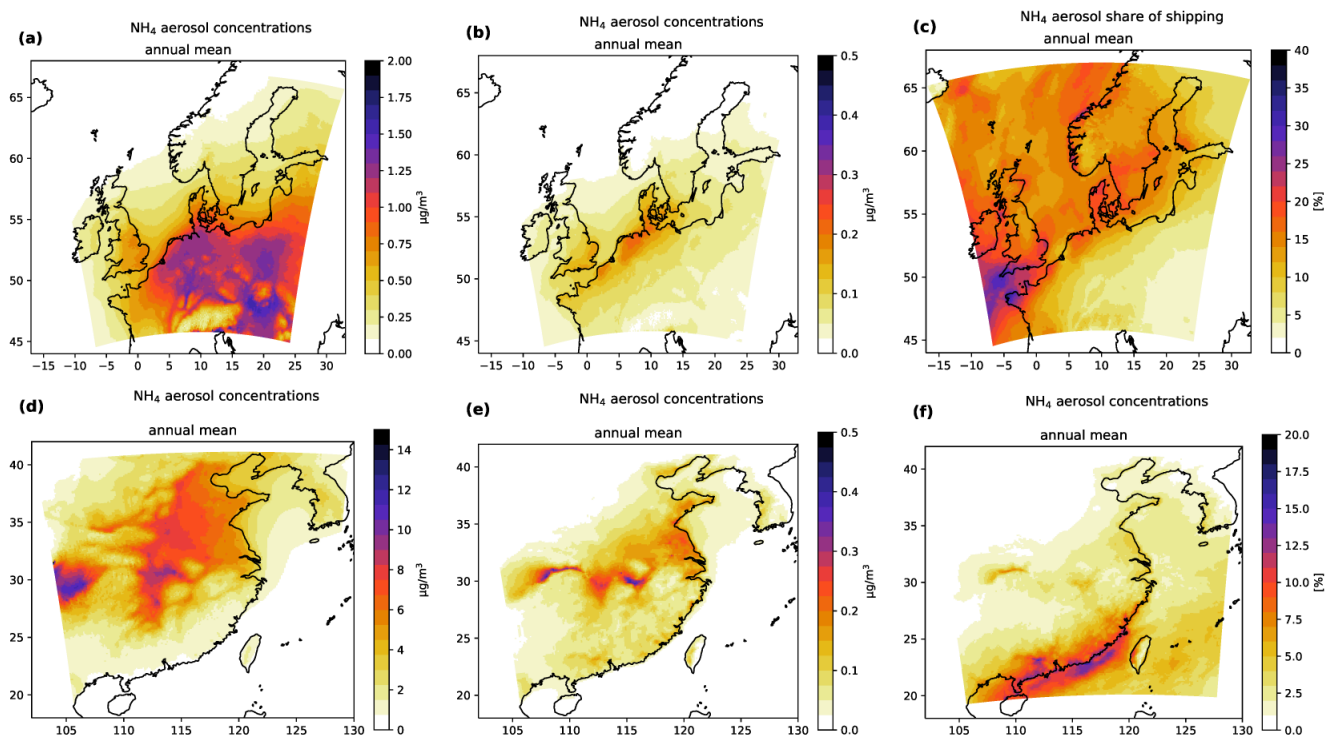


Figure 5.10.: Annual averages of  $\text{NH}_4$  concentrations in the SC12NSBS domain in Europe (a–c) and in the CNC12 domain in China (d–f).  $\text{NH}_4$  concentrations [ $\mu\text{g} \cdot \text{m}^{-3}$ ] from all emission sources are shown in (a,d);  $\text{NH}_4$  concentrations only from shipping are shown in (b,e); the share of  $\text{NH}_4$  concentrations from shipping in the  $\text{NH}_4$  concentrations from all sources [%] is shown in (c,f).

which was probably related to the overall higher  $\text{NH}_3$  emissions (Fig. A.28 and A.32). Despite the large agricultural sector in China and the high ammonia emissions during summer, no peak  $\text{NH}_4$  concentrations from fertilization were modeled, as in Europe during spring. A reason for this could be found in the high deposition rates during the rainy season in summer. Similar to  $\text{PM}_{2.5}$  concentrations, the remarkable seasonal concentration differences for ammonium from shipping in China were very different from the more uniform seasonality observed in Europe. They could be attributed to the high atmospheric background pollution in China and different weather phenomena.

#### 5.3.4.2. Sulfate ( $\text{SO}_4$ )

Sulfate particles form from  $\text{SO}_2$  in the atmosphere via a photoinduced gas-phase oxidation over the intermediate  $\text{SO}_3$  or in an aqueous phase reaction. Sulfate is deposited as sulfuric acid or irreversibly combines with ammonium in a reaction favored over the formation of ammonium nitrate (Seinfeld and Pandis, 2006).

In both domains, sulfate concentrations corresponded to the spatial and seasonal patterns of  $\text{SO}_2$  concentrations, although they were more diffuse due to a longer particle lifetime. Accordingly, sulfate from shipping played a subordinate role in the area of the northern European SECA (see also 5.3.2). However,  $\text{SO}_2$  emitted in the Celtic Sea, outside the SECA, was able to form aerosols that were transported by westerly winds to the United Kingdom and the French coastline in concentrations of approximately  $0.1$  to  $0.15 \mu\text{g} \cdot \text{m}^{-3}$  (Fig. 5.11 (b)). Sulfate concentrations were highest during summer due to increased shipping activity (Fig. A.43).

In China, sulfate from shipping impacts the air quality along the whole coastline and along the Yangtze River. The highest concentrations of approximately  $0.5 \mu\text{g} \cdot \text{m}^{-3}$  (5–10 %) were found near the port cluster in the YRD and PRD (Fig. 5.11 (e)). Similar to  $\text{PM}_{2.5}$  and ammonium, almost no  $\text{SO}_4$  concentrations from shipping were modeled in northeastern China during winter, while in summer, concentrations were reduced in southeastern China due to the rainy season (Fig. A.43). When compared to other particulates,

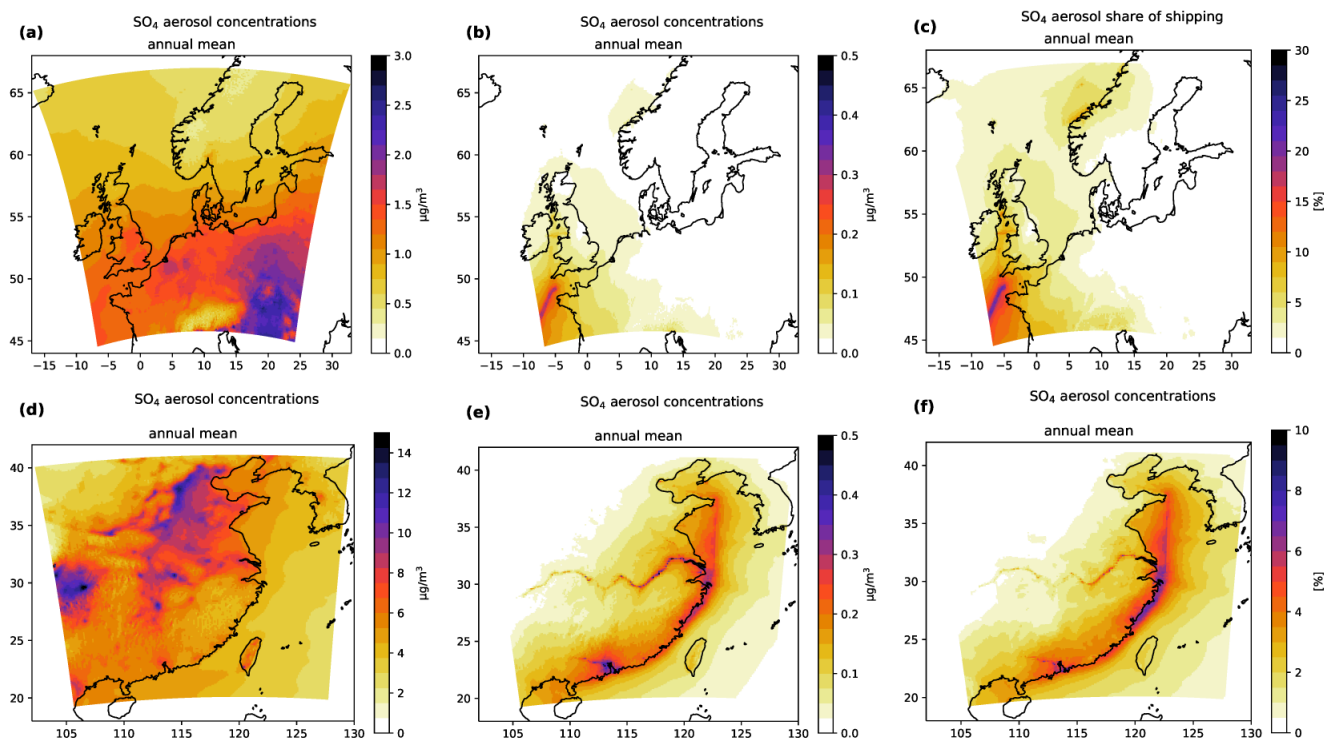


Figure 5.11.: Annual averages of  $\text{SO}_4$  concentrations in the SC12NSBS domain in Europe (a–c) and in the CNC12 domain in China (d–f).  $\text{SO}_4$  concentrations [ $\mu\text{g} \cdot \text{m}^{-3}$ ] from all emission sources are shown in (a,d);  $\text{SO}_4$  concentrations only from shipping are shown in (b,e); the share of  $\text{SO}_4$  concentrations from shipping in the  $\text{SO}_4$  concentrations from all sources [%] is shown in (c,f).

$\text{SO}_4$  from shipping was found closer to shipping lanes and coastal regions, which could be explained by its higher affinity to ammonium compared to nitrate.

### 5.3.4.3. Nitrate ( $\text{NO}_3$ )

Nitrate particles form from  $\text{NO}_2$  in a gas-phase oxidation with hydroxyl radicals during the day or via the intermediate  $\text{N}_2\text{O}_5$  in a nightly oxidation by ozone. Nitrate is deposited from the atmosphere as nitric acid or reacts with ammonia to form ammonium nitrate particles.

In Europe, especially the coastal regions bordering the English Channel, northern France, Belgium, the Netherlands, northern Germany and Denmark were affected by high  $\text{NO}_3$  loads (Fig. 5.12 (b)). In winter and autumn, higher concentrations were shifted towards the northeastern coastline of the European mainland, while in summer, they were shifted towards the southwest. Due to agricultural fertilization,  $\text{NO}_3$  concentrations were  $1.5 \mu\text{g} \cdot \text{m}^{-3}$  highest during spring (Fig. A.34).

In China, the Yangtze River, the LYP and NCP were most affected by nitrate aerosols from shipping in concentrations of  $0.5\text{--}1 \mu\text{g} \cdot \text{m}^{-3}$  (Fig. 5.12 (e)). The highest concentrations of  $1 \mu\text{g} \cdot \text{m}^{-3}$  were modeled during spring (Fig. A.37).

In both regions nitrate concentrations were found to correlate with ammonium concentrations. Especially in China, high  $\text{NO}_3$  concentrations were modeled in areas with low  $\text{SO}_2$  concentrations but abundant ammonium (Fig. 5.12 (a) and (d)). In general, the formation rate of  $\text{NO}_3$  particles showed a stronger seasonality than sulfate. A comparison of the nitrate and  $\text{NO}_2$  ratios suggested that the formation of nitrate aerosols was limited by available ammonium. The  $\text{NO}_3$  and  $\text{NH}_4$  concentrations were approximately 5 times higher in China than in Europe, while the ratio for  $\text{NO}_2$  was only 2.5. The highest  $\text{NO}_3$  concentrations were modeled in winter, when low temperatures enabled higher nucleation rates. Due to the SECA in the North and Baltic Seas,  $\text{SO}_2$  concentrations were smaller than those China, and emissions from regional shipping resulted in higher  $\text{NO}_3$  concentrations (Fig. 5.12 (b)).

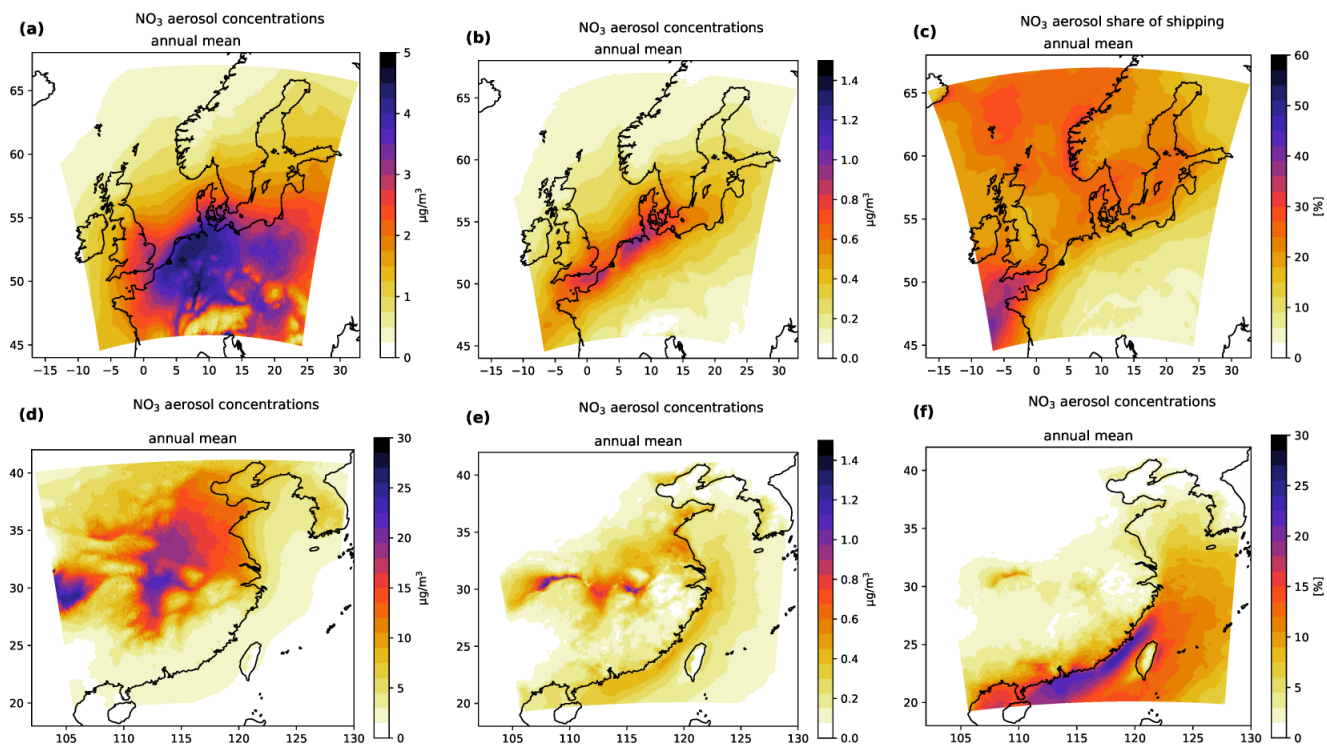


Figure 5.12.: Annual averages of  $\text{NO}_3$  concentrations in the SC12NSBS domain in Europe (a–c) and in the CNC12 domain in China (d–f).  $\text{NO}_3$  concentrations [ $\mu\text{g} \cdot \text{m}^{-3}$ ] from all emission sources are shown in (a,d);  $\text{NO}_3$  concentrations only from shipping are shown in (b,e); the share of  $\text{NO}_3$  concentrations from shipping in the  $\text{NO}_3$  concentrations from all sources [%] is shown in (c,f).

## 5.4. Conclusions

In this work, an air quality modelling system was applied to calculate and study pollutant concentrations for northern Europe, including the North and Baltic Seas, and eastern China, including the Yellow and South China Seas for 2015 in a harmonized approach. However, a noticeable difference between these two regions was, generally, the background air pollution, which could be classified as high in China and medium in Northern Europe. The goal of this study was a comparison of the impact of ship emissions between both regions, with a focus on the obvious differences and similarities.

An accurate representation of ship emissions was achieved by using two temporally and spatially high resolved bottom-up ship emission inventories, both created with the MoSES ship emission model using comparable input parameters. Anthropogenic emissions from other sectors were covered by the MEIC and EDGAR emissions inventories for China and CAMS emissions for Europe, which were distributed and generated using the HiMEMO emissions model. The emission data were fed into the chemical transport model CMAQ, as well as the meteorologic forcing, which was calculated with COSMO-CLM. Species concentrations of interest were those for  $\text{NO}_2$ ,  $\text{SO}_2$ ,  $\text{O}_3$ , PM and the secondary aerosol components ammonia, sulfate and nitrate. The contribution of ship traffic to air pollutant concentrations was determined by using the zero-out method.

The performance of the model was evaluated by a comparison of the modeled concentrations with measurement data from coastal air quality stations. Overall, the model performance proved to be satisfactory. However,  $\text{NO}_2$  concentrations were often predicted to be too low for Europe, and ozone concentrations were often predicted to be too high in both regions. A comparison between the results obtained with the MEIC inventory and the results obtained with the EDGAR v5 inventory for nonshipping land-based anthropogenic emissions in China pointed to an overestimation by the latter.

The comparison between China and Europe showed that air pollutant concentrations originating from ship emission were generally on a comparable scale, with slightly higher concentrations in China. However, a stronger seasonality was found for China, with the East Asian monsoon and different climate zones as

an important factors. Greater similarity was found between temperate northeastern China and Europe, while in the subtropical climate zone, the observed trends were often reversed. Compared to Europe, the overall higher concentrations of background air pollution in China modified the atmospheric chemistry of ship exhausts, especially for PM. This resulted in a smaller relative impact of ship emissions in China.

The relative contribution of ships to NO<sub>2</sub> concentrations was higher in Europe, with 30 % in moderately affected regions and 50 % in highly affected regions, compared to 10 and 30 % in China. In addition, NO<sub>2</sub> was transported further in the atmosphere during winter in China, which was related to an increased NO<sub>2</sub> lifetime due to oxidant-limited conditions.

As a result of the SECA implemented in the North and Baltic Seas in 2015, the amount of SO<sub>2</sub> emissions differed significantly between the compared regions.

Tropospheric ozone reductions through ship emissions in large ports were stronger in Europe than in China, by an average of 10–15 μg · m<sup>-3</sup> (10–15 %). In China's large ports, the shipping influence on ozone concentrations was mainly neutral due to the lower contribution of ships to total emissions. Along the Chinese coast, ship emissions had a stronger promoting effect on O<sub>3</sub> formation, particularly in the south, with 2–10 μg · m<sup>-3</sup> (3–10 %). In southern China, this could be attributed to a higher irradiation but also, an inland transport of ozone, whose formation is promoted by shipping in marine environments, was plausible.

In Europe, NO<sub>x</sub> and SO<sub>2</sub> from shipping led in combination with high ammonia emissions from agricultural fertilization during spring to peaking secondary PM concentrations (2 μg · m<sup>-3</sup>, 13 %). A similar seasonal peak of secondary PM could not be observed in China, despite high ammonia emissions from its large agricultural sector. Another notable observation was that during winter, no significant PM<sub>2.5</sub> concentrations from shipping were modeled in the eastern and northeastern parts of China. High aerosol precursor emissions from other sectors could deplete the reaction partners and oxidants necessary for secondary particle formation and inhibit the transformation of aerosol precursors from ship exhausts.

A comparison of the obtained model results with former studies by Aulinger et al. (2016) on the North Sea and Karl et al. (2019b) on the Baltic Sea, both for 2011, showed a similar impact of shipping on NO<sub>2</sub> concentrations. The results for SO<sub>2</sub> were not comparable due to differences in the sulfur regulation between these years. The impacts of ships on ozone concentrations were modeled slightly higher in this study for both, a promotion of ozone formation and depletion. PM<sub>2.5</sub> concentrations from ships were slightly lower in this study, which was reasonable due to the stricter fuel sulfur limits in 2015. Former studies on the impact of ship emissions on air quality for the YRD and PRD in 2015, by Feng et al. (2019) and Chen et al. (2019), respectively, were for most pollutants in agreement with the concentrations found in this study. However, the ozone reducing effect of ship emissions in the PRD was also found to be stronger in the present study.

The results from this study show the importance for a regulation of ship emissions in concert with other emission sectors, particularly in China. Otherwise, potential achievements from reducing ship emissions could be offset by emissions from other sectors. Indicators for such effects were the prolonged NO<sub>x</sub> lifetime and the impeded formation of secondary PM from ship emissions found in northern China. Furthermore this was indicated by the fact that ship-related PM<sub>2.5</sub> concentrations were in a similar range between Europe and China although sulfur-containing ship emissions, as precursors to secondary PM, were drastically reduced in Europe due to the implemented SECA. Since ammonia is an important precursor for ship-related PM, a regulation of NH<sub>3</sub> emissions could help in reducing PM concentrations. Such regulations could include a motivation to limit agricultural fertilization to specific seasons or by fertilization recommendations based on the current meteorologic situation to mitigate PM formation.



## 6. Summarising Discussion

This thesis deals with research on GHG emissions and air pollutants from the shipping sector. It is well-known that ship emissions contribute substantially to global warming, environmental problems, and health issues. Ships are operated in many regions worldwide, however, the extent of the impact of their emissions on air quality can vary regionally, depending on influences such as the regional shipping fleet, state of background atmospheric pollution, and meteorological aspects. Therefore, one objective of this thesis is to improve the understanding of these influences on the impact of ship emissions on air quality in populated regions. Northern Europe, including the North Sea and Baltic Sea (NBS), and eastern China, including the East China Sea, Yellow Sea, and Bohai Sea, were selected as study areas of interest. Both are regions with high shipping densities close to populated coastal areas and they include large port cities, such as Rotterdam or Shanghai. Furthermore, they have different levels of atmospheric background air pollution, which was higher for China and lower for Europe.

However, in ship emission research it is not only important to analyze regional differences but also to have a temporal perspective that focuses upcoming changes. Even more so in the current era of global warming, in which global greenhouse gases emissions must be drastically reduced in the coming years. A decarbonization of the shipping sector is pending, however, the exact pathway for achieving this goal is currently unclear. Thus, this thesis also investigates three future ship emission scenarios for the years 2025, 2040, and 2050 in a northern European study area that includes the North and Baltic Sea. The research focus for these scenarios was on a transition to cleaner and zero-carbon fuels. In this context, it should be noted that this measure also has an impact on the amount of air pollutants emitted, in addition to reducing greenhouse gas emissions.

Besides the application of established methods for regional air quality and emissions modeling, the modular ship emission modeling system (MoSES) was developed and applied. This model is able to produce spatially and temporally highly resolved ship emission inventories, which are the basis for studying ship-related air quality impacts. Furthermore, a novel approach for scenario generation was developed that can be used conjointly with the MoSES model.

### 6.1. Research Results

The first key scientific question of the present thesis is (see Sect. 2.1):

*What are the regional differences and/or similarities in air quality impacts of ship emissions between northern Europe and eastern China?*

This question was addressed by a comparative air quality modeling study for 2015. The study was conducted using an approach harmonized between the two regions, i.e. northern Europe and eastern China. The obtained results for each region were compared in an evaluation with the following results:

Air pollutant concentrations originating from ship emissions in eastern China and northern Europe were generally on a comparable level with slightly higher concentrations in China. The contribution of shipping to annually averaged concentrations of  $\text{NO}_2$  was in moderately affected coastal regions of both domains on the order of  $3 \mu\text{g} \cdot \text{m}^{-3}$ . In the regions heavily affected by shipping traffic, such as port clusters, shipping contributions were  $15 \mu\text{g} \cdot \text{m}^{-3}$ . With 30 % in moderately and 50 % in strongly affected regions, the relative contributions to the overall burden were higher in Europe, compared to 10 % and 30 % in China.

The contributions of shipping to  $\text{SO}_2$  concentrations differed considerably between the regarded regions due to a SECA implemented in the North and Baltic Seas. Thus, ship-related  $\text{SO}_2$  concentrations were only of minor importance in northern Europe, with contributions less than  $0.3 \mu\text{g} \cdot \text{m}^{-3}$ , which corresponded to less than 10 % of the total  $\text{SO}_2$ . In China, ship contributions to  $\text{SO}_2$  were on annual average  $1\text{--}3 \mu\text{g} \cdot \text{m}^{-3}$

along major parts of the Chinese coast and  $4\text{--}8\ \mu\text{g}\cdot\text{m}^{-3}$  in the large port clusters and along the Yangtze River. This corresponded to a share of 10–20 % and 30–40 % on the total ambient  $\text{SO}_2$  concentrations, respectively. In this context, it should be noted that in China's coastal regions the allowed fuel sulfur content is lower at present due to global limits and a new Chinese SECA.

The impact of ship emissions on tropospheric ozone concentrations was similar for coastal areas of both regions and in annual average  $2\text{--}3\ \mu\text{g}\cdot\text{m}^{-3}$  (2–4 %). In European ports, ship emissions reduced ozone concentrations on average by  $10\text{--}15\ \mu\text{g}\cdot\text{m}^{-3}$  (10–15 %). In contrast to this, the ship emission impact on ozone concentrations was negligible in the Chinese port clusters due to high emissions from other sectors and relatively small ship contributions.

In Europe, ambient  $\text{PM}_{2.5}$  concentrations from ship traffic were on annual average  $0.75\text{--}1.25\ \mu\text{g}\cdot\text{m}^{-3}$  (10 % of total). In China, these contributions were slightly larger,  $1\text{--}2\ \mu\text{g}\cdot\text{m}^{-3}$ . However, the relative share of ships on total  $\text{PM}_{2.5}$  concentrations was only 2–3 % in China, since other sectors have very high emissions of  $\text{PM}_{2.5}$  and of its precursors.

In the following, the subordinate questions related to the comparison of ship emission impacts are answered that were raised in Sect. 2.1:

*How do the different levels of air pollution influence atmospheric chemistry and the impact of ship emissions on air quality?*

The different levels of atmospheric background air pollution, which was higher for China and lower for Europe, led consequently to the fact that the relative impact of ship emissions on air quality was smaller in China. Furthermore, differences in their characteristic physicochemical transformations were identified. During winter, the atmospheric lifetime and thus the transport of  $\text{NO}_2$  in China was extended. Additionally, in northeastern China, the transformation of ship emissions to secondary PM was substantially impeded and no contribution from shipping to  $\text{PM}_{2.5}$  concentrations was found. The reason for both observations was a depletion of the necessary reaction partners and of atmospheric oxidants required for secondary particle formation. High emissions of aerosol precursor from other sectors could be held accountable for the lack of oxidants. Another difference with respect to secondary PM was connected to ammonia emission from agricultural fertilization. In combination with  $\text{NO}_x$  and  $\text{SO}_2$  emissions from ships, these are able to form ammonium nitrate and ammonium sulfate, respectively. In Europe, this reactivity led to a concise peak in ship-related  $\text{PM}_{2.5}$  concentrations of  $2\ \mu\text{g}\cdot\text{m}^{-3}$  (13 %) in spring. A similar observation was not made for China due to overall higher ammonia emissions throughout the year. All three of these observations are indicators that a successful regulation of ship emissions needs to be in concert with regulations for other emission sectors. Otherwise, potential achievements of reducing ship emissions could be offset by high emissions from other sectors.

*What role have meteorological aspects or regional weather phenomena in the impacts of ship emissions?*

In general, a stronger seasonality was found for the impact of ship emissions in China than in Europe. The East Asian monsoon and the characteristics of the two different climate zones of eastern China were the dominant factors for this observation. During the monsoon in summer, deposition rates of air pollutants were enhanced and the transport of ship-related air pollutants towards coastal regions was increased. The seasonality found for ship emissions in China was often reversed between the temperate climate zone in northeastern China and the subtropical climate zone of southeastern China. The impact of ship emissions and their seasonality were more similar between the temperate climate of northeastern China and Europe.

*Are there differences in the regional shipping fleet that can account for potential differences in ship emission impacts?*

An important difference in this modeling approach was the data availability for the vessel characteristics of the two regional fleets. The most important ship parameter for the calculation of ship emissions is the power of the main engine. For the Chinese shipping fleet, this quantity had to be estimated for a share of 67 % of the total main engine power installed on ships. In comparison, for the European shipping fleet, the main engine power had to be estimated for only 31 % of the total main engine power installed on ships. The

calculated ship emissions for China were therefore affected by a greater degree of uncertainty. Additionally, in Europe, more ships by number were found to use cleaner distillate fuels than in China (63 % compared to 35 %). The vast majority of the remaining ships used residual fuels, which produce more sulfur and PM emissions when burned.

However, distillate and residual fuels are both carbon-based fossil fuels and thus produce substantial amounts of GHGs emissions and air pollutants when combusted. As part of the current decarbonization efforts that also involve the shipping sector, a phasing-out of traditional marine fuels is an essential contribution to mitigate global warming. The investigation of such a pathway led to the second key scientific question that was raised in Section 2.1:

*How does a future transition to cleaner and carbon-free fuels affect ship emissions?*

In order to address this second key question, three ship emission scenarios were developed for the North and Baltic Sea regions for the years 2025, 2040, and 2050. The scenarios assume a technological transition to ammonia-fueled engines by 2050, via an extensive use of LNG fuel in 2040. Two different ammonia engine technology options were modeled with different effects on the amount of gases and particles emitted. These are a combustion ignition engine (CI) option using marine diesel engine as pilot fuel and a spark ignition engine (SI) option using hydrogen as pilot fuel. In general, stronger emission reductions were achieved with the SI technology, which is considered more advanced. Reductions or emission values calculated with the SI option are shown below in brackets if significantly different to the CI option.

CO<sub>2</sub> reductions of 40 % (47 %) were modeled for 2050, however, CO<sub>2</sub> equivalents were only reduced by 22 % (44 %). The decarbonization targets set by the IMO aim to reduce CO<sub>2</sub> emissions by at least 50 % until 2050. Thus, a difference must be compensated in other ways, e.g., by carbon capture and storage. Primarily responsible for the difference between emissions of CO<sub>2</sub> and CO<sub>2</sub> equivalents were increased nitrous oxide emissions from ammonia-fueled ships and methane slip from LNG-fueled ships. In 2050, methane emissions increased up to 613 % (decrease by 29 %) and nitrous oxide emissions up to 900 % compared to 2015. Therefore, for an effective mitigation of global warming, it is necessary to regulate the emissions of all GHGs from shipping and not only that of CO<sub>2</sub>.

The technology and fuel transition in the scenario for 2050 was also accompanied by substantial changes in air pollutant emission from ships. PM and SO<sub>2</sub> emissions were reduced by more than 73 %. CO emissions increased by 5 % and NMVOC emissions decreased by 27 %. NO<sub>x</sub> emissions were reduced by 39 % (61 %), mainly due to the NECA in the North and Baltic Sea, which is effective for ships built in 2021 or later.

With the deployment of ammonia-fueled ships, ammonia is introduced as a new ship emission species that originates from unburned NH<sub>3</sub>. In the North and Baltic Sea, the calculated ammonia emissions were 930 Gg (35 Gg) in 2050 and depend strongly on the applied engine technology. Besides the hazards resulting from the corrosiveness of NH<sub>3</sub>, ammonia emissions have the potential to substantially increase the formation of secondary PM near shipping lanes when reacting with NO<sub>x</sub> or SO<sub>2</sub>. Thus, to mitigate the adverse health effects of ammonia and PM when ammonia engines become established, NH<sub>3</sub> slip needs to be considered in legislation and technologies promoted that reduce NH<sub>3</sub> emissions.

## 6.2. The Modular Ship Emission Modeling System (MoSES)

Within the scope of this PhD project, the Modular Ship Emission Modeling System (MoSES) was developed which is capable of generating data that is fundamental for ship emission research and was required to answer the key scientific questions of this thesis. This model and the implemented approach for ship emission calculation provided also an answer to the following methodological question:

*What general approach is required to calculate useful and spatiotemporally highly resolved ship emission data?*

MoSES uses the data transmitted via signals of the automatic identification system (AIS) to generate spatially and temporally highly resolved ship emission data in a bottom-up approach. The model was designed in a modular approach that provides flexibility for the modeling procedure in terms of the calculation of the energy consumption of ships, the application of emission factors, and the regionally applicable

regulatory requirements. This ensures that the model is not only capable to meet current challenges in ship emission modeling, but can also be easily adapted to future requirements and changes in the shipping sector. Currently, there are freely selectable emission factors for 14 different pollutant species and GHGs implemented that cover 5 different fuel types. The model also distinguishes between 10 different ship types plus an undefined type, for ships which can not be classified. To deal with missing data, the MoSES model can draw on various estimation techniques for ship characteristics, such as main or auxiliary engine power, which are important for calculating ship emissions.

The model is independent of the region to which it is applied, and has been successfully used to generate the ship emission inventories for northern Europe and eastern China that were used in this thesis. In addition, MoSES has become a data source for ship emissions in current projects and publications, such as in the SEAIR project (2020) for the North and Baltic Sea or for the port of Hamburg in Lauenburg et al. (2022) or in Badeke (2022). Furthermore, it was applied for the derivation of ship traffic scaling factors in the beginning of the COVID-19 pandemic (Matthias et al., 2021) or for the estimation of ship-related parameters, such as the stack height for small-scale modeling in Badeke (2022).

The design of MoSES also focuses on a good capability for the development of ship emission scenarios. In accordance with the following second methodological question, scenarios that concern a decarbonization of the shipping sector were of particular interest:

*How can future ship emission scenarios be flexibly created, particularly scenarios related to a decarbonization of the shipping sector?*

To address this question, a novel approach was developed that benefits from the data structure of the MoSES model and uses its implemented toolbox for scenario creation. This novel approach is capable of evolving a virtual representation of a shipping fleet over time, e.g., to a potential future shipping fleet. This is done by exerting decommission and renewal cycles on the shipping fleet under selected scenario constraints. Subsequently, MoSES can be used to calculate ship emission inventories based on the scenario fleet of ships. This approach was successfully applied to create and investigate the three ship emission scenarios for the years 2025, 2040, and 2050 described earlier.

### 6.3. Outlook

As explained in previous sections, the decarbonization of the shipping sector in the next few decades is on the agenda of the IMO. A transformation of this magnitude is complex. It requires fundamental rethinking of the current structures and will be accompanied by many technological and economic challenges. An early investigation of decarbonization measures in terms of their effectiveness, requirements, and potential drawbacks is important. Only by this, a successful and target-oriented strategy can be developed to achieve the IMO's goal. Against this background, particularly research on ship emission scenarios becomes increasingly important.

The scenarios presented in this work cover only a small proportion of the possible pathways. A further utilisation of the scenario capabilities of MoSES is therefore obvious. As follow-up project to this thesis, an investigation of additional measures for decarbonizing the shipping sector is currently being done with the newly developed method presented in Chap. 4. These are, e.g., a transition to other fuel options, such as methanol or biofuels, and their comparison to ammonia. Operational measures for energy-saving, such as slow steaming or shore power, are also of interest for scenarios examining measures to mitigate GHG emissions. A quantification of the associated CO<sub>2</sub> savings can be achieved with an emission model, such as MoSES.

Different fleet development trends can be assumed for all of these scenarios, and their consideration helps to be prepared for the developments that are truly coming. Against the background of a global restructuring of production capacities due to the COVID-19 pandemic and the Ukraine war, with the associated uncertainties, the exploration of a broad field of potential pathways is currently of particular importance.

Future topics for ship emission scenarios should also investigate potential changes in trade flows and the rerouting of major shipping lanes. Such developments can result in shifts of the current ship emission

patterns and thus in changes of ship emission impacts on air quality. Examples for this are an Arctic shipping route, becoming navigable through climate warming, or a reduction of freight ship traffic due to a reduced transport volume necessary for fossil fuels as they are being phased out. The development and implementation of a methodology that allows the shifting of vessel traffic in MoSES can enable such investigations in future works. A basic functionality for the reduction of vessel traffic corresponding to a reduced freight volume is already implemented and was exemplified in Sect. 3.3.2.

An important additional step after the creation of scenario ship emission inventories is their application in a chemistry transport model to investigate the impacts on air quality. Using the CMAQ model, this is currently being done for the scenarios presented in Chap. 4.

Due to the wide range of applications for ship emission data, a steady improvement and augmentation of the MoSES model is also planned. Since missing data on ship characteristics proved to be one of the main uncertainties in the modeling procedure, an improvement of the implemented estimators is promising for enhancing the accuracy of the calculated emissions. This is particularly helpful for regions where the data situation is worse than for the North and Baltic Seas. Improved estimators could benefit from current methods from the field of machine learning.

Furthermore, a more elaborate method for determining the ship energy consumption could be implemented in MoSES that explicitly includes a ship resistance model and weather effects. However, the explicit consideration of such effects promises only a minor improvement in the emission calculation and can be computationally demanding (Jalkanen et al., 2012). Furthermore, specific ship design data is required as well as information on hull fouling, which are both hardly available. Therefore, priorities were set on other topics.

An improved description of the energy consumption of ships in ports is still necessary. For MoSES, a module was developed that integrates current information on ship activities in ports. (Sect. A.1.4). However, further developments are slowed down by a stagnating data availability.

Plans are also to link the MoSES model via an interface to the Highly Modular Emission Model (HiMEMO) that is currently under development and able to process and produce comprehensive emissions datasets for nonshipping sectors.

Following on from the regional comparison between China and Europe described in Chap. 5, a similar comparison for the impact of ship emissions in other regions can complement obtained results. Potential candidates for such studies are other densely shipped regions, such as the Mediterranean Sea, the eastern and western coast of North America, the Arabian Sea, or Southeast Asia. Important questions related to the results of the comparative study made are: How does the impact of ship emissions on air quality differ between regions with low and medium or low and high levels of background air pollution? What are the differences in the impacts of ship emissions between different climate zones?



# Acknowledgements

First of all I would like to thank my family for all the support they gave me throughout my education in every imaginable way. Thanks to this, I was able to pursue my career this far. I want to especially thank my partner Lisa for her endless patience with me working late, providing me with the emotional support and the endurance to finish this scientific marathon, and who never grew tired of providing me with snacks.

I also want to give my sincerest gratitude to my supervisors Dr. Volker Matthias, Prof. Dr. Markus Quante and Prof. Dr. Kay-Christian Emeis, as well as to the chair of my advisory panel Prof. Dr. Jürgen Scheffran. I was given the chance to pursue my scientific career on a current and interesting topic with all the necessary scientific guidance, teaching and feedback on my ideas to bring this PhD thesis to a fruitful end.

Thanks go of course to all the current and former members of the Chemistry Transport Modeling department from the Helmholtz-Zentrum Hereon. They make the working days lively, give the place a great atmosphere and are always available for interesting conversations, whether work-related or other topics during the coffee break. Many nice moments were shared with the group and not only in the office but also during the occasional company outings, the annual retreat, or in video conferences that, alas, dominated the mutual exchange in recent years. In particular, I would like to thank Dr. Ronny Petrik, whose mind is like a whirlwind of ideas and who was never tired of discussing new ideas, present concepts, and upcoming publications with me. No matter how big his current workload. He was not afraid to offer constructive criticism of my work when it was justified and necessary, but more importantly, he gave me reassurance when I needed it, which motivated me after each exchange.

I would like to thank the German Science Foundation/Deutsche Forschungsgemeinschaft (DFG) and the National Science Foundation of China (NSFC) for funding via the “ShipChem” project, to which a large parts of the work done in this PhD project contributed. Thanks are also due to our Chinese ShipCHEM project partners from Fudan University in Shanghai, Prof. Dr. Yan Zhang, Dr. Fan Zhang and Yming Liu for the cooperation and hospitality Furthermore to our roommate in Shanghai, Qingming, who made a place on the other side of the world a bit more familiar.

Furthermore, I want to thank the Helmholtz-Gemeinschaft Deutscher Forschungszentren e.V. and in particular the Helmholtz-Zentrum Hereon for its financial support and material equipment to successfully pursue my research.

I also thank the SICSS graduate school for accepting me as a member and the support for the advisory panel meetings that helped me to focus on the goal of my thesis and the organization of many interesting lectures, courses, and their annual retreat.

Finally, I would like to thank my reviewers, and especially Alessandro, for all corrections and comments on the draft of this dissertation.

Although there were ups and downs during the time of my PhD, despite the doubts and the many overtime hours I spent working, I am very happy about the plethora of things I learned during this time. I believe this experience taught me a lot and substantially drove me forward in my personal development and that is something I am proud of and I would not want to miss. All the people that aided in this task and supported me during this time and contributed to this: I want to genuinely thank you.





# Bibliography

- 23rd IMO Assembly. IMO Policies and Practices Related to the Reduction of Greenhouse Gas Emissions from Ships. Technical Report December, IMO, 2004.
- P. Aakko-Saksa and K. Lehtoranta. Ship emissions in the future - review. Technical report, VTT Technical Research Centre of Finland, 2019.
- ABS. Ship Energy Efficiency Measures Advisory - Status and Guidance. Technical report, American Bureau of Shipping, 2014.
- H. Agrawal, W. A. Welch, S. Henningsen, J. W. Miller, and D. R. Cocker. Emissions from main propulsion engine on container ship at sea. *J. Geophys. Res. Atmos.*, 115(23):1–7, 2010. ISSN 01480227. doi: 10.1029/2009JD013346.
- S. Ankathi, Z. Lu, G. G. Zaimes, T. Hawkins, Y. Gan, and M. Wang. Greenhouse gas emissions from the global transportation of crude oil: Current status and mitigation potential. *J. Ind. Ecol.*, pages 1–12, 3 2022. ISSN 1088-1980. doi: 10.1111/jiec.13262. URL <https://onlinelibrary.wiley.com/doi/10.1111/jiec.13262>.
- W. A. Asman, M. A. Sutton, and J. K. Schjørring. Ammonia: Emission, atmospheric transport and deposition. *New Phytol.*, 139:27–48, 1998. ISSN 0028646X. doi: 10.1046/j.1469-8137.1998.00180.x.
- A. Aulinger, V. Matthias, M. Zeretzke, J. Bieser, M. Quante, and A. Backes. The impact of shipping emissions on air pollution in the greater North Sea region - Part 1: Current emissions and concentrations. *Atmos. Chem. Phys. Discuss.*, 15(8):11277–11323, 2016. ISSN 16807375. doi: 10.5194/acpd-15-11277-2015.
- R. Badeke. *Small-scale modeling of dispersion and chemistry of ship plumes in urban areas*. PhD thesis, University of Hamburg, 2022.
- B. H. Baek, V. P. Aneja, and Q. Tong. Chemical coupling between ammonia, acid gases, and fine particles. *Environ. Pollut.*, 129(1):89–98, 2004. ISSN 02697491. doi: 10.1016/j.envpol.2003.09.022.
- P. Balcombe, J. Brierley, C. Lewis, L. Skatvedt, J. Speirs, A. Hawkes, and I. Staffell. How to decarbonise international shipping: Options for fuels, technologies and policies. *Energy Convers. Manag.*, 182:72–88, 2019. ISSN 01968904. doi: 10.1016/j.enconman.2018.12.080.
- M. Baldauf, A. Seifert, J. Förstner, D. Majewski, M. Raschendorfer, and T. Reinhardt. Operational Convective-Scale Numerical Weather Prediction with the COSMO Model: Description and Sensitivities. *Mon. Weather Rev.*, 139(12):3887–3905, 2011. ISSN 00270644. doi: 10.1175/MWR-D-10-05013.1.
- F. Baldi, H. Johnson, C. Gabrielli, and K. Andersson. Energy and Exergy Analysis of Ship Energy Systems - The Case study of a Chemical Tanker. *Int. J. Thermodyn.*, 18(2):82–93, 2015. ISSN 13019724. doi: 10.5541/ijot.5000070299.
- F. Baret, M. Weiss, R. Lacaze, F. Camacho, H. Makhmara, P. Pacholczyk, and B. Smets. GEOV1: LAI and FAPAR essential climate variables and FCOVER global time series capitalizing over existing products. Part1: Principles of development and production. *Remote Sens. Environ.*, 137:299–309, 10 2013. ISSN 00344257. doi: 10.1016/j.rse.2012.12.027. URL <https://linkinghub.elsevier.com/retrieve/pii/S0034425713000813>.
- D. M. Bates and D. G. Watts. *Nonlinear Regression Analysis and Its Applications*. Wiley-Interscience, 2007. ISBN 978-0-470-13900-4.

- S. Bengtsson, K. Andersson, and E. Fridell. A comparative life cycle assessment of marine fuels: Liquefied natural gas and three other fossil fuels. *Proc. IMechE Part M: Journal of Engineering for the Maritime Environment*, 225(2):97–110, 2011. ISSN 14750902. doi: 10.1177/1475090211402136.
- D. Bhattu. Primary Organic Aerosols. In *Air Pollution and Control*, chapter Primary Organic Aerosols, pages 109–117. Springer, Singapore, 2018. ISBN 9789811071850. doi: 10.1007/978-981-10-7185-0\_7.
- J. Bieser, A. Aulinger, V. Matthias, M. Quante, and P. Builtjes. SMOKE for Europe – adaptation, modification and evaluation of a comprehensive emission model for Europe. *Geosci. Model Dev.*, 4: 47–68, 1 2011a. ISSN 1991-9603. doi: 10.5194/gmd-4-47-2011. URL <https://gmd.copernicus.org/articles/4/47/2011/>.
- J. Bieser, A. Aulinger, V. Matthias, M. Quante, and H. A. Denier Van Der Gon. Vertical emission profiles for Europe based on plume rise calculations. *Environ. Pollut.*, 159(10):2935–2946, 2011b. ISSN 02697491. doi: 10.1016/j.envpol.2011.04.030. URL <http://dx.doi.org/10.1016/j.envpol.2011.04.030>.
- F. S. Binkowski. Aerosols in MODELS-3 CMAQ. In *Science Algorithms of the EPA Models-3 Community Multiscale Air Quality (CMAQ) Modeling System*, pages 10–23. 1999.
- T. C. Bond, S. J. Doherty, D. W. Fahey, P. M. Forster, T. Berntsen, B. J. Deangelo, M. G. Flanner, S. Ghan, B. Kärcher, D. Koch, S. Kinne, Y. Kondo, P. K. Quinn, M. C. Sarofim, M. G. Schultz, M. Schulz, C. Venkataraman, H. Zhang, S. Zhang, N. Bellouin, S. K. Guttikunda, P. K. Hopke, M. Z. Jacobson, J. W. Kaiser, Z. Klimont, U. Lohmann, J. P. Schwarz, D. Shindell, T. Storelvmo, S. G. Warren, and C. S. Zender. Bounding the role of black carbon in the climate system: A scientific assessment. *J. Geophys. Res.*, 118(11):5380–5552, 2013. ISSN 21698996. doi: 10.1002/jgrd.50171.
- D. Byun and K. L. Schere. Review of the Governing Equations, Computational Algorithms, and Other Components of the Models-3 Community Multiscale Air Quality (CMAQ) Modeling System. *Appl. Mech. Rev.*, 59:51–77, 3 2006. ISSN 0003-6900. doi: 10.1115/1.2128636. URL <https://asmedigitalcollection.asme.org/appliedmechanicsreviews/article/59/2/51/446394/Review-of-the-Governing-Equations-Computational>.
- D. W. Byun and J. K. S. Ching. Science Algorithms of the EPA Models-3 Community Multiscale Air Quality (CMAQ) modeling system. Technical report, United States Environmental Protection Agency, Washington DC, 1999.
- C. Chen, E. Saikawa, B. Comer, X. Mao, and D. Rutherford. Ship Emission Impacts on Air Quality and Human Health in the Pearl River Delta (PRD) Region, China, in 2015, With Projections to 2030. *GeoHealth*, 3(9):284–306, 2019. ISSN 24711403. doi: 10.1029/2019GH000183.
- D. Chen, Y. Zhao, P. Nelson, Y. Li, X. Wang, Y. Zhou, J. Lang, and X. Guo. Estimating ship emissions based on AIS data for port of Tianjin, China. *Atmos. Environ.*, 145:10–18, 2016. ISSN 18732844. doi: 10.1016/j.atmosenv.2016.08.086. URL <http://dx.doi.org/10.1016/j.atmosenv.2016.08.086>.
- D. Chen, X. Wang, Y. Li, J. Lang, Y. Zhou, X. Guo, and Y. Zhao. High-spatiotemporal-resolution ship emission inventory of China based on AIS data in 2014. *Sci. Total Environ.*, 609:776–787, 2017. ISSN 18791026. doi: 10.1016/j.scitotenv.2017.07.051. URL <http://dx.doi.org/10.1016/j.scitotenv.2017.07.051>.
- D. Chen, N. Zhao, J. Lang, Y. Zhou, X. Wang, Y. Li, Y. Zhao, and X. Guo. Contribution of ship emissions to the concentration of PM<sub>2.5</sub>: A comprehensive study using AIS data and WRF/Chem model in Bohai Rim Region, China. *Sci. Total Environ.*, 610-611:1476–1486, 2018. ISSN 18791026. doi: 10.1016/j.scitotenv.2017.07.255. URL <http://dx.doi.org/10.1016/j.scitotenv.2017.07.255>.
- China, Ministry of Transport. Action plan to establish a national emission control area for ship emission control. Technical report, China Ministry of Transport, 2018.

- China, State Council. Action Plan on Prevention and Control of Air Pollution, 2013. URL [http://www.gov.cn/zwqk/2013-09/12/content\\_2486773.htm](http://www.gov.cn/zwqk/2013-09/12/content_2486773.htm). Accessed: 2021-01-21.
- China, State Council. Air quality targets set by the Action Plan have been fully realized, 2018. URL [http://www.gov.cn/xinwen/2018-02/01/content\\_5262720.htm](http://www.gov.cn/xinwen/2018-02/01/content_5262720.htm). Accessed: 2021-01-21.
- M. F. Chislock, E. Doster, R. A. Zitomer, and A. E. Wilson. Eutrophication: Causes, Consequences, and Controls in Aquatic Ecosystems. *Nature Education Knowledge*, 4:10, 2013. URL <https://www.nature.com/scitable/knowledge/library/eutrophication-causes-consequences-and-controls-in-aquatic-102364466/>.
- C. Chuwah, T. van Noije, D. P. van Vuuren, E. Stehfest, and W. Hazeleger. Global impacts of surface ozone changes on crop yields and land use. *Atmos. Environ.*, 106:11–23, 2015. ISSN 18732844. doi: 10.1016/j.atmosenv.2015.01.062. URL <http://dx.doi.org/10.1016/j.atmosenv.2015.01.062>.
- CIMAC. Guide to diesel exhaust emissions control of NO<sub>x</sub>, SO<sub>x</sub>, particulates, smoke and CO<sub>2</sub>. Technical Report 28, The International Council on Combustion Engines (CIMAC), 2008.
- CNSS project. Clean North Sea Shipping Final Report: Key Findings and Recommendations. Technical Report March, 2014. URL [https://www.hereon.de/imperia/md/images/hzg/presse/pressemitteilungen/imperiamdimagesgksspressepressemitteilungen2014/cnss\\_finalreport.pdf](https://www.hereon.de/imperia/md/images/hzg/presse/pressemitteilungen/imperiamdimagesgksspressepressemitteilungen2014/cnss_finalreport.pdf). Accessed: 2022-05-30.
- J. Coello, I. Williams, D. A. Hudson, and S. Kemp. An AIS-based approach to calculate atmospheric emissions from the UK fishing fleet. *Atmos. Environ.*, 114:1–7, 2015. ISSN 18732844. doi: 10.1016/j.atmosenv.2015.05.011. URL <http://dx.doi.org/10.1016/j.atmosenv.2015.05.011>.
- D. Cooper and T. Gustafsson. Methodology for calculating emissions from ships. 1. Update of emission factors. Technical report, Swedish Environmental Protection Agency, 2004.
- J. J. Corbett and P. Fischbeck. Emissions from ships. *Science*, 278(5339):823–824, 1997. ISSN 00368075. doi: 10.1126/science.278.5339.823.
- J. J. Corbett and H. W. Koehler. Updated emissions from ocean shipping. *J. Geophys. Res.*, 108(D20), 2003. ISSN 0148-0227. doi: 10.1029/2003jd003751.
- J. J. Corbett, J. J. Winebrake, E. H. Green, P. Kasibhatla, V. Eyring, and A. Lauer. Mortality from ship emissions: A global assessment. *Environ. Sci. Technol.*, 41(24):8512–8518, 2007. ISSN 0013936X. doi: 10.1021/es071686z.
- M. Crippa, E. Solazzo, G. Huang, D. Guizzardi, E. Koffi, M. Muntean, C. Schieberle, R. Friedrich, and G. Janssens-Maenhout. High resolution temporal profiles in the Emissions Database for Global Atmospheric Research. *Sci. Data*, 7(1):1–17, 2020. ISSN 20524463. doi: 10.1038/s41597-020-0462-2. URL <http://dx.doi.org/10.1038/s41597-020-0462-2>.
- S. B. Dalsøren, M. S. Eide, O. Endresen, A. Mjelde, G. Gravir, and I. S. Isaksen. Update on emissions and environmental impacts from the international fleet of ships: The contribution from major ship types and ports. *Atmos. Chem. Phys.*, 9(6):2171–2194, 2009. ISSN 16807324. doi: 10.5194/acp-9-2171-2009.
- N. de Vries. Safe and effective application of ammonia as a marine fuel. Master’s thesis, Delft University of Technology, 5 2019.
- H. Denier van der Gon and J. Hulskotte. Methodologies for estimating shipping emissions in the Netherlands. A documentation of currently used emission factors and data on related activity. Technical report, Netherlands Environmental Assessment Agency, 2009.
- DNV-GL. Maritime forecast to 2050 - Energy Transition Outlook. Technical report, DNV-GL, 2020.

- M. Dodge. *Proceedings of the international conference on photochemical oxidant pollution and its control*, volume 2, chapter Combined use of modeling techniques and smog chamber data to derive ozone-precursor relationships, pages 881–889. U. S. Environmental Protection Agency, 1977.
- G. Doms and U. Schättler. A Description of the Nonhydrostatic Regional Model LM. Part I: Dynamics and Numerics. Technical report, Deutscher Wetterdienst, Offenbach, 2002.
- G. Doms, J. Foerstner, E. Heise, H. J. Herzog, T. Mrionow, D., Raschendorfer, M., Reinhart, B. Ritter, R. Schrodin, J. P. Schulz, and G. Vogel. A Description of the Nonhydrostatic Regional COSMO Model. Part II: Physical Parameterization. Technical report, Deutscher Wetterdienst, Offenbach, 2011.
- ECCAD. ECCAD - CAMS global emission inventories, 2021. URL <https://ads.atmosphere.copernicus.eu/cdsapp#!/dataset/cams-global-emission-inventories>. Accessed: 2022-04-27.
- ECMWF-CAMS. Data Store, 2021. URL <https://ads.atmosphere.copernicus.eu/cdsapp#!/dataset/cams-global-reanalysis-eac4?tab=overview>.
- EEA. Air Quality e-Reporting (AQER), 2021. URL <https://www.eea.europa.eu/data-and-maps/data/aqereporting-8>. Accessed: 2021-09-20.
- EMEP/EEA. EMEP/EEA air pollutant emission inventory guidebook 2019. Technical report, 2019.
- Ø. Endresen, E. Sjørgård, J. K. Sundet, S. B. Dalsøren, I. S. A. Isaksen, T. F. Berglen, and G. Gravir. Emission from international sea transportation and environmental impact. *J. Geophys. Res.*, 108(D17): 4560, 2003. ISSN 0148-0227. doi: 10.1029/2002JD002898.
- EU. Launch by united states, the european union, and partners of the global methane pledge to keep 1.5°C within reach, 2021. URL [https://ec.europa.eu/commission/presscorner/detail/en/statement\\_21\\_5766](https://ec.europa.eu/commission/presscorner/detail/en/statement_21_5766). Accessed: 2022-04-27.
- European Commission. Air Quality Standards, 2008. URL <https://ec.europa.eu/environment/air/quality/standards.htm>. Accessed: 2022-05-02.
- European Environmental Agency. Emissions of primary PM<sub>2.5</sub> and PM<sub>10</sub> particulate matter, 2018. URL <https://www.eea.europa.eu/data-and-maps/indicators/emissions-of-primary-particles-and-5>. Accessed: 2022-01-23.
- European Parliament and Council. European Union: Directive 2008/50/EC. *Off. J. Eur. Union*, L152: 1–44, 2008.
- Eurostat. Europe’s busiest container ports, 2018. URL [https://ec.europa.eu/eurostat/statistics-explained/index.php?title=File:Top\\_20\\_ports\\_handling\\_containers,\\_2008-2018\\_\(thousand\\_TEUs\).png](https://ec.europa.eu/eurostat/statistics-explained/index.php?title=File:Top_20_ports_handling_containers,_2008-2018_(thousand_TEUs).png). Accessed: 2020-08-20.
- V. Eyring, H. W. Köhler, J. Van Aardenne, and A. Lauer. Emissions from international shipping: 1. The last 50 years. *J. Geophys. Res. D Atmos.*, 110(17):171–182, 2005. ISSN 01480227. doi: 10.1029/2004JD005619.
- V. Eyring, I. S. Isaksen, T. Berntsen, W. J. Collins, J. J. Corbett, O. Endresen, R. G. Grainger, J. Moldanova, H. Schlager, and D. S. Stevenson. Transport impacts on atmosphere and climate: Shipping. *Atmos. Environ.*, 44(37):4735–4771, 2010. ISSN 13522310. doi: 10.1016/j.atmosenv.2009.04.059. URL <http://dx.doi.org/10.1016/j.atmosenv.2009.04.059>.
- Q. Fan, Y. Zhang, W. Ma, H. Ma, J. Feng, Q. Yu, X. Yang, S. K. Ng, Q. Fu, and L. Chen. Spatial and Seasonal Dynamics of Ship Emissions over the Yangtze River Delta and East China Sea and Their Potential Environmental Influence. *Environ. Sci. Technol.*, 50(3):1322–1329, 2016. ISSN 15205851. doi: 10.1021/acs.est.5b03965.

- A. Farrow, K. A. Miller, and L. Myllyvirta. *Toxic Air: The Price of Fossil Fuels*. Technical report, Greenpeace Southeast Asia, Seoul, 2020.
- J. Feng, Y. Zhang, S. Li, J. Mao, A. Patton, Y. Zhou, W. Ma, C. Liu, H. Kan, C. Huang, J. An, L. Li, Y. Shen, Q. Fu, X. Wang, J. Liu, S. Wang, D. Ding, J. Cheng, W. Ge, H. Zhu, and K. Walker. The influence of spatiality on shipping emissions, air quality and potential human exposure in the Yangtze River Delta/Shanghai, China. *Atmos. Chem. Phys.*, 19(9):6167–6183, 2019. ISSN 16807324. doi: 10.5194/acp-19-6167-2019.
- E. Flodström. *Energy and emission factors for ships in operation*. Swedish Transport and Communications Research Board, 1997. ISBN 91-88868-46-X.
- P. Forster, V. Ramaswamy, P. Artaxo, T. Berntsen, R. Betts, D. Fahey, J. Haywood, J. Lean, D. Lowe, G. Myhre, J. Nganga, R. Prinn, G. Raga, M. Schulz, and R. V. Dorland. *Changes in Atmospheric Constituents and in Radiative Forcing*. Technical report, IPCC, Cambridge, United Kingdom and New York, NY, USA, 2007.
- E. Fridell. *Emissions and Fuel Use in the Shipping Sector*. Elsevier Inc., 2018. ISBN 9780128140550. doi: 10.1016/B978-0-12-814054-3.00002-5. URL <http://dx.doi.org/10.1016/B978-0-12-814054-3.00002-5>.
- E. Fridell, R. Parsmo, B. Boteler, J. Troeltzsch, U. Kowalczyk, J. Piotrowicz, J.-P. Jalkanen, L. Johansson, V. Matthias, and E. Ytreberg. *Sustainable Shipping and Environment of the Baltic Sea Region (SHEBA) Deliverable 1.4, type RE*. Technical report, IVL, 2016.
- C. Geels, K. M. Hansen, J. H. Christensen, C. Ambelas Skjøth, T. Ellermann, G. B. Hedegaard, O. Hertel, L. M. Frohn, A. Gross, and J. Brandt. Projected change in atmospheric nitrogen deposition to the Baltic Sea towards 2020. *Atmos. Chem. Phys.*, 12(5):2615–2629, 2012. ISSN 16807316. doi: 10.5194/acp-12-2615-2012.
- R. Gelaro, W. McCarty, M. J. Suárez, R. Todling, A. Molod, L. Takacs, C. A. Randles, A. Darmenov, M. G. Bosilovich, R. Reichle, K. Wargan, L. Coy, R. Cullather, C. Draper, S. Akella, V. Buchard, A. Conaty, A. M. da Silva, W. Gu, G.-K. Kim, R. Koster, R. Lucchesi, D. Merkova, J. E. Nielsen, G. Partyka, S. Pawson, W. Putman, M. Rienecker, S. D. Schubert, M. Sienkiewicz, and B. Zhao. *The Modern-Era Retrospective Analysis for Research and Applications, Version 2 (MERRA-2)*. *J. Clim.*, 30(14):5419–5454, 2017. doi: <https://doi.org/10.1175/JCLI-D-16-0758.1>.
- German Federal Agency for Nature Conservation. *German Fisheries in the North Sea and Baltic Sea*, 2020. URL <https://www.bfn.de/en/activities/marine-nature-conservation/pressures-on-the-marine-environment/fisheries-and-fish-stocks/german-fisheries-in-the-north-sea-and-baltic-sea.html>. Accessed: 2020-12-09.
- L. Goldsworthy and B. Goldsworthy. Modelling of ship engine exhaust emissions in ports and extensive coastal waters based on terrestrial AIS data - An Australian case study. *Environ. Model. Softw.*, 63: 45–60, 2015. ISSN 13648152. doi: 10.1016/j.envsoft.2014.09.009. URL <http://dx.doi.org/10.1016/j.envsoft.2014.09.009>.
- C. Granier, S. Darras, H. Denier Van Der Gon, D. Jana, N. Elguindi, G. Bo, G. Michael, G. Marc, J.-P. Jalkanen, and J. Kuenen. *The Copernicus Atmosphere Monitoring Service global and regional emissions (April 2019 version)*. Technical report, Laboratoire d’Aérodologie, 2019. URL <https://hal.archives-ouvertes.fr/hal-02322431>.
- A. Guenther, X. Jiang, T. Shah, L. Huang, S. Kembell-Cook, and G. Yarwood. *Model of Emissions of Gases and Aerosol from Nature Version 3 (MEGAN3) for Estimating Biogenic Emissions*. In C. Mensink, W. Gong, and A. Hakami, editors, *Air Pollution Modeling and its Application XXVI*, pages 187–192. Springer International Publishing, 2020.

- A. B. Guenther, X. Jiang, C. L. Heald, T. Sakulyanontvittaya, T. Duhl, L. K. Emmons, and X. Wang. The model of emissions of gases and aerosols from nature version 2.1 (MEGAN2.1): An extended and updated framework for modeling biogenic emissions. *Geosci. Model Dev.*, 5(6):1471–1492, 2012. ISSN 1991959X. doi: 10.5194/gmd-5-1471-2012.
- P. Hammingh, M. Holland, G. Geilenkirchen, J. Jonson, and R. Maas. Assessment of the environmental impacts and health benefit of a nitrogen emission control area in the north sea. Technical report, PBL Netherlands Environmental Assessment Agency, 2012.
- G. B. Hamra, F. Laden, A. J. Cohen, O. Raaschou-Nielsen, M. Brauer, and D. Loomis. Lung cancer and exposure to nitrogen dioxide and traffic: A systematic review and meta-analysis. *Environ. Health Perspect.*, 123(11):1107–1112, 2015. ISSN 15529924. doi: 10.1289/ehp.1408882.
- Y. Harada, H. Kamahori, C. Kobayashi, H. Endo, S. Kobayashi, Y. Ota, H. Onoda, K. Onogi, K. Miyaoka, and K. Takahashi. The JRA-55 Reanalysis: Representation of atmospheric circulation and climate variability. *J. Meteor. Soc. Japan*, 94:269–302, 2016. doi: 10.2151/jmsj.2016-015.
- I. M. Held and B. J. Soden. Water Vapor Feedback and Global Warming. *Annu. Rev. Energy Environ.*, 25:441–475, 2000.
- J. Heywood. *Internal Combustion Engine Fundamentals*. McGraw-Hill Education Ltd, 2 edition, 2018. ISBN 978-1260116106.
- R. M. Hoesly, S. J. Smith, L. Feng, Z. Klimont, G. Janssens-Maenhout, T. Pitkanen, J. J. Seibert, L. Vu, R. J. Andres, R. M. Bolt, T. C. Bond, L. Dawidowski, N. Kholod, J.-i. Kurokawa, M. Li, L. Liu, Z. Lu, M. C. P. Moura, P. R. O'Rourke, and Q. Zhang. Historical (1750–2014) anthropogenic emissions of reactive gases and aerosols from the Community Emissions Data System (CEDS). *Geosci. Model Dev.*, 11:369–408, 2018. ISSN 1991-962X.
- L. Huang, Y. Wen, X. Geng, C. Zhou, and C. Xiao. Integrating multi-source maritime information to estimate ship exhaust emissions under wind, wave and current conditions. *Transp. Res. D Transp. Environ.*, 59:148–159, 2018. ISSN 13619209. doi: 10.1016/j.trd.2017.12.012.
- J. H. J. Hulskotte and H. A. C. Denier van der Gon. Fuel consumption and associated emissions from seagoing ships at berth derived from an on-board survey. *Atmos. Environ.*, 44(9):1229–1236, 2010. ISSN 13522310. doi: 10.1016/j.atmosenv.2009.10.018.
- P. Huszar, D. Cariolle, R. Paoli, T. Halenka, M. Belda, H. Schlager, J. Miksovsky, and P. Pisoft. Modeling the regional impact of ship emissions on NO<sub>x</sub> and ozone levels over the Eastern Atlantic and Western Europe using ship plume parameterization. *Atmos. Chem. Phys.*, 10(14):6645–6660, 2010. ISSN 16807316. doi: 10.5194/acp-10-6645-2010.
- IMO. Study of Greenhouse Gas Emissions from Ships. Technical report, International Maritime Organization, 2000.
- IMO. Second IMO Greenhouse Gas Study 2009. Technical report, International Maritime Organisation, 2009. URL [https://www.researchgate.net/publication/255890936\\_Second\\_IMO\\_Greenhouse\\_Gas\\_Study\\_2009/link/56e180ae08ae40dc0abf4db5/download](https://www.researchgate.net/publication/255890936_Second_IMO_Greenhouse_Gas_Study_2009/link/56e180ae08ae40dc0abf4db5/download).
- IMO. Third IMO Greenhouse Gas Study 2014. Technical report, International Maritime Organization, 2014. URL <http://www.imo.org/en/OurWork/Environment/PollutionPrevention/AirPollution/Documents/ThirdGreenhouseGasStudy/GHG3ExecutiveSummaryandReport.pdf>.
- IMO. Fourth IMO GHG Study. Technical report, International Maritime Organization, 2020. URL <https://wwwcdn.imo.org/localresources/en/OurWork/Environment/Documents/Fourth%20IMO%20GHG%20Study%202020%20-%20Full%20report%20and%20annexes.pdf>.

- IMO MEPC. Resolution MEPC.75(40) Protocol to the MARPOL Convention with added Annex VI. Technical report, International Maritime Organization Marine Environment Protection Committee, 1997.
- IMO MEPC. RESOLUTION MEPC.177(58). Technical report, International Maritime Organization Marine Environment Protection Committee, 2008a. URL [http://www.imo.org/en/KnowledgeCentre/IndexofIMOResolutions/Marine-Environment-Protection-Committee-\(MEPC\)/Documents/MEPC.177\(58\).pdf](http://www.imo.org/en/KnowledgeCentre/IndexofIMOResolutions/Marine-Environment-Protection-Committee-(MEPC)/Documents/MEPC.177(58).pdf).
- IMO MEPC. MEPC.176 (58). Technical report, International Maritime Organization Marine Environment Protection Committee, 2008b.
- IMO MEPC. MEPC.203(62). Technical report, International Maritime Organization Marine Environment Protection Committee, 2011.
- IMO MEPC. RESOLUTION MEPC.251(66). Technical report, International Maritime Organization Marine Environment Protection Committee, 2014. URL [http://www.imo.org/en/KnowledgeCentre/IndexofIMOResolutions/Marine-Environment-Protection-Committee-\(MEPC\)/Documents/MEPC.251\(66\).pdf](http://www.imo.org/en/KnowledgeCentre/IndexofIMOResolutions/Marine-Environment-Protection-Committee-(MEPC)/Documents/MEPC.251(66).pdf).
- IMO MEPC. MEPC 70/INF.34. Technical report, International Maritime Organization Marine Environment Protection Committee, 2016.
- IMO MEPC. MEPC 74/5/3. Technical report, International Maritime Organization Marine Environment Protection Committee, 2018a.
- IMO MEPC. Initial IMO Strategy on reduction of GHG emission from ships. Resolution MEPC.304(72) (adopted on 13 April 2018). Technical Report April, International Maritime Organization Marine Environment Protection Committee, 2018b.
- A. Inness, M. Ades, A. Agustí-Panareda, J. Barr, A. Benedictow, A. M. Blechschmidt, J. Jose Dominguez, R. Engelen, H. Eskes, J. Flemming, V. Huijnen, L. Jones, Z. Kipling, S. Massart, M. Parrington, V. H. Peuch, M. Razinger, S. Remy, M. Schulz, and M. Suttie. The CAMS reanalysis of atmospheric composition. *Atmos. Chem. Phys.*, 19(6):3515–3556, 2019. ISSN 16807324. doi: 10.5194/acp-19-3515-2019.
- IPCC. Climate Change 1995. Technical report, Intergovernmental Panel on Climate Change, 1995.
- IPCC. Climate Change, 2001. Technical report, Intergovernmental Panel on Climate Change, 2001.
- IPCC. Climate Change 2007: Synthesis Report. Technical report, Intergovernmental Panel on Climate Change, Geneva, Switzerland, 2007.
- IPCC. Climate Change 2013: The Physical Science Basis. Technical report, Cambridge, United Kingdom and New York, NY, USA, 2013. URL [https://www.researchgate.net/profile/Abha\\_Chhabra2/publication/271702872\\_Carbon\\_and\\_Other\\_Biogeochemical\\_Cycles/links/54cf9ce80cf24601c094a45e/Carbon-and-Other-Biogeochemical-Cycles.pdf](https://www.researchgate.net/profile/Abha_Chhabra2/publication/271702872_Carbon_and_Other_Biogeochemical_Cycles/links/54cf9ce80cf24601c094a45e/Carbon-and-Other-Biogeochemical-Cycles.pdf).
- IPCC. Reports, 2022. URL <https://www.ipcc.ch/reports/>. Accessed: 2022-05-03.
- ITF/OECD. Decarbonising maritime transport. pathways to zero-carbon shipping by 2035. Technical report, International Transport Forum, 2018. URL <https://www.itf-oecd.org/sites/default/files/docs/decarbonising-maritime-transport.pdf>.
- D. J. Jacob. *Introduction to Atmospheric Chemistry*. Princeton University Press, 1 edition, 1999. ISBN 978-0691001852.
- M. Z. Jacobson. *Air Pollution and Global Warming: History, Science, and Solutions*. Cambridge University Press, 2. edition, 2012. ISBN 110769115X.

- J. P. Jalkanen, A. Brink, J. Kalli, H. Pettersson, J. Kukkonen, and T. Stipa. A modelling system for the exhaust emissions of marine traffic and its application in the Baltic Sea area. *Atmos. Chem. Phys.*, 9(23):9209–9223, 2009. ISSN 16807324. doi: 10.5194/acp-9-9209-2009.
- J. P. Jalkanen, L. Johansson, J. Kukkonen, A. Brink, J. Kalli, and T. Stipa. Extension of an assessment model of ship traffic exhaust emissions for particulate matter and carbon monoxide. *Atmos. Chem. Phys.*, 12(5):2641–2659, 2012. ISSN 16807316. doi: 10.5194/acp-12-2641-2012.
- J. P. Jalkanen, L. Johansson, and J. Kukkonen. A comprehensive inventory of the ship traffic exhaust emissions in the Baltic Sea from 2006 to 2009. *Ambio*, 43(3):311–324, 2014. ISSN 00447447. doi: 10.1007/s13280-013-0389-3.
- L. Johansson, J. Jalkanen, J. Kalli, and J. Kukkonen. The evolution of shipping emissions and the costs of regulation changes in the northern EU area. *Atmos. Chem. Phys.*, 13:11375–11389, 2013. doi: 10.5194/acp-13-11375-2013.
- L. Johansson, J.-p. Jalkanen, and J. Kukkonen. Global assessment of shipping emissions in 2015 on a high spatial and temporal resolution. *Atmos. Environ.*, 167:403–415, 2017a. ISSN 1352-2310. doi: 10.1016/j.atmosenv.2017.08.042. URL <http://dx.doi.org/10.1016/j.atmosenv.2017.08.042>.
- L. Johansson, J. P. Jalkanen, and J. Kukkonen. Global assessment of shipping emissions in 2015 on a high spatial and temporal resolution. *Atmos. Environ.*, 167:403–415, 2017b. ISSN 18732844. doi: 10.1016/j.atmosenv.2017.08.042. URL <http://dx.doi.org/10.1016/j.atmosenv.2017.08.042>.
- L. Johansson, E. Ytreberg, J. P. Jalkanen, E. Fridell, K. Martin Eriksson, M. Lagerström, I. Maljutenko, U. Raudsepp, V. Fischer, and E. Roth. Model for leisure boat activities and emissions - Implementation for the Baltic Sea. *Ocean Sci.*, 16(5):1143–1163, 2020. ISSN 18120792. doi: 10.5194/os-16-1143-2020.
- J. E. Jonson, J. P. Jalkanen, L. Johansson, M. Gauss, and H. A. Van Der Gon. Model calculations of the effects of present and future emissions of air pollutants from shipping in the Baltic Sea and the North Sea. *Atmos. Chem. Phys.*, 15(2):783–798, 2015. ISSN 16807324. doi: 10.5194/acp-15-783-2015.
- J. E. Jonson, M. Gauss, M. Schulz, J. P. Jalkanen, and H. Fagerli. Effects of global ship emissions on European air pollution levels. *Atmos. Chem. Phys.*, 20(19):11399–11422, 2020. ISSN 16807324. doi: 10.5194/acp-20-11399-2020.
- J. Kalli, J. P. Jalkanen, L. Johansson, and S. Repka. Atmospheric emissions of European SECA shipping: Long-term projections. *WMU J. Marit. Aff.*, 12(2):129–145, 2013. ISSN 16541642. doi: 10.1007/s13437-013-0050-9.
- M. Karl, J. Bieser, B. Geyer, V. Matthias, J. P. Jalkanen, L. Johansson, and E. Fridell. Impact of a nitrogen emission control area (NECA) on the future air quality and nitrogen deposition to seawater in the Baltic Sea region. *Atmos. Chem. Phys.*, 19(3):1721–1752, 2019a. ISSN 16807324. doi: 10.5194/acp-19-1721-2019.
- M. Karl, J. E. Jonson, A. Uppstu, A. Aulinger, M. Prank, M. Sofiev, J. P. Jalkanen, L. Johansson, M. Quante, and V. Matthias. Effects of ship emissions on air quality in the Baltic Sea region simulated with three different chemistry transport models. *Atmos. Chem. Phys.*, 19(10):7019–7053, 2019b. ISSN 16807324. doi: 10.5194/acp-19-7019-2019.
- A. Kasper, S. Aufdenblatten, A. Forss, M. Mohr, and H. Burtscher. Particulate Emissions from a Low-Speed Marine Diesel Engine. *Aerosol. Sci. Technol.*, 41(1):24–32, 2007. ISSN 15217388. doi: 10.1080/02786820601055392.
- M. Y. Khan, S. Ranganathan, H. Agrawal, W. A. Welch, C. Laroo, J. W. Miller, and D. R. Cocker. Measuring in-use ship emissions with international and U.S. federal methods. *J. Air Waste Manag. Assoc.*, 63(3):284–291, 2013. ISSN 21622906. doi: 10.1080/10962247.2012.744370.



- S. Kinne. The MACv2 aerosol climatology. *Tellus B: Chem. Phys. Meteorol.*, 71:1–21, 1 2019. ISSN 16000889. doi: 10.1080/16000889.2019.1623639.
- S. Kobayashi, Y. Ota, Y. Harada, A. Ebita, M. Moriya, H. Onoda, K. Onogi, H. Kamahori, C. Kobayashi, H. Endo, K. Miyaoka, and K. Takahashi. The JRA-55 Reanalysis: General specifications and basic characteristics. *J. Meteor. Soc. Japan*, 93:5–48, 2015. doi: 10.2151/jmsj.2015-001.
- H. O. Kristensen. Statistical Analysis and Determination of Regression Formulas for Main Dimensions of Container Ships Based on IHS Fairplay Data. Technical report, Technical University of Denmark, 2013. URL <http://www.skibstekniskelskab.dk/public/dokumenter/Skibsteknisk/Foraar2013/25.02.2013/WP2-Report3-Regressionanalysisforcontainerships-February2013.pdf>.
- H. O. Kristensen and M. Lützen. Prediction of resistance and propulsion power of ships. Technical report, Technical University of Denmark, 2013. URL <http://www.skibstekniskelskab.dk/public/dokumenter/Skibsteknisk/Foraar2013/25.02.2013/WP2-Report4-ResistanceandPropulsionPower-FINAL-October2012.pdf>.
- H. O. H. Kristensen. Determination of Regression Formulas for Main Dimensions of Tankers and Bulk Carriers based on IHS Fairplay data. Technical report, Technical University of Denmark, 2012.
- Y. Kwon, H. Lim, Y. Lim, and H. Lee. Implication of activity-based vessel emission to improve regional air inventory in a port area. *Atmos. Environ.*, 203(February):262–270, 2019. ISSN 13522310. doi: 10.1016/j.atmosenv.2019.01.036. URL <https://doi.org/10.1016/j.atmosenv.2019.01.036>.
- D. A. Lack and J. J. Corbett. Black carbon from ships: A review of the effects of ship speed, fuel quality and exhaust gas scrubbing. *Atmos. Chem. Phys.*, 12(9):3985–4000, 2012. ISSN 16807316. doi: 10.5194/acp-12-3985-2012.
- D. A. Lack, C. D. Cappa, J. Langridge, R. Bahreini, G. Buffaloe, C. Brock, K. Cerully, D. Coffman, K. Hayden, J. Holloway, B. Lerner, P. Massoli, S. M. Li, R. McLaren, A. M. Middlebrook, R. Moore, A. Nenes, I. Nuaaman, T. B. Onasch, J. Peischl, A. Perring, P. K. Quinn, T. Ryerson, J. P. Schwartz, R. Spackman, S. C. Wofsy, D. Worsnop, B. Xiang, and E. Williams. Impact of fuel quality regulation and speed reductions on shipping emissions: Implications for climate and air quality. *Environ. Sci. Technol.*, 45(20):9052–9060, 2011. ISSN 0013936X. doi: 10.1021/es2013424.
- M. Lauenburg, M. Karl, V. Matthias, M. Quante, and M. O. P. Ramacher. City scale modeling of ultrafine particles in urban areas with special focus on passenger ferryboat emission impact. *Toxics*, 10, 3 2022. ISSN 23056304. doi: 10.3390/toxics10010003.
- A. Lauer, V. Eyring, J. J. Corbett, C. Wang, and J. J. Winebrake. Assessment of near-future policy instruments for oceangoing shipping: Impact on atmospheric aerosol burdens and the earth’s radiation budget. *Environ. Sci. Technol.*, 43(15):5592–5598, 2009. ISSN 0013936X. doi: 10.1021/es900922h.
- A. Laval, Hafnia, H. Topsoe, Vestas, and S. Gamesa. Ammonfuel - an industrial view of ammonia as a marine fuel. *Front. Mech. Eng.*, pages 1–61, 2020. URL <https://info.topsoe.com/ammonfuel>. Accessed: 2022-05-02.
- S. C. Leong, C. A. Hargreaves, P. Singhal, and J. Yuan. Estimation of CO<sub>2</sub> Emission from Marine Traffic in Singapore Straits Using Automatic Identification Systems Data. In *Environmental Science and Information Application Technology*, pages 177–185. 2015. ISBN 9781138028142. doi: 10.1201/b18559-31.
- C. Li, Z. Yuan, J. Ou, X. Fan, S. Ye, T. Xiao, Y. Shi, Z. Huang, S. K. Ng, and Z. Zhong. An AIS-based high-resolution ship emission inventory and its uncertainty in Pearl River Delta region, China. *Sci. Total Environ.*, 573:1–10, 2016. doi: <https://doi.org/10.1016/j.scitotenv.2016.07.219>.

- K. Li, D. J. Jacob, H. Liao, L. Shen, Q. Zhang, and K. H. Bates. Anthropogenic drivers of 2013–2017 trends in summer surface ozone in China. *Proceedings of the National Academy of Sciences of the United States of America*, 116(2):422–427, 2019a. ISSN 10916490. doi: 10.1073/pnas.1812168116.
- M. Li, Q. Zhang, D. G. Streets, K. B. He, Y. F. Cheng, L. K. Emmons, H. Huo, S. C. Kang, Z. Lu, M. Shao, H. Su, X. Yu, and Y. Zhang. Mapping Asian anthropogenic emissions of non-methane volatile organic compounds to multiple chemical mechanisms. *Atmos. Chem. Phys.*, 14:5617–5638, 2014. doi: 10.5194/acp-14-5617-2014.
- M. Li, H. Liu, G. Geng, C. Hong, F. Liu, Y. Song, D. Tong, B. Zheng, H. Cui, H. Man, Q. Zhang, and K. He. Anthropogenic emission inventories in China: a review. *Natl. Sci. Rev.*, 4:834–866, 2017. doi: 10.1093/nsr/nwx150.
- M. Li, Q. Zhang, B. Zheng, D. Tong, Y. Lei, F. Liu, C. Hong, S. Kang, L. Yan, Y. Zhang, Y. Bo, H. Su, Y. Cheng, and K. He. Persistent growth of anthropogenic non-methane volatile organic compound (NMVOC) emissions in China during 1990–2017: drivers, speciation and ozone formation potential. *Atmos. Chem. Phys.*, 19:8897–8913, 2019b. doi: 10.5194/acp-19-8897-2019.
- F. Liu, Q. Zhang, D. Tong, B. Zheng, M. Li, H. Huo, and K. B. He. High-resolution inventory of technologies, activities, and emissions of coal-fired power plants in China from 1990 to 2010. *Atmos. Chem. Phys.*, 15:13299–13317, 2015. doi: 10.5194/acp-15-13299-2015.
- H. Liu, M. Fu, X. Jin, Y. Shang, D. Shindell, G. Faluvegi, C. Shindell, and K. He. Health and climate impacts of ocean-going vessels in East Asia. *Nat. Clim. Chang.*, 6(11):1037–1041, 2016. ISSN 17586798. doi: 10.1038/nclimate3083.
- H. Liu, X. Jin, L. Wu, X. Wang, M. Fu, Z. Lv, L. Morawska, F. Huang, and K. He. The impact of marine shipping and its DECA control on air quality in the Pearl River Delta, China. *Sci. Total Environ.*, 625:1476–1485, 2018. ISSN 18791026. doi: 10.1016/j.scitotenv.2018.01.033. URL <https://doi.org/10.1016/j.scitotenv.2018.01.033>.
- J. Liu, D. Tong, Y. Zheng, J. Cheng, X. Qin, Q. Shi, L. Yan, Y. Lei, and Q. Zhang. Carbon and air pollutant emissions from China’s cement industry 1990–2015: trends, evolution of technologies and drivers. *Atmos. Chem. Phys. Discuss.*, 2020:1–39, 2020. doi: 10.5194/acp-2020-631.
- Lloyds’ List. One Hundred Ports 2020, 2020. URL <https://lloydslist.maritimeintelligence.informa.com/one-hundred-container-ports-2020>. Accessed: 2021-01-22.
- Z. Lv, H. Liu, Q. Ying, M. Fu, Z. Meng, and Y. Wang. Impacts of shipping emissions on PM<sub>2.5</sub> air pollution in China. *Atmos. Chem. Phys. Discuss.*, (June):1–27, 2018.
- V. Matthias, I. Bewersdorff, A. Aulinger, and M. Quante. The contribution of ship emissions to air pollution in the North Sea regions. *Environ. Pollut.*, 158(6):2241–2250, 2010. ISSN 02697491. doi: 10.1016/j.envpol.2010.02.013. URL <http://dx.doi.org/10.1016/j.envpol.2010.02.013>.
- V. Matthias, M. Quante, J. A. Arndt, R. Badeke, L. Fink, R. Petrik, J. Feldner, D. Schwarzkopf, E. M. Link, M. O. Ramacher, and R. Wedemann. The role of emission reductions and the meteorological situation for air quality improvements during the COVID-19 lockdown period in central Europe. *Atmospheric Chemistry and Physics*, 21:13931–13971, 9 2021. ISSN 16807324. doi: 10.5194/acp-21-13931-2021.
- MEGAN LAI. MEGAN, Leaf Area Index, 2021. URL <https://bai.ess.uci.edu/megan/data-and-code/lai>. Accessed: 2021-09-09.
- J. Moldanová, E. Fridell, O. Popovicheva, B. Demirdjian, V. Tishkova, A. Faccinnetto, and C. Focsa. Characterisation of particulate matter and gaseous emissions from a large ship diesel engine. *Atmos. Environ.*, 43(16):2632–2641, 2009. ISSN 13522310. doi: 10.1016/j.atmosenv.2009.02.008. URL <http://dx.doi.org/10.1016/j.atmosenv.2009.02.008>.

- C. Mounaïm-Rousselle and P. Brequigny. Ammonia as Fuel for Low-Carbon Spark-Ignition Engines of Tomorrow's Passenger Cars. *Front. Mech. Eng.*, 6(September):1–5, 2020. ISSN 22973079. doi: 10.3389/fmech.2020.00070.
- H. Müller. *Sulfur Dioxide*. Wiley-VCH Verlag GmbH & Co. KGaA, 6 2000. doi: 10.1002/14356007.a25\_569. URL [https://onlinelibrary.wiley.com/doi/10.1002/14356007.a25\\_569](https://onlinelibrary.wiley.com/doi/10.1002/14356007.a25_569).
- OECD. Reducing Sulphur Emissions from Ships - The Impact of International Regulation. Technical report, Organisation for Economic Co-operation and Development, 2016. URL [https://www.oecd-ilibrary.org/transport/reducing-sulphur-emissions-from-ships\\_5jlvvz8mq9s-en](https://www.oecd-ilibrary.org/transport/reducing-sulphur-emissions-from-ships_5jlvvz8mq9s-en).
- J. Olivier and J. Peters. Trends in Global CO<sub>2</sub> and Total Greenhouse Gas Emissions. Technical Report February, PBL Netherlands Environmental Assessment Agency, The Hague, 2020. URL [www.pbl.nl/en](http://www.pbl.nl/en).
- J. Olivier, A. Bouwman, C. van der Maas, J. Berdowski, C. Veldt, J. Bloos, A. Visschedijk, P. Zandveld, and J. Haverlag. Description of EDGAR Version 2.0: A set of global emission inventories of greenhouse gases and ozone-depleting substances for all anthropogenic and most natural sources on a per country basis and on 1 degree x 1 degree grid. Technical report, Natl. Inst. of Public Health and the Environ., Bilthoven, Netherlands, 1996.
- H. W. Paerl. Coastal eutrophication in relation to atmospheric nitrogen deposition: Current perspectives. *Ophelia*, 41(1):237–259, 1995. ISSN 00785326. doi: 10.1080/00785326.1995.10422046.
- R. K. Pathak, W. S. Wu, and T. Wang. Summertime PM<sub>2.5</sub> ionic species in four major cities of China: Nitrate formation in an ammonia-deficient atmosphere. *Atmos. Chem. Phys.*, 9(5):1711–1722, 2009. ISSN 16807324. doi: 10.5194/acp-9-1711-2009.
- K. Peng, L., Zhang, Q., Yao, Z., Mauzerall, D. L., Kang, S., Du, Z., Zheng, Y., Xue, T., and He. Underreported coal in statistics: A survey-based solid fuel consumption and emission inventory for the rural residential sector in China. *Appl. Energy*, 235:1169–1182, 2019. doi: 10.1016/j.apenergy.2018.11.043.
- R. Petrik, B. Geyer, and B. Rockel. On the diurnal cycle and variability of winds in the lower planetary boundary layer: evaluation of regional reanalyses and hindcasts. *Tellus A: Dyn. Meteorol. Oceanogr.*, 73:1–28, 2021. ISSN 16000870. doi: 10.1080/16000870.2020.1804294.
- A. Petzold, E. Weingartner, J. Hasselbach, P. Lauer, C. Kurok, and F. Fleischer. Physical properties, chemical composition, and cloud forming potential of particulate emissions from a marine diesel engine at various load conditions. *Environ. Sci. Technol.*, 44(10):3800–3805, 2010. ISSN 0013936X. doi: 10.1021/es903681z.
- A. Petzold, P. Lauer, U. Fritsche, J. Hasselbach, M. Lichtenstern, H. Schlager, and F. Fleischer. Operation of marine diesel engines on biogenic fuels: Modification of emissions and resulting climate effects. *Environ. Sci. Technol.*, 45(24):10394–10400, 2011. ISSN 0013936X. doi: 10.1021/es2021439.
- J. Pleim and J. Chang. A non-local closure model for vertical mixing in the convective boundary layer. *Atmos. Env.*, 26:965–981, 1992. doi: [https://doi.org/10.1016/0960-1686\(92\)90028-J](https://doi.org/10.1016/0960-1686(92)90028-J).
- Y. Qi, N. Stern, T. Wu, J. Lu, and F. Green. China's post-coal growth. *Nat. Geosci.*, 9(8):564–566, 2016. doi: 10.1038/ngeo2777.
- V. Ramanathan. Climate Change, Air Pollution, and Health: Common Sources, Similar Impacts, and Common Solutions. In W. Al-Delaimy, V. Ramanathan, and M. Sánchez Sorondo, editors, *Health of People, Health of Planet and Our Responsibility*, pages 49–59. Springer, Cham., 1 edition, 2020. ISBN 978-3-030-31125-4. doi: 10.1007/978-3-030-31125-4\_5.

- M. Rasche, M. Walther, R. Schiffner, N. Kroegel, S. Rupprecht, P. Schlattmann, P. C. Schulze, P. Franzke, O. W. Witte, M. Schwab, and F. Rakers. Rapid increases in nitrogen oxides are associated with acute myocardial infarction: A case-crossover study. *Eur. J. Prev. Cardiol.*, 25(16):1707–1716, 2018. ISSN 20474881. doi: 10.1177/2047487318755804.
- C. Redl, F. Hein, M. Buck, D. P. Graichen, and D. Jones. The European Power Sector in 2020: Up-to-Date Analysis on the Electricity Transistion. Technical report, 2021.
- S. Repka, J. Mellqvist, T. Borkowski, J.-P. Jalkanen, J. E. Jonson, L. Barregard, E. Olaniyi, G. Klaus, M. Gauss, J. Walden, E. Svensson, E. Genikhovich, D. Rumyantzev, J. Boyesen, C. Wenske, T. P. de Carvalho, A. Lähteenmäki-Uutela, L. Johansson, V. Conde, A. Erkkilä-Välimäki, J. Yliskylä-Peuralahti, K. Saarnio, A. Bakhtov, S. Tochanskaya, M. Bosch, T. Haukioja, J. Törrönen, A. Karppinen, J. Beecken, M. Alhosalo, J. Myskow, P. Kowalak, E. Bäck, H. Nguyen, P. Molnar, L. Stockfelt, S. Atari, and Y. Bakkar. Clean Shipping: Exploring the impact of emission regulation (EnviSuM). Technical report, 2019. URL <https://blogit.utu.fi/envisum/>.
- H. Ritchie, M. Roser, and P. Rosado. CO2 and Greenhouse Gas Emissions. *Our World in Data*, 2020. URL <https://ourworldindata.org/co2-and-other-greenhouse-gas-emissions>. Accessed: 2022-05-03.
- B. Rockel, A. Will, and A. Hense. The regional climate model COSMO-CLM (CCLM). *Meteorol. Zeitschrift*, 17(4):347–348, 2008. ISSN 09412948. doi: 10.1127/0941-2948/2008/0309.
- D. K. Sarkar. Fuels and Combustion. In *Thermal Power Plant*, chapter 3, pages 91–137. Elsevier, 2015. ISBN 9780128015759. doi: 10.1016/b978-0-12-801575-9.00003-2.
- G. Sarwar, K. W. Appel, A. G. Carlton, R. Mathur, K. Schere, R. Zhang, and M. A. Majeed. Impact of a new condensed toluene mechanism on air quality model predictions in the US. *Geosci. Model Dev.*, 4(1):183–193, 2011. ISSN 19919603. doi: 10.5194/gmd-4-183-2011.
- T. Schneider, P. A. O’Gorman, and X. J. Levine. Water vapor and the dynamics of climate changes. *Rev. Geophys.*, 48(1):1–22, 2010. ISSN 87551209. doi: 10.1029/2009RG000302.
- D. A. Schwarzkopf, R. Petrik, V. Matthias, M. Quante, E. Majamäki, and J.-P. Jalkanen. A ship emission modeling system with scenario capabilities. *Atmos. Environ.: X*, 12(September):100132, 2021. ISSN 25901621. doi: 10.1016/j.aeaoa.2021.100132.
- SEAIR project. Impact of shipping emissions on air quality and deposition in German marine and coastal areas (SEAIR), 2020. URL [https://www.bsh.de/DE/THEMEN/Forschung\\_und\\_Entwicklung/Aktuelle-Projekte/\\_Anlagen/Downloads/2-Sicherheit-und-Umweltschutz/SEAIR.html](https://www.bsh.de/DE/THEMEN/Forschung_und_Entwicklung/Aktuelle-Projekte/_Anlagen/Downloads/2-Sicherheit-und-Umweltschutz/SEAIR.html). Accessed: 2022-05-25.
- J. H. Seinfeld and S. N. Pandis. *Atmospheric Chemistry and Physics: From Air Pollution to Climate Change*. Wiley, 2. edition, 2006. ISBN 9780471720171. doi: 10.1063/1.882420.
- V. Shah, D. J. Jacob, K. Li, R. Silvern, S. Zhai, M. Liu, J. Lin, and Q. Zhang. Effect of changing NOx lifetime on the seasonality and long-term trends of satellite-observed tropospheric NO2 columns over China. *Atmos. Chem. Phys.*, 20(3):1483–1495, 2020. ISSN 16807324. doi: 10.5194/acp-20-1483-2020.
- SHEBA project. Sustainable shipping and environment of the baltic sea region, 2018. URL <https://www.sheba-project.eu/>. Accessed: 2021-01-26.
- F. Shen and X. Li. Effects of fuel types and fuel sulfur content on the characteristics of particulate emissions in marine low-speed diesel engine. *Environ. Sci. Pollut. Res.*, 27(30):37229–37236, 2020. ISSN 16147499. doi: 10.1007/s11356-019-07168-6.
- M. Simonsen, H. J. Walnum, and S. Gössling. Model for estimation of fuel consumption of cruise ships. *Energies*, 11(5), 2018. ISSN 19961073. doi: 10.3390/en11051059.

- M. Sofiev, J. J. Winebrake, L. Johansson, E. W. Carr, M. Prank, J. Soares, J. Vira, R. Kouznetsov, J. P. Jalkanen, and J. J. Corbett. Cleaner fuels for ships provide public health benefits with climate tradeoffs. *Nat. Commun.*, 9(1):1–12, 2018. ISSN 20411723. doi: 10.1038/s41467-017-02774-9.
- Starcrest. Port of Los Angeles Inventory of Air Emissions - 2012. Technical report, Starcrest Consulting Group, LLC, 2013.
- E. Tagaris, I. Stergiou, and R. E. P. Sotiropoulou. Impact of shipping emissions on ozone levels over Europe: assessing the relative importance of the Standard Nomenclature for Air Pollution (SNAP) categories. *Environ. Sci. Pollut.*, 24:14903–14909, 6 2017. ISSN 16147499. doi: 10.1007/s11356-017-9046-x.
- J. A. Thornton, P. J. Wooldridge, R. C. Cohen, M. Martinez, H. Harder, W. H. Brune, E. J. Williams, J. M. Roberts, F. C. Fehsenfeld, S. R. Hall, R. E. Shetter, B. P. Wert, and A. Fried. Ozone production rates as a function of NO<sub>x</sub> abundances and HO<sub>x</sub> production rates in the Nashville urban plume. *J. Geophys. Res. Atmos.*, 107(12):1–17, 2002. ISSN 01480227. doi: 10.1029/2001jd000932.
- D. Tong, Q. Zhang, F. Liu, G. Geng, Y. Zheng, T. Xue, C. Hong, R. Wu, Y. Qin, H. Zhao, L. Yan, and K. He. Current Emissions and Future Mitigation Pathways of Coal-Fired Power Plants in China from 2010 to 2030. *Environ. Sci. Technol.*, 52:12905–12914, 2018. doi: 10.1021/acs.est.8b02919.
- C. Trozzi and R. Vaccaro. Actual and future air pollutant emissions from ships. In *Transport and Air Pollution and Cost*, number 319, 1999. URL [https://www.researchgate.net/publication/236857872\\_Actual\\_and\\_future\\_air\\_pollutant\\_emissions\\_from\\_ships](https://www.researchgate.net/publication/236857872_Actual_and_future_air_pollutant_emissions_from_ships).
- M. C. Turner, M. Jerrett, C. A. P. Iii, D. Krewski, M. Susan, W. R. Diver, B. S. Beckerman, J. D. Marshall, J. Su, and L. Daniel. Long-Term Ozone Exposure and Mortality in a Large Prospective Study Michelle. *Am. J. Respir. Crit. Care Med.*, 193(10):1134–1142, 2016. doi: 10.1164/rccm.201508-1633oc.
- U. N. United Nations Framework Convention on Climate Change, 1992. URL [https://treaties.un.org/pages/ViewDetailsIII.aspx?src=TREATY&mtdsg\\_no=XXVII-7&chapter=27&Temp=mtdsg3&clang=\\_en](https://treaties.un.org/pages/ViewDetailsIII.aspx?src=TREATY&mtdsg_no=XXVII-7&chapter=27&Temp=mtdsg3&clang=_en). Accessed: 2022-05-02.
- U. S. Coast Guard, NOAA, BOEM. Marine Cadastre Project. Technical report, 2018. URL <https://coast.noaa.gov/data/marinecadastre/ais/VesselTypeCodes2018.pdf>.
- U. S. EPA. Science Algorithms of the EPA Models-3 Community Multiscale Air Quality (CMAQ) Modeling System, EPA/600/R-99/030. Technical report, U. S. Environmental Protection Agency, 1999. URL [https://www.cmascenter.org/cmaq/science\\_documentation/](https://www.cmascenter.org/cmaq/science_documentation/). Accessed: 2022-05-25.
- U. S. EPA. Integrated Science Assessment for Particulate Matter. Technical Report December 2009, U. S. Environmental Protection Agency, 2009.
- U. S. EPA. Health and Environmental Effects of Particulate Matter (PM). Technical report, U. S. Environmental Protection Agency, 2021a. URL <https://www.epa.gov/pm-pollution/health-and-environmental-effects-particulate-matter-pm>. Accessed: 2022-01-23.
- U. S. EPA. Sulfur Dioxide Basics, 2021b. URL <https://www.epa.gov/so2-pollution/sulfur-dioxide-basics>. Accessed: 2022-01-23.
- U. S. EPA. Emissions Models and Other Methods to Produce Emission Inventories, 2022. URL <https://www.epa.gov/moves/emissions-models-and-other-methods-produce-emission-inventories>. Accessed: 2022-06-03.
- U. S. Fish and Wildlife Service. Emissions-and-Effects.jpg, 2015. URL <https://www.fws.gov/refuges/airquality/images/Emissions-and-Effects.jpg>. Accessed: 2022-01-24.
- UNCTAD. Review of Maritime Transport 2019. Technical Report October, United Nations Conference on Trade and Development, 2019. URL [https://unctad.org/en/Pages/Publications/Review-of-Maritime-Transport-\(Series\).aspx](https://unctad.org/en/Pages/Publications/Review-of-Maritime-Transport-(Series).aspx).

- UNCTAD. Review of Maritime Transport 2020. Technical report, United Nations Conference on Trade and Development, 2020. URL [https://unctad.org/system/files/official-document/rmt2020\\_en.pdf](https://unctad.org/system/files/official-document/rmt2020_en.pdf). Accessed: 2022-05-02.
- UNCTAD STAT. Maritime Profile: China. URL <https://unctadstat.unctad.org/countryprofile/maritimeprofile/en-gb/156/index.html>. Accessed: 2021-01-22.
- UNFCCC. Kyoto Protocol to the United Nations Framework Convention on Climate Change, 1997. ISSN 24637807.
- UNFCCC. Paris Agreement, 2016.
- Z. Wan, S. Ji, Y. Liu, Q. Zhang, J. Chen, and Q. Wang. Shipping emission inventories in China's Bohai Bay, Yangtze River Delta, and Pearl River Delta in 2018. *Mar. Pollut. Bull.*, 151(November 2019): 110882, 2020. ISSN 18793363. doi: 10.1016/j.marpolbul.2019.110882. URL <https://doi.org/10.1016/j.marpolbul.2019.110882>.
- X.-T. Wang, H. Liu, Z.-F. Lv, F.-Y. Deng, H.-L. Xu, L.-J. Qi, M.-S. Shi, J.-C. Zhao, S.-X. Zheng, H.-Y. Man, and K.-B. He. Trade-linked shipping co2 emissions. *Nat. Clim. Change*, 2021. ISSN 1758-678X. doi: 10.1038/s41558-021-01176-6. URL <http://dx.doi.org/10.1038/s41558-021-01176-6>.
- Y. Wang and L. A. Wright. A comparative review of alternative fuels for the maritime sector: Economic, technology, and policy challenges for clean energy implementation. *World*, 2:456–481, 2021. doi: 10.3390/world2040029.
- F. R. Westlye, A. Ivarsson, and J. Schramm. Experimental investigation of nitrogen based emissions from an ammonia fueled SI-engine. *Fuel*, 111(2):239–247, 2013. ISSN 00162361. doi: 10.1016/j.fuel.2013.03.055. URL <http://dx.doi.org/10.1016/j.fuel.2013.03.055>.
- C. Whall, D. Cooper, K. Archer, L. Twigger, N. Thurston, D. Ock-well, A. McIntyre, and A. Ritchie. Quantification of emissions from ships associated with ship movements between ports in the European Community. *Tech. Rep.*, 2002.
- G. Z. Whitten, G. Heo, Y. Kimura, E. McDonald-Buller, D. T. Allen, W. P. Carter, and G. Yarwood. A new condensed toluene mechanism for Carbon Bond: CB05-TU. *Atmos. Environ.*, 44(40):5346–5355, 2010. ISSN 13522310. doi: 10.1016/j.atmosenv.2009.12.029. URL <http://dx.doi.org/10.1016/j.atmosenv.2009.12.029>.
- WHO. Air Quality Guidelines. Global update 2005. Technical report, World Health Organization, 2005.
- WHO. Health Effects of Black Carbon. Technical report, World Health Organization, 2012.
- WHO. 7 million premature deaths annually linked to air pollution, 2014. URL <https://www.who.int/news/item/25-03-2014-7-million-premature-deaths-annually-linked-to-air-pollution>. Accessed: 2022-01-23.
- WHO. WHO global air quality guidelines. Technical report, World Health Organization, 2021.
- WHO. Ambient air pollution data, 2022. URL <https://www.who.int/data/gho/data/themes/air-pollution/ambient-air-pollution#>. Accessed: 2022-01-23.
- H. Winnes, E. Fridell, K. Yaramenka, D. Nelissen, J. Faber, and S. Ahdour. NOx controls for shipping in EU Seas. Technical Report June, Transport & Environment, 2016a.
- H. Winnes, J. Moldanová, M. Anderson, and E. Fridell. On-board measurements of particle emissions from marine engines using fuels with different sulphur content. *Proc. Inst. Mech. Eng. M: J. Eng. Marit. Environ.*, 230(1):45–54, 2016b. ISSN 20413084. doi: 10.1177/1475090214530877.

- M. Winther, J. H. Christensen, M. S. Plejdrup, E. S. Ravn, Ó. F. Eriksson, and H. O. Kristensen. Emission inventories for ships in the arctic based on satellite sampled AIS data. *Atmos. Environ.*, 91(2014):1–14, 2014. ISSN 18732844. doi: 10.1016/j.atmosenv.2014.03.006. URL <http://dx.doi.org/10.1016/j.atmosenv.2014.03.006>.
- G. Yarwood, S. Rao, M. Yocke, and G. Whitten. Updates to the Carbon Bond Mechanism: CB05. Technical report, 2005.
- C. Yu, D. Pasternak, J. Lee, M. Yang, T. Bell, K. Bower, H. Wu, D. Liu, C. Reed, S. Bauguitte, S. Cliff, J. Trembath, H. Coe, and J. D. Allan. Characterizing the Particle Composition and Cloud Condensation Nuclei from Shipping Emission in Western Europe. *Environ. Sci. Technol.*, 2020. ISSN 15205851. doi: 10.1021/acs.est.0c04039.
- G. Yu, Y. Zhang, F. Yang, B. He, C. Zhang, Z. Zou, X. Yang, N. Li, and J. Chen. Dynamic ni/v ratio in the ship-emitted particles driven by multiphase fuel oil regulations in coastal china. *Environ. Sci. Technol.*, 55:15031–15039, 2021. ISSN 15205851. doi: 10.1021/acs.est.1c02612.
- Y. B. Zeldovich. The Oxidation of Nitrogen in Combustion and Explosions. *Acta Physicochimica U.S.S.R.*, 21:577–628, 1946. doi: 10.1515/9781400862979.364.
- M. Zeretzke. Entwicklung eines Modells zur Quantifizierung von Luftschadstoffen, die durch Schiffsdieselmotoren auf See emittiert werden. Master’s thesis, Technische Universität Hamburg-Harbug, 2013.
- Y. Zhang, X. Yang, R. Brown, L. Yang, L. Morawska, Z. Ristovski, Q. Fu, and C. Huang. Shipping emissions and their impacts on air quality in China. *Sci. Total Environ.*, 581-582:186–198, 2017. ISSN 18791026. doi: 10.1016/j.scitotenv.2016.12.098. URL <http://dx.doi.org/10.1016/j.scitotenv.2016.12.098>.
- Y. Zhang, J. C. Fung, J. W. Chan, and A. K. Lau. The significance of incorporating unidentified vessels into ais-based ship emission inventory. *Atmos. Environ.*, 203:102–113, 2019. ISSN 18732844. doi: 10.1016/j.atmosenv.2018.12.055.
- J. Zhao, Y. Zhang, A. P. Patton, W. Ma, H. Kan, L. Wu, F. Fung, S. Wang, D. Ding, and K. Walker. Projection of ship emissions and their impact on air quality in 2030 in Yangtze River delta, China. *Environ. Pollut.*, 263:114643, 2020. ISSN 18736424. doi: 10.1016/j.envpol.2020.114643. URL <https://doi.org/10.1016/j.envpol.2020.114643>.
- B. Zheng, D. Tong, M. Li, F. Liu, C. Hong, G. Geng, H. Li, X. Li, L. Peng, J. Qi, L. Yan, Y. Zhang, H. Zhao, Y. Zheng, K. He, and Q. Zhang. Trends in China’s anthropogenic emissions since 2010 as the consequence of clean air actions. *Atmos. Chem. Phys.*, 18:14095–14111, 2018. doi: 10.5194/acp-18-14095-2018.





# Abbreviations and Acronyms

## List of Abbreviations

AIS	Automatic Identification System
AQER	Air Quality e-Reporting
AQG	Air Quality Guideline
BC	Black Carbon
BSH	Bundesamt für Seeschifffahrt und Hydrographie (German Federal Office for Sea Shipping and Hydrography)
CAMS	Copernicus Atmosphere Monitoring Service
CARB	California Air Resources Board
CH <sub>4</sub>	Methane
Chap.	Chapter
CNC12	Descriptor for a domain located in western China
CNSS	Clean North Sea Shipping
CO	Carbon monoxide
CO <sub>2</sub>	Carbon dioxide
CTM	Chemistry Transport Model
DECA	Domestic Emission Control Area
<i>D</i>	Draught
DF	Distillate Fuel
<i>E</i>	Energy consumption
ECA	Emission Control Area
ECCAD	Emissions of Atmospheric Compounds and Compilation of Ancillary Data
ECMWF	European Centre for Medium-Range Weather Forecasts
EDGAR	Emissions Database for Global Atmospheric Research
EF	Emission Factor
EGR	Exhaust Gas Recirculation
EL	Engine Load
EI	Emission Inventory
EMEP	Co-operative Programme for Monitoring and Evaluation of the Long-range Transmission of Air Pollutants in Europe
EMSA	European Maritime Safety Agency
EPA	United States Environmental Protection Agency
Eq.	Equation
EU	European Union
FCR	Fuel Consumption Rate
Fig.	Figure
FMI	Finnish Meteorological Institute
FSC	Fuel Sulfur Content
GBO	Gas Boil-Off
GNFR	Guidelines for reporting emissions and projections data Nomenclature For Reporting
GPS	Global Positioning System
GT	Gross Tonnage

## Bibliography

HNO <sub>3</sub>	Nitric acid
H <sub>2</sub> SO <sub>4</sub>	Sulfuric acid
IFS	Integrated Forecast System
IMO	International Maritime Organization
3rd IMO GHGS	Third IMO Greenhouse Gas Study
4th IMO GHGS	Fourth IMO Greenhouse Gas Study
IPCC	Intergovernmental Panel on Climate Change
<i>L</i>	Length
LAI	Leaf Area Index
LM-MCIP	<i>Lokal-Modell</i> Meteorology–Chemistry Interface Processor
LNG	Liquefied Natural Gas
LYP	Lower Yangtze Plain
MA	Mineral Ash
MARPOL	International Convention for Prevention of Marine Pollution for Ships
MARS	Meteorological Archival and Retrieval System
MEIC	Multi-resolution Emission Inventory for China
MGO	Marine Gas Oil
MMSI	Maritime Mobile Service Identity
N <sub>2</sub> O	Dinitrogen oxide
NBS	North and Baltic Sea
NH <sub>3</sub>	Ammonia
NMB	Normalized Mean Bias
NCP	North China Plain
NECA	Nitrogen Emission Control Area
NMVOC	Non-Methane Volatile Organic Compound
NO	Nitrogen monoxide
NO <sub>2</sub>	Nitrogen dioxide
NO <sub>x</sub>	Nitrogen oxides
O <sub>3</sub>	Ozone
OC	Organic Compounds
<i>P<sub>aux</sub></i>	Total power of auxiliary engines
<i>P<sub>main</sub></i>	Total power of main engines
POA	Primary Organic Aerosol
PM	Particulate Matter
PRD	Pearl River Delta
RCEP	Regional Comprehensive Economic Partnership
RF	Residual Fuel
RPM	Revolutions Per Minute
S	Speed
<i>S<sub>ser</sub></i>	Service speed
SC12NSBS	Descriptor for a domain located in northern Europe
SCR	Selective Catalytic Reduction
SECA	Sulfur Emission Control Area
Sect.	Section
SFOC	Specific Fuel Oil Consumption
SHEBA	Sustainable Shipping and the Environment of the Baltic Sea Region
SNAP	Selected Nomenclature for Air Pollution
SO <sub>2</sub>	Sulphur dioxide
SO <sub>4</sub> <sup>2-</sup>	Sulfate
SO <sub>x</sub>	Sulfur oxides

TEU	Twenty-Foot Equivalent Unit
TNO	Netherlands Organisation for Applied Scientific Research
VOC	Volatile Organic Compounds
WHO	World Health Organization
YRD	Yangtze River Delta

## **List of Model Acronyms**

COSMOS-CLM	Consortium for Small Scale Modelling in Climate Mode
CMAQ	Community Multi-scale Air Quality model
HiMEMO	Highly Modular Emission Model
MEGAN	Model of Emissions of Gases and Aerosols from Nature
MoSES	Modular Ship Emission Modeling System
STEAM	Ship Traffic Emissions Assessment Model

# List of Figures

1.1.	Illustration of the atmospheric life-cycle of air pollutants from source to sink. Reprinted with permission from U.S. Fish & Wildlife Service (U. S. Fish and Wildlife Service, 2015).	3
1.2.	Growth of annual production-based emissions of carbon dioxide (CO <sub>2</sub> ) in tonnes by world region (Ritchie et al., 2020).	7
1.3.	Schematic representation of an Eulerian box model.	10
2.1.	Outline of the multi-model approach that was applied in this work to answer the scientific questions. External input data are marked by a dotted frame, model generated data by a dash-dotted frame and models are marked by a bold frame. An approximate reference of the work packages to the individual publications is given by the colorized, dashed frames.	19
3.1.	Schematic representation of the modeling process in MoSES. Black boxes represent modules and functions of the model. Blue boxes contain input data from AIS. Green boxes represent data from a ship database. Red boxes represent internal methods to fill in data gaps. Violet boxes represent data regarding emission factors.	22
3.2.	Calculated CO <sub>2</sub> emissions in $\text{g} \cdot (\text{m}^2 \cdot \text{year})^{-1}$ on a logarithmic scale for the year 2015 in the chosen model domain including the North and Baltic Sea. The spatial resolution is approximately $4 \times 4 \text{ km}^2$ ( <b>left</b> ). Monthly change of CO <sub>2</sub> emissions in 2015 for each ship type averaged to one day ( <b>right</b> ).	30
3.3.	Comparison of the daily CO <sub>2</sub> emissions [ $\text{g}/\text{km}^2$ ] calculated with MoSES and STEAM for the North Sea ( <b>left</b> ) and the Baltic Sea ( <b>right</b> ). The results are shown for January 2015 (top panel) and July 2015 (bottom panel).	34
3.4.	Ship type and gross tonnage distribution of ships traveling between the five busiest ports in the North and Baltic Sea Region and the English Channel.	38
4.1.	Development of total annual emissions from 2015 to 2050 in the North and Baltic Sea domain. For NH <sub>3</sub> -powered engines a compression-ignition engine with marine diesel oil as pilot fuel is considered, which is referred to as the “uncontrolled” case. Values for CO <sub>2</sub> were divided by 500, for NH <sub>3</sub> by 5, for NO <sub>x</sub> by 10, and for CO <sub>2</sub> equivalents by 500 to fit the scale.	45
4.2.	Development of total annual emissions from 2015 to 2050 in the North and Baltic Sea domain. For NH <sub>3</sub> -powered engines a spark-ignition engine with hydrogen as pilot fuel is considered, which is referred to as the “controlled” case. The figure shows only emission species whose development is different in the controlled case than in the uncontrolled case. Values for CO <sub>2</sub> were divided by 500, for NH <sub>3</sub> by 10, for NO <sub>x</sub> by 10 and for CO <sub>2</sub> equivalents by 500 to fit the scale.	46
4.3.	CO <sub>2</sub> emission fluxes in [ $\text{g} \cdot \text{m}^{-2} \cdot \text{year}^{-1}$ ] from the reference emission inventory (2015, <b>a</b> ) and the percentage change from the scenario emission inventories for the years 2025 ( <b>b</b> ), 2040 ( <b>c</b> ), and 2050 ( <b>d</b> ), compared to the reference.	47
5.1.	Modeled domains for northern Europe ( <b>left</b> , SC12NSBS) and eastern China ( <b>right</b> , CNC12) that were created for the comparison. Also shown are the air quality monitoring stations that were considered in an evaluation of the model performance. The red dots represent selected stations whose comparison data are exemplarily shown in the original publication in Sect. 5.2. The full evaluation data of all stations can be found in the appendix.	52

5.2.	Calculated CO <sub>2</sub> emission fluxes in $\text{g} \cdot \text{m}^{-2} \cdot \text{year}^{-1}$ plotted on a logarithmic scale for the Chinese domain 2015. The spatial resolution is approximately $4 \times 4 \text{ km}^2$ ( <b>left</b> ). Monthly emissions of black carbon (BC), CH <sub>4</sub> , CO, mineral ash (MA), nonmethane volatile organic compounds (NMVOCs), NO <sub>x</sub> , primary organic aerosols (POAs), SO <sub>2</sub> , SO <sub>4</sub> and SO <sub>4</sub> × H <sub>2</sub> O in 2015, normalized to one day ( <b>right</b> ). Values of NO <sub>x</sub> and SO <sub>2</sub> were divided by 10 to fit the scale. . . . .	57
5.3.	Annual averages of NO <sub>2</sub> concentrations in the SC12NSBS domain in Europe ( <b>a–c</b> ) and the CNC12 domain in China ( <b>d–f</b> ). NO <sub>2</sub> concentrations [ $\mu\text{g} \cdot \text{m}^{-3}$ ] from all emission sources are shown in ( <b>a,d</b> ), from shipping only in ( <b>b,e</b> ) and the share of NO <sub>2</sub> concentrations from shipping on total NO <sub>2</sub> concentrations [%] is shown in ( <b>c,f</b> ). . . . .	62
5.4.	Seasonal averages of NO <sub>2</sub> concentrations [ $\mu\text{g} \cdot \text{m}^{-3}$ ] from shipping in the CNC12 domain in China for winter ( <b>a</b> ) and summer ( <b>b</b> ). . . . .	63
5.5.	Annual averages of SO <sub>2</sub> concentrations in the SC12NSBS domain in Europe ( <b>a–c</b> ) and in the CNC12 domain in China ( <b>d–f</b> ). SO <sub>2</sub> concentrations [ $\mu\text{g} \cdot \text{m}^{-3}$ ] from all emission sources are shown in ( <b>a,d</b> ), from shipping only in ( <b>b,e</b> ) and the share of SO <sub>2</sub> concentrations from shipping on total SO <sub>2</sub> concentrations [%] is shown in ( <b>c,f</b> ). . . . .	63
5.6.	Annual averages of O <sub>3</sub> concentrations in the SC12NSBS domain in Europe ( <b>a–c</b> ) and in the CNC12 domain in China ( <b>d–f</b> ). Annual averages of 8-hour max. O <sub>3</sub> concentrations [ $\mu\text{g} \cdot \text{m}^{-3}$ ] from all emission sources are shown in ( <b>a,d</b> ), annual averages from shipping only in ( <b>b,e</b> ) and the share of O <sub>3</sub> concentrations from shipping on total O <sub>3</sub> concentrations [%] is shown in ( <b>c,f</b> ). . . . .	65
5.7.	Seasonal averages of O <sub>3</sub> concentrations [ $\mu\text{g} \cdot \text{m}^{-3}$ ] from shipping in the SC12NSBS domain in Europe for winter ( <b>a</b> ), summer ( <b>b</b> ) and in the CNC12 domain in China for winter ( <b>c</b> ) and summer ( <b>d</b> ). . . . .	66
5.8.	Annual averages of PM <sub>2.5</sub> concentrations in the SC12NSBS domain in Europe ( <b>a–c</b> ) and in the CNC12 domain in China ( <b>d–f</b> ). PM <sub>2.5</sub> concentrations [ $\mu\text{g} \cdot \text{m}^{-3}$ ] from all emission sources are shown in ( <b>a,d</b> ); PM <sub>2.5</sub> concentrations only from shipping are shown in ( <b>b,e</b> ); the share of PM <sub>2.5</sub> concentrations from shipping in the PM <sub>2.5</sub> concentrations from all sources [%] is shown in ( <b>c,f</b> ). . . . .	67
5.9.	Seasonal averages of PM <sub>2.5</sub> concentrations [ $\mu\text{g} \cdot \text{m}^{-3}$ ] from shipping in the SC12NSS domain in Europe for winter ( <b>a</b> ), spring ( <b>b</b> ), summer ( <b>c</b> ), autumn ( <b>d</b> ) and in the CNC12 domain in China for winter ( <b>e</b> ), spring ( <b>f</b> ), summer ( <b>g</b> ) and winter ( <b>h</b> ). . . . .	68
5.10.	Annual averages of NH <sub>4</sub> concentrations in the SC12NSBS domain in Europe ( <b>a–c</b> ) and in the CNC12 domain in China ( <b>d–f</b> ). NH <sub>4</sub> concentrations [ $\mu\text{g} \cdot \text{m}^{-3}$ ] from all emission sources are shown in ( <b>a,d</b> ); NH <sub>4</sub> concentrations only from shipping are shown in ( <b>b,e</b> ); the share of NH <sub>4</sub> concentrations from shipping in the NH <sub>4</sub> concentrations from all sources [%] is shown in ( <b>c,f</b> ). . . . .	69
5.11.	Annual averages of SO <sub>4</sub> concentrations in the SC12NSBS domain in Europe ( <b>a–c</b> ) and in the CNC12 domain in China ( <b>d–f</b> ). SO <sub>4</sub> concentrations [ $\mu\text{g} \cdot \text{m}^{-3}$ ] from all emission sources are shown in ( <b>a,d</b> ); SO <sub>4</sub> concentrations only from shipping are shown in ( <b>b,e</b> ); the share of SO <sub>4</sub> concentrations from shipping in the SO <sub>4</sub> concentrations from all sources [%] is shown in ( <b>c,f</b> ). . . . .	70
5.12.	Annual averages of NO <sub>3</sub> concentrations in the SC12NSBS domain in Europe ( <b>a–c</b> ) and in the CNC12 domain in China ( <b>d–f</b> ). NO <sub>3</sub> concentrations [ $\mu\text{g} \cdot \text{m}^{-3}$ ] from all emission sources are shown in ( <b>a,d</b> ); NO <sub>3</sub> concentrations only from shipping are shown in ( <b>b,e</b> ); the share of NO <sub>3</sub> concentrations from shipping in the NO <sub>3</sub> concentrations from all sources [%] is shown in ( <b>c,f</b> ). . . . .	71
A.1.	Seasonally averaged, modeled NO <sub>2</sub> concentrations in the ground layer from all emission sources in Europe. . . . .	121
A.2.	Seasonally averaged, modeled NO <sub>2</sub> concentrations in the ground layer from ships in Europe. . . . .	121
A.3.	Seasonally averaged, modeled percentage share of ships on NO <sub>2</sub> concentrations in the ground layer in Europe. . . . .	121

A.4. Seasonally averaged, modeled NO <sub>2</sub> concentrations in the ground layer from all sources in China. . . . .	121
A.5. Seasonally averaged, modeled NO <sub>2</sub> concentrations in the ground layer from ships in China. . . . .	122
A.6. Seasonally averaged, modeled percentage share of ships on NO <sub>2</sub> concentrations in the ground layer in China. . . . .	122
A.7. Seasonally averaged, modeled SO <sub>2</sub> concentrations in the ground layer from all sources in Europe. . . . .	122
A.8. Seasonally averaged, modeled SO <sub>2</sub> concentrations in the ground layer from ships in Europe. . . . .	122
A.9. Seasonally averaged, modeled percentage share of ships on SO <sub>2</sub> concentrations in the ground layer in Europe. . . . .	123
A.10. Seasonally averaged, modeled SO <sub>2</sub> concentrations in the ground layer from all sources in China. . . . .	123
A.11. Seasonally averaged, modeled SO <sub>2</sub> concentrations in the ground layer from ships in China. . . . .	123
A.12. Seasonally averaged, modeled percentage share of ships on SO <sub>2</sub> concentrations in the ground layer in China. . . . .	123
A.13. Seasonally averaged, modeled O <sub>3</sub> concentrations in the ground layer from all sources in Europe. . . . .	124
A.14. Seasonally averaged, modeled O <sub>3</sub> concentrations in the ground layer from ships in Europe. . . . .	124
A.15. Seasonally averaged, modeled percentage share of ships on O <sub>3</sub> concentrations in the ground layer in Europe. . . . .	124
A.16. Seasonally averaged, modeled O <sub>3</sub> concentrations in the ground layer from all sources in China. . . . .	124
A.17. Seasonally averaged, modeled O <sub>3</sub> concentrations in the ground layer from ships in China. . . . .	125
A.18. Seasonally averaged, modeled percentage share of ships on O <sub>3</sub> concentrations in the ground layer in China. . . . .	125
A.19. Seasonally averaged PM <sub>2.5</sub> concentrations in the ground layer from all sources in Europe. . . . .	125
A.20. Seasonally averaged, modeled PM <sub>2.5</sub> concentrations in the ground layer from ships in Europe. . . . .	125
A.21. Seasonally averaged, modeled percentage share of ships on PM <sub>2.5</sub> concentrations in the ground layer in Europe. . . . .	126
A.22. Seasonally averaged, modeled PM <sub>2.5</sub> concentrations in the ground layer from all sources in China. . . . .	126
A.23. Seasonally averaged, modeled PM <sub>2.5</sub> concentrations in the ground layer from ships in China. . . . .	126
A.24. Seasonally averaged, modeled percentage share of ships on PM <sub>2.5</sub> concentrations in the ground layer in China. . . . .	126
A.25. Seasonally averaged, modeled NH <sub>4</sub> concentrations in the ground layer from all sources in Europe. . . . .	127
A.26. Seasonally averaged, modeled NH <sub>4</sub> concentrations in the ground layer from ships in Europe. . . . .	127
A.27. Seasonally averaged, modeled percentage share of ships on NH <sub>4</sub> concentrations in the ground layer in Europe. . . . .	127
A.28. Seasonally averaged, modeled NH <sub>4</sub> concentrations in the ground layer from all sources in China. . . . .	127
A.29. Seasonally averaged, modeled NH <sub>4</sub> concentrations in the ground layer from ships in China. . . . .	128
A.30. Seasonally averaged, modeled percentage share of ships on NH <sub>4</sub> concentrations in the ground layer in China. . . . .	128
A.31. Seasonally averaged, modeled NH <sub>3</sub> emissions in the ground layer in the Europe. . . . .	128
A.32. Seasonally averaged, modeled NH <sub>3</sub> emissions in the ground layer in China. . . . .	128
A.33. Seasonally averaged, modeled NO <sub>3</sub> concentrations in the ground layer from all sources in Europe. . . . .	129
A.34. Seasonally averaged, modeled NO <sub>3</sub> concentrations in the ground layer from ships in Europe. . . . .	129
A.35. Seasonally averaged, modeled percentage share of ships on NO <sub>3</sub> concentrations in the ground layer in Europe. . . . .	129

A.36. Seasonally averaged, modeled NO <sub>3</sub> concentrations in the ground layer from all sources in China. . . . .	129
A.37. Seasonally averaged, modeled NO <sub>3</sub> concentrations in the ground layer from ships in China. . . . .	130
A.38. Seasonally averaged, modeled percentage share of ships on NO <sub>3</sub> concentrations in the ground layer in China. . . . .	130
A.39. Seasonally averaged, modeled SO <sub>4</sub> concentrations in the ground layer from all sources in Europe. . . . .	130
A.40. Seasonally averaged, modeled SO <sub>4</sub> concentrations in the ground layer from ships in Europe. . . . .	130
A.41. Seasonally averaged, modeled percentage share of ships on SO <sub>4</sub> concentrations in the ground layer in Europe. . . . .	131
A.42. Seasonally averaged, modeled SO <sub>4</sub> concentrations in the ground layer from all sources in China. . . . .	131
A.43. Seasonally averaged, modeled SO <sub>4</sub> concentrations in the ground layer from ships in China. . . . .	131
A.44. Seasonally averaged, modeled percentage share of ships on SO <sub>4</sub> concentrations in the ground layer in China. . . . .	131



# List of Tables

1.1.	World Health Organization (WHO) air quality guidelines (AQGs) for 2005 and 2021 (WHO, 2005, 2021), current European (European Commission, 2008) and Chinese air quality standards (class 2, GB 3095-2012 and HJ 633-2012). . . . .	4
3.1.	In MoSES considered gases and aerosols with the different implemented emission factors, their sources and dependencies. . . . .	27
3.2.	Modeled emissions in Gg/year for the North/Baltic Sea Domain 2015 in total and for each individual ship type. . . . .	32
3.3.	Hydrographic regions used for the comparison of MoSES with STEAM, along with the ratio between MoSES emission values and STEAM emission values, given as percentage. For the Baltic Sea region two data sets for comparison, STEAM-Worldpool (Baltic Sea Worldpool) and STEAM-HELCOM (Baltic Sea HELCOM), were available. Kattegat and Skagerrak were considered as an additional third region. . . . .	33
3.4.	The percentage of ships for which an attribute was estimated with the lower and upper percentual uncertainty this ship attribute has on the calculation of CO <sub>2</sub> emissions. The values are given as an average of the months January and July. . . . .	36
3.5.	Share in CO <sub>2</sub> emissions from ships sailing between the five busiest ports, the English Channel and all other implemented ports in the North/Baltic Sea region. The values cover both directions and are given as fraction of the total emissions in the model domain. Values that are not available or redundant are marked as “n.a.”. . . . .	38
3.6.	Reduction of trade volume and corresponding CO <sub>2</sub> emission reduction in an example scenario. 39	39
4.1.	Increase in number of ships and capacity increase in percent for all three scenarios, based on Fridell et al. (2016). Annual efficiency increases based on IMO Energy Efficiency Design Index and average ship lifetimes from Winnes et al. (2016a) for the ship types considered. . . . .	43
4.2.	Percentage of energy consumption by fuel type for the reference emissions inventory (2015) and the three scenarios created (2025, 2040, 2050), according to DNV-GL (2020). . . . .	43
4.3.	Emission factors (EFs) for ammonia-fueled engines for an “uncontrolled” case describing a compression-ignition engine using marine gas oil as pilot fuel and a “controlled” case describing a spark ignition engine using hydrogen as pilot fuel. The EFs are based on preliminary results from Ntziachristos et al. from the Laboratory of Applied Thermodynamics of the University of Thessaloniki. . . . .	44
5.1.	Gas and aerosol species included in the ship emission inventories (EIs), with sources of the emission factors (EFs) used. . . . .	55
5.2.	Modeled ship emissions in Gg · year <sup>-1</sup> for China in 2015 in total and for each individual ship type. . . . .	56
5.3.	Comparison of modeled NO <sub>2</sub> , SO <sub>2</sub> , O <sub>3</sub> 8-hour mean and PM <sub>2.5</sub> concentrations of the modeled “base” case in μg · m <sup>-3</sup> with measurements in the SC12NSBS domain. Based on all 29 considered stations in Europe, the mean correlation coefficient (Mean Corr.) and two values, calculated as the mean of either positive or negative normalized mean biases are shown (NMB <sub>pos</sub> , NMB <sub>neg</sub> ). For the latter two values, the number of stations used for the calculation is given in parentheses. . . . .	58

5.4. Comparison of modeled NO <sub>2</sub> , SO <sub>2</sub> , O <sub>3</sub> 8-hour mean and PM <sub>2.5</sub> concentrations of the modeled “base” case in $\mu\text{g} \cdot \text{m}^{-3}$ with measurements in the CNC12 domain. Based on all 20 considered stations in China, the mean correlation coefficient (Mean Corr.) and two values, calculated as the mean either from positive or negative normalized mean biases are shown (NMB <sub>pos</sub> , NMB <sub>neg</sub> ). For the latter two values, the number of stations used for the calculation is given in parentheses. . . . .	59
A.1. Parameters $a$ and $b$ for ship type specific fit functions with the gross tonnage ( $GT$ ) as dependent variable, determined from the ship length ( $L$ ) or draught ( $D$ ). . . . .	107
A.2. Parameter $a$ for the ship type specific fit functions with the total main engine power ( $P_{main}$ ) as dependent variable, determined from the gross tonnage ( $GT$ ). . . . .	108
A.3. Parameter $a$ for the ship type specific fit functions with the total auxiliary engine power ( $P_{aux}$ ) as dependent variable, determined from the total main engine power ( $P_{main}$ ). . . . .	108
A.4. Parameters $a$ , $b$ and $c$ for the ship type specific fit functions with the service speed ( $S_{ser}$ ) or the main engine RPM ( $RPM_{main}$ ) as dependent variables, determined from the total main engine power ( $P_{main}$ ). . . . .	109
A.5. Gross tonnage averages for different ship types. . . . .	109
A.6. Parameters $a$ , $b$ and $c$ for the engine size specific fit functions for different engine applications, with the specific fuel oil consumption (SFOC) as dependent variables, determined from the engine load ( $EL$ ). . . . .	110
A.7. Parameters $a$ , $b$ , $c$ , and $d$ for the engine size specific fit functions for different engine applications and NO <sub>X</sub> Tiers, with the NO <sub>X</sub> emission factor as dependent variables, determined from the engine load ( $EL$ ). . . . .	111
A.8. Parameter $a$ to determine the CO <sub>2</sub> emission factor for different fuel types. . . . .	112
A.9. Base emission factor ( $EF_{CO,base}$ ) for different engine or fuel types. . . . .	112
A.10. Methane emission factors ( $EF_{CH_4}$ ) for different engines or fuel types. . . . .	112
A.11. NMVOC emission factors ( $EF_{NMVOCb}$ ) for different engine type and engine load ( $EL$ ). . . . .	113
A.12. Dinitrogen oxide emission factors ( $EF_{N_2O}$ ) for different engine or fuel types. . . . .	113
A.13. Particulate matter emission factors ( $EF_{PMb}$ ) for different engine type, fuel types, and engine loads ( $EL$ ). . . . .	113
A.14. Parameter $a$ for the fuel consumption rate ( $FCR$ ) and fractional usage for the main engine, power generator, and boiler of a ship, for different ship types. . . . .	114
A.15. Modeled monthly emissions in Gg/month for the North/Baltic Sea Domain 2015. . . . .	115
A.16. Mapping of MEIC emission inventory sectors to SNAP sectors and EDGAR Activity Codes. . . . .	117
A.17. Comparison of modeled NO <sub>2</sub> concentrations in $\mu\text{g} \cdot \text{m}^{-3}$ with measurements in Europe. . . . .	118
A.18. Comparison of modeled SO <sub>2</sub> concentrations in $\mu\text{g} \cdot \text{m}^{-3}$ with measurements in Europe. . . . .	118
A.19. Comparison of modeled O <sub>3</sub> 8-hour mean concentrations in $\mu\text{g} \cdot \text{m}^{-3}$ with measurements in Europe. . . . .	118
A.20. Comparison of modeled PM <sub>2.5</sub> concentrations in $\mu\text{g} \cdot \text{m}^{-3}$ with measurements in Europe. . . . .	119
A.21. Comparison of modeled NO <sub>2</sub> concentrations in $\mu\text{g} \cdot \text{m}^{-3}$ with measurements in China. . . . .	119
A.22. Comparison of modeled SO <sub>2</sub> concentrations in $\mu\text{g} \cdot \text{m}^{-3}$ with measurements in China. . . . .	119
A.23. Comparison of modeled O <sub>3</sub> 8-hour average concentrations in $\mu\text{g} \cdot \text{m}^{-3}$ with measurements in China. . . . .	120
A.24. Comparison of modeled PM <sub>2.5</sub> concentrations in $\mu\text{g} \cdot \text{m}^{-3}$ with measurements in China. . . . .	120

# A. Appendix

## A.1. Appendix for Publication I

### A.1.1. Fit Functions

#### A.1.1.1. Gross Tonnage

Form of the fit function:

$$y(x) = a \cdot x^b.$$

$y$  is the gross tonnage ( $GT$ ) and  $x$  the ship length ( $L$ ) or draught ( $D$ ). The factors  $a$  and  $b$  can be found for the different ships types in Table A.1).

Table A.1.: Parameters  $a$  and  $b$  for ship type specific fit functions with the gross tonnage ( $GT$ ) as dependent variable, determined from the ship length ( $L$ ) or draught ( $D$ ).

Ship Type	Length		Draught	
	$a$	$b$	$a$	$b$
Bulk	0.0039	3.0	17.5	3.0
Cargo	0.0002	3.6	31.0	2.9
Cruise	0.0129	2.8	24.6	3.9
Fishing	0.0012	3.3	5.3	3.4
Military	0.6805	2.0	143.4	2.4
Passenger	0.0107	2.8	141.4	2.7
Pleasurecraft	0.0143	2.7	94.5	2.0
Tanker	0.0018	3.2	83.5	2.4
Tug	0.0192	2.8	37.6	2.1
Other	0.0041	2.9	565.5	1.8
Undefined	0.0012	3.3	5.3	3.4

#### A.1.1.2. Total Main Engine Power

Form of the fit function:

$$y(x) = a \cdot \sqrt{x}$$

$y$  is the total main engine power ( $P_{main}$ ),  $x$  is the gross tonnage ( $GT$ ). The factor  $a$  can be found for the different ship types in Table A.2.

Table A.2.: Parameter  $a$  for the ship type specific fit functions with the total main engine power ( $P_{main}$ ) as dependent variable, determined from the gross tonnage ( $GT$ ).

Ship Type	$a$
Bulk	51.0
Cargo	56.6
Cruise	165.5
Fishing	53.8
Military	178.3
Passenger	134.0
Pleasurecraft	123.2
Tanker	63.9
Tug	138.5
Other	153.1
Undefined	53.8

### A.1.1.3. Total Auxiliary Engine Power

Form of the fit function:

$$y(x) = a \cdot x$$

$y$  is the total auxiliary engine power ( $P_{aux}$ ),  $x$  is the total main engine power ( $P_{main}$ ). The factor  $a$  can be found for the different ship types in Table A.3.

Table A.3.: Parameter  $a$  for the ship type specific fit functions with the total auxiliary engine power ( $P_{aux}$ ) as dependent variable, determined from the total main engine power ( $P_{main}$ ).

Ship Type	$a$
Bulk	0.19
Cargo	0.24
Cruise	0.16
Fishing	0.14
Military	0.20
Passenger	0.18
Pleasurecraft	0.12
Tanker	0.26
Tug	0.15
Other	0.19
Undefined	0.14

### A.1.1.4. Service Speed and Main Engine RPM

Form of the fit function:

$$y(x) = a + (b - a) \cdot \exp^{-cx}$$

$y$  is the service speed ( $S_{ser}$ ) or the main engine RPM ( $RPM_{main}$ ),  $x$  is the total main engine power ( $P_{main}$ ). The factors  $a$ ,  $b$  and  $c$  can be found for different ship types in Table A.3.

Table A.4.: Parameters  $a$ ,  $b$  and  $c$  for the ship type specific fit functions with the service speed ( $S_{ser}$ ) or the main engine RPM ( $RPM_{main}$ ) as dependent variables, determined from the total main engine power ( $P_{main}$ ).

Ship Type	Service speed			Main Engine RPM		
	$a$	$b$	$c$	$a$	$b$	$c$
Bulk	16.0	9.3	-7.6	78.4	1066.4	-7.8
Cargo	24.1	10.8	-9.2	171.5	859.6	-8.2
Cruise	23.6	13.5	-9.5	541.6	2161.3	-7.9
Fishing	18.9	9.5	-7.9	701.5	1788.2	-6.2
Military	34.6	9.3	-9.7	718.5	2205.6	-7.7
Passenger	28.9	1.0	-7.1	509.8	1715.3	-9.4
Pleasurec.	31.5	9.5	-8.3	701.5	1788.2	-6.2
Tanker	17.4	12.0	-8.9	123.5	1176.5	-7.8
Tug	17.6	9.5	-8.8	917.5	1823.6	-7.7
Other	26.1	11.7	-9.8	71.2	1734.1	-9.2
Undefined	18.9	9.5	-7.9	701.5	1788.2	-6.2

### A.1.2. Gross Tonnage Class Averages

Gross tonnage class averages were used when no other data for the gross tonnage was available. They can be found for the different ship types in Table A.5.

Table A.5.: Gross tonnage averages for different ship types.

Ship Type	Class Average [GT]
Bulk	39000
Cargo	6900
Cruise	45000
Fishing	500
Military	13500
Passenger	3000
Pleasurecraft	700
Tanker	28000
Tug	500
Other	15000
Undefined	500

### A.1.3. Emission Factors

#### A.1.3.1. Specific Fuel Oil Consumption (SFOC)

The specific fuel oil consumption [ $g \cdot kWh^{-1}$ ] of a ship for the main engine applications E2 and E3 was estimated with Eq. (A.1) dependent on the engine load  $EL$  (Zeretzke, 2013).

$$SFOC(EL) = a \cdot EL^2 - b \cdot EL + c \quad (A.1)$$

The factors  $a$ ,  $b$  and  $c$  are given in Table A.6 for different engine applications and sizes.

For auxiliary engines with engine application D2 Eq. (A.2), which is dependent on the total auxiliary engine power  $P_{aux}$  [kW], was used,

$$SFOC(P_{aux}) = 254.9 \cdot P_{aux}^{-0.029}. \quad (A.2)$$

Table A.6.: Parameters  $a$ ,  $b$  and  $c$  for the engine size specific fit functions for different engine applications, with the specific fuel oil consumption (SFOC) as dependent variables, determined from the engine load ( $EL$ ).

Engine Power [kW]	E2			E3		
	$a$	$b$	$c$	$a$	$b$	$c$
< 2000	102.25	170.47	274.63	67.862	84.00	239.25
2,000–10,000	102.21	170.79	260.04	47.225	74.74	209.84
> 10,000	40.09	53.20	191.84	46.135	69.15	200.82

#### A.1.3.2. Sulfur Dioxide (SO<sub>2</sub>)

The emission factor  $EF_{SO_2}$  [ $g \cdot kWh^{-1}$ ] was determined according to Eq. (A.3), based on the specific fuel oil consumption  $SFOC$  in [ $g \cdot kWh^{-1}$ ] and the fuel sulfur content  $FSC$  as fraction.  $M(SO_2)$  and  $M(S)$  are the molar mass of SO<sub>2</sub> and sulfur (S), respectively.  $CR_{StoSO_2}$  is the conversion rate of sulfur to SO<sub>2</sub> which was assumed to be 0.98.

$$EF_{SO_2} = SFOC \cdot FSC \cdot \frac{M(SO_2)}{M(S)} \cdot CR_{StoSO_2} \quad (A.3)$$

#### A.1.3.3. Sulfate (SO<sub>4</sub>)

The emission factor  $EF_{SO_4}$  [ $g \cdot kWh^{-1}$ ] was determined with Eq. (A.4).  $M(SO_4)$  and  $M(S)$  are the molar mass of SO<sub>4</sub> and S, respectively.  $EL$  is the engine load,  $SFOC$  the specific fuel oil consumption in [ $g \cdot kWh^{-1}$ ] and  $FSC$  the fuel sulfur content as fraction. The factor  $a$  is 0.035 for residual fuels and 0.004 for distillate fuels.

$$EF_{SO_4}(EL) = SFOC \cdot FSC \cdot (0.01 + EL \cdot a) \cdot \frac{M(SO_4)}{M(S)} \quad (A.4)$$

#### A.1.3.4. Nitrogen Oxides (NO<sub>x</sub>)

The emission factor  $EF_{NO_x}$  [ $g \cdot kWh^{-1}$ ] was determined with Eq. (A.5).

$$EF_{NO_x}(EL) = a \cdot EL^3 + b \cdot EL^2 + c \cdot EL + d \quad (A.5)$$

The functions are only valid for engine loads  $EL$  equal or above 25%. The factors  $a$ ,  $b$  and  $c$ , as well as term  $d$ , are given in the Table A.7 for different NO<sub>x</sub> Tier regulations, engine applications and sizes.

Table A.7.: Parameters  $a$ ,  $b$ ,  $c$ , and  $d$  for the engine size specific fit functions for different engine applications and NO<sub>X</sub> Tiers, with the NO<sub>X</sub> emission factor as dependent variables, determined from the engine load ( $EL$ ).

Engine Power [kW] Tier 1	E2				E3			
	$a$	$b$	$c$	$d$	$a$	$b$	$c$	$d$
< 2000	0	0.70	1.18	9.07	-12.1	27.3	20.8	12.5
2,000–10,000	-6.36	11.47	-7.43	12.28	-13.8	23.8	15.2	17.0
> 10,000	0	-12.48	16.30	8.71	-25.7	44.3	25.2	19.7
Tier 2								
< 2000	0	4.15	5.39	7.91	-7.26	18.2	-15.48	10.72
2,000–10,000	-15.31	27.98	-14.50	11.18	-14.76	27.69	-18.99	17.21
> 10,000	0	-13.37	16.67	8.64	-31.99	57.16	-31.60	18.55

For auxiliary engines with engine application D2 the emission factor was determined using Eqs. (A.7) dependent on the total auxiliary engine power  $P_{aux}$ .

$$\text{Tier 1: } EF_{NOX}(P_{aux}) = (1.42 \cdot \log(P_{aux})) - 0.20 \quad (\text{A.6})$$

$$\text{Tier 2: } EF_{NOX}(P_{aux}) = (0.89 \cdot \log(P_{aux})) + 1.18 \quad (\text{A.7})$$

#### A.1.3.5. Black Carbon (BC)

$EF_{BCa}$  [ $\text{g} \cdot \text{kWh}^{-1}$ ] is the emission factor for black carbon (BC) reported by (Aulinger et al., 2016). It has for main engines using residual (RF) and distillate fuels (DF) the value 0.06 and 0.03, respectively and for auxiliary engines 0.15. Since BC emissions are known to increase at low engine loads this value is multiplied by a correction function  $EF_{BCa,corr}(EL)$  specific for the current load shown in Eq. (A.11).

$$EL \leq 0.25: EF_{BCa,corr}(EL) = (6 - 0.12 \cdot EL)/1.2 \quad (\text{A.8})$$

$$25 < EL \leq 0.5: EF_{BCa,corr}(EL) = (3 - 0.052 \cdot (EL - 0.25))/1.2 \quad (\text{A.9})$$

$$0.5 < EL \leq 0.75: EF_{BCa,corr}(EL) = (1.7 - 0.02 \cdot (EL - 0.5))/1.2 \quad (\text{A.10})$$

$$0.75 < EL: EF_{BCa,corr}(EL) = (1.2 - 0.008 \cdot (EL - 0.75))/1.2 \quad (\text{A.11})$$

#### A.1.3.6. Primary Organic Aerosols (POAs)

The emissions factor  $EF_{POAb}$  [ $\text{g} \cdot \text{kWh}^{-1}$ ] was reported by (Jalkanen et al., 2012). It has the value 0.2 for marine diesel engines using residual or distillate fuels. This value is multiplied by the correction function shown in Eq. A.13 that depends on the engine load  $EL$ .

$$EL \geq : EF_{BC,corr}(EL) = 1.024/(1 + -47.660 \cdot e^{-32.547 \cdot EL}) \quad (\text{A.12})$$

$$EL < 0.15: EF_{BC,corr}(EL) = 3.333 \quad (\text{A.13})$$

#### A.1.3.7. Mineral Ash (MA)

The emissions factor  $EF_{MAa}$  [ $\text{g} \cdot \text{kWh}^{-1}$ ] for Mineral Ash (MA) is calculated with Eq. (A.14). The  $FSC$  is the fuel sulphur content as fraction and  $SFOC$  is the specific fuel oil consumption in [ $\text{g} \cdot \text{kWh}^{-1}$ ].

$$EF_{MA} = FSC \cdot SFOC \cdot 0.02 \quad (\text{A.14})$$

#### A.1.3.8. Carbon Dioxide (CO<sub>2</sub>)

The emission factor  $EF_{CO_2}$  [ $\text{g} \cdot \text{kWh}^{-1}$ ] was determined with Eq. (A.15).

$$EF_{CO_2} = a \cdot SFOC \quad (\text{A.15})$$

$SFOC$  is the specific fuel oil consumption in  $[g \cdot kWh^{-1}]$ . The factor  $a$  is given in Table A.8 for residual (RF) and distillate fuel (DF).

Table A.8.: Parameter  $a$  to determine the  $CO_2$  emission factor for different fuel types.

	<b>RF</b>	<b>DF</b>	<b>LNG</b>
$a$	3.114	3.206	2.750

#### A.1.3.9. Carbon Monoxide (CO)

The emission factor  $EF_{CO}$   $[g \cdot kWh^{-1}]$  is originally described in the 3rd IMO GHGS 2014. The base emission factor  $EF_{CO,base}$  is shown in Table A.9 for different engine types.

Table A.9.: Base emission factor ( $EF_{CO,base}$ ) for different engine or fuel types.

	<b>Diesel Engines</b>	<b>Gas Turbine</b>	<b>Steam Turbine</b>	<b>LNG</b>
$EF_{CO,base}$	0.54	0.1	0.2	1.3

It is modified for small engine loads  $EL$ , below 20%, according to Eq. (A.16).

$$EF_{CO} = 0.84 \cdot EF_{CO,base}^{-1} + 0.15 \quad (A.16)$$

#### A.1.3.10. Methane (CH<sub>4</sub>)

The emission factor  $EF_{CH_4}$   $[g \cdot kWh^{-1}]$  is from the 3rd IMO GHGS 2014 is shown in Table A.10. It is given for differently rated diesel engines, gas or steam turbines and LNG-driven engines.

Table A.10.: Methane emission factors ( $EF_{CH_4}$ ) for different engines or fuel types.

<b>RPM <math>\leq</math> 300</b>	<b>RPM <math>&gt;</math> 300</b>	<b>Gas/Seam Turbine</b>	<b>LNG</b>
0.012	0.01	0.0023	8.5

#### A.1.3.11. Non-Methane Organic Volatile Compounds (NMVOCs)

The emission factor  $EF_{NMVOCb}$   $[g \cdot kWh^{-1}]$  originates from EMEP/EEA (2019) and is shown in Table A.11 for differently rated diesel engines, gas and steam turbines and auxiliary engines.



Table A.11.: NMVOC emission factors ( $EF_{NMVOCb}$ ) for different engine type and engine load (EL).

	RPM < 300	RPM ≥ 300	RPM ≥ 900	Gas Turbines	Steam Turbines	Aux. Engine
EL > 0.2	0.6	0.5	0.2	0.1	0.1	0.4
EL ≤ 0.2	1.8	1.5	0.6	0.5	0.3	0.4

### A.1.3.12. Dinitrogen Oxide ( $N_2O$ )

The emission factor  $EF_{N_2O}$  [ $g \cdot kWh^{-1}$ ] is originally from the 3rd IMO GHGS 2014. It is shown in Table A.12 for differently rated diesel engines, gas or steam turbines and LNG-driven engines.

Table A.12.: Dinitrogen oxide emission factors ( $EF_{N_2O}$ ) for different engine or fuel types.

	RPM ≤ 300	RPM > 300	Gas/Seam Turbine	LNG
EF Main Engine	0.031	0.034	0.049	0.018
EF Aux. Engine	—	0.0363	—	0.018

### A.1.3.13. Total Particulate Matter ( $PM_{tot}$ )

The emission factor  $EF_{PMb}$  [ $g \cdot kWh^{-1}$ ] is originally from (EMEP/EEA, 2019). It is shown in Table A.13 for residual (RF) and distillate fuel-driven (DF), differently-rated diesel main engines and steam and gas turbines. Emission factors for auxiliary engines are 0.8 and 0.3 for residual and distillate fuels, respectively.

Table A.13.: Particulate matter emission factors ( $EF_{PMb}$ ) for different engine type, fuel types, and engine loads (EL).

	RF		Gas/Steam Turbine	DF	
	RPM < 300	RPM ≥ 300		Diesel Engine	Gas Turbine
EL > 0.2	1.7	0.8	0.1	0.3	0
EL ≤ 0.2	2.4	2.4	1.5	0.9	0.9

### A.1.3.14. Correction Factor for the Fuel Sulfur Dependency of PM

$$EF_{PM}(FSC) = EF_{base} \cdot (0.52 \cdot FSC^{0.67}) \quad (A.17)$$

### A.1.4. Ship Energy Consumption at Berth

The fuel consumption and resulting emissions of ships at berth is, for the most part, difficult to model. This is due to scarce data availability of auxiliary engine usage and fuel consumption. Therefore, a model has been implemented that relies on the few studies conducted. Eq. A.18 is approximately the energy consumption rate of berthing ships  $E_{berth}$ , needed for the emission calculation, is dependent on the fuel consumption rate  $FCR_{berth}$ , energy density of the used fuel  $ED_{fuel}$ , fractional engine usage  $FU$  and efficiency  $\eta$ . The sum on the right side of the equation is the product of the main engine  $m$ , power generator  $p$  and boiler  $b$  fractional usage and efficiency, respectively.

$$E_{berth} = FCR_{berth} \cdot ED_{fuel} \cdot \sum_{i=m,p,b} (FU_i \cdot \eta_i) \quad (A.18)$$

## A. Appendix

It was distinguished between the two most important fuel types: RF and DF. The energy densities used were measured by Bengtsson et al. (2011) and are  $11.22 \text{ kW} \cdot \text{h} \cdot \text{kg}^{-1}$  and  $11.94 \text{ kW} \cdot \text{h} \cdot \text{kg}^{-1}$ , respectively. The a fuel consumption rate is available as a function, dependent on the gross tonnage, for the five ship types: “Bulk”, “Cargo”, “Passenger” and “Tanker” by Hulskotte and Denier van der Gon (2010) and “Cruise” by Simonsen et al. (2018). The other six ship types “Fishing”, “Pleasurecraft”, “Military”, “Tug” and “Undefined” were aggregated in the type “Other” due to the poor data condition. The basic fit function for the types “Bulk”, “Cargo”, “Passenger”, and “Tanker” is as follows,

$$FCR(GT) = a \cdot GT. \quad (\text{A.19})$$

The factor  $a$  for the different ship types is given in the table below. The functions to derive the fuel consumption rate for cruise ships between 25,000 and 70,000 gross tons is,

$$FCR(GT) = e^{-0.88+(0.71\ln(GT))}, \quad (\text{A.20})$$

and for cruise ships larger than 70,000,

$$FCR(GT) = e^{-13.141+(1.217\ln(GT))}. \quad (\text{A.21})$$

The main engine  $FU_m$ , power generator  $FU_p$  and boiler  $FU_b$  fractional usage for the different ship types used is from a survey of Hulskotte and Denier van der Gon (2010) and shown in Table A.14.

Table A.14.: Parameter  $a$  for the fuel consumption rate ( $FCR$ ) and fractional usage for the main engine, power generator, and boiler of a ship, for different ship types.

Ship Type	$a$	$FU_m$	$FU_p$	$FU_b$
Bulk	0.003	0	0.63	0.37
Cargo	0.005	0	0.45	0.55
Cruise	—	0.24	0.75	0.01
Passenger	0.007	0.18	0.5	0.32
Tanker < 30,000 GT	0.016	0.12	0.15	0.73
Tanker $\geq$ 30,000 GT	0.02	0.18	0.19	0.63
Other	0.012	0.24	0.75	0.01

The efficiency for different main engine types is taken from ABS Ship Energy and Efficiency Measures 2014 and is usually between 0.44 and 0.54 (ABS, 2014). A power generator and boiler efficiency value of 0.53 and 0.36, respectively, was used (Baldi et al., 2015).

### A.1.5. AIS Navigational Status Values

Navigational status values of vessels and their respective codes as usually transmitted in AIS signal data. The value is manually set by the crew.

- 0 = under way using engine
- 1 = at anchor
- 2 = not under command
- 3 = restricted maneuverability
- 4 = constrained by her draught
- 5 = moored
- 6 = aground
- 7 = engaged in fishing
- 8 = under way sailing
- 9 = reserved for future amendment of navigational status for ships carrying DG, HS, or MP, or IMO hazard or pollutant category C, high-speed craft (HSC)

- 10 = reserved for future amendment of navigational status for ships carrying dangerous goods (DG), harmful substances (HS) or marine pollutants (MP), or IMO hazard or pollutant category A, wing in ground (WIG)
- 11 = power-driven vessel towing astern (regional use)
- 12 = power-driven vessel pushing ahead or towing alongside (regional use)
- 13 = reserved for future use
- 14 = AIS-SART (active), MOB-AIS, EPIRB-AIS
- 15 = undefined = default (also used by AIS-SART, MOB-AIS and EPIRB-AIS under test)

### A.1.6. Engine Applications

The engine applications according to ISO 8178 emission test-bed cycles subdivide marine engines (IMO MEPC, 2008a).

- E2 *constant-speed main propulsion*
- E3 *propeller-law-operated main and auxiliary engine*
- D2 *constant-speed auxiliary engine*
- C1 *variable speed and load auxiliary engines*

### A.1.7. Total Monthly Ship Emissions in the North and Baltic Sea Domain

Table A.15.: Modeled monthly emissions in Gg/month for the North/Baltic Sea Domain 2015.

Month	SO <sub>2</sub>	SO <sub>4</sub>	SO <sub>4,H<sub>2</sub>O</sub>	NO <sub>X</sub>	BC	POA	MA	CO <sub>2</sub>	CO	CH <sub>4</sub>	NMVOC	N <sub>2</sub> O	PM <sub>tot</sub>
Jan.	2.24	0.05	0.04	66.05	1.10	1.35	0.02	3343.02	2.81	0.59	0.91	0.18	0.91
Feb.	2.15	0.05	0.04	64.02	1.01	1.29	0.02	3222.65	2.74	0.58	0.82	0.17	0.82
Mar.	2.49	0.06	0.05	73.45	1.15	1.47	0.03	3689.14	3.14	0.68	0.93	0.19	0.94
Apr.	2.56	0.06	0.05	74.63	1.15	1.48	0.03	3733.81	3.18	0.64	0.92	0.20	0.93
May	2.87	0.07	0.05	80.74	1.22	1.60	0.03	4008.28	3.44	0.66	0.96	0.21	0.97
Jun.	2.78	0.07	0.05	79.76	1.19	1.58	0.03	3948.29	3.39	0.66	0.94	0.21	0.95
Jul.	2.94	0.07	0.06	82.98	1.24	1.65	0.03	4105.22	3.53	0.69	0.98	0.22	1.00
Aug.	2.84	0.07	0.05	81.19	1.23	1.61	0.03	4009.11	3.45	0.72	0.98	0.21	0.99
Sep.	2.86	0.07	0.05	77.19	1.18	1.54	0.03	3843.57	3.29	0.71	0.94	0.20	0.95
Oct.	2.56	0.06	0.05	75.26	1.15	1.50	0.03	3766.97	3.20	0.59	0.91	0.20	0.92
Nov.	2.56	0.06	0.05	72.27	1.14	1.46	0.03	3645.94	3.10	0.64	0.92	0.19	0.91
Dec.	2.34	0.05	0.04	70.43	1.13	1.43	0.02	3570.43	3.02	0.60	0.92	0.19	0.91

### A.1.8. List of Implemented Harbors

#### A.1.8.1. North Sea

**Germany:** Brake, Bremen, Bremerhaven, Cuxhaven, Emden, Hamburg, Leer, Papenburg, Wilhelmshaven

**France:** Binic, Dieppe, Dunkirk, Le Havre, Portrieux, Saint Brieuc

**United Kingdom** Aberdeen, Arbroath, Brighton, Bristol, Clacton On Sea, Dover, Felixstowe Harwich, Fishbourne, Gillingham, Goole, Grangemouth, Grimsby, Immingham, Inverness, Kingston Upon Hull, Kirkwall, Leith, Lerwick, Liverpool, London, Lowestoft, Newcastle Upon Tyne, North Berwick, Peterhead, Portsmouth, Plymouth, Red Sands Fort, Ryde, Sheerness, Shoreham By Sea, Southampton, Sunderland, Teesport, Whitstable

**Belgium:** Antwerp, Bruges, Ghent, Ostend

**Denmark:** Aalborg, Esbjerg, Hanstholm, Hirtshals, Hvide Sande, Lemvig, Skive, Thiste, Thorsminde, Thyboron

**Netherlands:** Amsterdam, Delfzijl, Den Helder, Dordrecht, Eemshaven, Groningen, Ijmuiden, Rotterdam, Scheveningen, Terneuzen, Utrecht, Vlissingen

## A. Appendix

**Norway:** Alesund, Bergen, Brevik, Haugesund, Jelsa, Kragero, Kristiansund, Lavik, Moss, Oslo, Porsgrunn, Sandnes, Sauda, Stavanger, Trondheim, Vadheim, Ytre Oppedal

**Miscellaneous:** English Channel

### A.1.8.2. Baltic Sea

**Denmark:** Aarhus, Copenhagen

**Sweden:** Bohus Malmoen, Helsingborg, Goeteborg, Kungshamn, Lulea, Lysekil, Malmo, Norrkoping, Oernskoeldsvik, Oxelosund, Stockholm, Sundsvall, Trelleborg, Uddevalla, Visby, Ystad

**Poland:** Gdansk, Gdynia, Police, Stettin

**Finland:** Hamina, Helsinki, Kokkola, Kotka, Loviisa, Oulu, Pori, Porvoo, Rauma, Turku

**Russia:** Kaliningrad, Primorsk, Saint Petersburg, Sosnowy Bor, Ustluga, Visotsk

**Germany:** Kiel, Luebeck, Rostock, Wismar

**Estland:** Muuga, Paldiski, Tallin, Sillamaee

**Lithuania:** Klaipedia

**Latvia:** Liepaja, Riga, Ventspils

## A.2. Appendix for Publication III

### A.2.1. Mapping for MEIC to SNAP Sectors and EDGAR Activity Codes

The mapping of sectors present in the MEIC emission inventory for China to SNAP sectors and EDGAR activity codes is shown in Table A.16. The mapping to SNAP sectors was used to apply the vertical emission profile developed by TNO to the MEIC inventory. The mapping to EDGAR activity codes was used to apply the country and sector specific high resolution temporal profiles developed by Crippa et al. (2020) to the MEIC inventory and generate hourly resolved emission data.

Table A.16.: Mapping of MEIC emission inventory sectors to SNAP sectors and EDGAR Activity Codes.

MEIC sector	SNAP sector	EDGAR activity codes
Agriculture	L_AgriOther	AGS (agricultural soils), AWB (agricultural waste burning), ENF (enteric fermentation), MNM (manure management)
Industry	B_Industry	CHE (production of chemicals), FOO (production of foods), IND (manufacturing industry), IRO (production of iron and steel), NFE (production of non-ferrous metals), NMM (production of non-metallic minerals), PAP (production of pulp and paper), PRO (fuel production/transmission), PRU (production, use of products), REF (oil refineries), SOL (application of solvents), SWD (solid waste disposal), TRF (transformation industry)
Power	A_PublicPower	ENE (power industry)
Residential	C_OtherStationaryComb	RCO (residential)
Transportation	F_RoadTransport	TNR (non-road transportation), TRO (road transportation)

### A.2.2. Model Performance Data

Following, the comparison data of the modeled “base” case, that includes all emission sources, and the “no ships” case, that omits ships, with measurements is shown in Tables A.17 to A.24. For each pollutant and station the geometric mean, the normalized mean bias (NMB) and the Spearman correlation coefficient was calculated. Furthermore, the number of available hourly measurements is shown.

Table A.17.: Comparison of modeled NO<sub>2</sub> concentrations in  $\mu\text{g} \cdot \text{m}^{-3}$  with measurements in Europe.

Station	Mean <sub>base</sub>	NMB <sub>base</sub>	Corr. <sub>base</sub>	Mean <sub>noships</sub>	NMB <sub>noships</sub>	Corr. <sub>noships</sub>	Mean <sub>meas</sub>	No. samples
Dublin	3.05	-0.38	0.62	2.70	-0.47	0.63	4.94	8618
Blackpool	2.47	-0.63	0.69	1.83	-0.67	0.70	11.46	8343
Narberth	1.60	-0.14	0.53	1.10	-0.35	0.54	1.63	8572
Plymouth	2.27	-0.81	0.58	1.00	-0.90	0.60	13.53	8650
Brighton	4.77	-0.53	0.67	2.71	-0.67	0.63	10.72	8619
Lullington Heath	4.44	-0.09	0.66	1.91	-0.44	0.60	4.79	5834
Newcastle	6.06	-0.69	0.59	4.39	-0.76	0.61	25.56	8341
Houtem	7.19	-0.01	0.64	4.36	-0.35	0.63	7.12	8186
Gent	13.51	-0.29	0.63	7.05	-0.61	0.66	23.40	8022
Schoten	17.79	-0.05	0.63	10.18	-0.43	0.65	21.26	8388
Den Haag	17.91	-0.03	0.70	8.47	-0.51	0.66	22.20	8653
De Zilk	12.99	0.40	0.70	7.02	-0.19	0.66	9.83	8565
Wieringerwerf	5.30	-0.27	0.78	2.35	-0.62	0.75	8.55	8714
Ostfr. Inseln	3.43	-0.39	0.75	1.01	-0.68	0.75	6.39	8347
Elbmündung	5.33	-0.37	0.64	1.70	-0.72	0.62	9.56	8415
Hamburg	12.12	-0.45	0.51	5.49	-0.73	0.50	26.39	8727
Westerland	1.34	-0.55	0.79	0.51	-0.77	0.77	2.17	8287
Ulborg	1.54	-0.43	0.69	0.86	-0.62	0.66	2.77	7691
Århus	3.23	-0.67	0.61	1.61	-0.83	0.50	9.61	7962
Copenhagen	7.13	-0.36	0.51	4.71	-0.53	0.46	12.32	7965
Zingst	2.95	-0.19	0.71	1.04	-0.60	0.60	3.73	8216
Gdańsk Nowy Port	5.80	-0.41	0.58	3.21	-0.63	0.63	10.44	8353
Vilsandi	0.98	-0.42	0.62	0.35	-0.73	0.38	1.37	8444
Utö	1.16	-0.47	0.59	0.26	-0.85	0.33	2.25	8633
Öismäe	3.65	-0.42	0.52	1.23	-0.78	0.57	5.13	8603
Helsinki Kallio	5.90	-0.48	0.45	4.35	-0.60	0.41	14.01	8725
Lahemaa	1.33	-0.18	0.49	0.80	-0.46	0.45	1.61	8644
Virolahti	1.56	-0.36	0.53	0.88	-0.62	0.38	2.74	8601
Pyykösjärvi	3.00	-0.55	0.48	2.91	-0.55	0.47	6.61	8728

Table A.18.: Comparison of modeled SO<sub>2</sub> concentrations in  $\mu\text{g} \cdot \text{m}^{-3}$  with measurements in Europe.

Station	Mean <sub>base</sub>	NMB <sub>base</sub>	Corr. <sub>base</sub>	Mean <sub>noships</sub>	NMB <sub>noships</sub>	Corr. <sub>noships</sub>	Mean <sub>meas</sub>	No. samples
Narberth	0.37	0.04	-0.05	0.19	-0.12	-0.01	0.68	8367
Lullington Heath	0.28	-0.40	0.08	0.18	-0.46	0.08	0.95	8266
Houtem	1.19	1.20	0.19	1.08	1.13	0.19	1.07	8408
Gent	0.94	0.64	0.37	0.73	0.51	0.37	1.23	8335
De Zilk	0.73	0.22	0.32	0.54	0.10	0.32	0.95	7298
Ostfr. Inseln	0.14	0.12	0.35	0.08	0.03	0.35	0.40	6422
Hamburg	1.07	-0.50	0.29	0.83	-0.55	0.30	3.28	8727
Westerland	0.09	0.71	0.09	0.05	0.58	0.08	0.26	8315
Zingst	0.21	0.36	0.55	0.14	0.29	0.54	0.39	7830
Gdańsk Nowy Port	1.67	-0.04	0.44	1.59	-0.06	0.44	2.17	8690
Vilsandi	0.11	-0.03	0.37	0.07	-0.08	0.38	0.27	6862
Utö	0.10	-0.32	0.49	0.05	-0.38	0.51	0.30	8707
Öismäe	0.39	0.03	0.27	0.32	-0.05	0.26	0.47	7818
Helsinki Kallio	1.00	0.11	0.16	0.95	0.08	0.16	0.61	7491
Lahemaa	0.23	-0.31	0.15	0.19	-0.33	0.15	0.53	8079
Virolahti	0.26	0.24	0.41	0.23	0.19	0.41	0.21	8590

Table A.19.: Comparison of modeled O<sub>3</sub> 8-hour mean concentrations in  $\mu\text{g} \cdot \text{m}^{-3}$  with measurements in Europe.

Station	Mean <sub>base</sub>	NMB <sub>base</sub>	Corr. <sub>base</sub>	Mean <sub>noships</sub>	NMB <sub>noships</sub>	Corr. <sub>noships</sub>	Mean <sub>meas</sub>	No. samples
Blackpool	68.55	0.29	0.71	67.43	0.27	0.71	49.39	8662
Narberth	75.12	0.21	0.54	73.81	0.19	0.56	61.09	8647
Plymouth	76.77	0.54	0.57	75.80	0.52	0.55	45.59	8621
Brighton	72.40	0.31	0.66	72.39	0.31	0.60	51.52	8653
Lullington Heath	73.98	0.34	0.61	74.31	0.34	0.55	53.61	8603
Newcastle	66.52	0.63	0.68	67.14	0.64	0.64	36.56	8411
Phare d'Ailly	76.09	0.23	0.61	74.70	0.21	0.62	59.62	8700
Houtem	64.51	0.28	0.75	67.08	0.31	0.72	47.15	7829
Gent	50.48	0.42	0.72	61.01	0.55	0.71	32.78	7683
Schoten	45.04	0.36	0.78	56.81	0.52	0.78	29.50	8328
Den Haag	39.51	0.22	0.82	57.67	0.45	0.75	33.29	8657
De Zilk	48.49	0.12	0.80	59.38	0.23	0.73	42.27	8615
Wieringerwerf	68.96	0.42	0.68	72.78	0.46	0.57	44.15	8504
Ostfr. Inseln	72.08	0.20	0.70	72.72	0.20	0.60	55.72	8570
Elbmündung	67.33	0.28	0.72	69.55	0.30	0.65	47.54	8725
Westerland	77.55	0.18	0.64	76.30	0.15	0.52	61.91	8561
Ulborg	73.55	0.15	0.58	71.75	0.12	0.46	61.99	7664
Århus	72.37	0.33	0.65	72.26	0.32	0.55	50.36	8323
Räö	74.34	0.16	0.68	73.69	0.15	0.59	62.74	8647
Copenhagen	66.14	0.17	0.67	67.03	0.17	0.57	53.76	7973
Zingst	72.69	0.21	0.73	72.47	0.20	0.64	57.10	8596
Vilsandi	75.61	0.14	0.59	72.72	0.09	0.45	65.64	8504
Utö	74.56	0.12	0.59	72.21	0.08	0.46	66.32	8672
Öismäe	67.60	0.27	0.62	68.15	0.27	0.52	51.05	8482
Helsinki Kallio	58.39	0.26	0.61	58.41	0.25	0.54	44.94	8744
Lahemaa	65.52	0.24	0.63	64.04	0.21	0.61	50.24	8735
Virolahti	67.24	0.33	0.53	66.20	0.31	0.50	47.51	8622
Pyykösjärvi	51.92	0.16	0.61	51.19	0.14	0.61	43.39	8744

Table A.20.: Comparison of modeled PM<sub>2.5</sub> concentrations in  $\mu\text{g} \cdot \text{m}^{-3}$  with measurements in Europe.

Station	Mean <sub>base</sub>	NMB <sub>base</sub>	Corr <sub>base</sub>	Mean <sub>noships</sub>	NMB <sub>noships</sub>	Corr <sub>noships</sub>	Mean <sub>meas</sub>	No. samples
Blackpool	8.17	0.32	0.36	7.74	0.26	0.34	5.78	7508
Plymouth	8.52	0.01	0.29	7.79	-0.07	0.25	9.33	6502
Newcastle	7.96	0.03	0.32	7.58	-0.02	0.29	7.80	5540
Houtem	9.65	0.19	0.46	8.66	0.09	0.43	8.12	8632
Gent	10.57	-0.04	0.50	10.57	-0.04	0.50	11.15	8575
Schoten	10.87	-0.02	0.53	9.93	-0.09	0.53	10.79	8701
De Zilk	9.73	0.24	0.45	8.70	0.13	0.44	6.61	7868
Wieringerwerf	8.93	0.25	0.44	7.94	0.13	0.40	6.04	8140
Utö	4.00	0.11	0.28	3.71	0.04	0.28	3.45	8197
Helsinki Kallio	4.84	0.20	0.29	4.55	0.13	0.29	4.22	8366
Virolahti	3.87	0.13	0.21	3.66	0.08	0.20	4.19	8595

Table A.21.: Comparison of modeled NO<sub>2</sub> concentrations in  $\mu\text{g} \cdot \text{m}^{-3}$  with measurements in China.

Station	Mean <sub>base</sub>	NMB <sub>base</sub>	Corr <sub>base</sub>	Mean <sub>noships</sub>	NMB <sub>noships</sub>	Corr <sub>noships</sub>	Mean <sub>meas</sub>	No. samples
Dalian	53.68	1.03	0.33	45.60	0.68	0.42	29.53	8576
Huludao	16.78	-0.38	0.64	16.37	-0.40	0.64	29.73	8576
Qinhuangdao	29.04	-0.14	0.60	26.27	-0.22	0.62	38.01	8577
Tianjin	56.95	0.59	0.64	56.19	0.58	0.64	33.53	8575
Lianyungang	15.05	-0.14	0.66	13.95	-0.18	0.65	24.31	8576
Yancheng	18.57	0.17	0.61	17.30	0.10	0.60	19.60	8576
Nantong	36.79	0.35	0.60	31.98	0.13	0.60	30.45	8575
Shanghai	59.11	0.54	0.53	49.11	0.30	0.60	39.27	8576
Ningbo	44.97	0.34	0.57	36.53	0.11	0.58	37.27	8576
Wenzhou	30.72	-0.05	0.37	28.74	-0.11	0.37	38.75	8576
Fuzhou	23.77	0.04	0.34	22.86	0.01	0.34	28.91	8575
Quanzhou	24.96	0.29	0.40	23.66	0.22	0.39	21.22	8577
Shantou	15.01	0.05	0.48	12.55	-0.09	0.50	16.98	8576
Shenzhen	47.27	0.80	0.41	42.30	0.60	0.42	30.07	8576
Guangzhou	58.01	0.60	0.49	58.01	0.60	0.49	41.38	8576
Zhongshan	20.33	0.05	0.35	15.91	-0.17	0.35	23.39	8576
Zhuhai	14.25	-0.25	0.48	7.71	-0.57	0.45	23.30	8576
Haikou	6.92	-0.37	0.35	6.18	-0.45	0.38	11.34	8576
Beihai	5.38	-0.51	0.27	4.83	-0.57	0.32	12.10	8576
Fangchenggang	5.04	-0.42	0.42	4.07	-0.52	0.43	10.45	8578

Table A.22.: Comparison of modeled SO<sub>2</sub> concentrations in  $\mu\text{g} \cdot \text{m}^{-3}$  with measurements in China.

Station	Mean <sub>base</sub>	NMB <sub>base</sub>	Corr <sub>base</sub>	Mean <sub>noships</sub>	NMB <sub>noships</sub>	Corr <sub>noships</sub>	Mean <sub>meas</sub>	No. samples
Dalian	24.74	0.16	0.19	21.76	-0.07	0.27	19.59	8576
Huludao	7.85	-0.78	0.51	7.69	-0.78	0.51	33.10	8576
Qinhuangdao	14.51	-0.45	0.61	13.28	-0.50	0.64	28.64	8577
Tianjin	29.83	0.38	0.66	29.44	0.37	0.66	19.00	8575
Lianyungang	4.75	-0.60	0.63	4.23	-0.62	0.63	22.07	8576
Yancheng	3.75	-0.48	0.55	3.21	-0.52	0.55	15.53	8576
Nantong	11.84	-0.40	0.54	9.97	-0.52	0.52	23.50	8575
Shanghai	27.09	1.08	0.50	23.16	0.77	0.52	14.70	8576
Ningbo	16.06	0.34	0.47	12.32	0.01	0.47	14.36	8576
Wenzhou	9.05	-0.24	0.22	8.15	-0.31	0.21	11.96	8576
Fuzhou	6.19	0.22	0.17	5.79	0.14	0.17	5.78	8575
Quanzhou	9.87	0.12	0.23	9.26	0.07	0.23	8.60	8577
Shantou	6.05	-0.43	0.50	5.22	-0.51	0.50	11.64	8576
Shenzhen	15.55	1.18	0.24	14.43	1.03	0.24	7.93	8576
Guangzhou	20.86	1.02	0.30	20.86	1.02	0.30	10.96	8576
Zhongshan	7.03	-0.10	0.24	5.73	-0.26	0.26	9.99	8576
Zhuhai	5.03	-0.12	0.64	3.33	-0.38	0.64	7.03	8576
Haikou	3.00	-0.31	0.41	2.75	-0.38	0.41	4.84	8576
Beihai	4.93	-0.28	0.32	4.67	-0.33	0.31	7.90	8576
Fangchenggang	4.48	0.12	0.06	4.05	0.03	0.07	4.89	8578

Table A.23.: Comparison of modeled O<sub>3</sub> 8-hour average concentrations in  $\mu\text{g} \cdot \text{m}^{-3}$  with measurements in China.

Station	Mean <sub>base</sub>	NMB <sub>base</sub>	Corr. <sub>base</sub>	Mean <sub>noships</sub>	NMB <sub>noships</sub>	Corr. <sub>noships</sub>	Mean <sub>meas</sub>	No. samples
Dalian	26.280	-0.15	0.74	32.07	-0.09	0.77	64.12	8648
Huludao	52.85	0.50	0.79	53.57	0.46	0.80	48.38	8648
Qinhuangdao	31.46	0.91	0.73	34.27	0.94	0.73	30.50	8648
Tianjin	4.32	0.36	0.81	4.43	0.35	0.81	29.99	8648
Lianyungang	57.19	0.38	0.74	58.22	0.33	0.74	60.35	8648
Yancheng	59.14	0.14	0.70	60.01	0.10	0.70	72.76	8648
Nantong	37.06	0.12	0.70	45.14	0.14	0.69	62.88	8648
Shanghai	21.57	-0.05	0.67	29.85	-0.02	0.68	60.07	8648
Ningbo	36.73	0.21	0.67	44.06	0.22	0.65	50.95	8648
Wenzhou	51.90	0.65	0.55	47.63	0.51	0.54	33.98	8647
Fuzhou	70.80	0.85	0.49	62.36	0.69	0.51	40.27	8647
Quanzhou	63.49	0.56	0.57	54.04	0.41	0.58	46.82	8647
Shantou	78.48	0.35	0.61	71.36	0.23	0.60	61.95	8648
Shenzhen	27.79	0.15	0.64	27.50	0.07	0.62	48.69	8648
Guangzhou	22.08	0.53	0.67	22.73	0.48	0.67	26.21	8648
Zhongshan	64.65	0.97	0.47	66.04	0.90	0.43	33.83	8648
Zhuhai	79.18	0.64	0.62	81.63	0.62	0.61	51.72	8648
Haikou	85.70	0.85	0.62	80.24	0.73	0.60	44.20	8648
Beihai	92.03	0.41	0.30	85.43	0.30	0.30	65.84	8648
Fangchenggang	87.99	1.21	0.46	83.27	1.08	0.45	36.73	8648

Table A.24.: Comparison of modeled PM<sub>2.5</sub> concentrations in  $\mu\text{g} \cdot \text{m}^{-3}$  with measurements in China.

Station	Mean <sub>base</sub>	NMB <sub>base</sub>	Corr. <sub>base</sub>	Mean <sub>noships</sub>	NMB <sub>noships</sub>	Corr. <sub>noships</sub>	Mean <sub>meas</sub>	No. samples
Dalian	43.42	0.17	0.56	42.24	0.14	0.57	33.98	8576
Huludao	31.79	-0.16	0.67	31.44	-0.17	0.67	40.38	8576
Qinhuangdao	38.45	0.15	0.69	37.75	0.13	0.69	30.11	8577
Tianjin	59.93	0.19	0.64	59.46	0.19	0.64	50.52	8575
Lianyungang	42.26	0.10	0.61	41.19	0.08	0.61	39.82	8576
Yancheng	41.12	0.18	0.59	39.77	0.15	0.59	35.52	8576
Nantong	42.19	-0.04	0.53	40.75	-0.06	0.52	45.28	8575
Shanghai	41.51	0.02	0.50	39.76	-0.02	0.49	41.10	8576
Ningbo	37.51	0.07	0.43	35.83	0.03	0.42	35.30	8576
Wenzhou	36.03	-0.01	0.31	34.48	-0.04	0.30	37.30	8576
Fuzhou	34.67	0.37	0.28	33.44	0.33	0.27	24.41	8575
Quanzhou	44.64	0.86	0.32	43.34	0.81	0.32	23.66	8577
Shantou	42.11	0.46	0.25	40.73	0.42	0.23	28.22	8576
Shenzhen	48.70	0.79	0.17	47.48	0.75	0.16	25.08	8576
Guangzhou	52.25	0.51	0.30	52.25	0.51	0.30	32.91	8576
Zhongshan	48.02	0.59	0.12	46.64	0.55	0.10	26.30	8576
Zhuhai	45.85	0.66	0.20	44.41	0.61	0.17	23.98	8576
Haikou	37.56	1.10	0.47	37.05	1.08	0.46	17.73	8576
Beihai	42.38	0.66	0.38	41.59	0.63	0.36	19.20	8435
Fangchenggang	41.99	0.58	0.30	41.27	0.55	0.28	24.14	8578

### A.2.3. Pollutant Concentration Patterns

The following sections contain figures of seasonally averaged, modeled pollutant concentrations in the ground layer for the SC12NSBS domain in Europe and the CNC12 domain in China in 2015. These include the “base” case, modeled with all emission sources and for ships-only, determined by the zero-out method. Furthermore, the share of shipping on total concentrations is shown. Averages were calculated for the winter months: December, January, February; the spring months: March, April, May; the summer months: June, July, August; the autumn months: September, October, November. These are shown in that order from left to right.



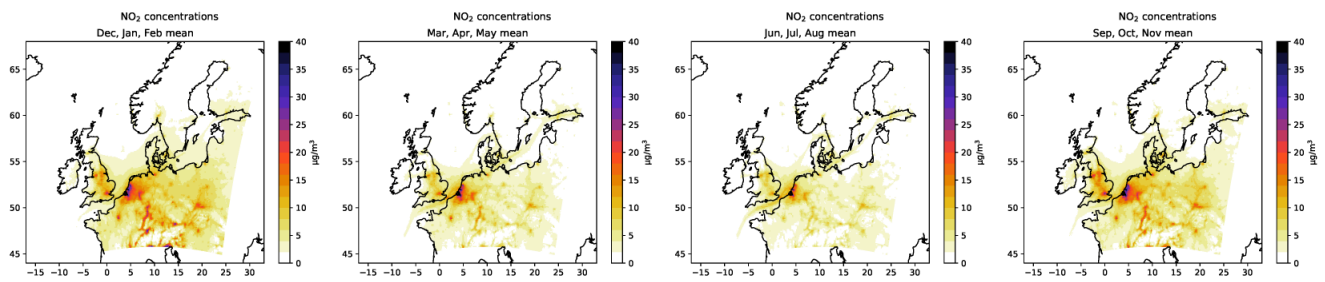
A.2.3.1. NO<sub>2</sub>

Figure A.1.: Seasonally averaged, modeled NO<sub>2</sub> concentrations in the ground layer from all emission sources in Europe.

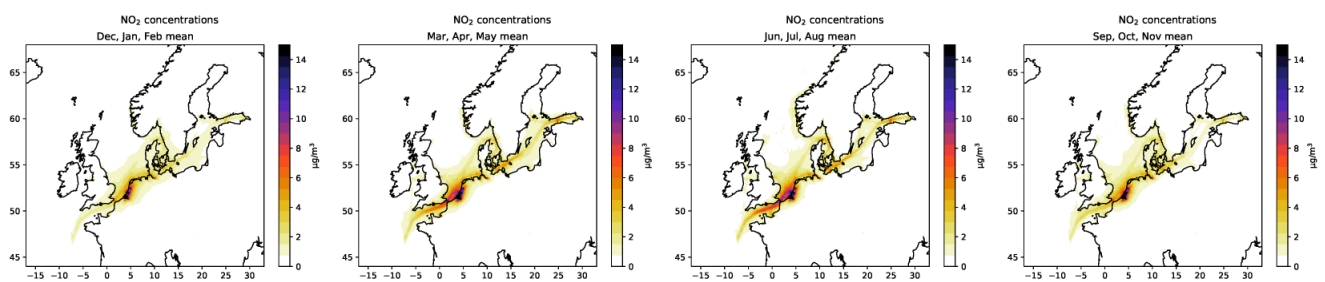


Figure A.2.: Seasonally averaged, modeled NO<sub>2</sub> concentrations in the ground layer from ships in Europe.

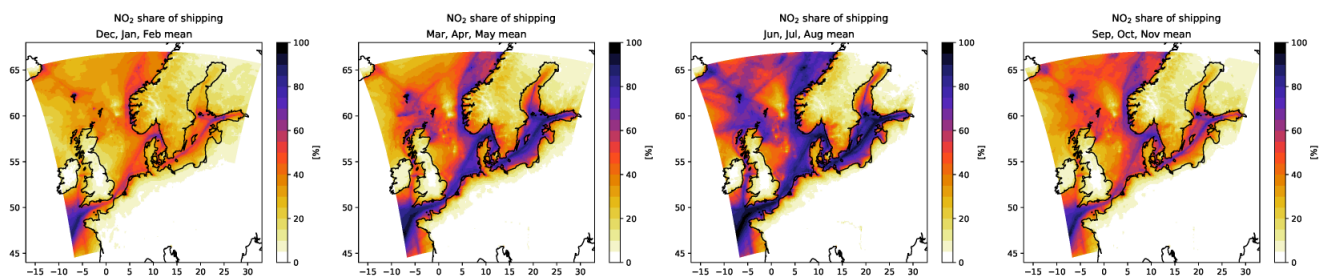


Figure A.3.: Seasonally averaged, modeled percentage share of ships on NO<sub>2</sub> concentrations in the ground layer in Europe.

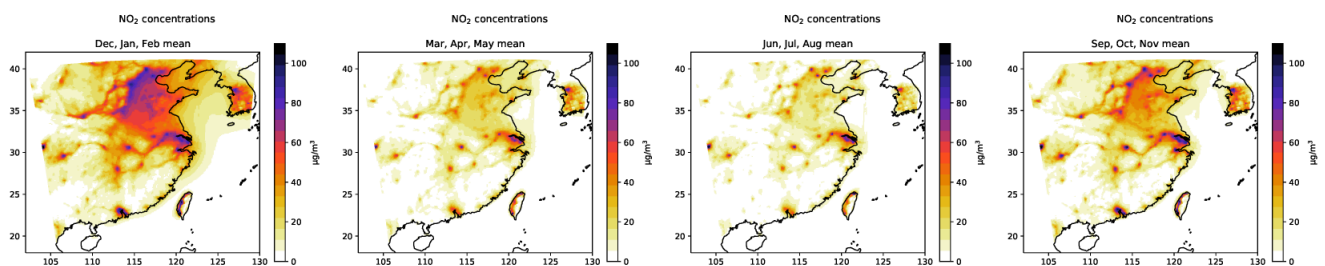


Figure A.4.: Seasonally averaged, modeled NO<sub>2</sub> concentrations in the ground layer from all sources in China.

## A. Appendix

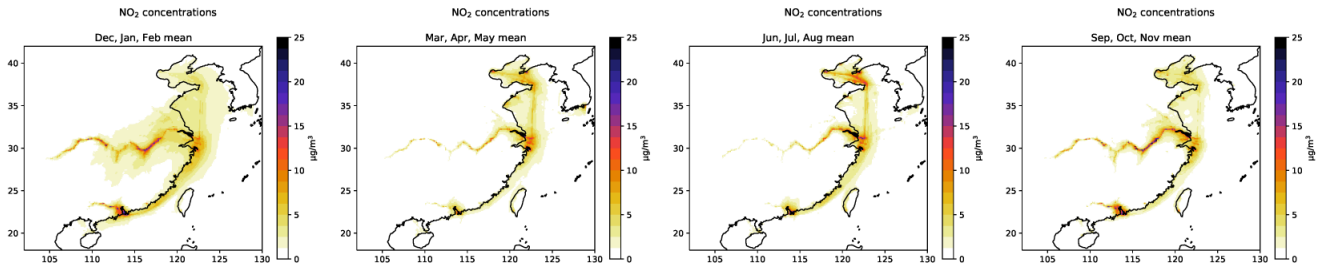


Figure A.5.: Seasonally averaged, modeled  $\text{NO}_2$  concentrations in the ground layer from ships in China.

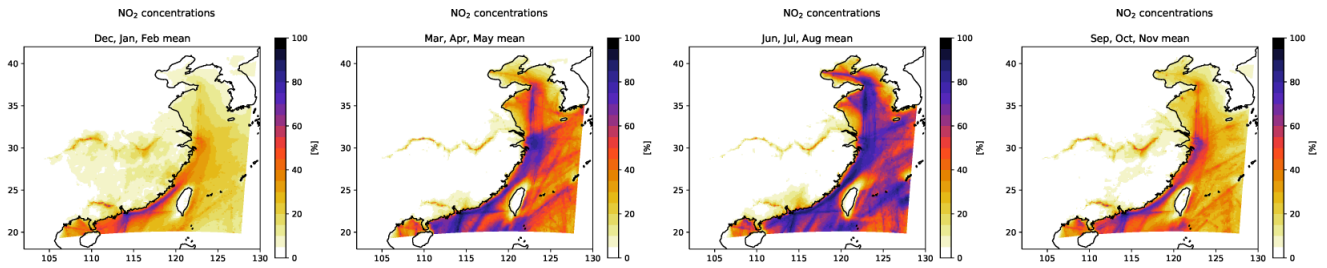


Figure A.6.: Seasonally averaged, modeled percentage share of ships on  $\text{NO}_2$  concentrations in the ground layer in China.

### A.2.3.2. $\text{SO}_2$

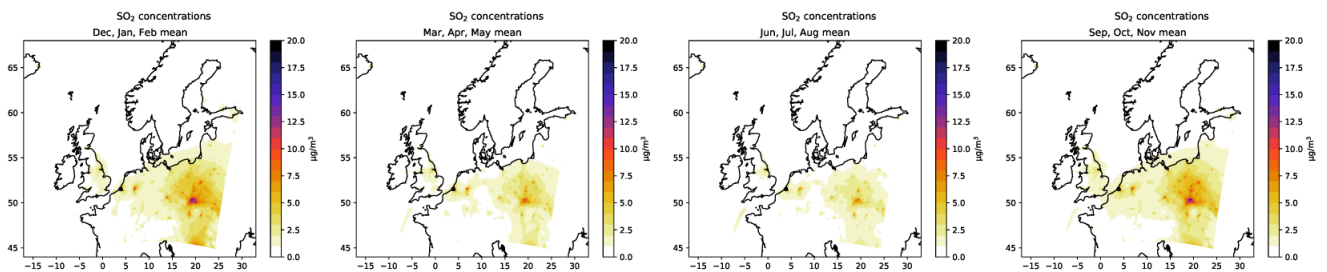


Figure A.7.: Seasonally averaged, modeled  $\text{SO}_2$  concentrations in the ground layer from all sources in Europe.

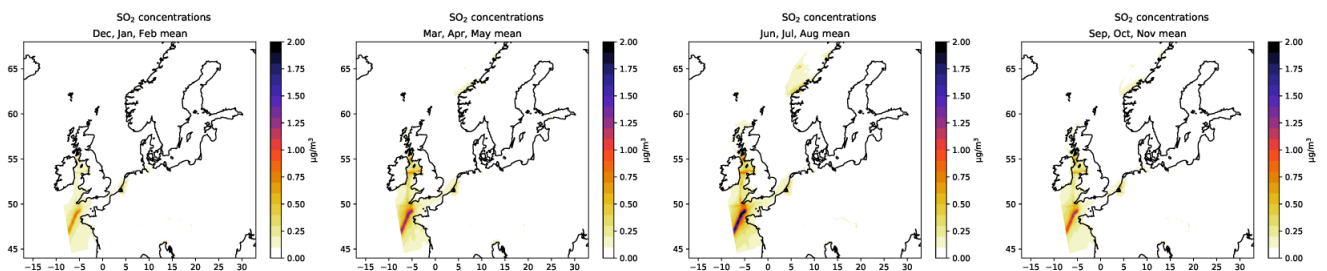


Figure A.8.: Seasonally averaged, modeled  $\text{SO}_2$  concentrations in the ground layer from ships in Europe.

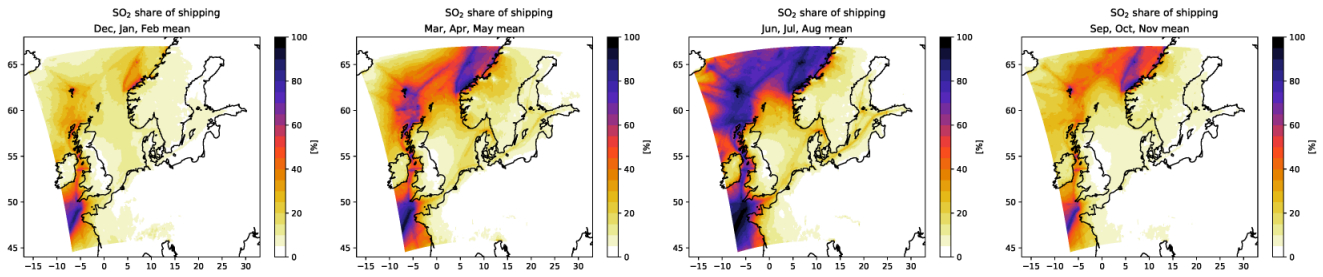


Figure A.9.: Seasonally averaged, modeled percentage share of ships on  $\text{SO}_2$  concentrations in the ground layer in Europe.

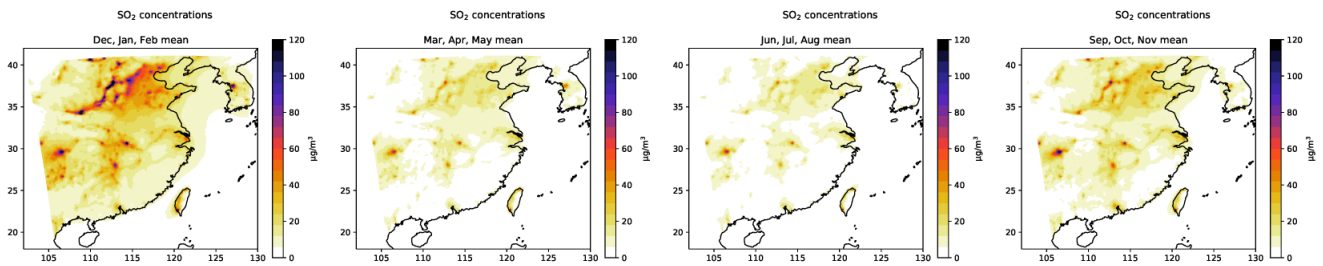


Figure A.10.: Seasonally averaged, modeled  $\text{SO}_2$  concentrations in the ground layer from all sources in China.

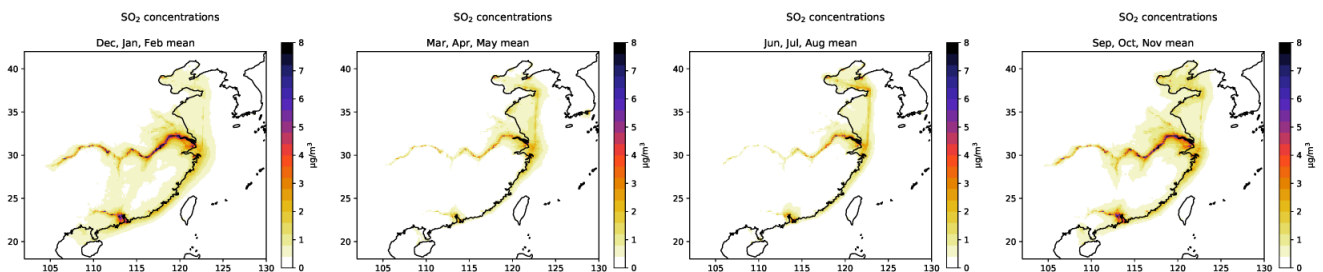


Figure A.11.: Seasonally averaged, modeled  $\text{SO}_2$  concentrations in the ground layer from ships in China.

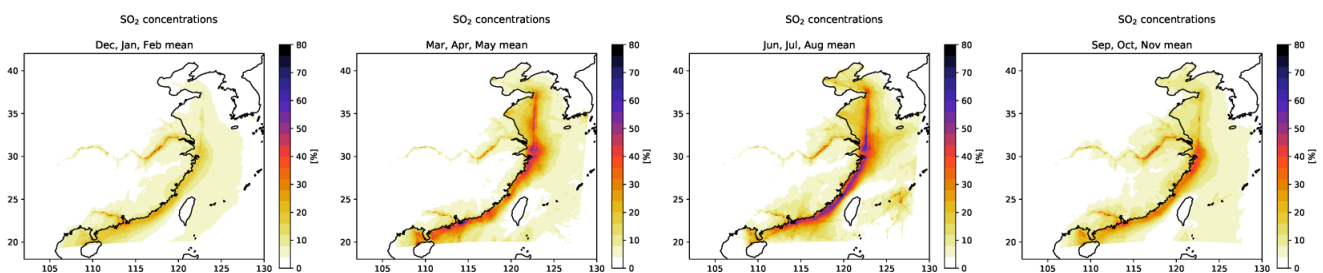


Figure A.12.: Seasonally averaged, modeled percentage share of ships on  $\text{SO}_2$  concentrations in the ground layer in China.

A.2.3.3. Ozone

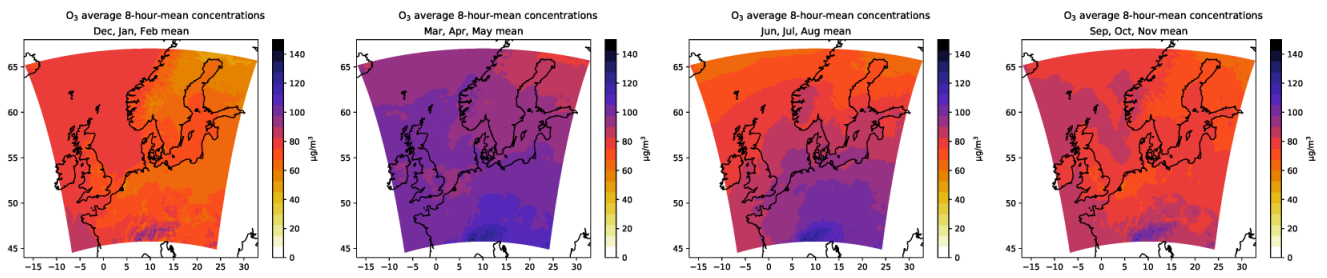


Figure A.13.: Seasonally averaged, modeled  $O_3$  concentrations in the ground layer from all sources in Europe.

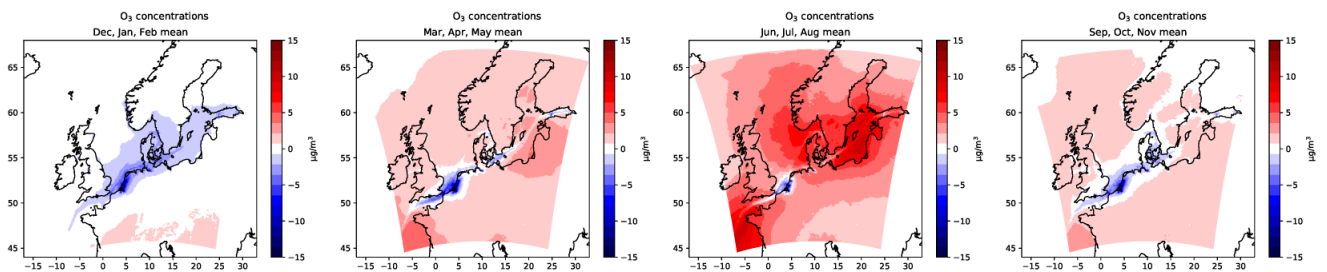


Figure A.14.: Seasonally averaged, modeled  $O_3$  concentrations in the ground layer from ships in Europe.

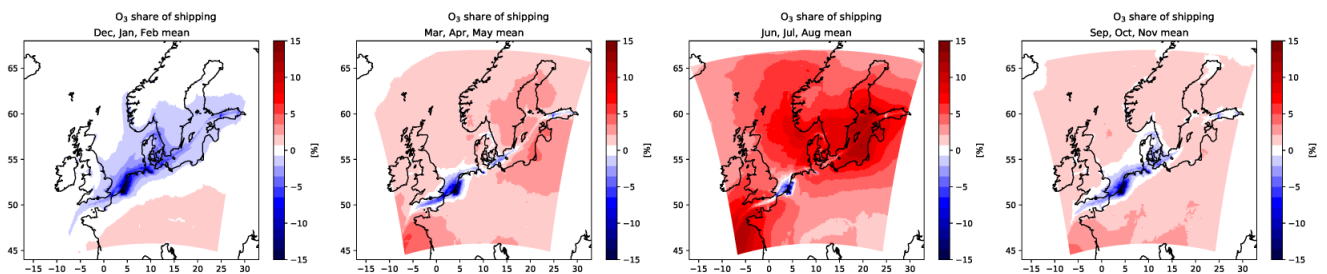


Figure A.15.: Seasonally averaged, modeled percentage share of ships on  $O_3$  concentrations in the ground layer in Europe.

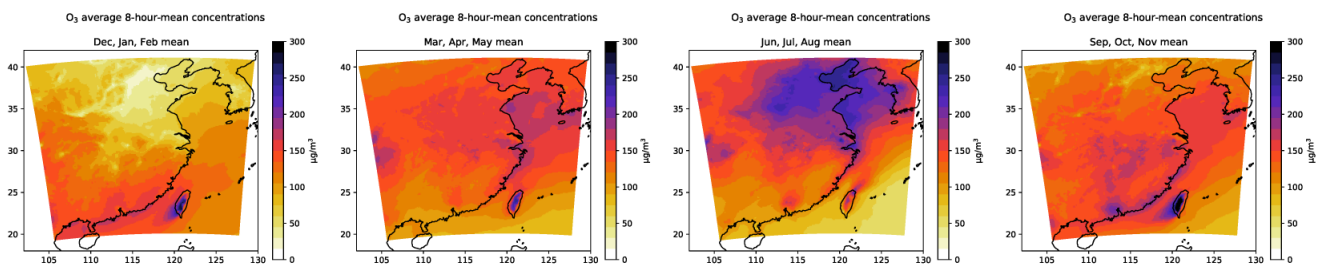


Figure A.16.: Seasonally averaged, modeled  $O_3$  concentrations in the ground layer from all sources in China.

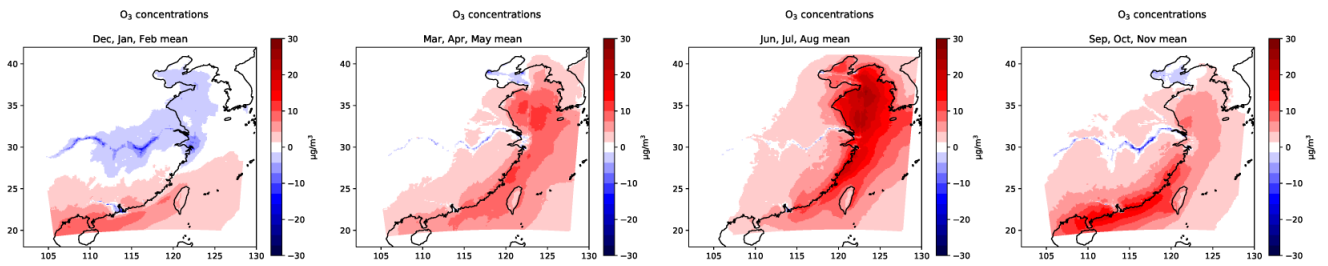


Figure A.17.: Seasonally averaged, modeled O<sub>3</sub> concentrations in the ground layer from ships in China.

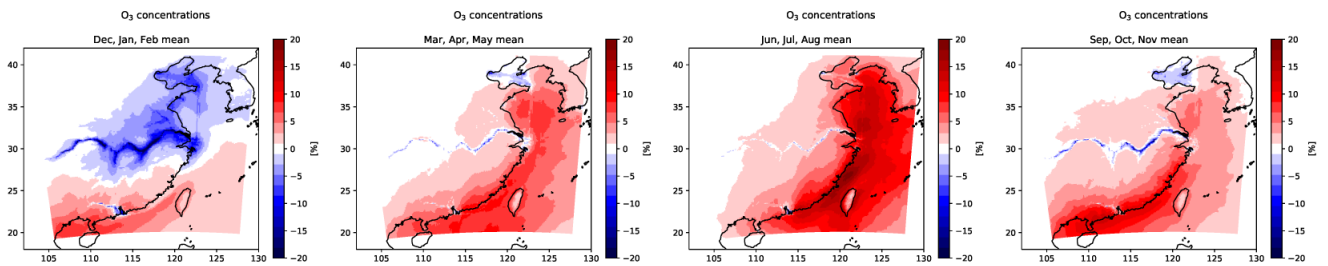


Figure A.18.: Seasonally averaged, modeled percentage share of ships on O<sub>3</sub> concentrations in the ground layer in China.

#### A.2.3.4. PM<sub>2.5</sub>

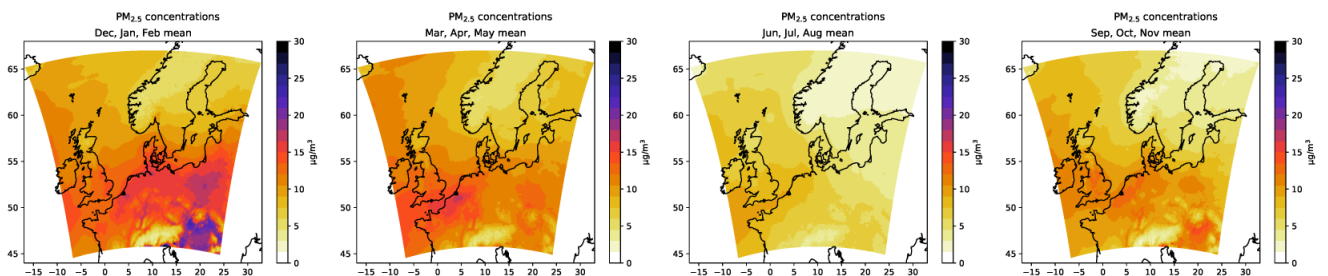


Figure A.19.: Seasonally averaged PM<sub>2.5</sub> concentrations in the ground layer from all sources in Europe.

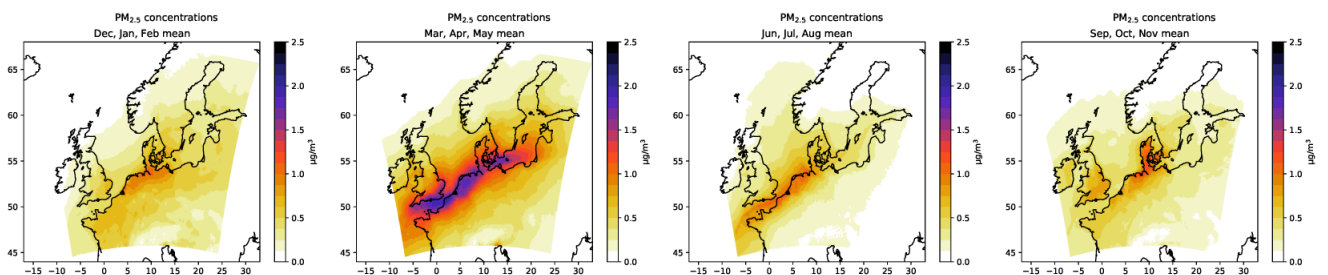


Figure A.20.: Seasonally averaged, modeled PM<sub>2.5</sub> concentrations in the ground layer from ships in Europe.

A. Appendix

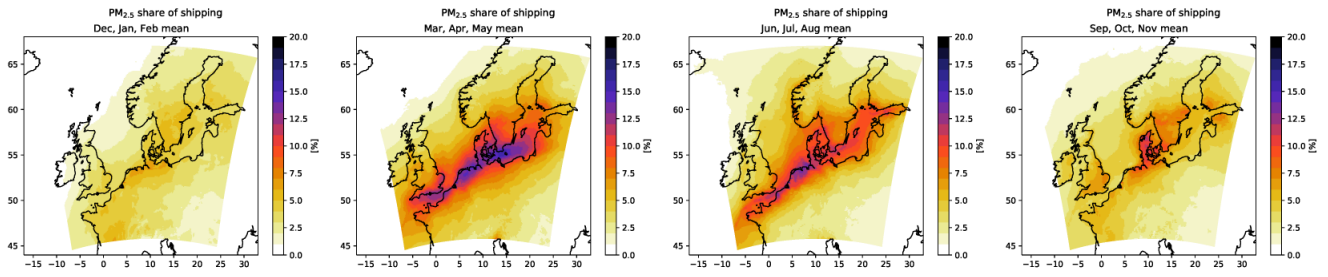


Figure A.21.: Seasonally averaged, modeled percentage share of ships on PM<sub>2.5</sub> concentrations in the ground layer in Europe.

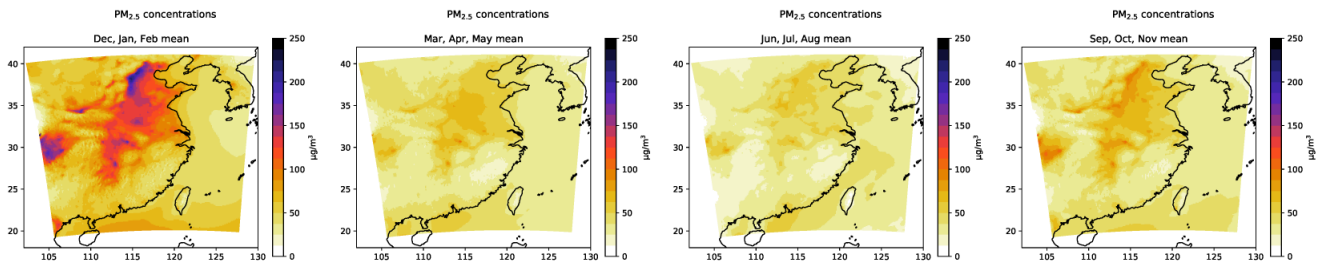


Figure A.22.: Seasonally averaged, modeled PM<sub>2.5</sub> concentrations in the ground layer from all sources in China.

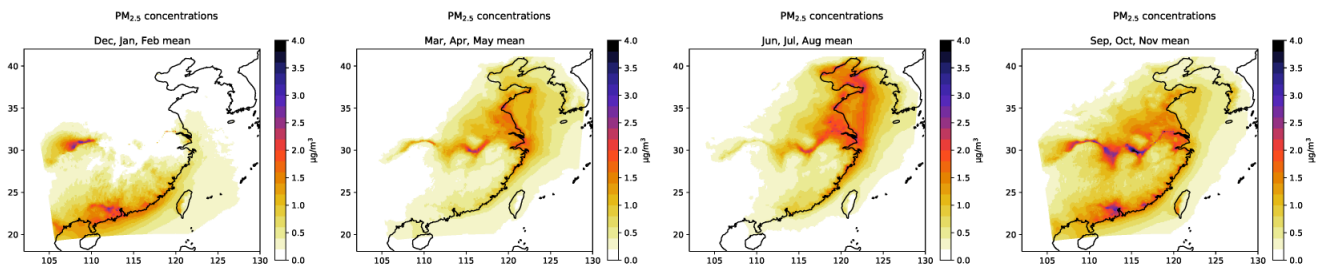


Figure A.23.: Seasonally averaged, modeled PM<sub>2.5</sub> concentrations in the ground layer from ships in China.

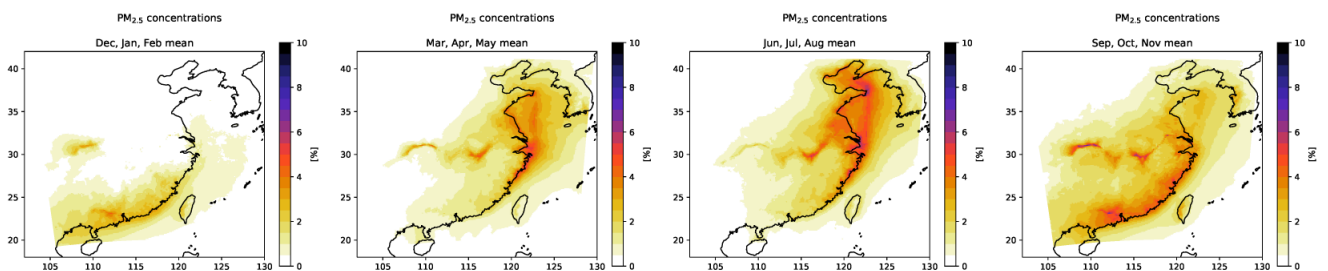


Figure A.24.: Seasonally averaged, modeled percentage share of ships on PM<sub>2.5</sub> concentrations in the ground layer in China.

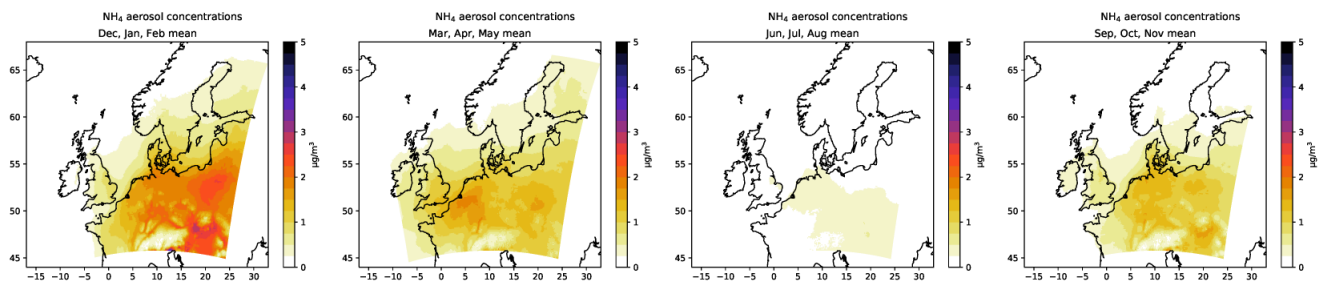
A.2.3.5.  $\text{NH}_4$ 

Figure A.25.: Seasonally averaged, modeled  $\text{NH}_4$  concentrations in the ground layer from all sources in Europe.

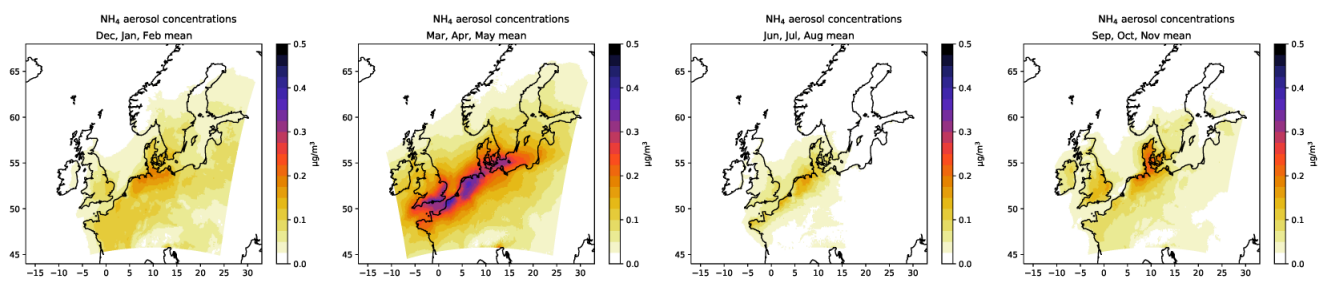


Figure A.26.: Seasonally averaged, modeled  $\text{NH}_4$  concentrations in the ground layer from ships in Europe.

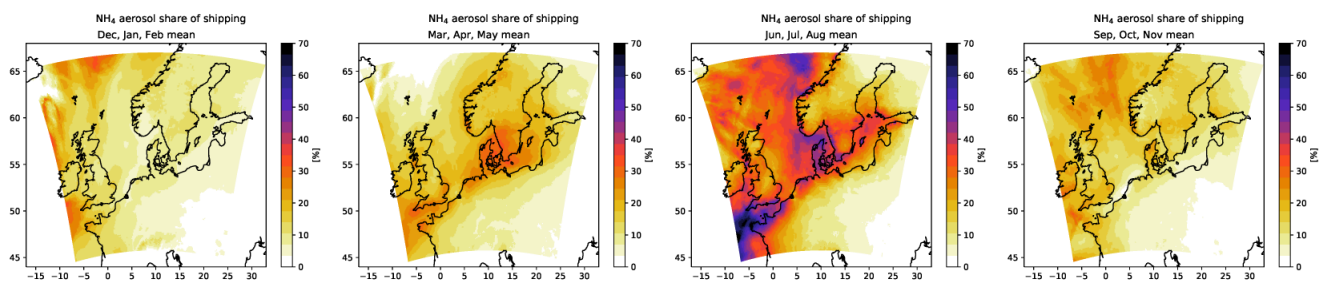


Figure A.27.: Seasonally averaged, modeled percentage share of ships on  $\text{NH}_4$  concentrations in the ground layer in Europe.

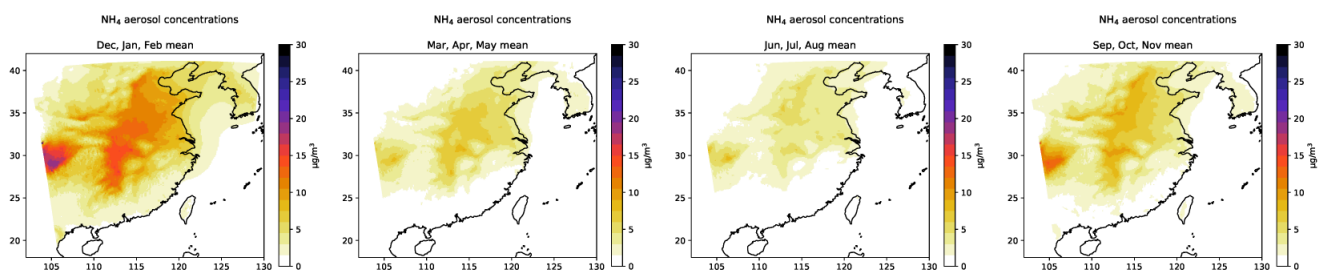


Figure A.28.: Seasonally averaged, modeled  $\text{NH}_4$  concentrations in the ground layer from all sources in China.

## A. Appendix

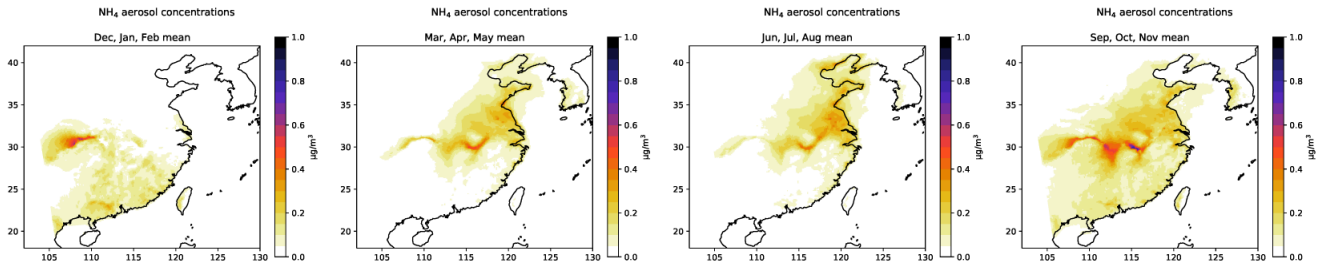


Figure A.29.: Seasonally averaged, modeled  $\text{NH}_4$  concentrations in the ground layer from ships in China.

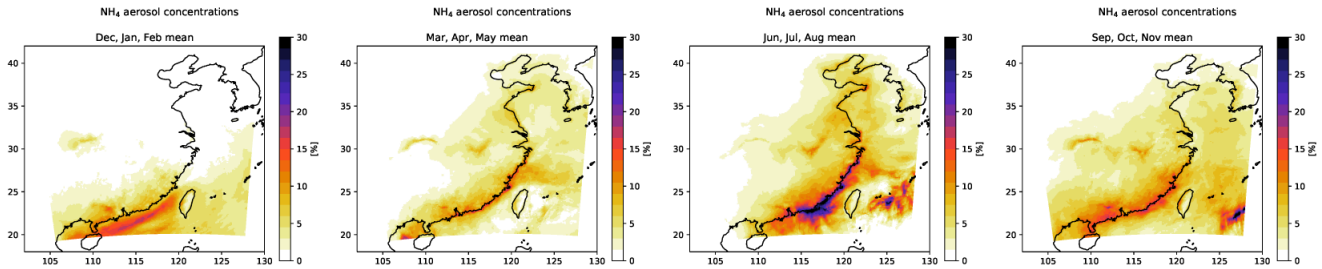


Figure A.30.: Seasonally averaged, modeled percentage share of ships on  $\text{NH}_4$  concentrations in the ground layer in China.

### A.2.3.6. $\text{NH}_3$ emissions

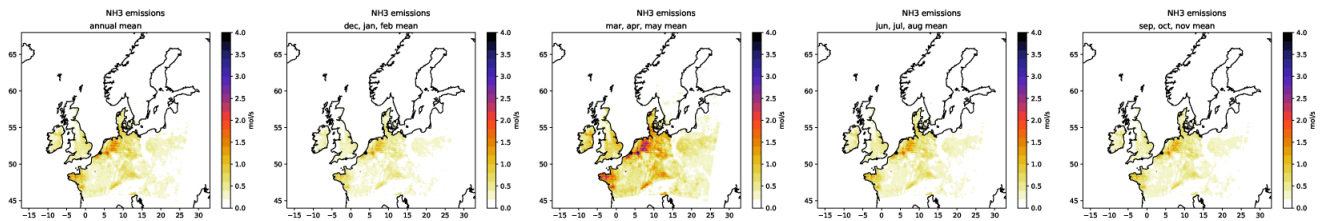


Figure A.31.: Seasonally averaged, modeled  $\text{NH}_3$  emissions in the ground layer in the Europe.

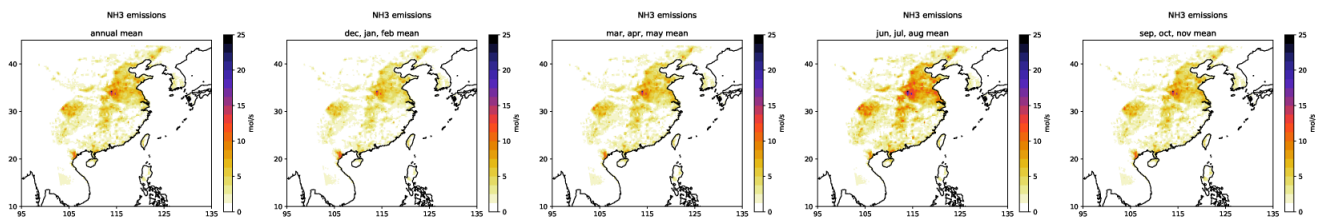


Figure A.32.: Seasonally averaged, modeled  $\text{NH}_3$  emissions in the ground layer in China.



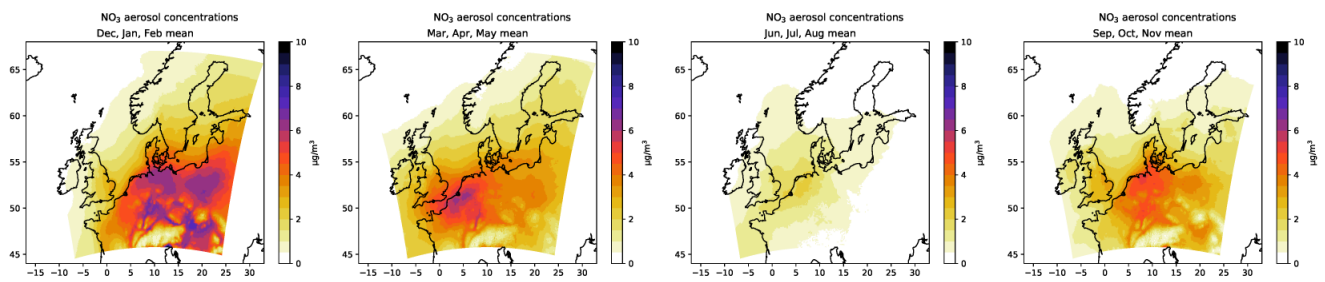
A.2.3.7. NO<sub>3</sub>

Figure A.33.: Seasonally averaged, modeled NO<sub>3</sub> concentrations in the ground layer from all sources in Europe.

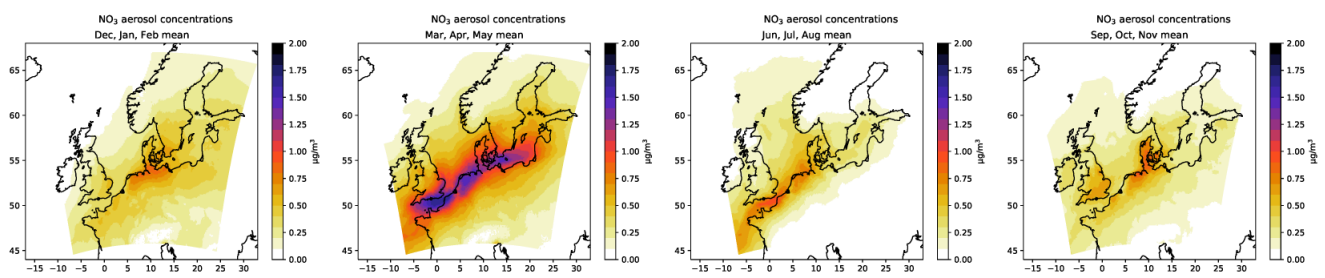


Figure A.34.: Seasonally averaged, modeled NO<sub>3</sub> concentrations in the ground layer from ships in Europe.

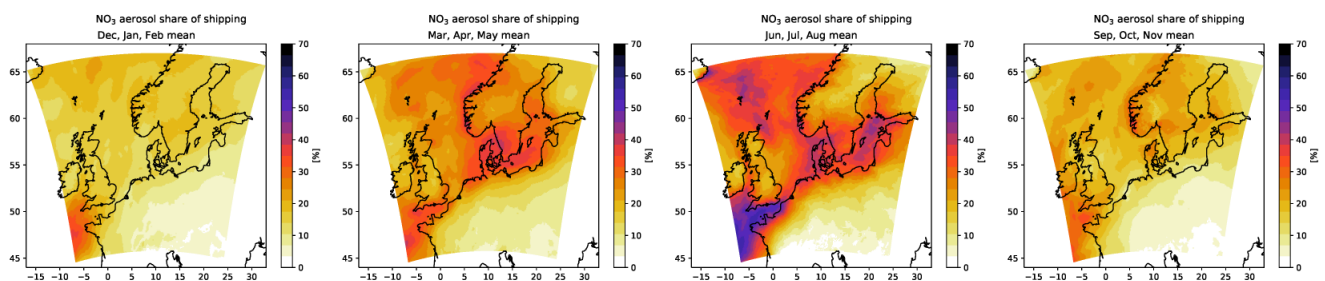


Figure A.35.: Seasonally averaged, modeled percentage share of ships on NO<sub>3</sub> concentrations in the ground layer in Europe.

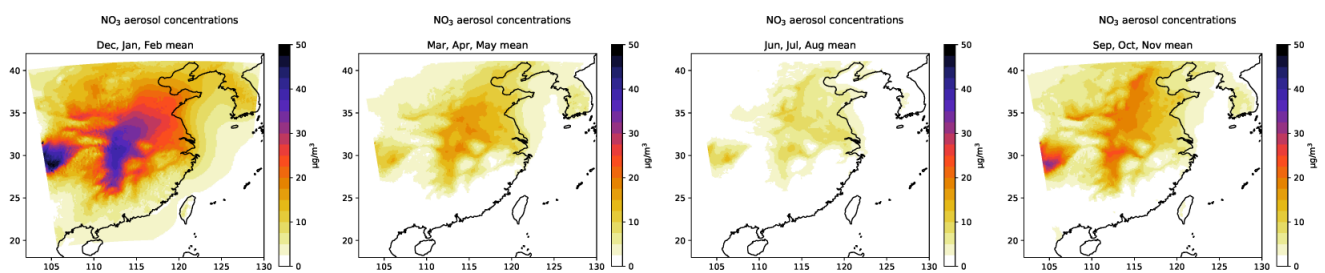


Figure A.36.: Seasonally averaged, modeled NO<sub>3</sub> concentrations in the ground layer from all sources in China.

## A. Appendix

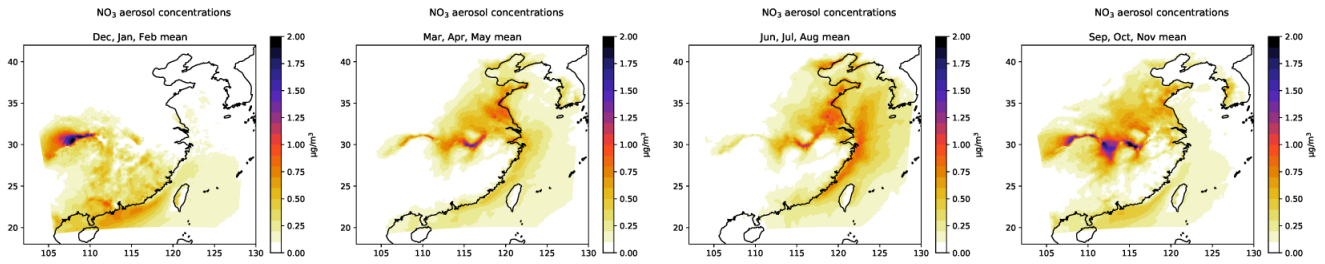


Figure A.37.: Seasonally averaged, modeled  $\text{NO}_3$  concentrations in the ground layer from ships in China.

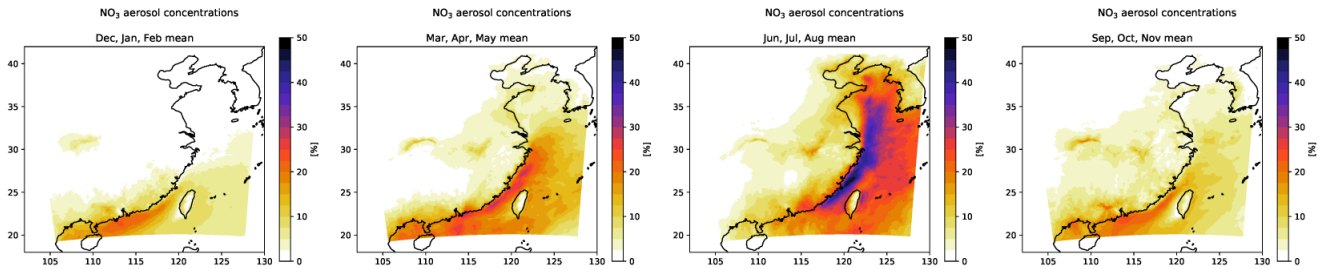


Figure A.38.: Seasonally averaged, modeled percentage share of ships on  $\text{NO}_3$  concentrations in the ground layer in China.

### A.2.3.8. $\text{SO}_4$

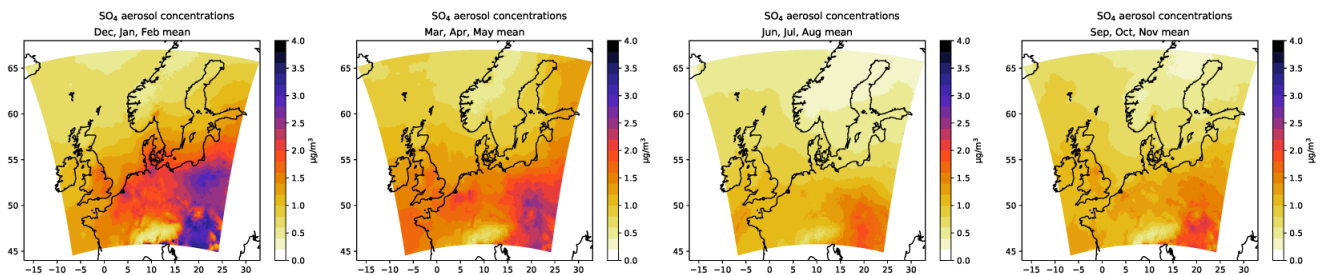


Figure A.39.: Seasonally averaged, modeled  $\text{SO}_4$  concentrations in the ground layer from all sources in Europe.

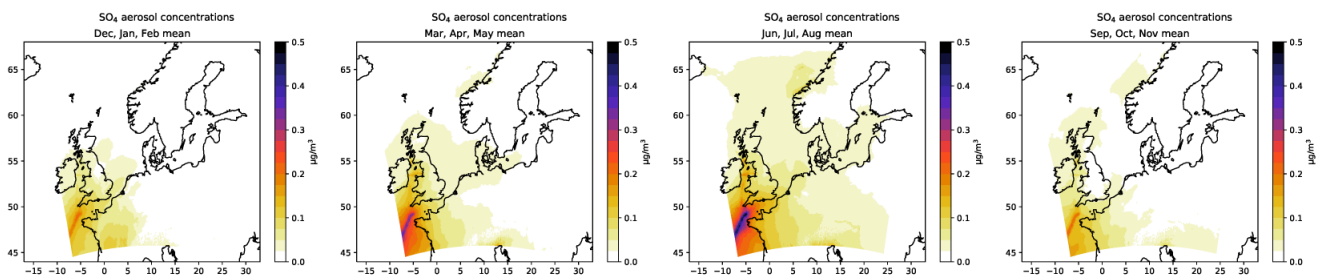


Figure A.40.: Seasonally averaged, modeled  $\text{SO}_4$  concentrations in the ground layer from ships in Europe.

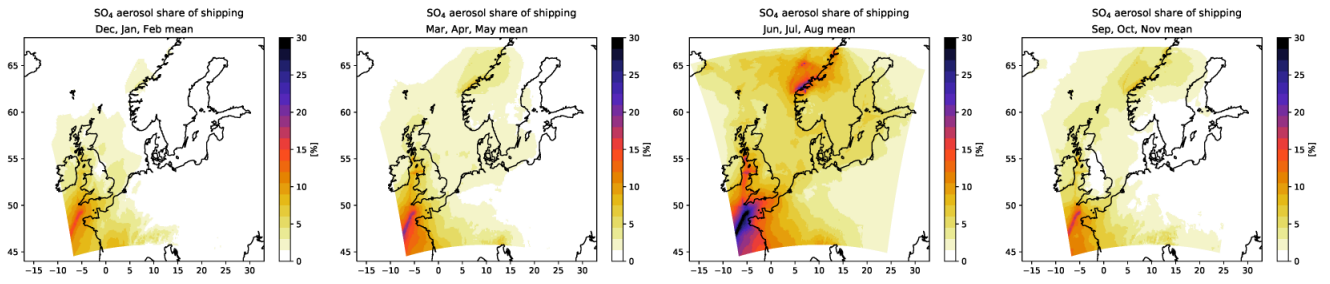


Figure A.41.: Seasonally averaged, modeled percentage share of ships on  $\text{SO}_4$  concentrations in the ground layer in Europe.

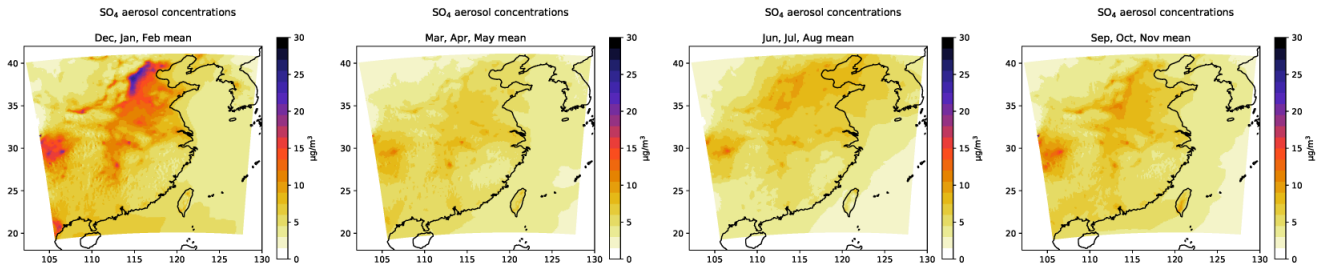


Figure A.42.: Seasonally averaged, modeled  $\text{SO}_4$  concentrations in the ground layer from all sources in China.

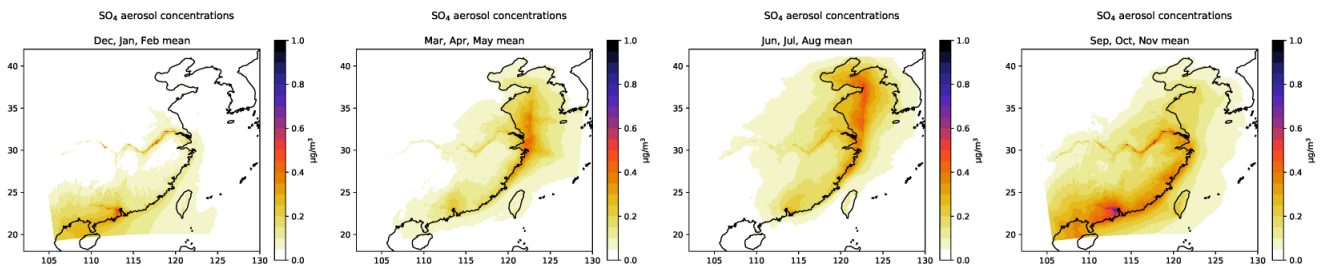


Figure A.43.: Seasonally averaged, modeled  $\text{SO}_4$  concentrations in the ground layer from ships in China.

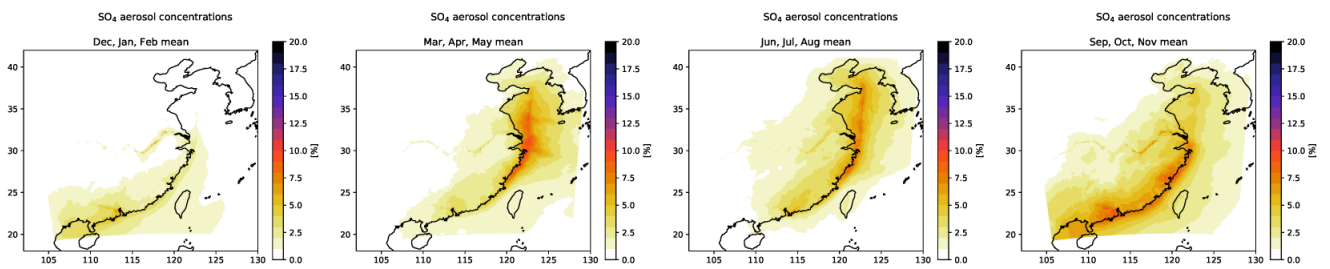


Figure A.44.: Seasonally averaged, modeled percentage share of ships on  $\text{SO}_4$  concentrations in the ground layer in China.